Open Science

Open Science Philosophy

Open science encompasses unrestricted access to scientific research articles, access to data from public research, and collaborative research enabled by information and communication technology tools, models, and incentives. Broadening access to scientific research publications and data is at the heart of open science. The objective of open science is to make research outputs and its potential benefits available to the entire world and in the hands of as many as possible:

- Open science promotes a more accurate verification of scientific research results. Scientific inquiry and discovery can be sped up by combining the tools of science and information technologies. Open science will benefit society and researchers by providing faster, easier, and more efficient availability of research outputs.
- Open science reduces duplication in collecting, creating, transferring, and re-using scientific material.
- Open science increases productivity in an era of tight budgets.
- Open science results in great innovation potential and increased consumer choice from public research.
- Open science promotes public trust in science. Greater citizen engagement leads to active participation in scientific experiments and data collection.

Open Science Index

The Open Science Index (OSI) currently provides access to over thirty thousand full-text journal articles and is working with member and non-member organizations to review policies to promote and assess open science. As part of the open science philosophy, and by making open science a reality; OSI is conducting an assessment of the impact of open science principles and restructuring the guidelines for access to scientific research. As digitalization continues to accelerate science, Open science and big data hold enormous promise and present new challenges for policymakers, scientific institutions, and individual researchers.

OSI is helping the global scientific research community discover, evaluate, and access high-quality research output. Renowned for its editorially curated and refereed collection of the highest-quality publications, OSI has always been and will remain free-of-charge.

OSI provides an efficient and thorough discovery process to the open science research database and provides links and free access to full-text articles. There are 50 open access journal categories that are curated and refereed by international scientific committees, the in-house editorial team, and trusted partners. Since its inception in 2007, OSI has made more than thirty thousand peer-reviewed open access full-text journal articles (PDF versions) freely available online without cost, barriers, or restrictions.

Open Science Access

With the Open Science Index, researchers can discover and access trusted peer-reviewed open access full-text scientific research articles with confidence. OSI helps researchers find appropriate non-profit open access journals to publish their work.

OSI gives one-click access to online full-text PDFs and expands the reach to global society by giving users free access from anywhere around the globe. Through cutting-edge open science collaboration, in an innovative public partnership, the non-profit OSI is devoted to making science open and reusable.

To learn more, visit online at waset.org

Open Science

Scholarly Research Review

The scholarly research review is a multidimensional evaluation procedure in which standard peer review models can be adapted in line with the ethos of scientific research, including accessible identities between reviewer and author, publishing review reports and enabling greater participation in the peer review process. Scholarly research review methods are employed to maintain standards of quality, improve performance, provide credibility, and determine suitability for publication. *Responsible Peer Review Procedure:* Responsible peer review ensures that scholarly research meets accepted disciplinary standards and ensures the dissemination of only relevant findings, free from bias, unwarranted claims, and unacceptable interpretations. Principles of responsible peer review:

• Honesty in all aspects of research
• Accountability in the conduct of research
• Professional courtesy and fairness in working with others
• Good stewardship of research on behalf of others

The responsibilities of peer review apply to scholarly researchers at all stages of peer review: Fairness, Transparency, Independence, Appropriateness and Balance, Participation, Confidentiality, Impartiality, Timeliness, Quality and Excellence, Professionalism, and Duty to Report.

Scholarly Research Review Traits:
• Scholarly Research Review Identities: Authors and reviewers are aware of each other's identity

• Scholarly Research Review Reports: Review reports are published alongside the relevant article

• Scholarly Research Review Participation: The wider academic community is able to contribute to the review process

• Scholarly Research Review Interaction: Direct reciprocal discussion between author(s) and reviewers, and/or between reviewers, is allowed and encouraged

• Scholarly Research Pre-review Manuscripts: Manuscripts are made immediately available in advance of any formal peer review procedures

• Scholarly Research Review Final-version Reviewing: Editorial revision of the language and format is conducted on the final version of the manuscript for publication

• Scholarly Research Review Platforms: The scholarly research review process is independent of the final publication of the manuscript and it is facilitated by a different organizational entity than the venue of publication

All submitted manuscripts are subject to the scholarly research review process, in which there are three stages of evaluation for consideration: pre-review manuscripts, chair-review presentation, and final-review manuscripts. All submitted full text papers, that may still be withstand the editorial review process, are presented in the conference proceedings. Manuscripts are tracked and all actions are logged by internal and external reviewers according to publication policy. External reviewers' editorial analysis consists of the evaluation reports of the conference session chairs and participants in addition to online internal and external reviewers' reports. Based on completion of the scholarly research review process, those manuscripts meeting the publication standards are published 10 days after the event date.

To learn more, visit online at waset.org

Open Science

Open Science Award

The International Research Conference (IRC) is an open science research organization dedicated to promoting advancement of science, engineering, and technology. The IRC's open science award program is pleased to announce research awards which are available to distinguished researchers who are currently based at or affiliated with a research university.

The purpose of this award is the recognition of open science research and publications. The award program coordinates and develops high impact scholarly research which seeks to promote multiscience approaches. The open science originates with the premise that universal scientific knowledge is a product of collective scholarly efforts. The social collaboration involves all stakeholders and knowledge belongs to the global society. Scientific outputs generated by public research are public good that should be available to all at no cost and without any barriers or restrictions.

The open science award is granted annually for outstanding achievements and excellence in scientific research. Any researcher who is interested in this award can submit their own and /or the colleagues' scholarly research articles for consideration for this honor. All respected researchers are warmly welcome to submit their research works for potential award consideration and evaluation. Qualitative and quantitative assessment of the open access articles submitted and published for consideration will be evaluation criteria for the award. The award emphasizes open science contributions, collaborations and communication, and the open publication of scholarly research knowledge.

This annual award will be given to one and up to three honorees (or research groups) in recognition of exceptional contributions to open science in the following three distinct research categories: Social Sciences, Life Sciences, and Physical Sciences. The selection committees (waset.org/Committees) are responsible for selecting the recipient(s) of the named award. The members of the open science award committee will promote excellence and transparency, allow broad input, recognition, diversity and commitment to equity so that the open science award is sufficiently representative of distinguished research groups.

Assignment of the open science award committee is performed primarily through the online submission and review system. The annual event is held to present awards and to celebrate distinguished researchers for their open science contributions.

Open Science Award Deadlines

Online Nomination Deadline: January 01, 2020 - December 31, 2020

Scoring Deadline: January 01, 2021 - March 31, 2021

Selection Deadline: April 30, 2021

Award Ceremony Date: June 30, 2021

Application Procedure

Applicants must submit the following to https://waset.org/profile/messages with the email subject line reading "OSA_surname_given name," e.g., OSA_Smith_John.

Open Science

Please include the following attachments to your email application:

1. Applicants should hold, at a minimum, a Ph.D. or its equivalent degree.

2. Cover letter to the Award Committee indicating interest in the award.

3. Curriculum vitae.

4. Research statement. Please include a description of your research accomplished (not more than two pages, single spaced), and published full text original research article in pdf format.

5. Two letters of recommendation. The applicant must request the letters (or the dossier service).

6. High-quality copies or scans of transcripts showing degrees (Bachelor, Masters, and Doctoral) and coursework.

To learn more, visit online at waset.org

Open Science

Postdoctoral Fellowship Award

The International Research Conference (IRC) is an open science research organization dedicated to promoting the advancement of science, engineering, and technology. The IRC's postdoctoral fellowship award is pleased to announce Fellowships which are available for postdoctoral researchers who are currently based at or affiliated with a research university. The postdoctoral fellowship award coordinates and develops high impact scholarly open science research which seeks to promote multiscience approaches. In addition, the fellowship award presents a unique opportunity for researchers who want to influence the future of open science through collaboration, communication, publication and data sharing within the global science community.

This postdoctoral fellowship award is looking for researchers with a passion for open science, open sources, open publications and data sharing. Applicants should already be working to promote research practices in a more collaborative, iterative and open dimension. Fellows will spend four months starting in June of 2020 as community catalysts at their own institutions creating, disseminating, and mentoring the next generation of open scientists, open data practitioners and researchers. The goal is to build lasting changes in the global open science community. Throughout the fellowship term, Fellows will receive training and support from the open science postdoctoral Fellowship award to develop and hone their skills around open science, open sources, data sharing, open science policy and licensing. Fellows will also craft policies and codes, write curriculum, teach their institutional peers, and be engaged in helping their local open science communities learn about open sources and open data practices.

Expectations: The open science postdoctoral Fellowship award anticipates applicants who:

- Create change within their university or other institution throughout open science, research, data sharing, and article publications.
- Create knowledge, policies and codes, curriculum and educational resources to promote open science.
- Participate in open science research workshops, symposia, conferences, and other activities.
- Participate in and help to lead regular open science research community call for proposals or papers.
- Serve as open science mentors and leaders within their research communities.
- Serve as reviewers for submitted open science abstracts and research papers for scholarly journals and conferences.
- Promote open science by communicating, publishing and sharing their high impact peer-reviewed research on an ongoing basis.

Note: Fellows are encouraged to continue their personal research for up to 20% of their time during the course of their fellowship (i.e., one day a week). Fellowship applicants must have buy-in from their advisors in advance and include their advisors' contact information on the application. The applicant's advisors will be interviewed should the applicant move on to the second round, and their support will be a critical consideration for the awarding of Fellowships.

Open Science

Fellowship Terms and Conditions

Award Scholarship Description

Application Deadline: April 30, 2020

- Fellowships are awarded to enhance the concept of open science and are open to scholars from all fields of science, engineering, and technology.

- The selected Fellow will receive a monthly stipend of $500.00 for four months during 2020 (June, July, August, and September). Fellows are responsible for remitting all applicable taxes and other government charges as required by their country of residence and by law.

Nationality: Fellowships are available to postdoctoral researchers in any country.

Requirements:

Fellows must:

• At a minimum, hold a Ph.D. or its equivalent by June 1, 2020, and should not have received the degree before 2018.

• Applicants should have working proficiency in the English language and should demonstrate their ability to read, write, and speak English.

• Applicants should be full-time academics or affiliated with a research university or institute.

• Funding will be direct to the Fellow and not distributed through their institution.

• Be able to travel.

• Obtain support from their advisors. Fellows will be based at their home institutions. Please note that a letter of support from the advisor is mandatory for consideration.

• Have experience participating in open science research.

Application Procedure:

Applicants must submit the following to https://waset.org/profile/messages with the email subject line reading "Postdoc_surname_given name," e.g., Postdoc_Smith_John.

Please include the following attachments to your email application:

1. Cover letter to the Search Committee indicating interest in the position.

2. Curriculum vitae.

3. Dissertation abstract.

Open Science

4. Research statement. Please include a description of your proposed research that would be accomplished during the fellowship (not more than two pages, single spaced).

5. Two letters of recommendation. The applicant must request the letters (or the dossier service).

6. High-quality copies or scans of transcripts showing degrees (Bachelor, Masters, and Doctoral) and coursework.

To learn more, visit online at waset.org

Article TABLE OF CONTENTS Page

Durability of a Non-Crimp Fabric Composite under Hygrothermal Aging

Hicham Bezzou

Abstract—The specific properties and durability of composite materials are particularly targeted by the aerospace, automotive, naval and aerospace industries to save consumable energy and improve the service life of structures. That's why research has multiplied in the development of new families of composite materials to address various issues, such as strength and durability. This last decade saw the emergence of a new generation of composite materials of NCF (Non-Crimp Fabric) type. It consists of composites composed of non-woven multiaxial reinforcements, and sewn with a textile thread. The presence of the sewing thread induces the formation of a specific morphology imposing a new approach concerning the study of durability of these composites. Indeed, the NCF composites consist of a stack of unidirectional layers whose fibers are sewn by a sewing thread. The layers are oriented together in directions selected to meet a given specification. Moreover, a laminated composite can crack by thermal cycling, and without any mechanical stress applied. High temperatures induce long-term drying of the material thus causing residual thermal stresses high enough to produce cracks in multiaxial composites. In this study, the NCF composite was solicited by an accelerated hygrothermal loading in which there are two different loading phases. A first phase from which the composite is conditioned at 95% RH for 12 hours at 50°C. Then, a second phase of one hour in which the composite is solicited 400 times by a temperature range of [-55 80]°C with a speed of 9°C/min. In order to quantify the cracks, a measurement variable called "crack density" is retained, which is based on optical micrographic observations. The cracks are then classified according to the number of folds they cross.

Keywords—durability, hygrothermal cycles, non-crimp fabric composite, microcracking

Corresponding Author
Bezzou Hicham from Université de Nantes, France
e-mail: hicham.bezzou@univ-nantes.fr

Corrosion Behavior of Organic-Inorganic Hybrid Coatings Fabricated by Electrostatic Method

Mohammed Ahmed, Ziba Nazarlou

Abstract**—**Mild steels has a limited alloying content which make them vulnerable to excessive corrosion rates in harsh medium. To overcome this issue, some protective coatings are used to prevent corrosion on the steel surface. the use of specialized coatings, mainly organic coatings (such as epoxies, polyurethanes, and acrylics) and inorganic coatings (such as Polysiloxanes) is the most common method of mitigating corrosion of carbon steel. Incorporating the benefits of organic and inorganic hybrid (OIH) compounds for the designing of hybrid protective coatings is still challenging for industrial applications. There are advantages of inorganic coatings have but purely inorganic siloxane-based coatings are difficult to use on industrial applications unless they are used at extremely low thicknesses (<1-2 microns). Hence, most industrial applications try to have a combination of Polysiloxanes with organic compounds.

A hybrid coating possesses an organic section, which transports flexibility and impact resistance, and an inorganic section, which usually helps in the decreasing of porosity and increasing thermal stability and hardness. A number of polymers including polyethylene glycol and polyvinyl pyrrolidone have been reported to inhibit the corrosion mild steel in acidic media. However, reports on the effect of polyethylene oxide (PEO) or its blends on corrosion inhibition of metals is very scarce. Different composition of OIH coatings was synthesized by using silica sol-gel, epoxy, and PEO. The effect of different coating types on the corrosion behavior of carbon steel in harsh solution has been studied by weight loss and electrochemical measurements using Gamry 1000 Interface Potentiostat. Coating structures were investigated by SEM. İt is revealed considerable reduction in corrosion rate for coated sample. Based on results, OIH coating prepared by epoxy-silica sol gel-PEO and epoxy-silica sol-gel exhibit %99.5 and %98 reduction of (Corrosion rate) C_R compares to baseline. cathodic Tafel constant (βc) shows that coatings change both Tafel constants but had more effect on the cathodic process. The evolution of the Potentiostatic scan with time displays stability in potential, some of them in a high value while the other in a low value which can be attributed to the formation of an oxide film covering substrate surface. The coated samples with the group of epoxy coating have a lower potential along with the time test while the silica group shows higher in potential with respect to time.

Keywords**—**Electrostatic; Hybrid Coating; Corrosion Tests, Silica Sol Gel.

M. A. is with the Department of Mechanical Engineering, Ozyegin university, Istanbul, Turkey (e-mail: salih.ahmed@ozu.edu.tr).

Z. N., Jr., was with Ozyegin university, Istanbul, Turkey She is now with the Department of Material Engineering, Koc University, Istanbul, Turkey (e-mail: znazarlou19@ku.edu.tr).

Development of Carrageenan-Psyllium/Montmorillonite Clay Hybrid Hydrogels for Agriculture Purpose

D. Aydınoğlu, N. Karaca, Ö. Ceylan

***Abstract*—**Limited water resources on the earth come first among the most alarming issues. In this respect, several solutions from treatment of waste water to water management have been proposed. Recently, use of hydrogels as soil additive, which is one of the water management ways in agriculture, has gained increasing interest. In traditional agriculture applications, water used with irrigation aim, rapidly flows down between the pore structures in soil, without enough useful for soil. To overcome this fact and increase the abovementioned limit values, recently several natural based hydrogels have been suggested and tested to find out their efficiency in soil. However, most of these researches have dealt with grafting of synthetic acrylate based monomers on natural gelling agents, most probably due to reinforced of the natural gels. These results motivated us to search a natural based hydrogel formulations, not including any synthetic component, and strengthened with montmorillonite clay instead of any grafting polymerization with synthetic monomer and examine their potential in this field, as well as characterize of them. With this purpose, carrageenan-psyllium/ montmorillonite hybrid hydrogels have been successively prepared. Their swelling capacities were determined both in deionized and tap water and were found to be dependent on the carrageenan, psyllium and montmorillonite ratios, as well as the water type. On the other hand, mechanical tests revealed that especially carrageenan and montmorillonite contents have a great effect on gel strengths, which is one of the essential features, preventing the gels from cracking resulted in readily outflow of all the water in the gel without beneficial for soil. They found to reach 0.23 MPa. The experiments carried out with soil indicated that hydrogels significantly improved the water uptake capacities and water retention degrees of the soil from 49 g to 85 g per g of soil and from 32 to 67%, respectively, depending on the ingredient ratios. Also, biodegradation tests demonstrated that all the hydrogels undergo biodegradation,as expected from their natural origin. The overall results suggested that these hybrid hydrogels have a potential for use as soil additive and can be safely used owing to their totally natural structure.

***Keywords*—**Carrageenan, hydrogel, montmorillonite, psyllium.

D. Aydınoğlu is with Yalova University, Armutlu Vocational School, Department of Food Processing, Yalova, 77500 Turkey (e-mail: demet.aydinoglu@yalova.edu.tr; daydinoglu@yahoo.com).

N. Karaca is with Yalova University, Central Research Laboratory, Yalova, 77200, Turkey (e-mail: nurcan.karaca@yalova.edu.tr).

Ö. Ceylan is with Yalova University, Central Research Laboratory, Yalova, 77200, Turkey (e-mail: ozgur.ceylan@yalova.edu.tr).

Current Status of Industry 4.0 in Material Handling Automation and In-house Logistics

Orestis K. Efthymiou, Stavros T. Ponis

***Abstract*—**In the last decade, a new industrial revolution seems to be emerging, supported -once again- by the rapid advancements of Information Technology in the areas of Machine-to-Machine (M2M) communication permitting large numbers of intelligent devices, e.g. sensors to communicate with each other and take decisions without any or minimum indirect human intervention. The advent of these technologies have triggered the emergence of a new category of hybrid (cyber-physical) manufacturing systems, combining advanced manufacturing techniques with innovative M2M applications based on the Internet of Things (IoT), under the umbrella term Industry 4.0. Even though the topic of Industry 4.0 has attracted much attention during the last few years, the attempts of providing a systematic literature review of the subject are scarce. In this paper, we present the authors' initial study of the field with a special focus on the use and applications of Industry 4.0 principles in material handling automations and in-house logistics. Research shows that despite the vivid discussion and attractiveness of the subject, there are still many challenges and issues that have to be addressed before Industry 4.0 becomes standardized and widely applicable.

***Keywords*—**Industry 4.0, internet of things, manufacturing systems, material handling, logistics.

I. Introduction

MATERIAL handling incorporates the movement, storage, protection and control of materials and products throughout the complete lifecycle of manufacturing, warehousing, distribution and disposal. The material handling process includes a wide range of manual, semi-automated and automated equipment and systems supporting logistics and making the supply chain work. The material handling systems and processes of a company are established to enhance customer service, decrease inventory, shorten shipping times and decrease general production, distribution and transportation expenses.

The term Industry4.0 which first appeared at Hannover Fair in 2011, refers to the Fourth Industrial Revolution which is characterized by the need to attain a higher level of operational efficiency and productivity, but also a greater level of automation as well. The primary characteristics are digitization, manufacturing optimization and customization; automatic data sharing and communication; enhanced human-machine interaction; automation and adaptation; and value-added services [2]. Consequently, the result of all the above is to build "smart" factories. Factories that are able to adapt quickly to modifications in order to satisfy leadership objectives, use resources at the greatest level, and do all this autonomously, without the need for human intervention [3].

Material handling incorporates the movement, storage, protection and control of materials and products throughout the complete lifecycle of manufacturing, warehousing, distribution and disposal. The material handling process includes a wide range of manual, semi-automated and automated equipment and systems supporting logistics and making the supply chain work. The material handling systems and processes of a company are established to enhance customer service, decrease inventory, shorten shipping times and decrease general production, distribution and transportation expenses.

Key technologies of Industry 4.0 are IoT including Industrial Wireless Networks (IWN) that can sense, identify, process and communicate [4], Cyber-Physical Systems [2], Cloud Computing [5], Robotics [6], Big Data analytics [7], Augmented Reality [8], Artificial Intelligence and Machine Learning [9], Digital Twins and Simulation [10] and Additive Manufacturing [11]. The more these trends converge (i.e. adoption of such technologies by people and companies), the bigger the effect becomes. Each of these technologies and trends disrupts almost every aspect of our lives, our society, the economy and all industries and countries with an exponential pace and impact. The more devices, machines, production modules and products that can connect and exchange data independently, the more actions will be generated between them, and a more linked and intelligent environment for production and services will be developed [12].

Although there is increasing interest in Industry 4.0, literature on how this new technology revolution affects supply chain activities and intralogistics and material handling has been restricted up to now. This paper seeks to determine the current Industry 4.0 state of the art, study its main applications in the area of in-house logistics, analyze its impact and potential consequences and identify grey research areas and shortcomings in the current state of the art. Therefore, the objective of this paper is to contribute to improving knowledge of Industry 4.0 in relation to material handling and in-house logistics.

This paper is organized in four discrete sections. The current one introduces the basic concepts and states the objectives of this paper. Section II presents the detailed analysis of the collected material. Section III discusses the review of collected material and Section IV concludes the

Orestis K. Efthymiou, is with the National Technical University Athens, Heroon Polytechniou 9, Zografos, Athens, Greece (phone: +30210 7722384; fax: +30210 7723571, e-mail: orestisefthymiou@mail.ntua.gr

Stavros T. Ponis is with the National Technical University Athens, Heroon Polytechniou 9, Zografos, Athens, Greece (phone: +30210 7722384; fax: +30210 7723571, e-mail: staponis@central.ntua.gr.

review, by presenting the research contributions and limitations of this study.

II. Analysis

The authors provide an analysis and discussion of the impact and potential consequences of Industry 4.0 on material handling & contemporary in-house logistics. In doing so, the authors focus on supply chain & logistics and discuss how Industry 4.0 technologies and digitalization affect the different elements of material handling and in-house logistics through the reviewed literature.

According to [13], developments of Industry 4.0 have a heavy impact on logistics. These developments, lead to improvements in different areas of logistics, such as better efficiency, increased traceability and improved responsiveness to customers, which in turn impact the basic elements of businesses. In other words, this new "version" of logistics provides opportunities to significantly change business models that companies operate with. Technologies such as IoT and Cyber-Physical Systems (CPS) are able to tackle challenges of traditional supply chains and logistics by monitoring and synchronizing information between physical processes and cyber computational space [13]. Based on [14], within the procurement, transport logistics, warehouse and order fulfillment functions, results showed that the areas most affected by the launch of Industry 4.0 are order fulfillment and transport logistics. It is evident from the same analysis that the application of specific techniques, such as Virtual Reality, Augmented Reality, simulation and 3D-Printing, has favorable outcomes for the logistics tasks under research. Big Data Analytics, cloud computing, IoT, RFID, cybersecurity, robotics, drones, and BI, on the other hand, could have both beneficial and negative consequences for organizations. The clear advantages of Industry 4.0 application are enhanced flexibility, quality standards, efficiency and productivity [14].

Reference [15] mentions the fields of transportation and warehousing as areas impacted by digitization and Industry 4.0 techniques. CPS will be the primary initiator of change in the field of warehousing. In the intelligent warehouse of the future, individuals, machines and resources will all interact easily and continually with each other, which literally implies that standard warehousing activities will totally alter as products are uniquely recognizable, can be located at all times and know their own history, current status and alternative paths to attain their target state. In [16], the authors discover a correlation between Industry 4.0 technologies and improved operational efficiency in transport services and warehousing facilities. They demonstrate that technologies such as IoT, automation, Cloud computing, Big Data Analytics, simulation and Augmented and Virtual Reality can be applied with beneficial effect on logistics and material handling. Furthermore, they also recognize five significant technological elements that will lead to future logistics tasks being fully automated, being: intelligent robots & autonomous vehicles, RFID technology & Quick Response Codes, sensors & conveyors, smart devices, and lastly CPS [16].

Another region that Industry 4.0 technologies could assist in the supply chain is the optimization of issues and processes for factories and warehouses. Logistic systems demand a shorter delivery cycle, reduced inventory levels, fewer working hours, and more on-time manufacturing and distribution in the context of Industry 4.0. The range and level of logistics planning within the prism of Industry 4.0 is therefore more comprehensive than in traditional logistics planning [17]. According to [18], broader logistics sector, including material handling and in-house logistics, is a suitable application area for Industry 4.0, with significant impacts expected.

According to [19], digitalization in logistics is based on cooperation, connectivity, adaptiveness, integration, autonomous control and cognitive improvement. Industry 4.0 technologies play a crucial role on the implementation of these characteristics and they enable the ability for integrated planning & execution systems, logistics visibility, autonomous logistics, smart procurement, smart warehousing and intralogistics, and advanced analytics among others. The characteristic of adaptiveness is also vital for intralogistics operations, since it allows systems to be able to change its components and their relations over time in order to be influenced by events outside of its system boundaries [19].

Reference [20] uses the term "Smart Logistics", which is the same that is used also for defining "Smart Products" and "Smart Services". A Smart Logistics system is one that can increase flexibility by bringing the business closer to client requirements and adapting to market modifications. An effective and powerful Logistics 4.0 should use and depend on the following four technological apps, according to [20]: 1) Smart Warehouse Management Systems to transform warehouse operations according to future demands in compliance with the paradigm of Industry 4.0. 2) Advanced transport management systems capable of providing better end-to-end visibility of the supply chain by using IoT technology. 3) Intelligent Transportation Systems (ITS), an area that interacts with distinct fields of transport systems, such as transport management, control, operations, infrastructure, policies and methods of control and finally 4) Information Security is, crucial and challenging requirement in Logistics 4.0, since dependence on technology is increasing [20].

On a more detailed level, Industry 4.0 will trigger changes that affect material handling and in-house Logistics, through improvements in materials and information, robotics and cloud technologies, RFID, Autonomous Guided Vehicles (AGVs) and autonomous decisions and configuration of material handling systems. According to [21], future warehouses and factories will have all of their components represented as individual agents in the cloud. All devices such as AGVs, industrial robots and operators, through their smart tablets or PDAs, will be interconnected and also have the ability to make their own decisions. Through the cloud architecture, the current hierarchical control structures will be replaced by decentralized web-like control architectures, which will offer additional services like data storage and outsourcing computational power.

Reference [22] describes that automated systems comprised

by AGVs or some form of freely autonomous robots allow the warehouse area to become far more flexible than with the use of a fixed automation system, such as a conveyor. Extensions or modifications to such systems can be quite quick and cost adequate, which is one of the most important aspects during our times, where trends change quickly and future can be much different than the present. Another advantage of fleets of freely autonomous robots is that they are able to deal with dynamic changes, such as obstacles in the environment, and when a route is blocked, they can find a way to navigate around in order to continue their task [22]. Reference [23] describes the advantages of using AGVs in industrial environments, whether they are warehouses, container terminals, or manufacturing facilities. They state that according to the 2016 Material Handling Industry Report, which documents the utilization of AGVs in supply chains, the role of robotics and automation is catalytic in disruptively shaping competitive advantages. Reference [24] also explains the positive impact of mobile robots in material handling, through the different solutions they have provided. Todays' smart manufacturing systems rely on intelligent machines and devices in order to meet the challenges of consumer demands. They present a solution to the problem of mobile robot Artificial Intelligence programming in smart manufacturing systems. According to [25], cloud computing can be of great help in robotics, since it helps to manage data flow more efficiently. Within a warehouse, each individual robot does not have to keep its massive data storage, since combined data pools can help to use and update data on the basis of individual capability. Transferring computational and data analysis load to the cloud releases robot resources and enhances their capacity for executing tasks at the shop floor level [25].

According to [26], RFID technology can be of great assistance in a warehouse environment. Other than tracking inventory items, it can be used on storage equipment too, which allows for real-time response. Reference [26] introduces a concept of flexible warehousing, which is based on real-time decision support system that is enabled by RFID generated data. In this concept, all racking and inventory items are RFID enabled, which permits their visibility at any time. The outcome of such a system is that depositing and picking trips within the warehouse can be greatly reduced, which in turn reduces costs and lead time [26]. According to [27], in order to navigate a warehouse or a factory, some form of information regarding the mapping of the facility is required. Reference [28] also mentions the positive effects of RFID on AGV systems. In their paper, they introduce an AGV system for smart factories which uses RFID in order to create a flexible and intelligent environment. What they found out is that RFID enables smart decision making for the AGVs, it improves fixed form guidance methods and remains flexible in case of future reconfigurations of warehouse or factory space [28].

Reference [29] describes another way that Industry 4.0 technologies could help in material handling. They say that based on technological advances, like intelligent industrial robots and M2M communication, new possibilities open up in order to reduce throughput losses in case of equipment failure. Machines have become intelligent enough in order to reconfigure themselves automatically in case they detect a failure in the overall system. In [29], they consider a planning of configuring automated flow lines that allows for downstream stations to perform the operations of failed stations in addition to those operations that were initially assigned to them, in the event of a failure [29].

Reference [30] describes the importance of knowing the abilities and overall effectiveness of material handling system, and therefore they discuss about the Overall Equipment Effectiveness (OEE) standard and simulation and show how these two techniques can help identify possible problems. The paper designs and studies the execution of an intelligent material handling system for material distribution with utilizing an agent-based algorithm as control architecture. A time based methodology is applied to evaluate the OEE. On the second stage, each of the optimization solutions is implemented on the simulation model in order to verify and validate the effects of the OEE percentage [30].

III. Discussion

Through a detailed evaluation process of the selected papers, four dominant literature categories were identified. A discussion for each one of these categories follows in the remainder of this section.

Industry 4.0 Applications for General Supply Chain & Logistics

This category includes papers that study Industry 4.0 technologies and their impact on logistics in general. Their main outcome shows that the shift towards Industry 4.0 will result in a profound change in the related information flow, affecting the entire logistics distribution system. This will inevitably lead to a deeper integration of logistics in business operations and create a shift toward service-oriented logistics on demand. According to the literature reviewed, the key organizational change in logistics sector will be the higher autonomy of decision-making accessible to logistics partners. This implies that decentralized decision-making promotes leaner planning of logistics, as connectivity guarantees that the actors have access to a virtual process model. Therefore, a thorough knowledge of upstream and downstream procedures enables a close integration of logistics into the value network.

Industry 4.0 Applications for Material Handling and Its Support by Information Flows

This category includes papers related to information flow and the intensified ability that Industry 4.0 has provided through technologies such as the IoT. With thousands of different kinds and forms of products being stored in today's average warehouse, every square meter of warehouse room needs to be optimally utilized to guarantee that particular products can be retrieved, processed and supplied as quickly as possible. Industry 4.0 promises a technology-driven, high-speed environment allowing executives to know what happens

in a warehouse or factory space at a specified time; machine performance, environmental conditions, energy consumption, stock status or material flow. Key technology of papers in this category is undoubtedly RFID, which by using active and passive readers, can provide precise localization of mobile devices in indoor environments. At the same time, sensors can also be incorporated into the infrastructure of the warehouse itself. Smart warehouse energy management connects various utilities, including connected lights and ventilation systems in order to optimize energy consumption, which in turn results in lower costs and lower carbon footprint of the facility. Finally, preventive maintenance is another key use case of IoT once data analytics is involved, and this is particularly critical in a warehouse or factory environment. This can have significant consequences in terms of OEE, a main metric of production productivity.

Industry 4.0 Applications for Material Handling Physical Activities

In this category, we classified papers that discuss about Industry 4.0 technologies and their impact on physical activities of material handling, such as picking, packing, storage and retrieval among others. Therefore in this category papers mention and analyze subjects that refer to CPSs, AGVs, picking robots, mobile robots, swarm intelligence, wearable devices and AR and VR. Material handling equipment and packaging are increasingly equipped with information technologies, which makes assets such as forklift trucks able to autonomously identify themselves, determine their present location and collect data on their status and the products being transported. Another point that was addressed on the examined literature is the human-to-machine interaction. In the near future, workers will join the IoT environment and through connecting via their smartphones, scanners, tablets and wearables, such as smart glasses and other AR and VR devices, they will possibly elevate human-to-machine interaction within the warehouse even further. The advent of connected workforce offers innovative possibilities for monitoring workers' health and fatigue, tracking workers' specified process routes and analyzing, where warehouse executives can enhance walkways or alter a process to make the work of employees easier and safer.

Industry 4.0 Applications for Material Handling Managerial & Strategic Planning

This category includes papers focusing in Industry 4.0 technologies and their impact on managerial and strategic planning of material handling, with subjects such as big data analytics, simulation and digital twins being in the center of discussion. It is often still the case that very little information is gathered for tasks such as production, logistics and services, even in centralized operations. Moreover, in many cases the data captured can only be seen or accessed by a limited number of people who can decrypt and understand the respective domain systems. The fact that warehousing facilities, transport units and autonomous vehicles are fitted with sensors and are connected to systems that share and organize their produced data creates a digital shadow of the real world. Thus, by employing analytics to sensor data, not only imminent issues, but possibly hazardous developments can be predicted well in advance. Therefore we see that as time progresses, logistics decisions are becoming more data based, in order to allow continuous process improvement and the efficacy of these data based decisions is guaranteed by the systematic use of information technology and systems.

IV. Conclusions

Logistics have developed from just an activity providing services, i.e. delivering the right goods to the right place at the right time, to become a key driver of digital and societal change. Topics like autonomous driving, IoT and Big Data are closely intertwined with logistics today. In this process, logistics both as a science and an economic sector drives both the application and the development of basic methods, algorithms and technologies. Therefore, Logistics plays a key role in the all-encompassing digitization of the economy and society. This means it is even more essential as a subject of research than was already the case, because Logistics is the backbone of developments concerning Industry 4.0. The goal is to create flexibly interconnected, complex and distributed material handling and in-house logistics systems based on a continuous and autonomous exchange of data and information between human actors and physical, technical objects [31].

In this paper, an analysis of Industry 4.0 technologies is presented in an attempt to understand their effect on material handling and in-house logistics. The study of literature reveals that Industry 4.0 is currently populated by small-scale test installations that try to depict real-life situations, thus lacking large-scale applications of its technologies in material handling and in-house logistics. Therefore the impact of Industry 4.0 in the studied areas in terms of efficiency, flexibility and availability has not yet been tested in detail. In addition, existing studies on the impact of automation in terms of human employees and the future qualifications and competencies needs of the workforce are scarce and relatively limited in their empirical findings. Finally, we have to note down that the choice of language limits the results of our study, since it is anticipated that a substantial number of publications is using a language other than English, especially in German where the Industry 4.0 term was firstly introduced.

Acknowledgments

The present work is co-funded by the European Union and Greek national funds through the Operational Program "Competitiveness, Entrepreneurship and Innovation" (EPAnEK), under the call “RESEARCH-CREATE-INNOVATE” (project code: T1EΔK-01168 and Acronym: SMARTFLEX

References

[1] Kagermann, V. H., Lukas, W.-D., & Wahlster, W. (2011). Industrie 4 0 Mit dem Internet der Dinge auf dem Weg zur vierten industriellen Revolution 2. Retrieved from VDI nachrichten website: http://www.wolfgang-wahlster.de/wordpress/wp-

content/uploads/Industrie_4_0_Mit_dem_Internet_der_Dinge_auf_dem_Weg_zur_vierten_industriellen_Revolution_2.pdf

[2] Lu, Y. (2017). Industry 4.0: A survey on technologies, applications and open research issues. Journal of Industrial Information Integration, Vol. 6, 1–10. https://doi.org/10.1016/j.jii.2017.04.005

[3] Kamble, S. S., Gunasekaran, A., & Gawankar, S. A. (2018). Sustainable Industry 4.0 framework: A systematic literature review identifying the current trends and future perspectives. Process Safety and Environmental Protection, Vol. 117, 408–425. https://doi.org/10.1016/j.psep.2018.05.009

[4] Li, X., Li, D., Wan, J., Vasilakos, A. V., Lai, C. F., & Wang, S. (2017). A review of industrial wireless networks in the context of industry 4.0. Wireless networks, 23(1), 23-41. https://doi.org/10.1007/s11276-015-1133-7

[5] Givehchi, O., Trsek, H., & Jasperneite, J. (2013, September). Cloud computing for industrial automation systems—A comprehensive overview. In 2013 IEEE 18th Conference on Emerging Technologies & Factory Automation (ETFA) (pp. 1-4). IEEE. https://ieeexplore.ieee.org/document/6648080

[6] Bahrin, M. A. Kamarul, Othman, M. F., Nor Azli, N. H., & Talib, M. F. (2016). Industry 4.0: A Review on Industrial Automation and Robotic. Jurnal Teknologi, 78(6–13). https://doi.org/10.11113/jt.v78.9285

[7] Wang, L., & Wang, G. (2016). Big data in cyber-physical systems, digital manufacturing and industry 4.0. International Journal of Engineering and Manufacturing (IJEM), 6(4), 1-8. https://doi.org/10.5815/ijem.2016.04.01

[8] Fraga-Lamas, P., Fernández-Caramés, T. M., Blanco-Novoa, Ó., & Vilar-Montesinos, M. A. (2018). A review on industrial augmented reality systems for the industry 4.0 shipyard. IEEE Access, 6, 13358-13375. https://doi.org/10.1109/ACCESS.2018.2808326

[9] Zhong, R. Y., Xu, X., Klotz, E., & Newman, S. T. (2017). Intelligent manufacturing in the context of industry 4.0: a review. Engineering, 3(5), 616-630. https://doi.org/10.1016/J.ENG.2017.05.015

[10] Uhlemann, T. H. J., Lehmann, C., & Steinhilper, R. (2017). The digital twin: Realizing the cyber-physical production system for industry 4.0. Procedia Cirp, 61, 335-340. https://doi.org/10.1016/j.procir.2016.11.152

[11] Ngo, T. D., Kashani, A., Imbalzano, G., Nguyen, K. T., & Hui, D. (2018). Additive manufacturing (3D printing): A review of materials, methods, applications and challenges. Composites Part B: Engineering, 143, 172-196. https://doi.org/10.1016/j.compositesb.2018.02.012

[12] Pereira, A. C., & Romero, F. (2017). A review of the meanings and the implications of the Industry 4.0 concept. Procedia Manufacturing, Vol. 13, 1206–1214. https://doi.org/10.1016/j.promfg.2017.09.032

[13] Strandhagen, J. O., Vallandingham, L. R., Fragapane, G., Strandhagen, J. W., Stangeland, A. B. H., & Sharma, N. (2017). Logistics 4.0 and emerging sustainable business models. Advances in Manufacturing, 5(4), 359–369. https://doi.org/10.1007/s40436-017-0198-1

[14] Tjahjono, B., Esplugues, C., Ares, E., & Pelaez, G. (2017). What does Industry 4.0 mean to Supply Chain? Procedia Manufacturing, 13, 1175–1182. https://doi.org/10.1016/j.promfg.2017.09.191

[15] Kagermann, V. H. (2014). Change Through Digitization—Value Creation in the Age of Industry 4.0. Management of Permanent Change, 23–45. https://doi.org/10.1007/978-3-658-05014-6_2

[16] Edirisuriya, A., Weerabahu, S., & Wickramarachchi, R. (2018). Applicability of Lean and Green Concepts in Logistics 4.0: A Systematic Review of Literature. 2018 International Conference on Production and Operations Management Society (POMS). https://doi.org/10.1109/poms.2018.8629443

[17] LI, F., Sijun, L., & Cui, Y. (2018). Logistics Planning and Its Applications for Engine Plant under 'Industry 4.0.' SAE Technical Paper Series. https://doi.org/10.4271/2018-01-1205

[18] Hofmann, E., & Rüsch, M. (2017). Industry 4.0 and the current status as well as future prospects on logistics. Computers in Industry, 89, 23–34. https://doi.org/10.1016/j.compind.2017.04.002

[19] Kayikci, Y. (2018). Sustainability impact of digitization in logistics. Procedia Manufacturing, 21, 782–789. https://doi.org/10.1016/j.promfg.2018.02.184

[20] Barreto, L., Amaral, A., & Pereira, T. (2017). Industry 4.0 implications in logistics: an overview. Procedia Manufacturing, 13, 1245–1252. https://doi.org/10.1016/j.promfg.2017.09.045

[21] Martin, J., May, S., Endres, S., & Cabanes, I. (2017). Decentralized Robot-Cloud Architecture for an Autonomous Transportation System in a Smart Factory. SEMANTICS Workshops.

[22] Lutz, M., Verbeek, C., & Schlegel, C. (2016). Towards a robot fleet for intra-logistic tasks: Combining free robot navigation with multi-robot coordination at bottlenecks. 2016 IEEE 21st International Conference on Emerging Technologies and Factory Automation (ETFA). https://doi.org/10.1109/etfa.2016.7733602

[23] Bechtsis, D., Tsolakis, N., Vouzas, M., & Vlachos, D. (2017). Industry 4.0: Sustainable material handling processes in industrial environments. Computer Aided Chemical Engineering, 2281–2286. https://doi.org/10.1016/b978-0-444-63965-3.50382-2

[24] Naidoo, N., Bright, G., & Stopforth, R. (2019). A Distributed Framework for Programming the Artificial Intelligence of Mobile Robots in Smart Manufacturing Systems. 2019 Southern African Universities Power Engineering Conference/Robotics and Mechatronics/Pattern Recognition Association of South Africa (SAUPEC/RobMech/PRASA). https://doi.org/10.1109/robomech.2019.8704788

[25] Hussnain, A., Ferrer, B. R., & Lastra, J. L. M. (2018). Towards the deployment of cloud robotics at factory shop floors: A prototype for smart material handling. 2018 IEEE Industrial Cyber-Physical Systems (ICPS). https://doi.org/10.1109/icphys.2018.8387635

[26] Zhou, W., Piramuthu, S., Chu, F., & Chu, C. (2017). RFID-enabled flexible warehousing. Decision Support Systems, 98, 99–112. https://doi.org/10.1016/j.dss.2017.05.002

[27] Zou, O., & Zhong, R. Y. (2018). Automatic Logistics in a Smart Factory using RFID-enabled AGVs. 2018 IEEE/ASME International Conference on Advanced Intelligent Mechatronics (AIM). https://doi.org/10.1109/aim.2018.8452349

[28] Mehami, J., Nawi, M., & Zhong, R. Y. (2018). Smart automated guided vehicles for manufacturing in the context of Industry 4.0. Procedia Manufacturing, 26, 1077–1086. https://doi.org/10.1016/j.promfg.2018.07.144

[29] Müller, C., Grunewald, M., & Spengler, T. S. (2016). Redundant configuration of automated flow lines based on "Industry 4.0"-technologies. Journal of Business Economics, 87(7), 877–898. https://doi.org/10.1007/s11573-016-0831-7

[30] Ghafoorpoor Yazdi, P., Azizi, A., & Hashemipour, M. (2019). A Hybrid Methodology for Validation of Optimization Solutions Effects on Manufacturing Sustainability with Time Study and Simulation Approach for SMEs. Sustainability, 11(5), 1454. https://doi.org/10.3390/su11051454

[31] Delfmann, W., Ten Hompel, M., Kersten, W., Schmidt, T., & Stölzle, W. (2018). Logistics as a science: Central research questions in the era of the fourth industrial revolution. Logistics Research, 11(9), 1–13. https://doi.org/doi:10.23773/2018_9

Separation of Water/Organic Mixtures Using Micro- and Nanostructured Membranes of Special Type of Wettability

F. R. Sultanov[1,2*], Ch. Daulbayev[1], B. Bakbolat[1], Z. A. Mansurov[1,2], A. A. Zhurintaeva[1], R. I. Gadilshina[2], A. B. Dugali[1]

***Abstract*—**Both hydrophilic-oleophobic and hydrophobic-oleophilic membranes were obtained by coating of the substrate of membranes, presented by stainless steel meshes with various dimensions of their openings, with a composition that forms the special type of their surface wettability via spray-coating method. The surface morphology of resulting membranes was studied using SEM, the type of their wettability was identified by measuring the contact angle between the surface of membrane and a drop of studied liquid (water or organic liquid) and efficiency of continuous separation of water and organic liquid was studied on self-assembled setup.

***Keywords*—**membrane, stainless steel mesh, oleophobicity, hydrophobicity, separation, water, organic liquids

I. INTRODUCTION

Separation of water and organic liquids is an important area not only in scientific view, but also in an economical, social, while influencing the state of the environment [1,2]. It is known that wastewater contaminated with organic pollutants, formed as a result of large-scale production of steels, aluminum, food, textiles, petrochemicals are the largest pollutant to date [3]. At the same time, the notorious oil spills on the surface of water carry both a huge environmental threat and a large loss of energy [4].

In recent years, the phenomenon of wettability of the surface in the separation of water and organic liquids started to play an important role. Wetability is an inherent property of a solid surface, which determines the phenomenon of wetting the surface upon contact with the liquid. In the synthesis process it is possible to obtain materials with a specific type of wettability (superhydrophobic, superhydrophilic, superoleophobic, superolephilic) by varying the structure and composition. In this case, surfaces for special purpose can be obtained by usual combination of these properties. Summarizing the literature data, materials for controlled separation of water and organic liquids depending on the type of their wettability can be divided into two broad groups: materials that remove organic liquids from a mixture of “organic liquid - water” (hydrophobic) and materials that remove water from a mixture of “water - organic liquid”.

Typically, mesh structures (metal or polymeric) are used as the basis for creation of micro-porous filters. Superhydrophobic and superolephilic membranes were obtained in [5, 6] by etching a metallic mesh in acids (monoalkylsulfonic) at which nano-flakes of lamellar crystals were formed as a result of self-assembly of alkylphosphonates. These membranes have shown high efficiency in the separation of water and organic liquids.

Polyurethane and melamine surfaces can be used as polymer networks, which are coated with a certain composition that forms the type of its wettability. In [7], the authors coated polyurethane membrane with polystyrene microspheres, which increased its degree of hydrophobicity and oleophilicity, thus making it possible to use it in the separation of water and organic liquids.

Metal meshes, such as stainless steel and copper meshes formed by metal fibers, can be used as semipermeable barriers with a porous structure. Due to their strong mechanical properties, their simplicity of production, excellent performance and adjustable pore size, metal mesh membranes have always been of great scientific interest. To achieve the desired separation efficiency of a mixture of oil and water, the metal mesh must have selective permeability to water or oil due to increased wettability. As a rule, membranes of a metal mesh with special wettability are obtained by forming a micro-nanostructure and modifying the surface of a metal mesh substrate, which can enhance the surface roughness and enhance its wetting [8].

Materials that remove organic liquids from the "water-organic liquid" mixture can be obtained by two methods: chemical modification of porous surface by substances with a specific wettability and creation of a porous structure of a material with a specific wettability. The aim of this research is focused on obtaining membranes of special type of their wettability by spray-coating the substrate of membrane with compositions, which form their type of wettability and study their water-organic liquid separation efficiencies. For creation of hydrophilic-oleophobic membranes the composition based on polydiallyldimethylammonium chloride (PDDA) with additions of nanostructured particles of SiO_2 was used and for hydrophobic-oleophilic membranes the composition based on polytetrafluoroethylene (PTFE) was used [9, 10].

II. EXPERIMENTAL

A. Synthesis of hydrophilic-oleophobic membranes based on PDDA with addition of nanostructured particles of SiO_2

To obtain a hydrophilic-oleophobic compound, silica particles (0.1 g) were dispersed in an aqueous PDDA solution (35 ml, 1 mg/ml) by ultrasonic treatment for 30 minutes. After creating a homogeneous dispersion of silicon dioxide particles in the PDDA solution, 8 ml of a 0.1 M solution of the ammonium salt of pentadecafluorooctanoic acid was added dropwise with constant stirring. When a

[1]Institute of Combustion Problems, Kazakhstan, Almaty
[2]al-Farabi Kazakh National University, Kazakhstan, Almaty
(e-mail: fail_23@bk.ru)

certain concentration of the ammonium salt of pentadecafluorooctanoic acid in the mixture was reached, a pulp precipitate was formed due to the coordination of the anions of the ammonium salt of pentadecafluorooctanoic acid with the quaternary amine groups of PDDA. The resulting precipitate was repeatedly washed with distilled water and dried at room temperature.

A certain amount of a dried compound based on PDDA, pentadecafluorooctanoic acid with the addition of particles of silicon dioxide was dissolved in ethanol (95%), after which the resulting mixture was applied to a substrate - a pre-cleaned metal mesh with specific openings sizes by spray-coating methods. The mesh coated with the compound was dried at room temperature for 2 hours until ethanol was completely evaporated, after which it was exposed to microwave air plasma (50 W) for one minute with the formation of polar hydrophilic groups on the membrane surface to enhance the hydrophilic-oleophobic effect.

B. Synthesis of hydrophobic-oleophilic membranes based on polytetrafluoroethylene

Teflon was selected to create a hydrophobic compound that is applied to the substrate of the membrane. A homogeneous emulsion containing Teflon - PFTE 30 wt. %, adhesive - PVA, 10 wt. %, dispersant - polyvinyl acetate, 8 wt. %, surfactant - sodium dodecylbenzenesulfonate, 2 wt. % and diluent - distilled water, 50 wt. % was prepared. The starting reagents were mixed in a proportional amount by stirring until the mixture was completely homogenized.

When applying a hydrophobic-oleophilic compound to a metal mesh by spraying, a spray gun was used. A mixture under pressure of 0.2 MPa sprayed with a thin film to the surface of the metal mesh.

Then, the samples were heated at 350 ° C in an electric furnace for 30 minutes for thermal decomposition of the adhesive and dispersion agent, after which a thin film of a hydrophobic-oleophilic reaction component remained on the surface.

C. Study of the efficiency of separation of water/organic liquids by obtained membranes

The efficiency of separation of water and organic liquids by the obtained hydrophilic-oleophobic membranes was studied on an assembled setup, which consisted of two fittings screwed into each other and glass tubes attached to them. The membrane with the size less than the internal diameter of the fittings was placed in the internal cavity of fitting, where it was tightly sealed. The fittings were tightened, thereby ensuring the tightness of the entire system to eliminate the slightest smudges (Figure 1).

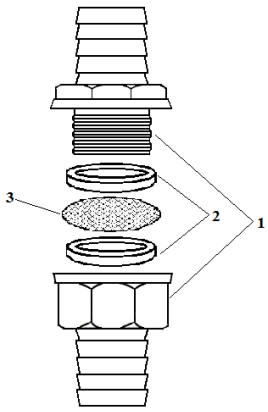

where 1 is fittings, 2 is rubber seals, 3 is obtained membrane

Figure 1 - Installation for determining the efficiency of separation of water and organic liquids obtained hydrophilic-oleophobic membranes

III. RESULTS AND DISCUSSION

Figure 2, which shows the surface morphology of the membrane based on a stainless steel mesh 200 coated with the PDDA/SiO_2 compound, shows that in this case the coating is uniform along all the wires that make up the grid framework. With an increase, it is seen that the PDDA/SiO_2 compound forms a large number of globules and protrusions, which can favorably affect the membrane oleophobicity.

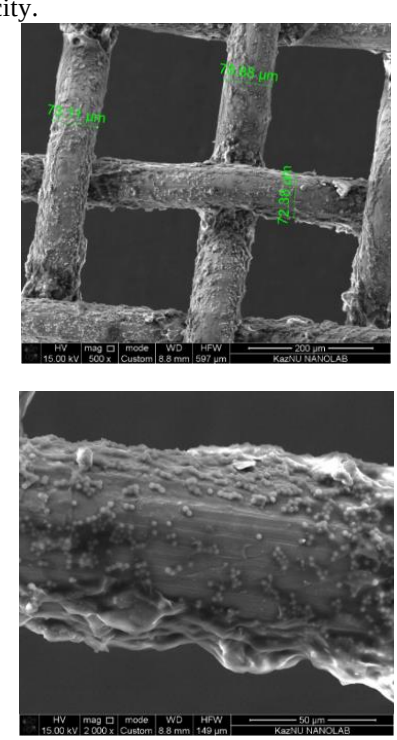

Figure 2 - SEM images of the surface of membranes based on a stainless steel mesh 200 coated with PDDA/SiO_2

Figure 3 presents SEM images of the surface of a membrane based on a stainless steel mesh 200 coated with a hydrophobic-oleophilic compound based on PFTE by spray-coating method. Figure shows that the hydrophobic-oleophilic compound is evenly distributed along the entire surface of the membrane substrate, some protrusions that reduce the actual size of the holes of the membrane base are

seen. The coating has globular formations, tightly adjacent to the surface of the wires of the membrane base.

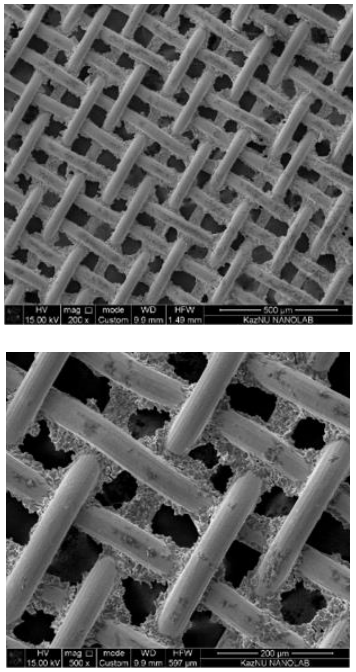

Figure 3 - SEM images of surface morphology of membranes based on stainless steel mesh 200 coated with PTFE

To determine the quality of the coating of the substrate with the developed compounds, the wetting angle of the surface of the obtained membrane with a drop of the studied liquid (water or organic liquid) was measured. For this, a drop of liquid was applied to the surface of the membrane, after which the contact angle between the drop and the surface of the membrane was measured (Figure 4).

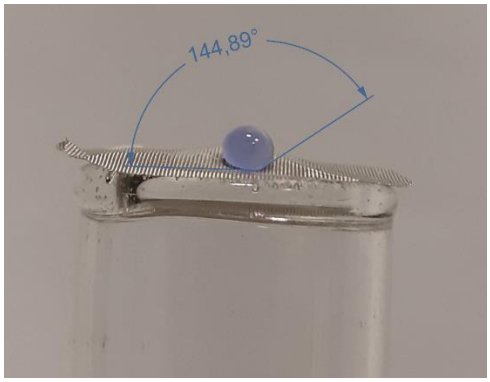

Figure 4 - The wetting angle of the membrane based on a stainless steel mesh 200 coated with PTFE

Table 1 presents data on the wetting angles of the synthesized membranes. The Table shows that membranes based on stainless steel meshes coated with PDDA/SiO_2 exhibit hydrophilic-oleophobic properties. The membrane based on the mesh 400, which has smaller dimensions of its openings than mesh 200, exhibits the greatest oleophobicity, the contact angle between its surface and a drop of organic liquid is 116 °, while water passes through it easily. On the other hand membranes coated with PTFE are hydrophobic, the wetting angles of their surfaces is up to 145°. At the same time, the synthesized membranes exhibit high oleophilicity, a drop of organic liquid does not stay on the membrane surface, passing through it.

Table I
Values of wetting angles of the synthesized membranes

Type of mesh	Membrane wetting angle depending on the coating composition, organic liquid / water, °	
	PDDA/SiO_2	PTFE
Stainless steel mesh 200	103/-	-/131
Stainless steel mesh 400	116/-	-/145

To study the process of separation of water and organic liquids using the obtained membranes the setup was assembled. The setup consists of two metal fittings into which glass tubes are tightly inserted (for visualization of the process of separation of water and organic liquids) with a diameter of 10 mm A membrane with a diameter of 10 mm is inserted into the cavity between the two fittings, where it is tightly fixed with rubber seals. As a result, a cavity with a diameter of 6-7 mm is formed, on the surface of which there is a contact of water and organic liquid with the membrane.

Figure 5 shows the process of separation of water and kerosene, dyed with a special dye for organic liquids "Sudan", by a hydrophilic-oleophobic membrane based on a mesh 400 coated with PDDA/SiO_2 compound. It can be seen from the figure that this membrane effectively transmits water (20 ml of water in 4-5 seconds), however, after complete passage of water, this membrane does not pass kerosene through its structure.

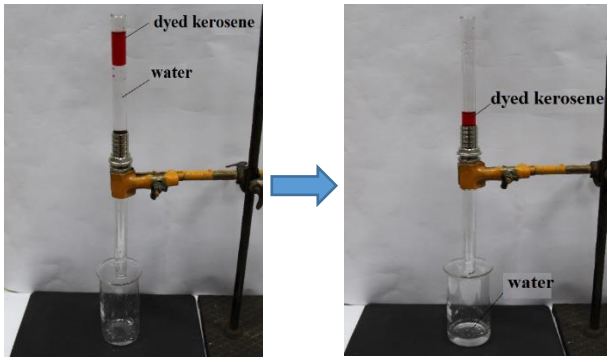

Figure 5- The process of gravitational separation of water and organic liquid using hydrophilic oleophobic membranes

In the case of chloroform, whose density is higher than water, it is clearly seen that it displaces water and sinks to the bottom of the system. Wetting the membrane chloroform passes through it at high speed due to its oleophilicity. After complete passage of chloroform through the membrane, it is clear that water repelled by its surface due to the formed hydrophobicity, not passing through the membrane (Figure 6).

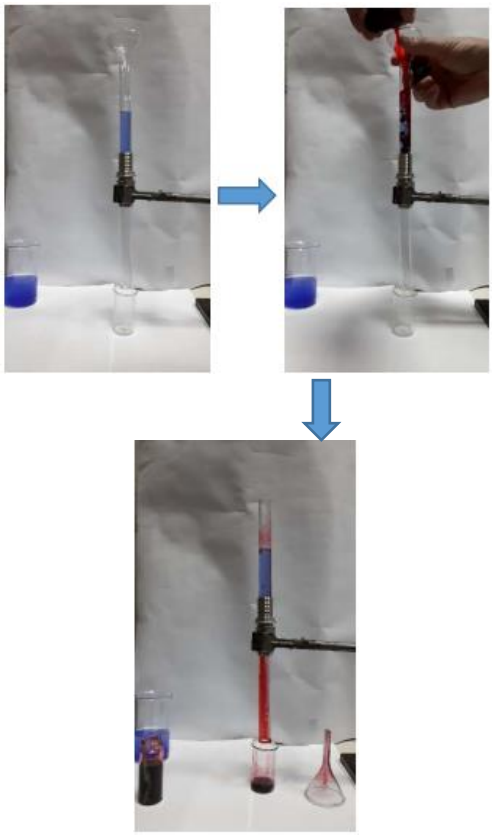

Figure 6 - Study of the efficiency of separation of chloroform and water by a hydrophobic oleophilic membrane based on a stainless steel mesh of grade 400, coated with PTFE

A mixture of water and organic liquid was fed from above through a glass tube into the assembled setup, after which the liquids decomposed in densities, i.e. water, having a higher density than that of an organic liquid, fell down, contacting and wetting the membrane. The efficiency of separation of water and organic liquids by membranes was determined by the rate of separation of measured volumes of liquids and the presence of organic liquid in the receiving tank after complete separation.

As a result of study the efficiencies of oil-organic liquid separation the following results were obtained: a membrane based on mesh 400 coated with PDDA/SiO_2 exhibits excellent hydrophilic properties, the flow rate of 20 ml of water is 4-5 seconds (as with a mesh-based membrane 200), however, this membrane does not pass through its structure kerosene. The passage of 10 ml of kerosene through the membrane was not observed within 40 minutes of pressure of a liquid column on its surface. At the same time, the passage rate of 10 ml of oil decreased to 20-21 minutes. A membrane based on stainless steel mesh 400 coated with PFTE exhibits a high degree of hydrophobicity. It was experimentally confirmed that it practically does not pass water, the waiting time was 2 hours, while the presence of water in the receiving tank was not visually observed. Moreover, this membrane exhibits oleophilicity - the passage rates of 10 ml of chloroform and kerosene were 90 and 50 seconds, respectively.

IV. CONCLUSION

The membranes of special type of wettability based on stainless steel meshes spray-coated with developed compositions were obtained. The surface morphology of membranes is presented by rough structure, with formed protrusions and pores influencing on their wetting properties. The efficiency of separation of organic liquids from mixture of water and organic liquids of hydrophilic and oleophobic membrane coated with PDDA/SiO_2 is following: the flow rate of 20 ml of water through the membrane is 4-5 seconds, while the passage of 10 ml of kerosene through the membrane was not observed within 40 minutes of pressure of a liquid column on its surface, the passage rate of 10 ml of oil decreased to 20-21 minutes. In case of hydrophobic and oleophilic membrane coated with PTFE the results of study of their oil/water separation efficiencies are following: it practically does not pass water, the waiting time was 2 hours, while the passage rates of 10 ml of chloroform and kerosene through it were 90 and 50 seconds, respectively. We believe that these materials are perspective candidates for complex and continuous separation of water and organic liquids.

ACKNOWLEDGMENT

Scientific results presented in this article were obtained in the framework of project #AP05131745 “Obtaining of micro and nanoporous membranes of special type of wettability for complex purification of water from organic pollutants and salts” with support of Ministry of Education and Science of Republic of Kazakhstan.

REFERENCES

1. Lin Feng, Zhongyi Zhang, Zhenhong Mai, Yongmei Ma, Biqian Liu, Lei Jiang, Daoben Zhu. A Super-Hydrophobic and Super-Oleophilic Coating Mesh Film for the Separation of Oil and Water // Angew. Chem. Int. Ed. –2004. –V. 43. –P.2012–2014
2. J. K. Yuan, X. Liu, O. Akbulut, J. Hu, S. L. Suib, J. Kong and F. Stellacci. Superwetting nanowire membranes for selective absorption // Nat. Nanotechnol. –2008. –V. 3. –P. 332-336
3. V. Singh, M.K.Purkait, C. Das. Cross flow Ultrafiltration of Industrial Oily Wastewater: Experimental and Theoretical Consideration // Sci Technol. –2011. –V. 46. –№8. –P. 1213-1223
4. Kammerer, M., Mastain, O., Le Deran-Quenech'du, S., Pouliquen, H., Larhantec-Verdier, M. Liver and kidney concentrations of vanadium in oiled seabirds after the Erika wreck // Science of the Total Environment. –2004. –V. 333. –№1-3. –P. 295-301.
5. M. Li, J. Xu and Q. Lu. Creating superhydrophobic surfaces with flowery structures on nickel substrates through a wet-chemical-process // Journal of Materials Chemistry. –2007. –V. 17. –P. 4772-4776
6. C. Wang, T. Yao, J. Wu, C. Ma, Z. Fan, Z. Wang, Y. Cheng, Q. Lin and B. Yang. Facile approach in fabricating superhydrophobic and superoleophilic surface for water and oil mixture separation // ACS Appl Mater Interfaces. –2009. –V. 1. –№11. –P. 2613-2617
7. J. Zhang, W. Huang and Y. Han. A Composite Polymer Film with both Superhydrophobicity and Superoleophilicity // Macromolecular Rapid Communications. –2006. –V.27. –P. 804-808
8. X. Yue, T. Zhang, D. Yang, F. Qiu, Z. Li, G. Wei, Y. Qiao. Ag nanoparticles coated cellulose membrane with high infrared reflection, breathability and antibacterial property for human thermal insulation // J. Colloid Interface Sci. –2019. –V. 535. –P. 363-370.
9. F.R. Sultanov, Ch. Daulbayev, B. Bakbolat, A. Zhurintayeva, O.Daulbayev and Z.A. Mansurov. Comparison of oil/water separating efficiency of oleophobic membranes based on fluorine containing and fluorine non-containing coatings // Rasayan J. Chem, 12 (3), 1091 - 1097 (2019)
10. F.R. Sultanov, Ch. Daulbayev, B. Bakbolat, Z.A. Mansurov. Separation efficiency of water/oil mixtures by hydrophilic and oleophobic membranes based on stainless steel meshes with openings of various sizes // Eurasian Chemico-Technological Journal. –2018. –V. 20, №3. –P. 195-200.

A Study on Weddernburn – Artin Theorem for Rings

Fahad Suleiman, Sammani Abdullahi

Department of Statistics, School of Science & Technology, Federal Polytechnic Kaura Namoda, Zamfara State – Nigeria (phone: +2348037346623, +2347068706358, e-mail: fssalai.stat@fedponam.edu.ng, dagasammaniabdullahi@gmail.com)

Abstract: The study depicts that a Wedderburn Artin – theorem for rings is considered to be a semisimple ring R which is isomorphic to a product of finitely many $m_i by m_i$ matrix rings over division rings D_i, for some integers n_i, both of which are uniquely determined up to permutation of the index *i*.

Keywords: Commutivity, matrix, ring, Wedderburn – Artin theorem.

1. INTRODUCTION

According to Ref. [1], the subject of determining structure of rings and algebras, over which all modules are direct sum of certain cyclic modules has a long a long history. Ref. [1] showed that every module over a finite dimensional K – algebra A is a direct sum of simple modules if and only if $A \cong \prod_{i=1}^{m} M_{n_i}(D_i)$ where $m, n_{1,\ldots\ldots,\in N}$ and each D_i is finite dimensional division algebra over k.

It has been observed from the study of [2] that the first Wedderburn Artin theorem has two parts one dealing with finite simple algebra. We let R be a ring with identity. The ring R is called left semisimple ring if the left R module is a semisimple module, i.e. if R is a direct sum of minimal left ideals. In this case $R = \oplus_{i \in S} I_i$.

Examples of semisimple rings were stated in [4] as:

i. If D is a division ring, then the ring $R = M_n(D)$ is left semisimple in the of the definition of Wedderburn Artin theorem. It revealed that R as a left R module is given by $M_n(D) \cong D^n \ldots \oplus D^n$, where each D^n is a simple left $M_n(D)$ module and the j^{th} summand D^n corresponds to the matrices whose only non – zero entries are in the j^{th} column. The left R module $M_n(D)$ has a composition series whose terms are partial sumsof the n summandsD^n.

ii. If $R_1, \ldots R_n$ are left semisimple rings, then the direct product $R \cong \prod_{i=1}^{n} R_i$. Each minimal left ideal of R_i, when included into R, is a minimal left ideal of R. Hence R is the sum of minimal left ideals and is left semisimple.

2. MAIN RESULT

The main result of this paper is given below

Theorem 2.1: If R is any left semisimple ring, then

$$R \cong M_{n_i}(D_1) \times \ldots \times M_{n_r}(D_r)$$

Where each D_i is a division ring and $M_n(D)$ denotes the ring of $n \times n$ matrices over D

Theorem 2.2: Let R be a finite dimensional algebra with identity over field F. If R is a semisimple ring, then R is a semisimple and hence is isomorphic to $M_n(D)$ for some integer $n \geq 1$ and some finite dimensional algebra D over F. the integer n is uniquely determined by R, and D is unique upto isomorphic.

In order to obtain our main result, we begin prove the above stated theorems.

Proof of theorem 2.1: By the work of [2] we write R as direct sum of minimal left ideals, and then regroup the summand according to their R isomorphic type as $R \cong \oplus_{j=1}^{r} n_j V_j$, where $n_i V_j$ is the direct sum of n_j submodules R isomorphic to V_j and where $V_i \ncong V_j$ for $i \neq j$. The isomorphison is one of unital left R modules. Now put $D_i^o = End_{R(V_i)}$. This is a division ring by Schur's Lemma as it was proved in [5] research.

Using proposition 10.14 of [2], we obtain an isomorphism of rings of rings

$$R^0 \cong End_R R \cong Hom_R\left(\oplus_{i=1}^{r} n_i V_i, \oplus_{j=1}^{r} n_j V_j\right) \qquad 2.1$$

Define a map $p_i: \oplus_{j=1}^{r} n_j V_j \to n_i V_i$ to be the i^{th} projection and $q_i: n_i V_i \to \oplus_{j=1}^{r} n_j V_j$ to be the i^{th} inclusion. Let us see that the right side of 2.1 is isomorphic as a ring to $\prod_i End_{R(n_i V_i)}$ via mapping $f \mapsto (p_1 f q_1, \ldots p_r f q_r)$. What is to be presented here is that $p_j f q_j = 0 for i \neq j$. Now $p_j f q_i$ is a member of $Hom_R\left(n_i V_i, n_j V_j\right)$.

Referring to (2.1) above, we therefore obtain

$$R^0 \cong \prod_{i=1}^{r} Hom_R\left(n_i V_i, n_j V_j\right) = \prod_{i=1}^{r} End_{R(n_i V_i)}$$

$\cong \prod_{i=1}^{r} M_{n_i}\left(End_{R(V_i)}\right)$ by corollary 10.13 of [3]

$\cong \prod_{i=1}^{r} M_{n_i}(D_i^o)$ by definition of D_i^o

Reversing the order of multiplication in R^0 and using transpose map to reverse the order of multiplication in each $M_{n_i}(D_i^o)$, we conclude that $R \cong \prod_{i=1}^{r} M_{n_i}(D_i)$. This proves the existence of the decomposition in the given theorem of the main result. We still need to identify the simple left R module and prove its an appropriate unique statement as contained in [2]. In example (i) above, we have decomposition $M_n(D_i) \cong D_i^{n_1} \ldots \oplus D_i^{n_i}$ of left $M_{n_i}(D_i)$ modules, and each term $D_i^{n_i}$ is a simple left $M_{n_i}(D_i)$ module. The decomposition proved allows the researchers to regard each term $D_i^{n_i}$ as simple left R module, $1 \leq i \leq r$. Each of these modules is acted upon by a different coordinate of R, and hence we have projected at least r non – isomorphic simple left R modules as in [3]. The researcher added that any simple R module must be a quotient of R by a maximal left ideal, as we observed in example (ii) hence a composition factor as consequences of the Jordan – Holder theorem in [6]. There are only r non - isomorphic such $V_{j's}$, and we conclude that the number of simple left R modules, up to isomorphism, is exactly r.

For uniqueness, we consider [3] which opined that supposed that $R \cong M_{n_1'}(D_i) \times \ldots \times M_{n_s'}(D_s)$ as rings. Let $V_j' = \left(D_j'\right)^{n_j'}$ be the unique simple left $M_{n_j'}\left(D_j'\right)$ module up to isomorphison, and regard V_j' as a simple left R module. Then we have $R \cong \oplus_{j=1}^{s} n_j' V_j'$ as left R modules. By the Jordan Holder Theorem, we must have r=s and, after a suitable numbering, $n_i = n_i'$ and $V_i \cong V_i'$ for $1 \leq i \leq r \leq$. Thus we have ring isomorphison

$$\left(D_j'\right)^0 \cong End_{M_{n_i'}(D_i')} \quad \text{by lemma 2.1 of [3]}$$

$$\cong End_{R(V_i')}$$

$$\cong End_{R(V_i)} \quad \text{since } V_i \cong V_i'$$

$$\cong D_i^0$$

Reversing the order of multiplication gives $D_i' \cong D_i$, and hence proved.

Proof of theorem 2.2: from the work of [2] and by finite dimensionality, R has a minimal left ideal V. For r in R, form the set Vr . This is a left ideal, and we claim that it is minimal or is 0. In fact, the function $v \to vr$ is R linear from V onto Vr . Since V is simple as a left R module, Vr is simple or 0. The sum $I = \sum_r \; withr \neq 0\, Vr$ is a two-sided ideal in R, and it is not 0 because $V1 \neq 0$. Since R is simple, $I = R$. Then the left R module R is exhibited as the sum of simple left R modules and is therefore semisimple. The isomorphism with $M_n(D)$ and the uniqueness now follow from Theorem 2.1 above.

3. CONCLUSION

The prove yield a very good main result in which it shows that a ring R with unity is semisimple, or left semisimple to be precise, if the free left R-module underlying R is a sum of simple R-module. In his short prove of Wedderburn's theorem, [7] states that when R is simple the Wedderburn – Artin theorem is known as Wedderburn's theorem.

REFERENCES

[1] Behhoodi, M., Daneshvar, A. & Vedadi, M.R. (2016). Two Generalizations of the Wedderburn-Artin Theorem with Applications. *Algebras and Representation Theory*, Vo. 21 No.1, pp 1 – 18.

[2] Knapp, A.W. (2016). Advanced Algebra. New York: East Setauket

[3] Jacobson, Nathan (1989), Basic algebra II (2nd ed.), W. H. Freeman, Lam,

[4] Tsit-Yuen (2001), A First Course in Noncommutative Rings (2nd ed.), Berlin, New York: Springer-Verlag, doi:10.1007/978-1-4419-8616-0,

[5] Kostov, V.P. (1995). A Generalization of the Burnside Theorem and Of Schur's Lemma For Reducible Representations. *Journal of Dynamical and Control Systems*, Vol. 1 No. 4, Pp 551 – 580. DOI: 10.1007/s10468-017-9748-2

[6] Natale, S. (2015). Jordan-Holder Theorem for Finite Dimensional ¨ Hopf Algebras. *Proceedings Of The American Mathematical Society, Vol. 143 No. 12.* Pp 5195 – 5211.

[7] Nicholson, W.K. (1993). A Short Proof of the Wedderburn Artin Theorem. *New Zealand Journal of Mathematics*, Vo. 22 No. 1. Pp 83 – 86.

Crystallized Colored Towels Obtained by Special Coloration of Yarns

Hasan Eskin, Gizem Özmen, A. Nazmi Çeler

***Abstract*—**When we examine the home textile development process, it follows a parallel line with the other textile products especially in the garment fabrics in terms of raw materials, production technologies and pattern characteristics. As a result, the expectations of people regarding textile, comfort, pattern (texture) and color properties are increasing. One of the places where comfort is most sought after is bath, pool, sea and baths. In addition to the material and technique that make up the physical structure in woven fabrics, color has an impressive importance with its strong effects. Color is the most prominent element in the fabric and the color and texture are visually reinforcing.

Evaluation of color in fabric is a personal phenomenon. Factors that determine color determination in fabric are the amount of color used, color ratio and its relationship with other colors.

In this project; Considering the effect of color dimensions on human, we are talking about the crystallized colored towel that we developed in terms of comfort and texture properties.

The basis of the effect created in the towel; It is formed by bending the yarn from its own special blend and the harmonious appearance of the natural crystallized rainbow colors with the pattern effect it determines on the warp yarns by using the weft yarns in the weaving. In addition, by using different weaving techniques and colors, alternatives can be created and personalized patterns can be created. One side of the towel determines the properties related to color, while the pile part determines the comfort characteristics with its soft touch and water absorbency.

***Keywords*—**Color effect, comfort, towel, weaving technique.

Hasan Eskin is with Denizli Rateks Tekstil, Turkey (e-mail: hasaneskin@goldstarteks.com).

Conducting Polymer Composites for the Adsorption and Reduction of Toxic Hexavalent Chromium in Water

N. H. Kera, M. Bhaumik, K. Pillay, S. S. Ray, A. Maity

***Abstract*—**Electroplating, mining, textile, tanning and other industries produce wastewater containing high concentrations of toxic hexavalent chromium, Cr(VI). The release of Cr(VI) into water sources is a serious concern due to its high toxicity to humans and animals and high mobility in the environment. Therefore, industrial wastewater must be treated prior to discharge into the environment to ensure Cr(VI) levels are well below the maximum allowable limits prescribed by water quality standards.

Conducting polymers such as polypyrrole (PPy) and polyaniline (PANI) have been widely studied as adsorbents for Cr(VI) removal from water due to their ion-exchange properties and inherent ability to reduce Cr(VI) to less toxic, Cr(III). In this study, conducting polymers were modified by incorporating suitable dopants and magnetic nanoparticles to improve their Cr(VI) adsorption capacity and impart other properties important for water treatment applications. Polypyrrole/2,5-diaminobenzenesulfonic acid (PPy/DABSA) composite and magnetic polypyrrole-polyaniline/iron oxide (PPy-PANI/Fe_3O_4) nanocomposite, were synthesized

The conducting polymer composites were synthesized by using a simple and effective method, namely, *in situ* chemical oxidative polymerization with $FeCl_3$ as an oxidant. PPy/DABSA was synthesized with pyrrole monomer in the presence of 2,5-diaminobenzenesulfonic acid dopant and PPy-PANI/Fe_3O_4 nanocomposite was synthesized from pyrrole and aniline monomers with Fe_3O_4 nanoparticles present.

Field emission scanning electron microscopy (FE-SEM) and high resolution transmission electron microscopy (HR-TEM) analyses showed that PPy/DABSA composite and PPy-PANI/Fe_3O_4 nanocomposite consisted of agglomerations of roughly spherical particles similar to that observed for PPy. The specific surface areas of PPy/DABSA composite and PPy-PANI/Fe_3O_4 nanocomposite were found to be 22 m^2/g and 57 m^2/g, respectively, from BET surface area studies.

Batch adsorption studies were conducted to investigate Cr(VI) removal from water by the conducting polymer composites. Cr(VI) removal by PPy/DABSA composite and PPy-PANI/Fe_3O_4 nanocomposite was found to be strongly dependant on pH and maximum removal was achieved when the initial solution pH was 2. EDX analyses confirmed adsorption of Cr(VI) while XPS analyses and IC-ICP-MS analyses (carried out in some studies) confirmed that some of the adsorbed Cr(VI) was reduced to Cr(III). The mechanism of Cr(VI) removal by PPy/DABSA composite at pH 2 (**Figure 1**) was proposed to involve the adsorption of Cr(VI) anions by protonated amino groups present in the composite. In the case of PPy-PANI/Fe_3O_4 nanocomposite, it was suggested that Cr(VI) was adsorbed through ion exchange with dopant Cl^- ions in the structure of the PPy-PANI/Fe_3O_4 nanocomposite. In both cases, for initial solution pH 2, it was suggested that some of the adsorbed Cr(VI) was reduced to Cr(III) by the electron-rich conducting polymers.

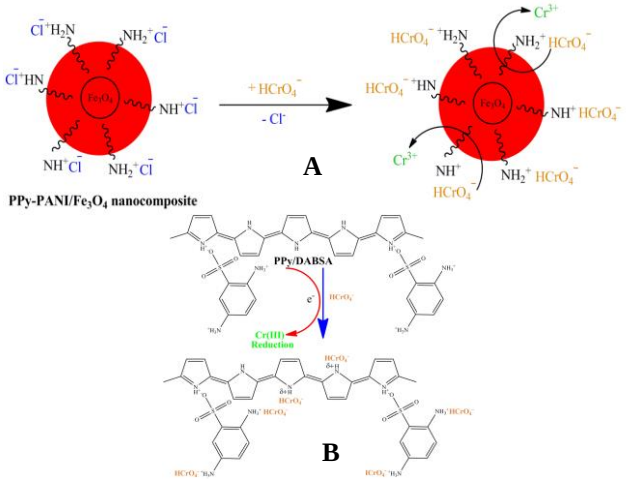

Figure 1 Proposed mechanisms of Cr(VI) removal by (A) PPy-PANI/Fe_3O_4 nanocomposite and (B) PPy/DABSA composite.

It was determined from the effect of dose studies that the optimum mass of adsorbent required for the treatment of Cr(VI) solution of 100 mg/L concentration was 1 g/L for both PPy/DABSA composite and PPy-PANI/Fe_3O_4 nanocomposite. The maximum adsorption capacities of both PPy/DABSA composite and PPy-PANI/Fe_3O_4 nanocomposite were calculated to be 303 mg/g (for initial solution pH 2) by fitting the adsorption isotherm data obtained to the linear form of the Langmuir models.

PPy/DABSA composite and PPy-PANI/Fe_3O_4 nanocomposite were found to be highly selective for the removal of Cr(VI) from aqueous solution when selected cations (Cu^{2+}, $Zn^{2+}$and Ni^{2+}) and anions (Cl^-, NO_3^- and SO_4^{2-}) were co-existing in the aqueous solution.

Desorption studies showed that PPy/DABSA composite and PPy-PANI/Fe_3O_4 nanocomposite could be used for three adsorption cycles without any loss in Cr(VI) removal efficiency.

In this study, the modification of PPy with compounds containing amino functional groups, namely DABSA resulted in PPy composites with high adsorption capacities for Cr(VI). The modification of PPy-PANI polymer with magnetic Fe_3O_4 nanoparticles improved its Cr(VI) adsorption capacity and the resulting composite had magnetic properties which could simplify recovery of the adsorbent from water after treatment. The conducting polymer based adsorbents also showed high selectivity for Cr(VI) removal from aqueous solution.

Conducting polymer composites were therefore shown to be promising adsorbents for the treatment of Cr(VI) wastewater.

***Keywords*—**Adsorption, hexavalent chromium, polyaniline, polypyrrole, reduction.

N. H. Kera is with the Department of Chemical Sciences, University of Johannesburg, Johannesburg, South Africa (phone: 012-842-7839; e-mail: nazia.kera@gmail.com).

M. Bhaumik is with the Department of Chemical Sciences, University of Johannesburg, Johannesburg, South Africa (phone: 012-842-7839; e-mail: bhaumikmadhu@gmail.com).

K. Pillay is with the Department of Chemical Sciences, University of Johannesburg, Johannesburg, South Africa (phone: 011-559-6128; e-mail: kriveshinip@uj.ac.za).

S. S. Ray is with the DST-CSIR National Centre for Nanostructured Materials, Council for Scientific and Industrial Research, South Africa (phone: 012-841-2388; fax: 012-841-2135; e-mail: RSuprakas@csir.co.za).

A. Maity is with the DST-CSIR National Centre for Nanostructured Materials, Council for Scientific and Industrial Research, South Africa (phone: 012-841-2658; fax: 012-841-3553; e-mail: AMaity@csir.co.za).

Atomic Hydrogen Storage in Hexagonal GdNi5 and GdNi4Cu Rare Earth Compounds: A Comparative DFT Study

A. Kellou, L. Rouaiguia, L. Rabahi

***Abstract*—**In the present work, the atomic hydrogen absorption trend in the GdNi5 and GdNi4Cu rare earth compounds within the hexagonal CaCu5 type of crystal structure (space group P6/mmm) is investigated. The density functional theory (DFT) combined with the generalized gradient approximation (GGA) is used to study the site preference of atomic hydrogen at 0K. The octahedral and tetrahedral interstitial sites are considered. The formation energies and structural properties are determined in order to evaluate hydrogen effects on the stability of the studied compounds. The energetic diagram of hydrogen storage is established and compared in GdNi5 and GdNi4Cu. The magnetic properties of the selected compounds are determined using spin polarized calculations. The obtained results are discussed with and without hydrogen addition taking into account available theoretical and experimental results.

***Keywords*—**Density Functional Theory, Hydrogen storage, Rare earth compounds, Structural and magnetic properties.

A. Kellou is with University of Science and Technology Houari Boumediene (USTHB), Algeria (e-mail: afkellou@usthb.dz).

Experimental Investigation on Effect of Different Heat Treatments on Phase Transformation and Superelasticity of NiTi Alloy

Erfan Asghari Fesaghandis, Reza Ghaffari Adli, Abbas Kianvash, Hossein Aghajani, Homa Homaie

Abstract—NiTi alloys possess magnificent superelastic, shape memory, high strength and biocompatible properties. For simproving mechanical properties, foremost, superelasticity behavior, heat treatment process is carried out. In this paper, two different heat treatment methods were undertaken: (1) solid solution, and (2) aging. The effect of each treatment in a constant time is investigated. Five samples were prepared to study the structure and optimize mechanical properties under different time and temperature. For measuring the upper plateau stress, lower plateau stress and residual strain, tensile test is carried out. The samples were aged at two different temperatures to see difference between aging temperatures. The sample aged at 500 °C has a bigger crystallite size and lower amount of Ni which causes the mentioned sample to possess poor pseudo elasticity behaviour than the other aged sample. The sample aged at 460 °C has shown remarkable superelastic properties. The mentioned sample's higher plateau is 580 MPa with the lowest residual strain (0.17%) while other samples have possessed higher residual strains. X-ray diffraction was used to investigate the produced phases.

Keywords—Heat treatment, phase transformation, superelasticity, NiTi alloy.

I. Introduction

TECHNOLOGY and new era's necessities, pulls humans to use new materials and systems. Shape memory alloys are one of those mentioned systems to assign a big importance in the world of technology [1]. The "pseudo elasticity" behavior of shape memory alloys (SMAs), which is well known as "super elasticity", is the reversible reaction of these materials against the applied stress [2], [3]. Super elastic materials, recover their initial shape with or without a thermal process, which is named as shape memory effect (SME) [4]-[6]. The mentioned effect is related to the reversible transformation between two crystalline phases named austenite and detwinned martensite [7], [8] and it has been a real concern in different experiences [9], [10].

NiTi SMAs has attracted a lot of attention lately because of all its special applications in human body implants and joints, stents, sensors, elevators [11]-[13]. Also, the structure of NiTi alloys helps the body cells and tissues to grow [14]. Heat treatment of these alloys affects the mechanical properties by producing precipitations such as Ti_3Ni_4, $Ni_{14}Ti_{11}$, etc. [15]-[17]. These small sized and distributed precipitations in the main phase of NiTi make barriers against slipping of dislocations and achieving to super elastic properties. Also the mentioned precipitation could modify the phase deformation temperature which is an important factor on the mechanical properties [18]-[20]. Liu and McCromics [21] showed that NiTi samples were fractured at a strain of 8%. Also, ultimate tensile strength of the samples is 300 MPa. Sadrnezhad et al. study, on SME of Nitinol, has increased the Ms temperature which could be effective on fatigue life [22]-[24].

Due to biocompatibility, excellent mechanical properties such as high ultimate tensile strength and a long fatigue life, unique shape memory, effect and twinning mechanism [25], there is a wide range of NiTi and other SMA applications. So there is a necessity to enhance its mechanical properties, to grow them better than before, which could be obtained via heat-treatment techniques [26], [27]. Also, Paryab et al. showed that temperatures of selected treatment could even affect properties such as pseudo elasticity [35]. Using other cycles such as two step cycles or just annealing cycles may cause a shorter fatigue life or fraction of sample in tensile testing in a low strain amount [28]. As an example of thermal treatments to nitinol wires, shape setting operations also could be mentioned. Normally, shape setting operations occurs in a specific shape of the sample, for a specific temperature [29]. This paper reports an optimized heat treatment to improve the mechanical properties, such as martensitic transformation temperature which is directly in contact with super elasticity behavior [30]. Also, the effects of heat treatment on mechanical properties and shape memory behavior are investigated by scanning electron microscope (SEM), Energy Dispersive X-ray Spectroscopy (EDS), X-ray Diffraction (XRD), tensile test and differential scanning calorimetry (DSC).

II. Experimental

The chemical composition of NiTi SMA was determined by EDS with an EDAX Element Silicon drift 2017 machine. Also, microstructure of the samples was studied by SEM, FEI Quanta 200 ESEM machine. Phase studies were conducted by XRD, PW1730 device. The crystallite size and lattice parameter were calculated via Williamson-Hall equations [31]. Quantity of the phases and lattice parameter were obtained by High Score software. Also, lattice parameter was calculated by Bragg's law through the following equations [32]:

$$b\cos\Theta = (0.9\,\lambda)/d + 2\eta\sin\Theta \quad \text{(Williamson-hall equation)}$$

$$n\lambda = 2d\sin\Theta \quad \text{(Bragg's law)}$$

Erfan Asghari Fesaghandis is MSc student, Reza Ghaffari Adli is MSc educated, Abbas Kianvash is Professor, and Homa Homaie is BSc educated of Department of Materials Engineering, University of Tabriz, Tabriz, Iran (e-mail: erfan.asgharioskui1997@gmail.com, rghaffari2012@gmail.com, akianvash@tabrizu.ac.ir, homahmh97@gmail.com)

Hossein Aghajani is Associate professor of Department of Materials Engineering, University of Tabriz, Tabriz, Iran (corresponding author, e-mail: h_aghajani@tabrizu.ac.ir)

$$a = d\sqrt{(h^2+k^2+l^2)}$$

In Williamson-hall equation, b is the width of a peak at its half intensity obtained from the Expert software, Θ is the angle of the peak at the pattern, **λ** is the wavelength of X-ray, η is the lattice strain and a is the lattice parameter [33]. Tensile test was carried at room temperature. In the first step, samples were elongated and when reached to 6% strain, after one second, the stress was removed and they returned to their initial state. In tensile test which was carried out by ETM-200/300KN High Speed universal tester, hysteresis diagrams were obtained. Also re-crystallization and transformation temperatures were analyzed by DSC under nitrogen atmosphere. NiTi alloy used in this process was a commercial alloy with nominal composition of 49%Ti-51%Ni. Effects of heat-treatment cycles and their parameters such as time and temperature of aging and annealing and cooling rate on the microstructure and mechanical properties were investigated. It is also necessary to remind that high amount of titanium could result a high risk of oxidation of NiTi samples at high temperatures [34]. To avoid this destructive issue, a controlled atmosphere furnace with a 200 ml/min argon flow was used. NiTi Specimen was purchased from G&H Orthodontics, Earlywood, Franklin, USA as an arch wire. The diameter of the specimen was 0.5 millimeter. For carrying out the tensile test, they were cut into samples with a length of 10 centimeters. The specifications of each cycle are presented in Table I.

TABLE I
PERFORMED HEAT TREATMENT (TIME AND TEMPERATURE)

	Annealing		Aging	
cycle	Time (min)	temperature (◦C)	Time (min)	temperature (◦C)
1	60	850	-	-
2	60	850	30	500
3	-	-	60	500
4	-	-	17	460

In the cycle.1 the sample was just annealed to determine the effects of anneal treatment on the mechanical properties and also microstructure of sample. It is also necessary to say that the applied temperature of annealing is used for cycle.2 samples. In the cycle.2, after quenching of the sample in the water, aging treatment was performed. Among the multi-step cycles, cycle 2 was the optimum cycle which was selected after testing different temperatures. The cycle.3 is just a one-step cycle which has a bigger hysteresis diagram with better pseudo elasticity effect and SME. Cycle.4 is the optimum cycle. It has the biggest hysteresis diagram with the minimum amount of residual strain. After the tensile test, the samples were electro-polished to have a clear surface and then electro-etched to reveal their microstructure under optical microscope. Chemical etch solutions may solve the cold mount material, thus, electro-polishing is the best way to achieve a clear surface of the samples. Intended electro-polish solution contains 5% perchloric acid, 25% glycerin in the main phase of ethanol for 30 seconds and voltage of 20 volts with current of 0.7 A of electricity.

III. RESULTS AND DISCUSSION

A. Characterization

Figs. 1 and 2 indicate the SEM results of the materials in which (a) and (b) are related to the raw sample, (c) and (d) for sample aged at 460 ℃. Figs. 2 (a) and (b) are for sample aged at 500 ℃, (c) and (d) for samples solution treated at 850 ℃ and aged at 500 ℃, (e) and (f) for solution treated at 850 ℃. In these figures some oxide inclusions as well as porosity could be seen in the microstructure. In Figs. 1 (c), (d) and 2 (a) and (b) the precipitations are detected which can cause an incomparable super elasticity behaviour. As it can be seen in the mentioned figures, precipitations get larger by increasing the aging temperature. In Figs. 2 (a) and (b) precipitations are bigger than Figs. 1 (c) and (d), which is related to the time and temperature of aging treatments. Also, bigger size of precipitations could have a negative effect on mechanical properties. Samples aged at high temperatures, may have high amount of residual strain, which may cause a short fatigue life.

The precipitations consist of two kinds: Ni rich and Ti rich. Here, the formed precipitation is Ni_4Ti_3. Precipitations of aged samples which could be seen in SEM images are the reason of low residual strain and remarkable tensile stress. Oxide inclusions are detected in all images but at images related to annealed samples there are more oxide inclusions which may cause fraction even at low amount of loads. In Figs. 2 (c)-(f), grains have become so small. Small grains of NiTi samples affect the mechanical properties of the samples by decreasing tensile stress and increasing residual strain.

B. Phase Analysis and Chemical Compositions

EDS is carried out to measure the amount of the elements in each sample. Moreover, the composition of the samples is calculated via the atomic amount of the elements. These measurements are shown in Table II. Main phase in NiTi samples is austenite. However, by applying heat treatment cycles, the other unwanted phases, such as Ni_3Ti, could be removed. These phases cause a decrease in A_f (Austenite finish temperature). To utilize shape memory behavior of the alloy, A_f temperature has to be under 25 °C. So, if the mentioned phases are not removed, instead of detwinning mechanism, transfiguration of the samples will be affected from slip of boundaries and residual strain will not be returnable, therefore, the samples will not be able to return to their first state. It can be figured out by applying solution treatment that amount of “Ti” precipitations increases. The EDX spectra are indicated in Fig. 3. It can be concluded that the sample “aged at 460 °C” has the same amount of Ni and Ti.

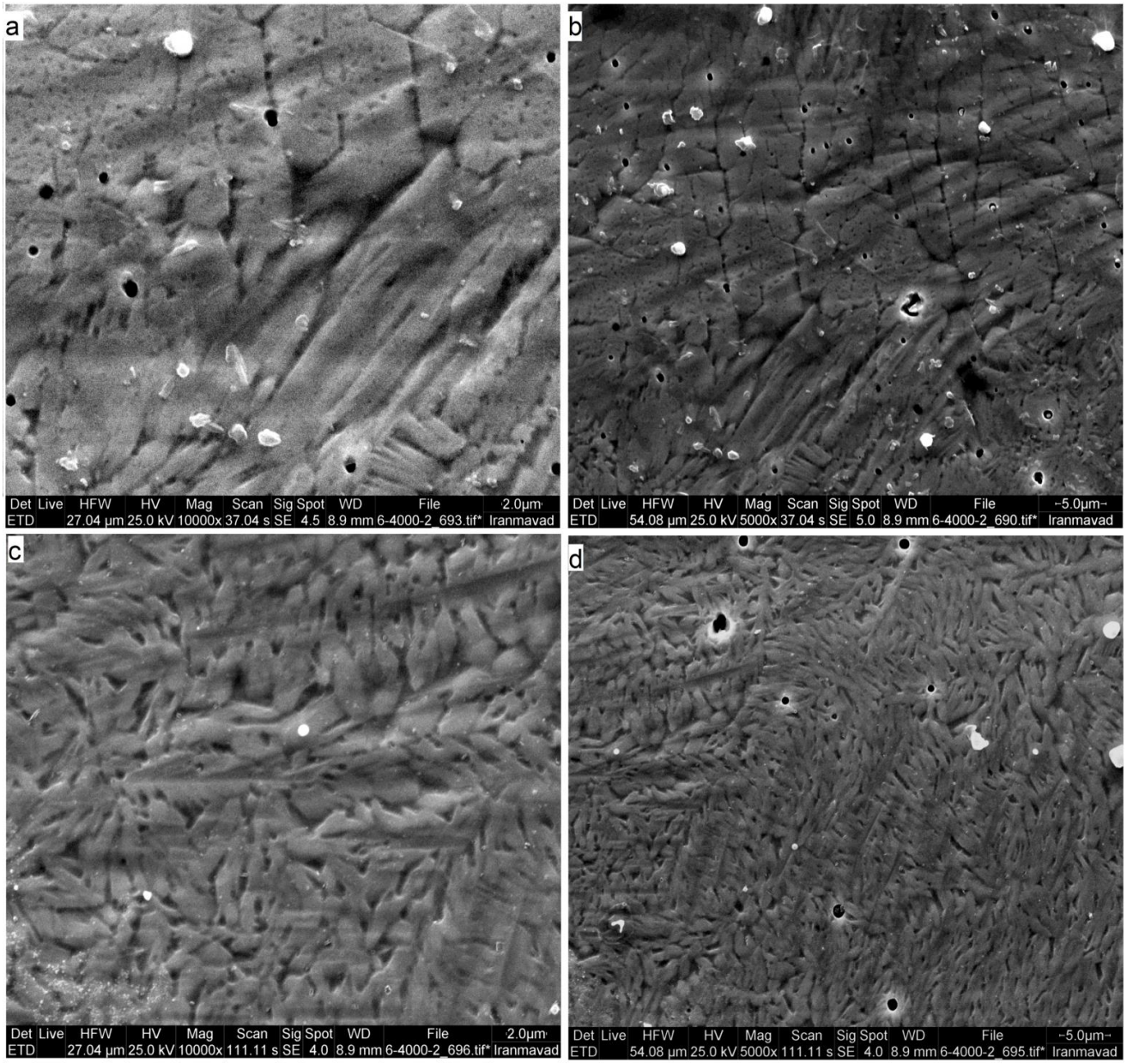

Fig. 1 SEM images of the etched samples in two magnifications: 5000X and 10000X (a) and (b) for raw sample, (c) and (d) for sample aged at 460 ℃

TABLE II
COMPOSITION, AND ATOMIC AND WEIGHT PERCENTAGES OF THE SAMPLES ACCORDING TO THE EDX SPECTRA

Sample	Atomic% of Ni	Atomic% of Ti	Weight% of Ni	Weight% of Ti	Element% of Ni in Map	Element% of Ti in Map	Composition
Raw	48.91	51.09	59.99	46.01	41	59	$Ni_{0.49}Ti_{0.51}$
Aged at 460	49.32	50.68	54.39	45.61	41	59	$Ni_{0.49}Ti_{0.51}$
Aged at 500	48.17	51.83	53.26	46.74	42	58	$Ni_{0.48}Ti_{0.52}$
Solution treated at 850 ℃	5.61	94.39	6.79	93.21	42	58	$Ni_{0.05}Ti_{0.95}$
Solution treated at 850 ℃ and aged at 500 ℃	65.19	34.81	69.65	30.35	41	59	$Ni_{0.65}Ti_{0.35}$

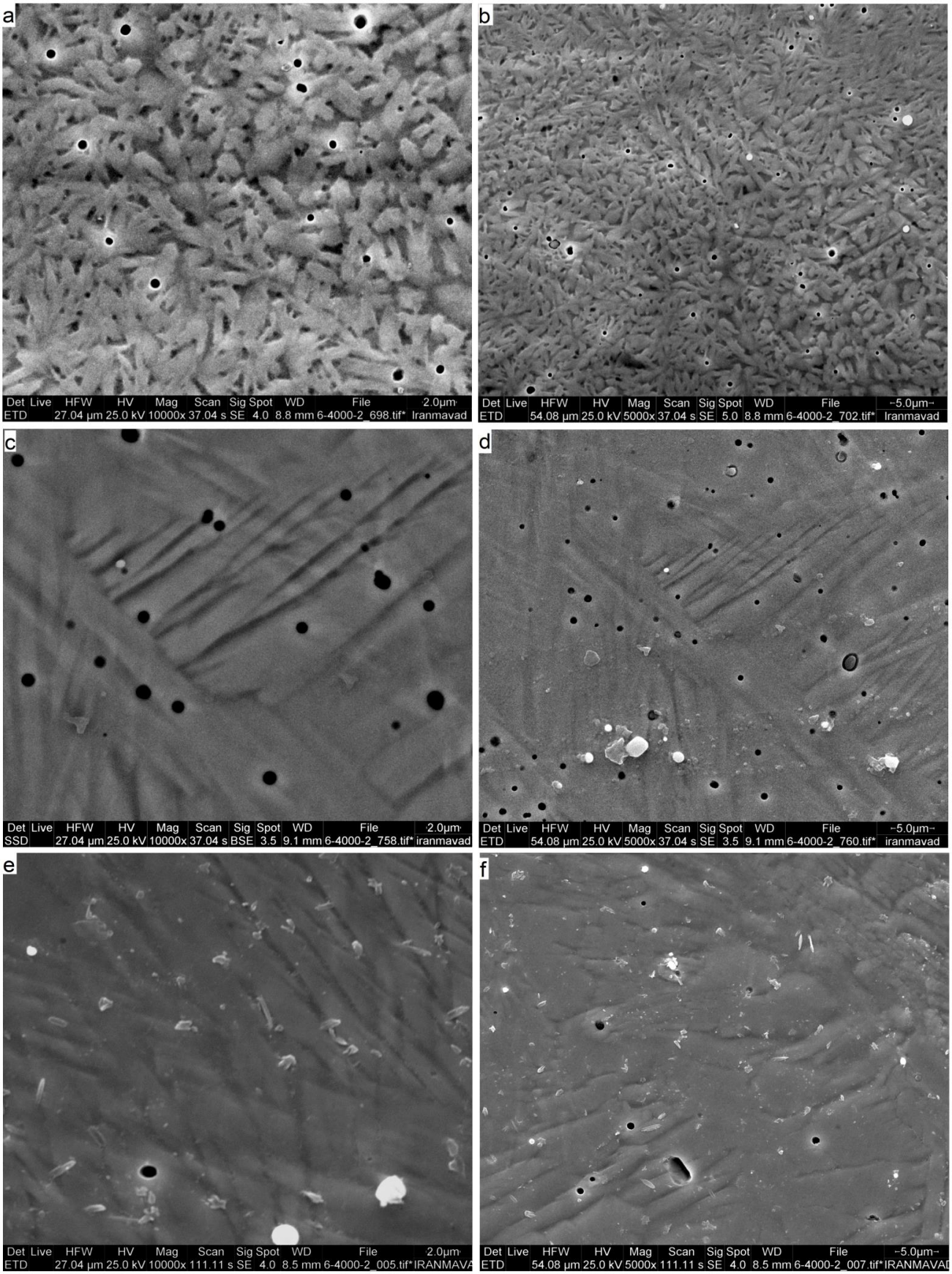

Fig. 2 FESEM images in two magnification of (a) and (b) sample aged at 500 ℃, (c) and (d) sample solution treated at 850 ℃, and (e) and (f) sample solution treated at 850 ℃ then aged at 500 ℃

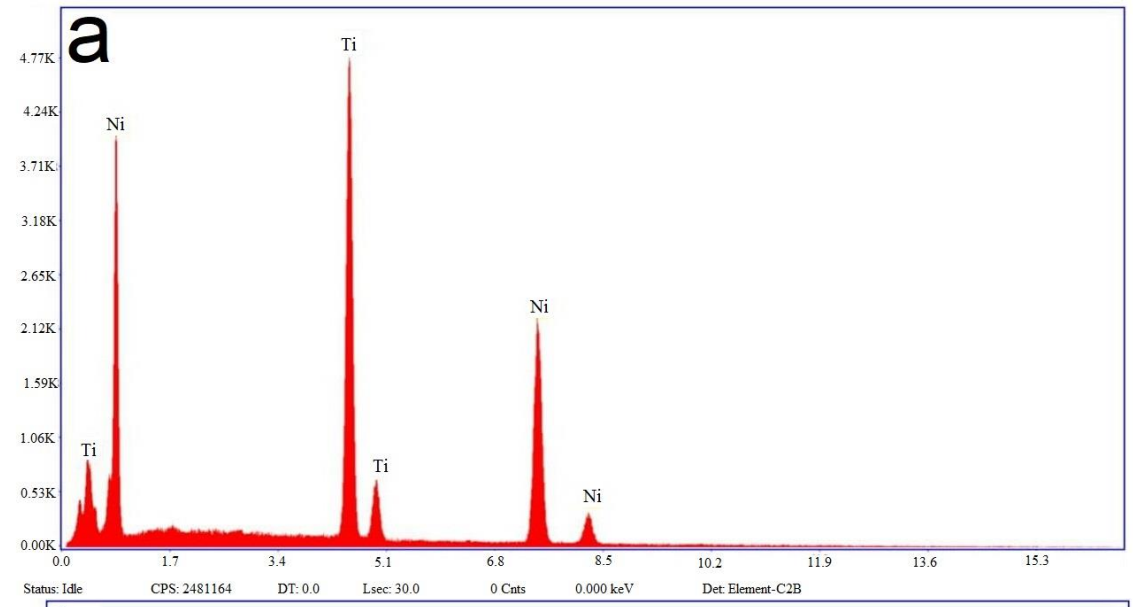
a
Ti
Ni
Ti
Ni
Ti
Ni
4.77K
4.24K
3.71K
3.18K
2.65K
2.12K
1.59K
1.06K
0.53K
0.00K
0.0
1.7
3.4
5.1
6.8
8.5
10.2
11.9
13.6
15.3
Status: Idle
CPS: 2481164
DT: 0.0
Lsec: 30.0
0 Cnts
0.000 keV
Det: Element-C2B

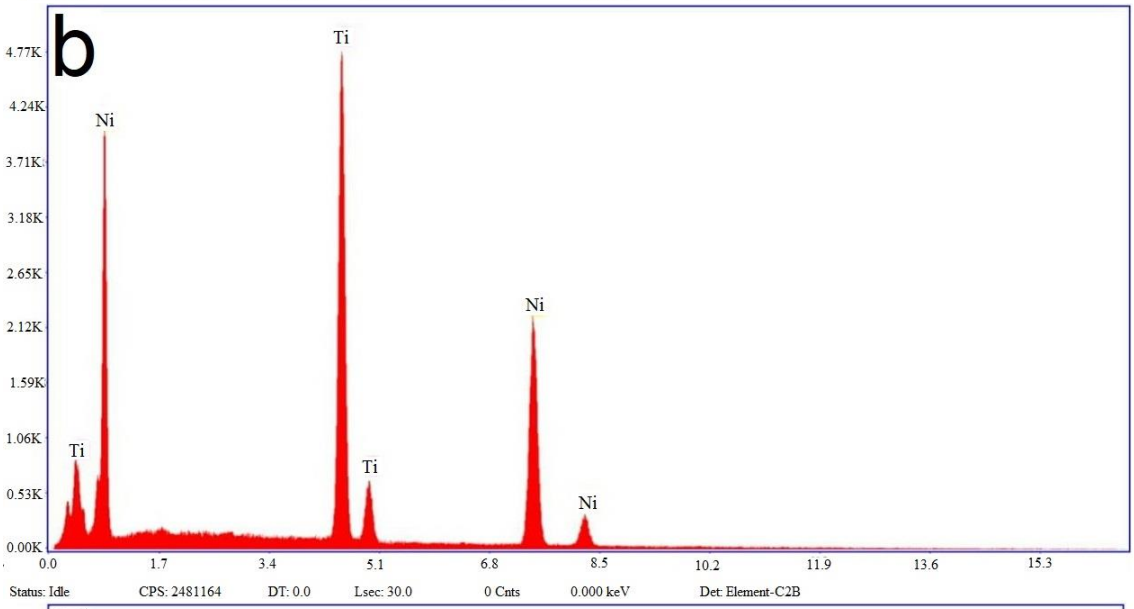
b
Ti
Ni
Ti
Ni
Ti
Ni
4.77K
4.24K
3.71K
3.18K
2.65K
2.12K
1.59K
1.06K
0.53K
0.00K
0.0
1.7
3.4
5.1
6.8
8.5
10.2
11.9
13.6
15.3
Status: Idle
CPS: 2481164
DT: 0.0
Lsec: 30.0
0 Cnts
0.000 keV
Det: Element-C2B

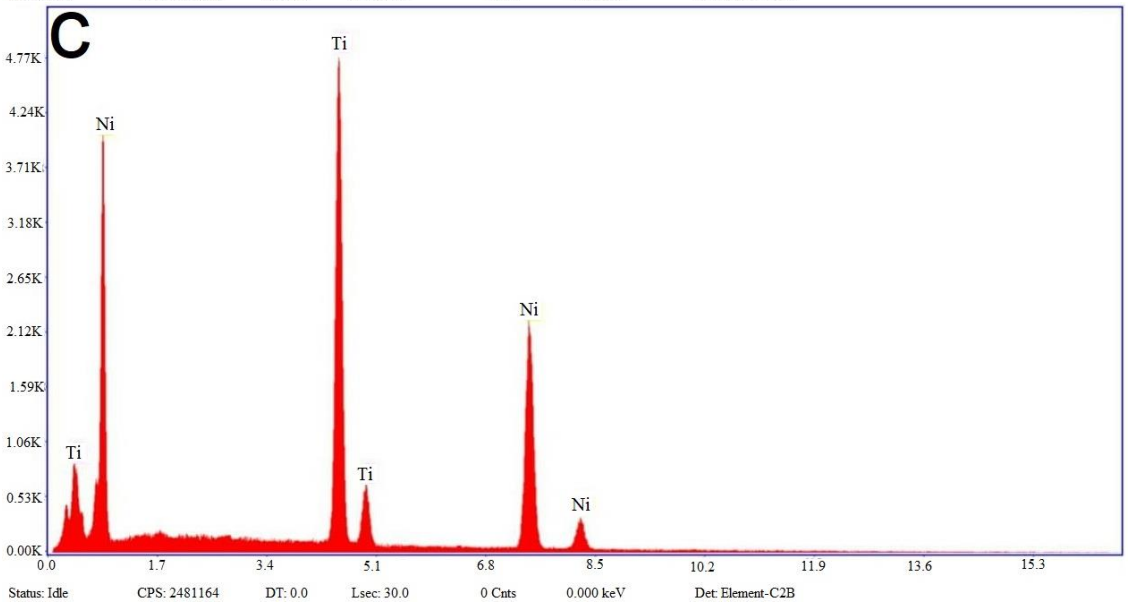
c
Ti
Ni
Ti
Ni
Ti
Ni
4.77K
4.24K
3.71K
3.18K
2.65K
2.12K
1.59K
1.06K
0.53K
0.00K
0.0
1.7
3.4
5.1
6.8
8.5
10.2
11.9
13.6
15.3
Status: Idle
CPS: 2481164
DT: 0.0
Lsec: 30.0
0 Cnts
0.000 keV
Det: Element-C2B

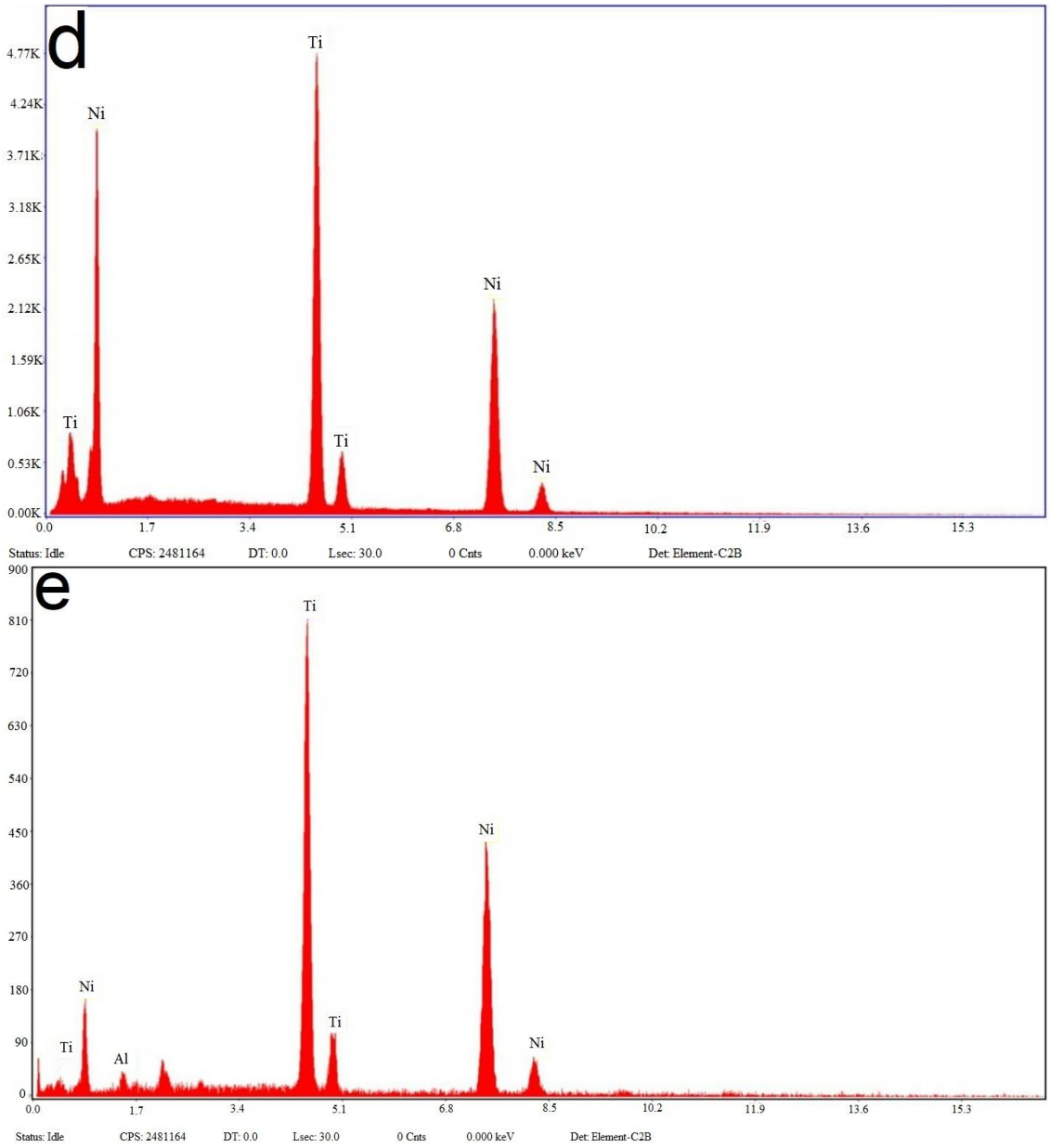

Fig. 3 EDX spectra of the samples: (a) raw, (b) aged at 460 ℃, (c) aged at 500 ℃, (d) solution treated at 850 ℃ and (e) solution treated at 850℃ then aged at 500 ℃

Fig. 4 illustrates the XRD analysis of the samples. Figs. 3 (a)-(e) refer to raw, aged at 460 °C, aged at 500°C, annealed at 850 °C and annealed at 850 then aged at 500 °C samples, respectively. Formed phases are analyzed using High Score software. The raw material (Fig. 3 (a)), as it was expected, consists of NiTi single phase. The peaks correspond with the reference code 03-065-7711. Figs. 3 (b) and (c) are the same as the raw material. It means that aging at 460 and 500 °C does not change the single phase. The sample that was solution treated at 850 °C (Fig. 3 (d)) consists of three phases: Ni, NiTi, and TiO_2. But in the sample that was solution treated at 850 °C and then aged at 500 °C (Fig. 3 (e)), beside mentioned phases, Ni_3Ti precipitation has been formed. The reference codes for these phases are 98-009-0603, 03-065-5537 and 01-076-0318, respectively [21].

Crystallite sizes of the samples are calculated via Williamson-Hall equation. These calculations are illustrated in Table III. It can be recognized that the minimum crystallite size is according to the sample aged at 460 °C.

TABLE III
CRYSTALLITE SIZE OF THE SAMPLES

Sample	Crystallite size (nm)
Raw	26.7
Aged at 460°c	18.573
Aged at 500°c	69.609
Solution treated at 850 ℃	40.527
Solution treated at 850 ℃ and aged at 500 ℃	73.384

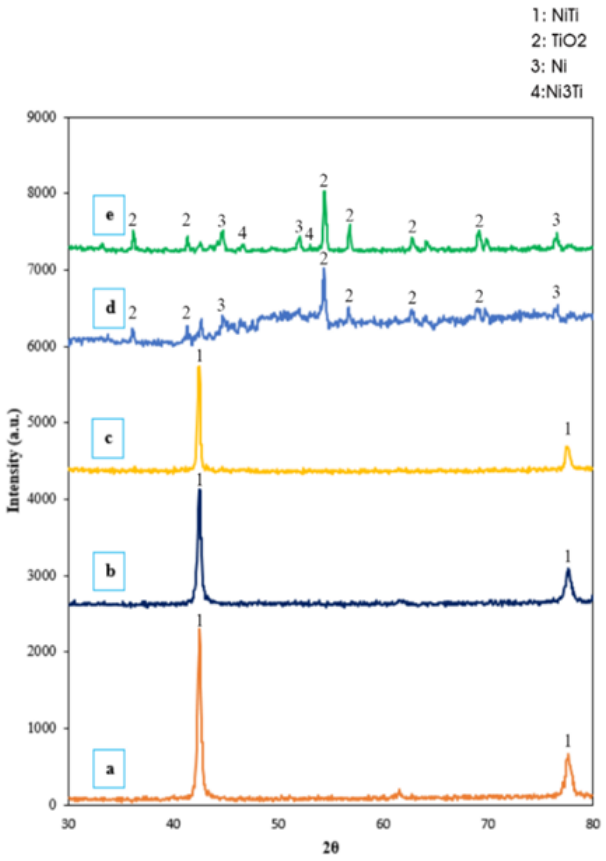

Fig. 4 XRD patterns of the samples: (a) raw, (b) aged at 460 ℃, (c) aged at 500 ℃, (d) solution treated at 850 ℃ and (e) solution treated at 850 ℃ then aged at 500 ℃

C. Thermal Analysis

Fig. 5 shows the DSC measurements of the samples. The number of developed peaks for all of the samples is the same. However, there is a little temperature difference. Three endothermic peaks can be seen in every sample which means there are three transformations. The transformation of martensite to austenite occurs due to heating the NiTi alloys. Ni_4Ti_3 precipitations preparation is between the austenite and martensitic transformation which develops another peak in the DSC curves. So, there should be three peaks. The third peak can be corresponding to the non-homogeneous precipitation of the Ni_4Ti_3 near the grain boundaries [36].

D. Mechanical Properties

Fig. 6 shows the stress-strain diagram of the samples. In this figure the ultimate strain is constant (6.5%). It can be determined from this figure that the sample aged at 460 °C has the highest upper plateau stress (580 MPa), the maximum curve area and the least residual strain (0.17%). So, the best heat treatment process for obtaining both the higher upper plateau stress and lower residual strain is aging at 460 °C (the optimum sample). The minimum of the lower plateau is for the raw sample. This sample has the least upper plateau. However, it has an acceptable residual strain (0.17%) in comparison with the sample solution treated at 850 °C. The highest plateau stress is due to the formation of the dislocations. These dislocations act as an obstacle to the austenite martensite interface which is the cause of the highest upper plateau stress [1].

TABLE IV
M_s AND A_s TEMPERATURES OF THE SAMPLES

Sample	M_s	A_s
Raw	-137.28°C	2.7°C
Aged at 460°c	-138.56°C	31.43°C
Aged at 500°c	-137.17°C	17.82°C
Solution treated at 850 ℃	-137.82°C	-6.82°C
Solution treated at 850 ℃ and aged at 500 ℃	-138.56°C	29.43°C

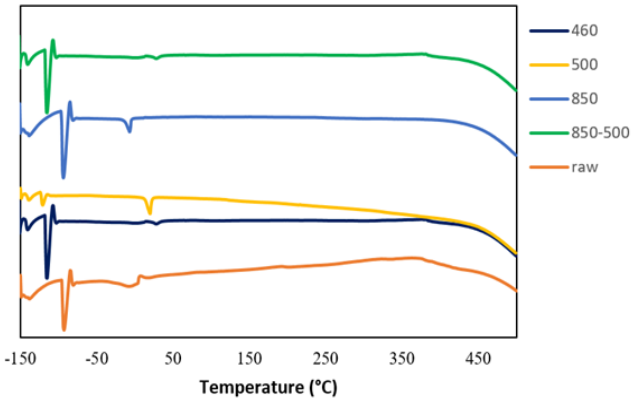

Fig. 5 DSC curves of the samples: raw, aged at 460 ℃, aged at 500 ℃, solution treated at 850 ℃ and solution treated at 850 ℃ then aged at 500 ℃ in the temperature range of -150 to 500 ℃

The sample which is just solution treated has the maximum amount of residual strain (3%). So it is clear that, annealing the samples would cause a decrease in mechanical properties of Nitinol. It may result in increasing residual strain and accordingly, a short fatigue life. The achieved data from stress-strain curves (Fig. 6) are given in Table V. The M_s temperature of the samples are close to each other but, the A_s temperature differs widely for each sample. These temperatures are reported in Table IV. It can be seen that the austenite temperature of the sample aged at 460 °C has the highest value of all. As much as M_s temperature grows bigger, yield stress increases. In other words, as much as M_s grows bigger, martensitic transformation occurs at high temperatures. Therefore, yield stress of samples will increase. Higher difference between M_s and A_s improves super-elasticity.

Martensitic transformation takes place via shear phenomena. If this transformation takes place with an external stress simultaneously, the superelasticity occurs. There are two kinds of martensitic transformation: thermal and athermal. If the temperature of the tensile test is around martensitic transformation, the thermal transformation helps its counterpart to improve the superelasticity [29].

According to Fig. 6, it can be seen that grade of each tension graph is different from other samples. This happens when Yang's modulus changes and it fluctuates when chemical composition is changed. After heat treatment of samples, new compounds such as Ni_3Ti, Ni_4Ti_3 form. The highest value of Yang's modulus is related to the aged sample at 460 ℃. Higher Yang's modulus helps mechanical properties grow better. As it is known, Yang's modulus is directly connected with tensile stress. In other words, by increasing Yang's modulus, tensile stress of the samples would increase. Also, with a decreasing Yang's modulus at high temperatures, operations which cause an increase in

Yang's modulus provide high temperature applications.

TABLE V
UPPER PLATEAU, LOWER PLATEAU AND RESIDUAL STRESS OF THE SAMPLES

Sample	Upper plateau (MPa)	Lower plateau (MPa)	Residual stress
Raw	100	22.5	0.61
Aged at 460°c	580	55	0.17
Aged at 500°c	388	32	0.7
Solution treated at 850 ℃	222	34	3
Solution treated at 850 ℃ and aged at 500 ℃	208	72	0.44

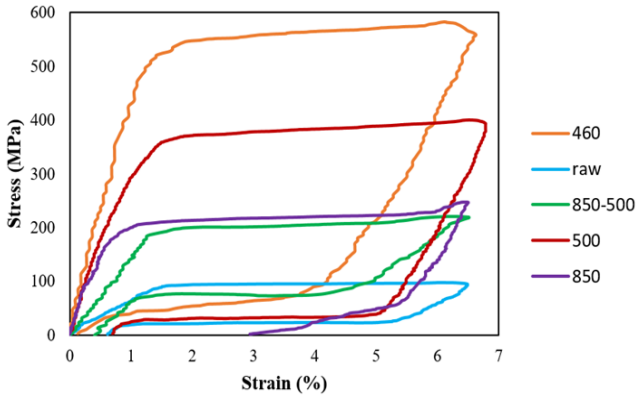

Fig. 6 Stress-strain curves of the samples: raw, aged at 460 ℃, aged at 500 ℃, solution treated at 850 ℃ and solution treated at 850 ℃ then aged at 460 ℃ in the constant strain of 6.5%

As it was mentioned, in addition to the phases which were formed in the solution treated sample at 850 ℃, Ni_3Ti precipitation was formed at the sample which was solution treated at 850 ℃ and aged at 500 ℃. According to Fig. 6, it could be seen that residual strain in solution treated sample is 3% while, in solution treated sample and aged sample, amount of residual strain is 0.3%. It is related to the formed precipitation which improves SME. However, it has not affected tensile strength.

IV. CONCLUSION

NiTi alloys have superelastic behavior that differs in various heat treatments. It is illustrated that the grain size of the samples gets larger when the aging temperature gets higher. For this alloy, solution treatment is not a helpful issue. The cause of the high super elasticity is the precipitation of the Ni_4Ti_3. Some porosity and oxidation can be seen due to SEM and XRD results, respectively. According to DSC curves, three transformations occur while heating the samples from -150 to 500 °C (Martensite, Austenite and Ni_4Ti_3 precipitation). Furthermore, the optimum aging temperature is 460 °C which is concluded from tensile test. The sample aged at 460 ℃ has the highest upper plateau (580 MPa) and the lowest residual strain (0.17%).

REFERENCES

[1] J.M. Jani, M. Leary, A. Subic, M.A. Gibson, Materials and Designs, 2014, 56, 1078-1113.
[2] L. Lecce, A. Concilio, Shape Memory Alloys Engineering, Elsevier publication, 2014.
[3] K.K. Alaneme, E.A. Okotete, N. Maledi, Materials Research and Technology, 2017, 6, 2, 136-146.
[4] K. Yamauchi, I. Ohkata, K. Tsuchiya, s. Miyazaki, Shape memory and super elastic alloys, Woodhead Publishing, 2011.
[5] R.K. Miller, T. Walker. Survey on Shape Memory Alloys' Survey Reports, Future Technology Surveys, 1989, 17-27.
[6] D. J. Hartl, D. C. Lagoudas, Thermomechanical Characterization of Shape Memory Alloy Materials, shape memory alloys, springer publication 2008.
[7] R. Abeyaratne, J.K. Knowles, 1993, 41, 3, 541-571.
[8] K. Otsuka, C.M. Wayman, Shape Memory Materials, Cambridge University Press, 1998.
[9] S.Y. Yang, G.S. Dui, Solids and Structures, 2013, 50, 20-21, 3254-3265.
[10] H. Yin, Y. He, 2014, 67, 100-128.
[11] T. Saburi, in Shape Memory Materials, Cambridge University Press, 1998.
[12] T. Duerig, A. Pelton, D. Stockel, Materials Science Engineering, 1999, 273-275,149-160.
[13] M.J. Garcia-Ramirez, R. Lopez-sesenes, I. Rosales-Cadena, J.G. Gonzalez-Rodriguez, Materials Research and Technology, 2017.
[14] C. L. Chu, J. CY. Chung, P.K. Chu, Transactions of Nonferrous Metals Society of China, 2006, 16, 1, 49-53.
[15] B. Yuan, CY Chung, M Zhu, Materials Science and Engineering, 2004, 382, 1-2, 181-187.
[16] K. Yamauchi, I. Ohkata, K. Tsuchiya, S. Miyazaki, shape memory and super elastic alloys, Woodhead Publishing, 2011.
[17] M. Nishida, C.M. Wayman, T. Honma, Metallurgical Transactions, 1986, 17, 9, 1505-1515.
[18] [18] D. J. Hartl, D. C. Lagoudas, Thermomechanical Characterization of Shape Memory Alloy Materials, shape memory alloys, Springer Publication's, 2008.
[19] T.S. Spini, F.P. Valarelli, R.H. Cançado, Rodrigo Hermont, K.M. Salvatore de, D.J. Villarinho, Applied Oral Science, 2013, 22.
[20] S.Y. Jiang, Y.G. Zhang, Y.N. Zhao, S.W. Liu, L. Hu, C.Z. Zhao, Transaction of non-ferrous metals society of china, 2015, 25, 12, 4063-4071.
[21] P.G. McCormick, Yinong liu, Acta Metallurgica et Materialia, 1994, 42, 7, 2407-2413.
[22] K. Sadrnezhad, F. Mashhadi, R. Sharghi, Materials and Manufacturing Process, 1997, 12, 1, 107-115.
[23] C. Chluba, W. Ge, R de Miranda, J. Strobel, L Kienle, E. Quandt, M. Wuttig, science, 2015, 348, 6238, 1004-1007.
[24] C. Yu, G. Kang, D. Song, Q. Kan, plasticity, 2015, 67, 69-101.
[25] M.L. Lethabane, P.A. Olubambi, H.K. Chikwanda, Materials Research and Technology, 2015, 4, 4, 367-376.
[26] D.A. Miller, D.C. Lagoudas, Materials Science and Engineering, 2001, 308, 1-2, 161-175.
[27] V. Birman, Applied Mechanic Reviews, 1997, 50, 11, 629-645.
[28] X. Wang, B. Verlinden, J.V. Humbeeck, Intermetallics, 2015, 62, 43-49.
[29] Y. Liu, Acta Materialia, 2015, 95, 411-427.
[30] M.S. Shakeri, H. Aghajani, Alloys and Compounds, 2013, 574, 119-123.
[31] G.K. Williamson, W.H. Hall, Acta metallurgica, 1, 1, 1953, 22-31.
[32] J. B. Holt, Z. A. Munir, materials science, 1986, 21, 1, 251-259.
[33] A. Hajalilou, M. Hashim, M. Nahavandi, I. Ismaila, Advanced Powder Technology, 2014, 25, 1, 423–429.
[34] C.N. Elias, M.A. Meyers, R.Z. Valiev, S.N. Monteiro, Materials Research and Technology, 2013, 2, 4, 340-350.
[35] A. Paryab, M. Asghar, N. Omid, B. Abouei, V. Eshraghi, Association of Metallurgical Engineers of Serbia, 2010, 16, 123–131.
[36] K. Kazemi-Choobi, J. Khalil-Allafi, A. Elhami, P. Asadi, Metallurgical and Materials Transactions A: Physical Metallurgy and Materials Science, 2013, 44, 10, 4429–4433.

Aliasing Free and Additive Error in Spectra for Alpha Stable Signals

R. Sabre

***Abstract*—**This work focuses on the symmetric alpha stable process with continuous time frequently used in modeling the signal with indefinitely growing variance, often observed with an unknown additive error. The objective of this paper is to estimate this error from discrete observations of the signal. For that, we propose a method based on the smoothing of the observations via Jackson polynomial kernel and taking into account the width of the interval where the spectral density is non-zero. This technique allows avoiding the "Aliasing phenomenon" encountered when the estimation is made from the discrete observations of a process with continuous time. We have studied the convergence rate of the estimator and have shown that the convergence rate improves in the case where the spectral density is zero at the origin. Thus, we set up an estimator of the additive error that can be subtracted for approaching the original signal without error.

***Keywords*—**Spectral density, stable processes, aliasing, p-adic.

I. Introduction

RECENT years have shown an increasing interest in the study of stationary stable processes and in general stationary processes with infinite variance. The harmonizable process is an important example of a symmetric α -stable stationary process, and its proprieties have been considered by numerous authors like [1]-[10] to name a few.

Stable symmetric processes find applications in various fields including: signal and image processing, hydrology, economies, electronic and electric, communications and radar applications ... see [11]-[23].

In this work, we consider, as in [4], a complex stationary symmetric α -stable (SαS) process: $X=\{X(t),-\infty<t<+\infty\}$, with $\alpha\in(0,2)$; more specifically, X is a complex-valued stochastic process for which the finite dimensional characteristic function is:

$$E\exp\left\{i\Re e\sum_{j=1}^{n}z_jX(t_j)\right\}=\exp\left\{-C_\alpha\int_{-\infty}^{+\infty}\left|\sum_{j=1}^{n}z_je^{it_ju}\right|^\alpha\phi(u)du\right\}$$

with $z_j=x_j-iy_j$ and $C_\alpha=(\alpha\pi)^{-1}\int_0^\pi|\cos(\theta)|^\alpha\,d\theta$, where ϕ is a nonnegative integrable function called the spectral density of X. This spectral density plays a role analogous to that played by the usual power spectral density function of a second order stationary process. It is clear that the spectral density ϕ fully describes the distribution of the process X. Alternatively X has the integral representation

$$X(t)=\int_{-\infty}^{\infty}e^{itu}d\xi(u) \tag{1}$$

where ξ is a complex-valued SαS process with independent isotropic increments. The stochastic integral in (1) is defined by means of convergence in probability, for details see [1], [5].

The spectral density function was already estimated by [4], when the process is continuous-time, by [24] when the process is discrete-time and by [25] when the process is p-adic-time.

This paper deals with the fairly common situation in practice, namely that the observations of the process are tainted by an unknown and constant error. The process $X_t=a+Z_t$ is observed instead of the process Z alone. The constant a is estimated in [26] when the process is discrete-time.

Our goal is to establish nonparametric estimate of a, from sample of the process $X(t_n)$ at instants t_n, where the sampling instants t_n are equally distant, i.e., $t_n=n\tau$, $\tau>0$. It is known that aliasing occurs. For more details about aliasing phenomenon, see [27], [28]. To avoid this difficulty, we suppose that the spectral density ϕ is vanishing for $|\lambda|>\Omega$ where Ω is a nonnegative real number. The value of τ is chosen such that $\tau\Omega<\pi$.

In this paper we particularly study some cases where the spectral density is zero at the origin: $\phi(\lambda)=\sin^{2k\alpha}(\lambda/2)g(\lambda)$ and $\phi(\lambda)=|\lambda|^\beta g(\lambda)$. We show that the rate of convergence of the estimator of the constant "a" is improved.

This paper is organized as follows: The second section gives some definitions and proprieties of Jackson polynomial kernel and an estimator of the constant a is defined. We show that this estimate converges in probability to a. Then we show that the estimate converges to a in L_p $(p<\alpha)$. Since the second moment of this process does not exist, the convergence in *Lp* substitutes the quadratic. In third section, the spectral density of Z is assumed vanishing at origin precisely: $\phi(\lambda)=|\lambda|^\beta g(\lambda)$. We improve the rate of convergence depending to the value of β. The fourth section is reserved to numerical studies.

R. Sabre is with the Laboratory Biogeoscience Laboratory Biogeosciences UMR CNRS, University of Burgundy, Agrosup, Department DSIP, Dijon, France (e-mail: r.sabre@agrosupdijon.fru).

II. Estimation of the Constant Error

As in [20], [24], we give the definition of the Jackson polynomial kernel: Let $Z_1,\ldots,Z_N$ observations of the process $Z:\ \left(Z_{(n)}\right)_{0\le n\le N-1}$, where *N* satisfies:

$$N-1=2k(n-1) \qquad with \quad n\in N \quad k\in N\cup\{1/2\}$$

if $k=1/2$ then $n=2n_1-1, n_1\in N$.

The Jackson's polynomial kernel is defined by:

$$\left|H_N(\lambda)\right|^{\alpha}=\left|A_N H^{(N)}(\lambda)\right|^{\alpha}$$

where

$$H^{(N)}(\lambda)=\frac{1}{q_{k,n}}\left(\frac{\sin(\frac{n\lambda}{2})}{\sin(\frac{\lambda}{2})}\right)^{2k} \qquad with$$

$$q_{k,n}=\frac{1}{2\pi}\int_{-\pi}^{\pi}\left(\frac{\sin(\frac{n\lambda}{2})}{\sin(\frac{\lambda}{2})}\right)^{2k} d\lambda.$$

In addition, we have $A_N=(B_{\alpha,N})^{-\frac{1}{\alpha}}$ with

$$B_{\alpha,N}=\int_{-\pi}^{\pi}\left|H^{(N)}(\lambda)\right|^{\alpha} d\lambda.$$

We give the following lemmas which are used in the reminder of this paper. Their proofs are given in [24].

Lemma1. There is a non negative function h_k such as:

$$H^{(N)}(\lambda)=\sum_{m=-k(n-1)}^{k(n-1)} h_k\left(\frac{m}{n}\right)\cos(m\lambda)$$

Lemma2. Let

$$B'_{\alpha,N}=\int_{-\pi}^{\pi}\left|\frac{\sin\frac{n\lambda}{2}}{\sin\frac{\lambda}{2}}\right|^{2k\alpha} d\lambda \quad and$$

$$J_{N,\alpha}=\int_{-\pi}^{\pi}|u|^{\gamma}|H_N(\lambda)|^{\alpha} d\lambda,$$

where $\gamma\in]0,2]$. Then

$$B'_{\alpha,N}\begin{cases}\ge 2\pi\left(\frac{2}{\pi}\right)^{2k\alpha} n^{2k\alpha-1} & if\ 0<\alpha<2\\ \le\frac{4\pi k\alpha}{2k\alpha-1} n^{2k\alpha-1} & if\ \frac{1}{2k}<\alpha<2\end{cases} \quad and$$

$$J_{N,\alpha}\le\begin{cases}\frac{\pi^{\gamma+2k\alpha}}{2^{2k\alpha}(\gamma-2k\alpha+1)}\frac{1}{n^{2k\alpha-1}} & if \quad \frac{1}{2k}<\alpha<\frac{\gamma+1}{2k}\\ \frac{2k\alpha\pi^{\gamma+2k\alpha}}{2^{2k\alpha}(\gamma+1)(2k\alpha-\gamma-1)}\frac{1}{n^{\gamma}} & if \quad \frac{\gamma+1}{2k}<\alpha<2\end{cases}$$

The estimator of the *a* is constructed as follows:

$$\hat{a}=\frac{\tau^{\frac{1}{\alpha}}A_N}{H_N(0)}\sum_{n'=-k(n-1)}^{k((n-1)} h_k\left(\frac{n'}{n}\right)X(\tau n'+\tau k(n-1)). \qquad (2)$$

Theorem1. Let p a real number such that $0<p<\alpha$. Then

$$|\hat{a}-a|^{p}=O\left(\frac{1}{n^{p\alpha}}\right)$$

Proof. From (1) and (2), we have

$$\hat{a}=\frac{\tau^{\frac{1}{\alpha}}A_N}{H_N(0)}\sum_{n'=-k(n-1)}^{k((n-1)} h_k\left(\frac{n'}{n}\right)\int_{-\infty}^{\infty} exp\left[i([\tau n'+\tau k(n-1)]\lambda)\right] d\xi(\lambda) + a.$$

As in [1], the characteristic function of $(\hat{a}-a)$ can be written as:

$$E\exp\left[i\Re e\bar{r}(\hat{a}-a)\right]=$$

$$\exp[-C_\alpha|r|^{\alpha}\int_{-\infty}^{\infty}\tau\left|\frac{A_N}{H_N(0)}\sum_{n'=-k(n-1)}^{k((n-1)} h_k\left(\frac{n'}{n}\right)e^{in'\tau\lambda}\right|^{\alpha} d\xi(\lambda)].$$

where $r=r_1+ir_2$. It is easy to show that:

$$E\exp\left[i\Re e\bar{r}(\hat{a}-a)\right]=\exp\left(-C_\alpha|r|^{\alpha}\psi_N\right),$$

where

$$\psi_N=\int_{-\infty}^{\infty}\frac{|H_N(\lambda)|^{\alpha}}{|H_N(0)|^{\alpha}}\phi\left(\frac{\lambda}{\tau}\right)d\lambda=\sum_{j\in Z}\int_{(2j-1)\pi}^{(2j+1)\pi}\frac{|H_N(\lambda)|^{\alpha}}{|H_N(0)|^{\alpha}}\phi\left(\frac{\lambda}{\tau}\right)d\lambda.$$

Putting $\lambda=y-2\pi j$ and using the fact that H_N is 2π-periodic, we obtain

$$\psi_N=\sum_{j\in Z}\int_{-\pi}^{\pi}\frac{|H_N(\lambda)|^{\alpha}}{|H_N(0)|^{\alpha}}^{a}\ \phi_j(y)dy,$$

where $\phi_j(y)=\phi\left(\frac{y}{\tau}-\frac{2\pi}{\tau}j\right)$. Let j be an integer such that

$-\Omega < \frac{y-2\pi j}{\tau} < \Omega$. Using the fact that $\pi\Omega < \pi$ and $|y| < \pi$, we get $|j| < \frac{\pi\Omega}{2\pi} + \frac{1}{2} < 1$ and then $j = 0$. Consequently:

$$\psi_N = \int_{-\pi}^{\pi} \frac{|H_N(\lambda)|^{\alpha}}{|H_N(0)|^{\alpha}} \phi\left(\frac{y}{\tau}\right) dy.$$

The function ϕ being bounded on $[-\pi,\pi]$ and $|H_N(.)|^{\alpha}$ being a kernel, it can be shown that $\int_{-\pi}^{\pi} |H_N(\lambda)|^{\alpha} \phi(\lambda) d\lambda$ is converging to $\phi(0)$. On the other hand, from lemma 2, we have:

$$\frac{1}{|H_N(0)|^{\alpha}} = \frac{B'_{\alpha,N}}{n^{2k\alpha}} = O(1/n). \tag{3}$$

Therefore ψ_N converges to 0. Consequently, the characteristic function of $\hat{a} - a$ converges to 1 when N approaches infinity. Hence we have the convergence in probability of $\hat{a}$ to a.

We study now the convergence of $\hat{a}$ to a in L_p where $0 < p < \alpha$, which replaces the convergence in mean square, because the second order moment of X is infinity. Let

$$D_p = \Re e \int_{-\infty}^{\infty} \int_{-\frac{\pi}{4}}^{\frac{\pi}{4}} \frac{1 - e^{ir\cos\theta}}{|r|^{1+p}} dr d\theta.$$

Let $t = r' e^{i\theta'}$ and $x = \rho e^{i\tau_0}$. Assuming now $r = \varepsilon r', \quad \tau = \tau' - \tau_0$

$$D_p = \Re e \int_{-\infty}^{\infty} \int_{-\frac{\pi}{4}+\tau_0}^{\frac{\pi}{4}+\tau_0} \frac{1 - e^{i\varepsilon r' \cos(\tau' - \tau_0)}}{|\varepsilon|^{1+p} |r'|^{1+p}} \varepsilon dr' d\theta'$$

$$D_p |x|^p = \Re e \int_{0}^{\infty} \int_{-\frac{\pi}{4}+\tau_0}^{\frac{\pi}{4}+\tau_0} \frac{1 - e^{i\Re e(\bar{t}x)}}{|t|^{1+p}} d|t| d\theta'$$

$$- \Re e \int_{-\infty}^{0} \int_{-\frac{\pi}{4}+\tau_0}^{\frac{\pi}{4}+\tau_0} \frac{1 - e^{i\Re e(\bar{t}x)}}{|t|^{1+p}} d|t| d\theta'.$$

Replacing in this formula x by $\hat{a} - a$, from the previous result we have

$$D_p E|x|^p = \int_{-\infty}^{\infty} \int_{-\frac{\pi}{4}+\tau_0}^{\frac{\pi}{4}+\tau_0} \frac{1 - e^{-C_\alpha |t|^{\alpha} \psi_N}}{|t|^{1+p}} d|t| d\theta'$$

$$= \frac{\pi}{2} \int_{-\infty}^{\infty} \frac{1 - e^{-C_\alpha |t|^{\alpha} \psi_N}}{|t|^{1+p}} dt.$$

Let $u = t[\psi_N]^{\frac{1}{\alpha}}$ and using (3), we obtain

$$\frac{2}{\pi} C_{p,\alpha} E|\hat{a} - a|^p = (\psi_N)^{\frac{p}{\alpha}} = O\left(\frac{1}{n^{p/\alpha}}\right)$$

where $C_{p,\alpha} = R_p F_{p,\alpha}^{-1} (C_\alpha)^{-\frac{p}{\alpha}}$ with $R_p = \int \frac{1 - \cos(u)}{|u|^{1+p}} du$ and $F_{p,\alpha} = \int \frac{1 - e^{-|u|^{\alpha}}}{|u|^{1+p\alpha}} du$.

III. The Rate of Convergence for Particular Cases

Suppose that the spectral density is zero at the origin. This assumption gives our estimator a better convergence rate.

Theorem2. Assume that the spectral density is satisfying: $\phi(\lambda) = |\lambda|^{\beta} g(\lambda)$ where $\beta \in]0, 2k\alpha - 1[$, $\lambda \in [-\pi,\pi]$ and $g(\lambda)$ is a bounded function on $[-\pi,\pi]$ and vanishing for $|\lambda| > \Omega$, continuous in neighborhood of 0 and $g(0) \neq 0$. Then

$$2^{4kp} L \tau^{2k\alpha - \beta} \leq \lim_{N \to \infty} n^{\frac{p(\beta+1)}{\alpha}} E|\hat{a} - a|^p \leq \tau^{\beta} \pi^{4kp} L,$$

where L is the following constant:

$$L = \frac{\pi}{2C_{p,\alpha}} \left[g(0) \int_{-\infty}^{\infty} \frac{|\sin u2|^{2k\alpha}}{|u|^{2k\alpha - \beta}} du \right]^{\frac{p}{\alpha}}.$$

Proof. The function ψ_N can be written as:

$$\psi_N = n^{-2k\alpha} \int_{-\pi}^{\pi} \left| \frac{\sin\frac{n\lambda}{2}}{\sin\frac{\lambda}{2}} \right|^{2k\alpha} \left|\frac{\lambda}{\tau}\right|^{\beta} g\left(\left(\frac{\lambda}{\tau}\right) d\lambda\right.$$

Using the inequality: $\left|\sin\frac{x}{2}\right| \geq \frac{x}{\pi} \quad 0 \leq x \leq \pi,$ we maximize ψ_N as:

$$\psi_N \leq \pi^{4k\alpha} n^{-2k\alpha} \tau^{-\beta} \int_{-\pi}^{\pi} \frac{\left|\sin\frac{n\lambda}{2}\right|^{2k\alpha}}{|\lambda|^{2k\alpha - \beta}} g\left(\frac{\lambda}{\tau}\right) d\lambda.$$

Putting $n\lambda = u$, we have

$$\psi_N \leq \pi^{4k\alpha} \tau^{-\beta} n^{-1-\beta} \int_{-\infty}^{\infty} \frac{\left|\sin\frac{u}{2}\right|^{2k\alpha}}{|u|^{2k\alpha - \beta}} g\left(\frac{u}{n\tau}\right) du$$

The Lebesgue's dominated convergence theorem gives the following convergence:

$$\lim_{N\to\infty}\int_{-\infty}^{\infty}\frac{\left|\sin\frac{u}{2}\right|^{2k\alpha}}{|u|^{2k\alpha-\beta}}g\left(\frac{u}{n\tau}\right)du=g(0)\int_{-\infty}^{\infty}\frac{\left|\sin\frac{u}{2}\right|^{2k\alpha}}{|u|^{2k\alpha-\beta}}du.$$

Lemma 2 gives:

$$\lim_{N\to\infty}n^{\frac{p(\beta+1)}{\alpha}}\left(\psi_N\right)^{\frac{p}{\alpha}}\le\pi^{4kp}\left(g(0)\int_{-\infty}^{+\infty}\frac{\left|\sin\frac{u}{2}\right|^{2k\alpha}}{|u|^{2k\alpha-\beta}}du\right)^{\frac{p}{\alpha}}. \quad (4)$$

Thus ψ_N converges to zero. Using the following inequality $|\sin x|\le|x| \quad \forall x\in[-\pi,\pi]$, we obtain:

$$\psi_N\ge 2^{4k\alpha}n^{-2k\alpha}\tau^{2k\alpha-\beta}\int_{-\pi}^{\pi}\frac{\left|\sin\frac{n\lambda}{2}\right|^{2k\alpha}}{|\lambda|^{2k\alpha-\beta}}g\left(\frac{\lambda}{\tau}\right)d\lambda.$$

Therefore

$$\psi_N\ge 2^{4k\alpha}n^{-\beta-1}\tau^{2k\alpha-\beta}\int_{-\pi}^{\pi}\frac{\left|\sin\frac{u}{2}\right|^{2k\alpha}}{|u|^{2k\alpha-\beta}}g(\frac{u}{n\tau})du$$

$$\lim_{N\to\infty}n^{\frac{p(\beta+1)}{\alpha}}\left(\psi_N\right)^{\frac{p}{\alpha}}\ge 2^{4kp}\tau^{2k\alpha-\beta}\left(g(0)\int_{-\infty}^{+\infty}\frac{\left|\sin\frac{u}{2}\right|^{2k\alpha}}{|u|^{2k\alpha-\beta}}du\right)^{\frac{p}{\alpha}}.$$

The first equality of (4) reaches the result of this theorem.

Theorem3. Assuming that the spectral density satisfies:

$$\phi(\lambda)=\sin^{2k\alpha}\left(\frac{\lambda}{2}\right)g(\lambda)$$

where the function g is integrable on $[-\pi,\pi]$, $g(0)\neq 0$ and vanishing for $|\lambda|>\Omega$. Then

$$cte\pi 2C_{p,\alpha}\tau^{p\alpha}\left(\int_{-\pi}^{\pi}g(\lambda)d\lambda\right)^{\frac{p}{\alpha}}\le\lim_{N\to\infty}n^{2pk}E\,|\hat{a}-a|^{p}$$
$$\le\frac{\pi}{2C_{p,\alpha}}\tau^{\frac{p}{\alpha}}\left(\int_{-\pi}^{\pi}g(\lambda)d\lambda\right)^{\frac{p}{\alpha}}$$

Proof. From the definition of ψ_N, we have

$$\psi_N=n^{-2k\alpha}\int_{-\pi}^{\pi}\left|\sin\frac{n\lambda}{2\tau}\right|^{2k\alpha}g\left(\frac{\lambda}{\tau}\right)d\lambda.$$

As $1\le k\alpha$ and the sinus function is smaller than 1, the next expression is connected to

$$\psi_N\le n^{-2k\alpha}\int_{-\pi}^{\pi}\left|\sin\frac{n\lambda}{2\tau}\right|^{2k\alpha}g\left(\frac{\lambda}{\tau}\right)d\lambda$$

$$\psi_N\le n^{-2k\alpha}\left[\int_{-\pi}^{\pi}g\left(\frac{\lambda}{\tau}\right)d\lambda\right].$$

So, from lemma 2, we have:

$$\lim_{N\to\infty}\psi_N n^{2k\alpha}\le\tau\int_{-\pi}^{\pi}g(\lambda)d\lambda.$$

Using the fact that the sinus function is between -1 and 1 and $k\alpha<[k\alpha]+1$ where $[k\alpha]$ represents the integer part of $k\alpha$, we obtain

$$\psi_N\ge n^{-2k\alpha}\int_{-\pi}^{\pi}\left[\left(\sin\frac{n\lambda}{2\tau}\right)^2\right]^{[k\alpha]+1}g\left((\frac{\lambda}{\tau}\right)d\lambda$$

$$\psi_N\ge n^{-2k\alpha}\frac{n^{-1}}{2B'_{\alpha,N}}\int_{-\pi}^{\pi}\left[\frac{1-\cos\left(\frac{n\lambda}{\tau}\right)}{2}\right]^{[k\alpha]+1}g\left(\frac{\lambda}{\tau}\right)d\lambda.$$

The binomial formula gives:

$$2^{[k\alpha]+1}\psi_N\ge n^{-2k\alpha}\tau\int_{-\pi}^{\pi}g(\lambda)d\lambda$$

IV. SIMULATION

The proposed estimator can be applied to concrete situations. For example, the arrival time of a signal sent by Wi-Fi using new wireless transmission technologies can be modeled by alpha stable process. Indeed, [29] proposed an arrival time model based on Poisson distributions. Reference [15] provided a model based on stable alpha distributions. The sum of arrival times modeled by independent and isotropic Poisson distributions can be represented by a stable harmonizable process like that given in (1), see [30]. When these signals are collected in an aquatic environment with a constant disturbance, the process will be added with a constant error ($X_n=Z_n+a$).

Throughout this section, we give the simulation of the studied process:

$$Z_t = \int_{-\infty}^{\infty} e^{it\lambda} d\xi(\lambda),$$

where $1 < \alpha < 2$ and ξ is a complex symmetric SαS measure on R with independent and isotropic increments and with control measure m such that $mdx = \phi(x)dx$. In order to achieve this, we use the series representation defined in [26]. Therefore, the process Z given in (8) can be expressed as:

$$Z_t = C_\alpha \left(\int \phi(x)dx \right)^{1\alpha} \sum_{j=1}^{\infty} \varepsilon_j \Gamma_j^{-1\alpha} e^{inV_j} e^{i\theta_j}$$

where ε_j is a sequence of i.i.d. random variables such as $P[\varepsilon_j = 0] = P[\varepsilon_j = 1] = 12$, Γ_k is a sequence of arrival times of Poisson process, V_j is a sequence of i.i.d. random variables independent of ε_k and of Γ_k having the same distribution of control measure m, which has probability density ϕ, θ_j are independent random variables, having the uniform distribution on $[-\pi, \pi]$, independent of ε_j, Γ_j and V_j.

To generate N values $(N = 101,501,1001)$ of the process Z_{t_n}, we use the following steps:

- generate 2000 values of ε_j
- generate 2000 values of Γ_j
- generate 2000 values of V_j
- generate 2000 values of θ_j

Then we calculate for all $0 \le n \le N$: $Z_{t_n} = C_\alpha \left(\int \phi(x)dx \right)^{\frac{1}{\alpha}} \sum_{j=1}^{2000} \varepsilon_j \Gamma_j^{-1\alpha} e^{it_n V_j} e^{i\theta_j}$ where the spectral density is chosen as $\phi(x) = |x|^{\beta} e^{-|x|}$ for $x \in [-\pi, \pi]$ and $\phi(x) = 0$ otherwise and $\alpha = 1,7$ and $k = 4$. The β is taken as 2, between 0 and $2k\alpha - 1$ g Afterwards, we generate $X_{t_n} = a + Z_{t_n}$ where a is chosen equal to 40.

We calculate the estimator $\hat{a}$ given in (1) for different sizes of sample $N = 101,501,1001$. The result is given in Table I.

TABLE I
THE VALUE OF THE ERROR ESTIMATOR FOR DIFFERENT SIZES OF SAMPLES

$2k\alpha - 1 = 12.6$	$\beta = 2$
N=101	$\hat{a} = 31,5$
N=501	$\hat{a} = 36,3$
N=1001	$\hat{a} = 41,05$

Comparing $\hat{a}$ to 40 (value of the constant a), we find that the estimator $\hat{a}$ increasingly approaches the constant error a when the sample size is large.

V. CONCLUSIONS

We give an estimator of the constant additive error in spectral representation of SαS process. This work could be applied to several cases when processes have an infinite variance and the observation of these processes is perturbed by a constant noise. For example:

- the decomposition of audio signals with background noise by separating the different musical instruments.
- the denoising of a degraded historical record. The signal is considered infinitely variable.

The perspective of this work is to optimize the smoothing parameters to have a better speed of convergence. For this purpose, the cross-validation method will be the most appropriate tool.

REFERENCES

[1] S. Cambanis (1983) "Complex symetric stable variables and processes" In P.K.SEN, ed, Contributions to Statistics": Essays in Honour of Norman L. Johnson North-Holland. New York,(P. K. Sen. ed.), pp. 63-79

[2] S. Cambanis, and M. Maejima (1989). "Two classes of self-similar stable processes with stationary increments". Stochastic Process. Appl. Vol. 32, pp. 305-329

[3] M.B. Marcus and K. Shen (1989). "Bounds for the expected number of level crossings of certain harmonizable infinitely divisible processes". Stochastic Process. Appl., Vol. 76, no. 1 pp 1-32.

[4] E. Masry, S. Cambanis (1984). "Spectral density estimation for stationary stable processes". Stochastic processes and their applications, Vol. 18, pp. 1-31 North-Holland.

[5] G. Samorodnitsky and M. Taqqu (1994). "Stable non Gaussian processes ». Chapman and Hall, New York.

[6] K., Panki and S. Renming (2014). "Stable process with singular drift". Stochastic Process. Appl., Vol. 124, no. 7, pp. 2479-2516

[7] C. Zhen-Qing and W. Longmin (2016). "Uniqueness of stable processes with drift." Proc. Amer. Math. Soc., Vol. 144, pp. 2661-2675

[8] K. Panki, K. Takumagai and W. Jiang (2017). "Laws of the iterated logarithm for symmetric jump processes". Bernoulli, Vol. 23, n° 4 pp. 2330-2379.

[9] M. Schilder (1970). "Some Structure Theorems for the Symmetric Stable Laws". Ann. Math. Statist., Vol. 41, no. 2, pp. 412-421.

[10] R. Sabre (2012b). "Missing Observations and Evolutionary Spectrum for Random". International Journal of Future Generation Communication and Networking, Vol. 5, n° 4, pp. 55-64.

[11] E. Sousa (1992). "Performance of a spread spectrum packet radio network link in a Poisson of interferences". IEEE Trans. Inform. Theory, Vol. 38, pp. 1743-1754

[12] M. Shao and C.L. Nikias (1993). "Signal processing with fractional lower order moments: Stable processes and their applications", Proc. IEEE, Vol.81, pp. 986-1010

[13] C.L. Nikias and M. Shao (1995). "Signal Processing with Alpha-Stable Distributions and Applications". Wiley, New York

[14] S. Kogon and D. Manolakis (1996). "Signal modeling with self-similar alpha- stable processes: The fractional levy motion model". IEEE Trans. Signal Processing, Vol 44, pp. 1006-1010

[15] N. Azzaoui, L. Clavier, R. Sabre, (2002). "Path delay model based on stable distribution for the 60GHz indoor channel" IEEE GLOBECOM, IEEE, pp. 441-467

[16] J.P. Montillet and Yu. Kegen (2015). "Modeling Geodetic Processes with Levy alpha-Stable Distribution and FARIMA", Mathematical Geosciences. Vol. 47, no. 6, pp. 627-646.

[17] M. Pereyra and H. Batalia (2012). "Modeling Ultrasound Echoes in Skin Tissues Using Symmetric alpha-Stable Processes". IEEE Transactions on Ultrasonics, Ferroelectrics, and Frequency Control, Vol. 59, n°. 1, pp. 60-72.

[18] X. Zhong and A.B. Premkumar (2012). "Particle filtering for acoustic source tracking in impulsive noise with alpha-stable process". IEEE Sensors Journal, Vol. 13, no. 2, pp. 589 - 600.

[19] Wu. Ligang and W. Zidong (2015). "Filtering and Control for Classes of Two-Dimensional Systems". The series Studies in Systems of, Decision

and Control, Vol.18, pp. 1-29.
[20] N. Demesh (1988). “Application of the polynomial kernels to the estimation of the spectra of discrete stable stationary processes”. (Russian) Akad.Nauk.ukrain. S.S.R. Inst.Mat. Preprint 64, pp. 12-36
[21] F. Brice, F. Pene, and M. Wendler, (2017) “Stable limit theorem for U-statistic processes indexed by a random walk”, Electron. Commun. Prob., Vol. 22, no. 9, pp.12-20.
[22] R. Sabre (2019). “Alpha Stable Filter and Distance for Multifocus Image Fusion”. IJSPS, Vol. 7, no. 2, pp. 66-72.
[23] JN. Chen, J.C. Coquille, J.P. Douzals, R. Sabre (1997). “Frequency composition of traction and tillage forces on a mole plough”. Soil and Tillage Research, Vol. 44, pp. 67-76.
[24] R. Sabre (1995). “Spectral density estimate for stationary symmetric stable random field”, Applicationes Mathematicaes, Vol. 23, n°. 2, pp. 107-133
[25] R. Sabre (2012a). “Spectral density estimate for alpha-stable p-adic processes”. Revisita Statistica, Vol. 72, n°. 4, pp. 432-448.
[26] R. Sabre (2017). “Estimation of additive error in mixed spectra for stable prossess”. Revisita Statistica, Vol. LXXVII, n°. 2, pp. 75-90.
[27] E. Masry, (1978). “Alias-free sampling: An alternative conceptualization and its applications”, IEEE Trans. Information theory, Vol. 24, pp.317-324.
[28] R. Sabre (1994). « Estimation de la densité de la mesure spectrale mixte pour un processus symétrique stable strictement stationnaire », C. R. Acad. Sci. Paris, Vol. 319, série I, pp. -1310.
[29] L. Clavier, M. Rachdi, Y. Delignon, V. Letuc, C. Garnier, P.A. Roland (2001). “Wide band 60GHz indoor channel: characterization and statistical modelling“. IEEE 54th VTC fall, Atantic City, NJ USA, 7-11October, 2001.
[30] A. Janicki and A. WERON (1993). “Simulation and Chaotic Behavior of Alpha-stable Stochastic Processes”. Series: Chapman and Hall/CRC Pure and Applied Mathematics, New York.

R.Sabre received the PhD degree in statistics from the University of Rouen, France, in 1993 and Habilitation to direct research (HdR) from the University of Burgundy, Dijon, France, in 2003. He joined Agrosup Dijon, France, in 1995, where he is an Associate Professor. From 1998 through 2010, he served as a member of Institut de Mathématiques de Bourgogne, France. He was a member of the Scientific Council AgroSup Dijon from 2009 to 2013. From 2012 to 2019, he has been a member of Laboratoire Electronic, Informatique, and Image (LE2I), France. Since 2019 he has been a member of Laboratory Biogeosciences UMR CNRS University Burgundy. He is author/co-author of numerous papers in scientific and technical journals and conference proceedings. His research interests lie in areas of statistical process and spectral analysis for signal and image processing.

An analysis of a BJT high frequency phase shift oscillator by root locus of current consumption and impedance matching using MATLAB

Kittipong Tripetch[1], Member, IEEE

[1]Division of Electronic and Telecommunication, Faculty of Engineering and Architecture, Rajamangala University of Technology Suvarnabhumi, Nonthaburi Campus, Thailand

Corresponding author: Kittipong Tripetch (e-mail: Kittipong.tripetch.mr@ ieee.org).

ABSTRACT A Design of a BJT phase shift oscillator is proposed with a detail polynomial form. The numerator and denominator polynomial form are derived which can be seen as a symbolic coefficient. A detail analysis is very laborious but it is presented some of the coefficients which are a function of the small signal parameters of the equivalent circuit such as transconductance, output resistance, based resistance, pi resistance, mu resistance and two parasitic capacitances and passive capacitors and resistors. The SPICE transistor model of high frequency transistor array is currently used so that the phase shift oscillator can be design to operating at the highest frequency of transition frequency by design of dc biasing according so that one can write the current consumption as a function of transition frequency. Complex pole-zero diagram is plotted against current consumption so that it can be seen how complex pole frequency is moving in the complex frequency plate and how it is transformed into imaginary pole as a function of the current consumption of the BJT transistor amplifier. If it is impossible for the designer to simulate the polynomial form of the BJT phase shift oscillator to have complex pole frequencies which have real part of the pole frequency approaching zero ohm. The negative resistance oscillator concept should be used to search for the input impedance matching circuit which can make this circuit oscillate to have any type of time domain periodic waveform.

INDEX TERMS BJT Microwave Oscillators, Voltage Controlled Oscillator, Bipolar transistor circuits, Bipolar integrated circuits, Impedance matching circuit, BJT Negative Resistance Oscillator

I. INTRODUCTION

The phase shift oscillator design was existed and published before 1941 [1]. The oscillator topology can be characterized as a resistance capacitance oscillator and as a resistance inductance oscillator. Since the time, the transistor topology was not existed even though a transistor was invented since the late 1940 because someone used tube amplifier which is connected with passive network in a phase shift oscillator topology. The resistance inductance oscillator is not a popular topology because it is bulky and expensive than a resistance capacitance oscillator. Since that time, the transfer function can be derived based on an application of the control theory which separates a phase shift oscillator circuit diagram into a network of passive circuit and an amplifier which composed of resistors and capacitors. The gain necessary for oscillation can be derived by determining the ratio of the output voltage and input voltage, then substituting a complex frequency s with $j\omega$ so that the denominator polynomial is transformed into symbolic complex number. The next step is to equate the symbolic real part and symbolic imaginary part with zero. Someone is derived oscillation frequency as a function of resistors and capacitors. The problem is that the tube amplifier equivalent circuit is not well described in that paper, instead it used Thevinin voltage source and serie source resistors to represent a tube amplifier. The following section briefly reviews a classical design concept of a phase shift oscillator. In section III, we present the matrix form of six nodal equations, the small signal parameters which is mixed with passive parameters in the phase shift oscillator circuit diagram can be group to make a new coefficient so that it can be written in a more compact matrix form, the input impedance of the BJT phase shift oscillator can be derived by a symbolic Gaussian elimination, by keeping only single node variable for each column and eliminating all other node variable for each column (for the same node voltage). The ratio of the input impedance can be derived in symbolic polynomial form. The section IV, we present the

graph of input impedance which is written as a basic program in MATLAB by using SPICE high frequency transistor model.

II. An Original Concept of a BJT Phase shift oscillator topolgy

There are four topologies of the phase shift oscillator in the original paper which is published since 1941 [1]. But this paper has four section of RC network which are composed of four capacitors and three resistors, the two bias resistors are not included in the RC network. It is described in [1] that the phase shift oscillator has a magnitude response or voltage gain and phase response of an amplifier stage and feedback stage which are written as a function of passive network. Its multiplication of the magnitude response of the amplifier and feedback network should be higher or equal to one while the addition of the phase response of the amplifier network and the passive network should be zero at an oscillation frequency.

After KCL is written by analyzing the circuit diagram of the phase shift oscillator. By assigning the direction of the current which should be flow from higher dc voltage to lower dc voltage. There are six nodes in this circuit diagram. Therefore, all of the equations in this circuit should be equal to six equations. The matrix which is a system of current equation at all nodes after group could not be written compactly without grouping which short variable names with subscript which are numbers.

$$\begin{bmatrix} -a_1 & a_2 & 0 & 0 & 0 & a_3 \\ a_4 & -a_5 & a_6 & 0 & 0 & 0 \\ 0 & a_7 & -a_8 & a_9 & 0 & 0 \\ 0 & 0 & a_{10} & -a_{11} & a_{12} & 0 \\ 0 & 0 & 0 & a_{13} & -a_{14} & a_{15} \\ a_{16} & 0 & 0 & 0 & a_{17} & -a_{18} \end{bmatrix} \begin{bmatrix} V_1 \\ V_2 \\ V_3 \\ V_4 \\ V_5 \\ V_6 \end{bmatrix} = \begin{bmatrix} -I_{in}R_6 \\ 0 \\ 0 \\ 0 \\ 0 \\ 0 \end{bmatrix} \quad (1)$$

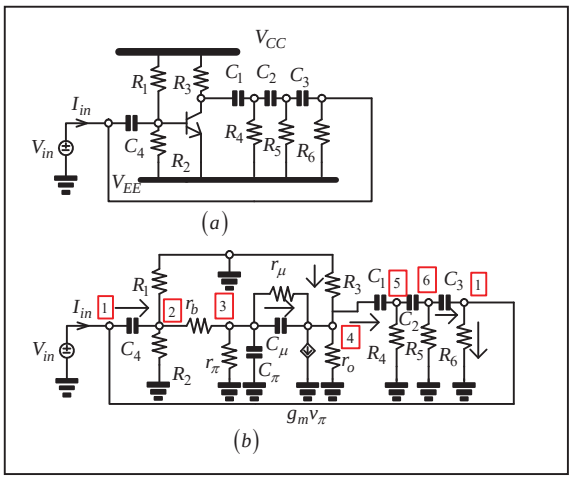

FIGURE 1. **A BJT Phase Shift Oscillator Circuit**

(a) A Circuit Diagram of A BJT Phase Shift Oscillator

(b) Equivalent circuit of A BJT Phase Shift Oscillator

All the coefficients in the matrix form of equation (1) can be defined as follows.

$$\begin{aligned} &a_1 = s(C_3 + C_4)R_6 + 1, a_2 = (sC_4R_6), a_3 = (sC_3R_6), a_4 = (sC_4) \\ &a_5 = \left[sC_4 + \left(\frac{1}{R_1} + \frac{1}{R_2} + \frac{1}{r_b} \right) \right] = \left[sC_4 + a_{52} \right] \\ &a_6 = \left(\frac{1}{r_b} \right), a_7 = \left[\frac{1}{r_b} \right], a_8 = \left[\frac{1}{r_b} + \frac{1}{r_\pi} + sC_\pi + \frac{1}{r_\mu} + sC_\mu \right] \\ &a_9 = \left[\frac{1}{r_\mu} + sC_\mu \right], a_{10} = \left[sC_\mu + \frac{1}{r_\mu} - g_m \right], a_{11} = \left[sC_\mu + \frac{1}{r_\mu} + \frac{1}{r_o} + sC_1 \right] \\ &a_{12} = sC_1, a_{13} = sC_1, a_{14} = \left[sC_1 + \frac{1}{R_4} + sC_2 \right] \\ &a_{15} = (sC_2), a_{16} = (sC_3), a_{17} = (sC_2), a_{18} = \left[sC_2 + \frac{1}{R_5} + sC_3 \right] \end{aligned} \quad (2)$$

III. An Input Impedance Analysis of A BJT Phase Shift Oscillator

By substituting the small signal high frequency equivalent circuit of a BJT transistor in figure 1(a). As a result, the whole circuit diagram of the small signal circuit of the BJT phase shift oscillator can be drawn in figure 1(b). It can be seen that the voltage source is injecting at node1 in figure 1(b). The total of 6 nodes can be counted and assigned in the equivalent circuit of figure 1(b). After performing the KCL at all nodes. The system of equations are written as a matrix in frequency domain, after admittance grouping are defined as the short coefficients as follows.

$$Z_{in} = \frac{V_1}{I_{in}} = \frac{f_{17}}{a_{17}} \quad (3)$$

The next step of an input impedance analysis of the BJT phase shift oscillator is to write a function of the node voltage V_1 of the first row of the matrix as a function of the other node voltage so that the same variable can be eliminated for the purpose of the next column has no recursive of the same variable in the first column when someone want to eliminate the variable V_2 with the second row equation which is written as a function of the other node voltage. The same procedure can be repeated until the last column has only one variable left. As a result, the derivation will be finished.

$$f_{17}=\left[f_{13}-\frac{f_{16}f_{14}}{f_{15}}\right],f_{16}=\left[f_{12}-\frac{f_9f_{10}}{f_7}\right],f_{15}=\left[\frac{f_8f_{10}}{f_7}+f_{11}\right]$$
$$f_{14}=\left[d_{15}-\frac{f_8d_{14}}{f_7}\right],f_{13}=\left(d_{13}+\frac{f_9d_{14}}{f_7}\right),f_{12}=\left[\frac{d_9d_{11}}{d_7}-d_{10}\right]$$
$$f_{11}=\left[-\frac{d_8d_{11}}{d_7}+d_{12}\right],f_{10}=\left[\frac{a_{12}d_{11}}{d_7}+a_{17}\right],f_9=\left[\frac{d_9a_{13}}{d_7}\right]$$
$$f_8=\left[\frac{d_8a_{13}}{d_7}+a_{15}\right],f_7=\left(\frac{a_{12}a_{13}}{d_7}+a_{14}\right),f_6=\left[b_{10}-\frac{d_9a_9}{d_7}\right] \quad (4)$$
$$f_5=\left[\frac{d_8a_9}{d_7}-b_{12}\right],f_4=\left(\frac{a_{12}a_9}{d_7}\right),f_3=\left[d_6-\frac{d_9d_4}{d_7}\right]$$
$$f_1=\left(\frac{a_{12}d_4}{d_7}\right),f_2=\left[\frac{d_8d_4}{d_7}+d_5\right]$$

All the intermediate coefficients are defined as an addition or negation of another intermediate coefficients as follows

$$d_1=\left[b_7+\frac{b_{10}b_8}{b_{11}}\right],d_2=\left(\frac{a_9b_8}{b_{11}}\right),d_3=\left[\frac{b_{12}b_8}{b_{11}}+b_9\right]$$
$$d_4=\left(\frac{a_9a_6}{b_{11}}\right),d_5=\left(b_3-\frac{b_{12}a_6}{b_{11}}\right),d_6=\left[\frac{b_{10}a_6}{b_{11}}-b_1\right]$$
$$d_7=\left[\frac{a_9a_{10}}{b_{11}}-a_{11}\right],d_8=\left(\frac{b_{12}a_{10}}{b_{11}}\right),d_9=\left(\frac{b_{10}a_{10}}{b_{11}}\right) \quad (5)$$
$$d_{10}=\left[b_{13}+\frac{b_{10}b_{14}}{b_{11}}\right],d_{11}=\left(\frac{a_9b_{14}}{b_{11}}\right),d_{12}=\left[b_{15}+\frac{b_{12}b_{14}}{b_{11}}\right]$$
$$d_{13}=\left(d_1-\frac{d_9d_2}{d_7}\right),d_{14}=\left(\frac{a_{12}d_2}{d_7}\right),d_{15}=\left(\frac{d_8d_2}{d_7}-d_3\right)$$

The parameter names d_i which are coefficients name in equation (5) can be written as a function of parameter names b_i and prior subscripts d_i as follows.

$$b_1=\left(\frac{R_6a_4}{a_1}\right),b_2=\left(\frac{a_2a_4}{a_1}-a_5\right),b_3=\left(\frac{a_3a_4}{a_1}\right)$$
$$b_4=\left(\frac{a_2a_{16}}{a_1}\right),b_5=\left(\frac{a_3a_{16}}{a_1}-a_{18}\right),b_6=\left(\frac{R_6a_{16}}{a_1}\right)$$
$$b_7=\left[R_6-\frac{b_1a_2}{b_2}\right],b_8=\left(\frac{a_6a_2}{b_2}\right),b_9=\left(a_3-\frac{b_3a_2}{b_2}\right) \quad (6)$$
$$b_{10}=\left(\frac{b_1a_7}{b_2}\right),b_{11}=\left(\frac{a_6a_7}{b_2}+a_8\right),b_{12}=\left(\frac{b_3a_7}{b_2}\right)$$
$$b_{13}=\left(b_6-\frac{b_1b_4}{b_2}\right),b_{14}=\left(\frac{a_6b_4}{b_2}\right),b_{15}=\left(b_5-\frac{b_3b_4}{b_2}\right)$$

After this step, the polynomial form can be manipulated by substituting the coefficients from equation (2) into equation (6). Then, some of the polynomial form of the coefficients can be substituting further into equation (5) for the next step.

$$d_1=\frac{\left(s^5g_{24}+s^4g_{25}+s^3g_{26}+s^2g_{27}-sg_{28}+g_{29}\right)}{\left[s^2g_1r_b^2-\left(sg_2r_b^2+a_{52}r_b^2\right)\right]\left[s^3g_{11}+s^2g_{12}+sg_{13}+g_{14}\right]}$$
$$g_{24}=\left(g_5g_{11}r_b^2\right),g_{25}=\left(g_5g_{12}r_b^2-g_2R_6g_{11}r_b^2\right),g_{26}=\left(g_5g_{13}r_b^2-g_2R_6g_{12}r_b^2-a_{52}R_6g_{11}r_b^2+R_6C_4g_6\right)$$
$$g_{27}=\left(g_5g_{14}r_b^2-g_2R_6g_{13}r_b^2-a_{52}R_6g_{12}r_b^2+R_6C_4g_7\right),g_{28}=\left(g_2R_6g_{14}r_b^2+a_{52}R_6g_{13}r_b^2\right),g_{29}=\left(a_{52}R_6g_{14}r_b^2\right)$$

(7.1)

$$d_2=\frac{\left(s^3g_{30}+s^2g_{31}+sg_{32}\right)}{\left(s^3g_{11}r_b+s^2g_{12}r_b+sg_{13}r_b+g_{14}r_b\right)}$$
$$g_{30}=C_\mu g_6,g_{31}=\left(C_\mu g_7+\frac{g_6}{r_\mu}\right),g_{32}=\left(\frac{g_7}{r_\mu}\right)$$

(7.2)

$$d_3=\frac{\left[s^6g_{33}+s^5g_{34}+s^4g_{35}+s^3g_{36}-s^2g_{37}-sg_{38}\right]}{\left(s^3g_{11}+s^2g_{12}+sg_{13}+g_{14}\right)\left(s^2g_1r_b-\left(sg_2r_b+a_{52}r_b\right)\right)}$$
$$g_{33}=\left(g_8r_bg_{11}\right),g_{34}=\left(g_8g_{12}r_b-g_9r_bg_{11}\right),g_{35}=\left(g_8g_{13}r_b-g_9g_{12}r_b-g_{10}r_bg_{11}+\left(C_3R_6C_4g_6\right)\right)$$
$$g_{36}=\left(g_8g_{14}r_b-g_9g_{13}r_b-g_{10}g_{12}r_b+\left(C_3R_6C_4g_7\right)\right),g_{37}=\left(g_9g_{14}r_b+g_{10}g_{13}r_b\right)$$
$$g_{38}=\left(g_{10}g_{14}r_b\right)$$

(7.3)

$$d_4=\frac{\left(s^3g_{39}+s^2g_{40}-sg_{41}-g_{42}\right)}{\left(s^3g_{11}+s^2g_{12}+sg_{13}+g_{14}\right)}$$
$$g_{39}=\left(\frac{C_\mu g_1}{r_b}\right),g_{40}=\left(\frac{g_1}{r_\mu r_b}-\frac{C_\mu g_2}{r_b}\right),g_{41}=\left(\frac{g_2}{r_\mu r_b}+\frac{C_\mu a_{52}}{r_b}\right),g_{42}=\frac{a_{52}}{r_\mu r_b}$$

(7.4)

$$d_5=\frac{s^2\left(C_3R_6\right)\left(C_4\right)}{\left(s^3g_{11}r_b^2+s^2g_{12}r_b^2+sg_{13}r_b^2+g_{14}r_b^2\right)}$$

(7.5)

$$d_6=\frac{-s^4g_{43}-s^3g_{44}-s^2g_{45}+sg_{46}}{\left(s^3g_{11}r_b^2+s^2g_{12}r_b^2+sg_{13}r_b^2+g_{14}r_b^2\right)\left[s\left(C_3+C_4\right)R_6+1\right]}$$
$$g_{43}=\left(R_6C_4g_{11}r_b^2\right),g_{44}=\left(R_6C_4g_{12}r_b^2\right),g_{45}=\left(R_6C_4g_{13}r_b^2\right),g_{46}=\left(R_6C_4\left(1-g_{14}r_b^2\right)\right)$$

(7.6)

$$d_7=\frac{\left[s^4g_{47}+s^3g_{48}+s^2g_{49}-sg_{50}-g_{51}\right]}{\left(s^3g_{11}+s^2g_{12}+sg_{13}+g_{14}\right)}$$
$$g_{47}=\left(C_\mu^2g_1-\left(g_{11}a_{11a}\right)\right),g_{48}=\begin{pmatrix}C_\mu\left(\frac{2}{r_\mu}-g_m\right)g_1-C_\mu^2g_2\\-\left(g_{11}a_{11b}+g_{12}a_{11a}\right)\end{pmatrix},g_{49}=\begin{pmatrix}\left(\frac{1}{r_\mu}\right)\left(\frac{1}{r_\mu}-g_m\right)g_1-C_\mu\left(\frac{2}{r_\mu}-g_m\right)g_2\\-C_\mu^2a_{52}-\left(g_{12}a_{11b}+g_{13}a_{11a}\right)\end{pmatrix}$$
$$g_{50}=\begin{pmatrix}C_\mu\left(\frac{2}{r_\mu}-g_m\right)a_{52}+\left(\frac{1}{r_\mu}\right)\left(\frac{1}{r_\mu}-g_m\right)g_2\\-\left(g_{13}a_{11b}+g_{14}a_{11a}\right)\end{pmatrix},g_{51}=\left[\left(\frac{1}{r_\mu}\right)\left(\frac{1}{r_\mu}-g_m\right)a_{52}+g_{14}a_{11b}\right]$$

(7.7)

$$d_8=\frac{s^3g_{52}+s^2g_{53}}{\left(s^3g_{11}r_b+s^2g_{12}r_b+sg_{13}r_b+g_{14}r_b\right)}$$
$$g_{52}=\left(C_3R_6C_4C_\mu\right),g_{53}=\left(C_3R_6C_4\left(\frac{1}{r_\mu}-g_m\right)\right)$$

(7.8)

$$d_9=\frac{sC_4R_6\left(sC_\mu+\frac{1}{r_\mu}-g_m\right)}{\left(s^3g_{11}r_b+s^2g_{12}r_b+sg_{13}r_b+g_{14}r_b\right)}=\frac{s^2g_{54}+sg_{55}}{\left(s^3g_{11}r_b+s^2g_{12}r_b+sg_{13}r_b+g_{14}r_b\right)}$$

$$g_{54}=\left(C_4C_\mu R_6\right),g_{55}=\left(C_4R_6\left(\frac{1}{r_\mu}-g_m\right)\right)$$

(7.9)

$$d_{10}=\frac{\left(-s^6g_{56}+s^5g_{57}+s^4g_{58}+s^3g_{59}+s^2g_{60}+sg_{61}\right)}{\left[s\left(C_3+C_4\right)R_6+1\right]\left(s^2g_1r_b-s\left(g_2r_b\right)+\left(a_{52}r_b\right)\right)\left(s^3g_{11}+s^2g_{12}+sg_{13}+g_{14}\right)}$$

$$g_{56}=\left(g_{15}r_bg_{11}\right),g_{57}=\left(g_{16}r_bg_{11}-g_{15}r_bg_{12}\right),g_{58}=\left(g_{17}r_bg_{11}+g_{16}r_bg_{12}-g_{15}r_bg_{13}+\left(R_6^2C_4g_{18}\left(C_3+C_4\right)\right)\right)$$

$$g_{59}=\left(-g_{15}r_bg_{14}+g_{16}r_bg_{13}+g_{17}r_bg_{12}+\left(R_6C_4g_{18}\right)\right),g_{60}=\left(g_{16}r_bg_{14}+g_{17}r_bg_{13}\right),g_{61}=\left(g_{17}r_bg_{14}\right)$$

(7.10)

$$d_{11}=\frac{s^3\left(C_\mu g_{18}\right)+s^2\left(\frac{g_{18}}{r_\mu}\right)}{\left(s^3g_{11}+s^2g_{12}+sg_{13}+g_{14}\right)}$$

(7.11)

$$d_{12}=\frac{\left(s^7g_{62}+s^6g_{63}+s^5g_{64}+s^4g_{65}+s^3g_{66}+s^2g_{67}+sg_{68}+g_{69}\right)}{\left[s\left(C_3+C_4\right)R_6+1\right]\left(s^2g_1r_b-\left(sg_2r_b+a_{52}r_b\right)\right)\left(s^3g_{11}+s^2g_{12}+sg_{13}+g_{14}\right)}$$

$$g_{62}=\left(g_{19}r_bg_{11}\right),g_{63}=\left(g_{19}r_bg_{12}-g_{20}r_bg_{11}\right),g_{64}=\left(g_{19}r_bg_{13}-g_{20}r_bg_{12}+g_{21}r_bg_{11}+\left(C_3+C_4\right)R_6C_3R_6C_4g_{18}\right)$$

$$g_{65}=\left(g_{19}r_bg_{14}-g_{20}r_bg_{13}+g_{21}r_bg_{12}+g_{22}r_bg_{11}+C_3R_6C_4g_{18}\right)$$

$$g_{66}=\left(-g_{20}r_bg_{14}+g_{21}r_bg_{13}+g_{22}r_bg_{12}+g_{23}r_bg_{11}\right)$$

$$g_{67}=\left(g_{21}r_bg_{14}+g_{22}r_bg_{13}+g_{23}r_bg_{12}\right),g_{68}=\left(g_{22}r_bg_{14}+g_{23}r_bg_{13}\right),g_{69}=\left(g_{23}r_bg_{14}\right)$$

(7.12)

$$d_{13}=\frac{\left[s^9g_{70}+s^8g_{71}+s^7g_{72}+s^6g_{73}+s^5g_{74}+s^4g_{75}+s^3g_{76}+s^2g_{77}+s^1g_{78}-g_{79}\right]}{\left[s^2g_1r_b^2-\left(sg_2r_b^2+a_{52}r_b^2\right)\right]\left[s^3g_{11}+s^2g_{12}+sg_{13}+g_{14}\right]\left[s^4g_{47}+s^3g_{48}+s^2g_{49}-sg_{50}-g_{51}\right]}$$

$$g_{70}=\left(g_{24}g_{47}\right),g_{71}=\left(g_{24}g_{48}+g_{25}g_{47}\right),g_{72}=\left(g_{24}g_{49}-g_{25}g_{48}-g_{26}g_{47}\right)$$

$$g_{73}=\left(-g_{24}g_{50}+g_{25}g_{49}+g_{26}g_{48}+g_{27}g_{47}\right),g_{74}=\left(-g_{24}g_{51}-g_{25}g_{50}+g_{26}g_{49}+g_{27}g_{48}-g_{28}g_{47}\right)$$

$$g_{75}=\left(-g_{25}g_{51}-g_{26}g_{50}+g_{27}g_{49}-g_{28}g_{48}+g_{29}g_{47}\right),g_{76}=\left(-g_{26}g_{51}-g_{27}g_{50}-g_{28}g_{49}+g_{29}g_{48}\right)$$

$$g_{77}=\left(-g_{27}g_{51}-g_{28}g_{50}+g_{29}g_{49}\right),g_{78}=\left(+g_{28}g_{51}-g_{29}g_{50}\right),g_{79}=g_{29}g_{51}$$

(7.13)

$$d_{14}=\left(\frac{a_{12}d_2}{d_7}\right)=\left(\frac{\frac{\left(s^3g_{30}+s^2g_{31}+sg_{32}\right)sC_1}{\left(s^3g_{11}r_b+s^2g_{12}r_b+sg_{13}r_b+g_{14}r_b\right)}}{\frac{\left[s^4g_{47}+s^3g_{48}+s^2g_{49}-sg_{50}-g_{51}\right]}{\left(s^3g_{11}+s^2g_{12}+sg_{13}+g_{14}\right)}}\right)=\frac{\left(s^4\left(g_{30}C_1\right)+s^3\left(g_{31}C_1\right)+s^2\left(g_{32}C_1\right)\right)}{\left[s^4g_{47}r_b+s^3g_{48}r_b+s^2g_{49}r_b-sg_{50}r_b-g_{51}r_b\right]}$$

(7.14)

$$d_{15}=\left[\frac{\left(-\left(s^{10}g_{80}+s^9g_{81}\right)-s^8g_{82}+s^7g_{83}+s^6g_{84}+s^5g_{85}+s^4g_{86}-s^3g_{87}-s^2g_{88}-sg_{89}\right)}{\left[s^4g_{47}r_b+s^3g_{48}r_b+s^2g_{49}r_b-sg_{50}r_b-g_{51}r_b\right]\left(s^3g_{11}r_b+s^2g_{12}r_b+sg_{13}r_b+g_{14}r_b\right)\left(s^2g_1-\left(sg_2+a_{52}\right)\right)}\right]$$

$$g_{80}=\left(g_{47}g_{33}\right),g_{81}=\left(g_{47}g_{34}+g_{48}g_{33}\right),g_{82}=\left(g_{52}g_{30}g_1+\left(g_{47}g_{35}+g_{48}g_{34}+g_{49}g_{33}\right)\right)$$

$$g_{83}=\left(g_{52}g_{31}g_1+g_{53}g_{30}g_1-\left(g_{52}g_{30}g_2\right)-\left(g_{47}g_{36}+g_{48}g_{35}+g_{49}g_{34}-g_{50}g_{33}\right)\right)$$

$$g_{84}=\left(-g_{52}g_{30}a_{52}-\left(g_{52}g_{31}+g_{53}g_{30}\right)g_2+\left(g_{52}g_{32}+g_{53}g_{31}\right)g_1-\left(-g_{47}g_{37}+g_{48}g_{36}+g_{49}g_{35}-g_{50}g_{34}-g_{51}g_{33}\right)\right)$$

$$g_{85}=\left(-\left(g_{52}g_{31}+g_{53}g_{30}\right)a_{52}-\left(g_{52}g_{32}+g_{53}g_{31}\right)g_2+\left(g_{53}g_{32}\right)g_1-\left(-g_{47}g_{38}-g_{48}g_{37}+g_{49}g_{34}-g_{50}g_{35}-g_{51}g_{34}\right)\right)$$

$$g_{86}=\left(-\left(g_{52}g_{32}+g_{53}g_{31}\right)a_{52}-\left(g_{53}g_{32}\right)g_2-\left(-g_{48}g_{38}-g_{49}g_{37}-g_{50}g_{36}-g_{51}g_{35}\right)\right)$$

$$g_{87}=\left(g_{53}g_{32}a_{52}+\left(-g_{49}g_{38}+g_{50}g_{37}-g_{51}g_{36}\right)\right)$$

$$g_{88}=\left(-g_{50}g_{38}+g_{51}g_{37}\right),g_{89}=\left(g_{51}g_{38}\right)$$

(7.15)

The intermediate coefficients f_i can be manipulated as a polynomial form as follows

$$f_1=\left(\frac{a_{12}d_4}{d_7}\right)=\frac{\frac{\left(sC_1\right)\frac{\left(s^3g_{39}+s^2g_{40}-sg_{41}-g_{42}\right)}{\left(s^3g_{11}+s^2g_{12}+sg_{13}+g_{14}\right)}}{\frac{\left[s^4g_{47}+s^3g_{48}+s^2g_{49}-sg_{50}-g_{51}\right]}{\left(s^3g_{11}+s^2g_{12}+sg_{13}+g_{14}\right)}}=\frac{\left(s^4\left(C_1g_{39}\right)+s^3\left(C_1g_{40}\right)-s^2\left(C_1g_{41}\right)-s\left(C_1g_{42}\right)\right)}{\left[s^4g_{47}+s^3g_{48}+s^2g_{49}-sg_{50}-g_{51}\right]}$$

(8.1)

$$f_2=\frac{\left[s^6g_{90}+s^5g_{91}+s^4g_{92}+s^3g_{93}-s^2g_{94}\right]}{\left(s^3g_{11}r_b^2+s^2g_{12}r_b^2+sg_{13}r_b^2+g_{14}r_b^2\right)\left[s^4g_{47}+s^3g_{48}+s^2g_{49}-sg_{50}-g_{51}\right]}$$

$$g_{90}=\left(g_{52}r_bg_{39}+\left(g_{47}C_3R_6C_4\right)\right),g_{91}=\left(g_{52}r_bg_{40}+g_{53}r_bg_{39}+\left(g_{48}C_3R_6C_4\right)\right),g_{92}=\left(g_{53}r_bg_{40}-g_{52}r_bg_{41}+\left(g_{49}C_3R_6C_4\right)\right)$$

$$g_{93}=\left(-g_{52}r_bg_{42}-g_{53}r_bg_{41}-\left(g_{50}C_3R_6C_4\right)\right),g_{94}=\left(g_{53}r_bg_{42}+g_{51}C_3R_6C_4\right)$$

(8.2)

$$f_3=\frac{\left(-s^8g_{95}-s^7g_{96}-s^6g_{108}+s^5g_{109}+s^4g_{110}+s^3g_{111}+s^2g_{112}-sg_{113}\right)}{\left(s^3g_{11}r_b^2+s^2g_{12}r_b^2+sg_{13}r_b^2+g_{14}r_b^2\right)\left[s\left(C_3+C_4\right)R_6+1\right]\left[s^4g_{47}+s^3g_{48}+s^2g_{49}-sg_{50}-g_{51}\right]}$$

$$g_{108}=\left(g_{97}+g_{103}g_{54}\right),g_{109}=\left(g_{98}-\left(g_{103}g_{55}+g_{104}g_{54}\right)\right),g_{110}=\left(g_{99}-\left(g_{104}g_{55}+g_{105}g_{54}\right)\right)$$

$$g_{111}=\left(g_{100}-\left(g_{105}g_{55}+g_{106}g_{54}\right)\right),g_{112}=\left(g_{101}-\left(g_{106}g_{55}-g_{107}g_{54}\right)\right),g_{113}=\left(g_{102}-\left(g_{107}g_{55}\right)\right)$$

(8.3)

$$f_4=\frac{\left[s^5g_{114}+s^4g_{115}+s^3g_{116}+s^2g_{117}+sg_{118}\right]}{\left[s^4g_{47}+s^3g_{48}+s^2g_{49}-sg_{50}-g_{51}\right]}$$

$$g_{114}=\left(C_1C_\mu g_{11}\right),g_{115}=\left(C_1C_\mu g_{12}+\frac{C_1g_{11}}{r_\mu}\right),g_{116}=\left(C_1C_\mu g_{13}+\frac{C_1g_{12}}{r_\mu}\right),g_{117}=\left(C_1C_\mu g_{14}+\frac{C_1g_{13}}{r_\mu}\right),g_{118}=\left(\frac{C_1g_{14}}{r_\mu}\right)$$

(8.4)

$$f_5=\left[\frac{\left[s^6g_{119}+s^5g_{120}+s^4g_{121}+s^3g_{122}-s^2g_{123}\right]}{\left[s^4g_{47}+s^3g_{48}+s^2g_{49}-sg_{50}-g_{51}\right]\left(s^2g_1r_b-\left(sg_2r_b+a_{52}r_b\right)\right)}\right]$$

$$g_{119}=\left(g_{52}C_\mu g_1-\left(C_3R_6C_4g_{47}\right)\right),g_{120}=\left(g_{53}C_\mu g_1+\frac{g_{52}g_1}{r_\mu}-\left(g_{52}C_\mu g_2\right)-\left(C_3R_6C_4g_{48}\right)\right)$$

$$g_{121}=\left(\left(\frac{g_{53}g_1}{r_\mu}\right)-\left(g_{53}C_\mu+\frac{g_{52}}{r_\mu}\right)g_2-\left(g_{52}C_\mu a_{52}\right)-\left(C_3R_6C_4g_{49}\right)\right),g_{122}=\left(-\left(\frac{g_{53}g_2}{r_\mu}\right)-\left(g_{53}C_\mu+\frac{g_{52}}{r_\mu}\right)a_{52}+\left(C_3R_6C_4g_{50}\right)\right)$$

$$g_{123}=\left(\frac{g_{53}a_{52}}{r_\mu}-\left(C_3R_6C_4g_{51}\right)\right)$$

(8.5)

$$f_6=\frac{\left[s^5g_{124}+s^4g_{125}+s^3g_{126}+s^2g_{127}+sg_{128}\right]}{\left[s^2g_1r_b-s\left(g_2r_b\right)+\left(a_{52}r_b\right)\right]\left[s^4g_{47}+s^3g_{48}+s^2g_{49}-sg_{50}-g_{51}\right]}$$

$$g_{124}=\left(R_6C_4g_{47}-\left(g_1g_{54}C_\mu\right)\right),g_{125}=\left(R_6C_4g_{48}-\left(\left(g_1g_{55}-g_2g_{54}\right)C_\mu+\frac{\left(g_1g_{54}\right)}{r_\mu}\right)\right)$$

$$g_{126}=\left(R_6C_4g_{49}-\left(\frac{\left(g_1g_{55}-g_2g_{54}\right)}{r_\mu}+\left(a_{52}g_{54}-g_2g_{55}\right)C_\mu\right)\right)$$

$$g_{127}=\left(\left(\frac{\left(a_{52}g_{54}-g_2g_{55}\right)}{r_\mu}+\left(a_{52}g_{55}\right)C_\mu\right)-R_6C_4g_{50}\right),g_{128}=\left(\left(\frac{a_{52}g_{55}}{r_\mu}\right)-R_6C_4g_{51}\right)$$

(8.6)

$$f_7=\frac{\left[s^6k_1+s^5k_2+s^4k_3+s^3k_4+s^2k_5-sk_6-k_7\right]}{\left[s^4g_{47}+s^3g_{48}+s^2g_{49}-sg_{50}-g_{51}\right]}$$

$$k_1=\left(C_1C_2g_{47}\right),k_2=\left(C_1C_2g_{48}+C_1^2g_{11}\right)$$

$$k_3=\left(C_1C_2g_{49}+\frac{g_{47}}{R_4}+C_1^2g_{12}\right),k_4=\left(-C_1C_2g_{50}+\frac{g_{48}}{R_4}+C_1^2g_{13}\right)$$

$$k_5=\left(-C_1C_2g_{51}+\frac{g_{49}}{R_4}+C_1^2g_{14}\right),k_6=\left(\frac{g_{50}}{R_4}\right),k_7=\left(\frac{g_{51}}{R_4}\right)$$

(8.7)

$$f_8=\frac{\left(s^5g_{129}+s^4g_{130}+s^3g_{131}-s^2g_{132}-sg_{133}\right)}{\left[s^4g_{47}r_b+s^3g_{48}r_b+s^2g_{49}r_b-sg_{50}r_b-g_{51}r_b\right]}$$
$$g_{129}=\left(g_{47}r_bC_2\right),g_{130}=\left(g_{48}r_bC_2+\left(g_{52}C_1\right)\right)$$
$$g_{131}=\left(g_{49}r_bC_2+\left(g_{53}C_1\right)\right),g_{132}=\left(g_{50}r_bC_2\right),g_{133}=\left(g_{51}r_bC_2\right)$$

(8.8)

$$f_9=\frac{\left(s^3\left(g_{54}C_1\right)+s^2\left(g_{55}C_1\right)\right)}{\left[s^4g_{47}r_b+s^3g_{48}r_b+s^2g_{49}r_b-sg_{50}r_b-g_{51}r_b\right]}$$

(8.9)

$$f_{10}=\frac{\left(s^5g_{134}+s^4g_{135}+s^3g_{136}-s^2g_{137}-sg_{138}\right)}{\left[s^4g_{47}+s^3g_{48}+s^2g_{49}-sg_{50}-g_{51}\right]}$$
$$g_{134}=\left(g_{47}C_2\right),g_{135}=\left(g_{48}C_2+\left(C_1C_\mu g_{18}\right)\right),g_{136}=\left(g_{49}C_2+\left(\frac{C_1g_{18}}{r_\mu}\right)\right),g_{137}=\left(g_{50}C_2\right),g_{138}=\left(g_{51}C_2\right)$$

(8.11)

$$f_{11}=\frac{\left[\begin{array}{l}s^{14}g_{157}+s^{13}g_{158}+s^{12}g_{159}+s^{11}g_{160}+s^{10}g_{161}+s^9g_{162}+s^8g_{163}+s^7g_{164}\\+s^6g_{165}+s^5g_{166}+s^4g_{167}+s^3g_{168}+s^2g_{169}+sg_{170}-g_{171}\end{array}\right]}{\left[\begin{array}{l}\left(s^3g_{11}r_b+s^2g_{12}r_b+sg_{13}r_b+g_{14}r_b\right)\left[s^4g_{47}+s^3g_{48}+s^2g_{49}-sg_{50}-g_{51}\right]\\\times\left[s\left(C_3+C_4\right)R_6+1\right]\left(s^2g_1r_b-\left(sg_2r_b+a_{52}r_b\right)\right)\end{array}\right]}$$
$$g_{139}=\left(g_{52}C_\mu g_{18}\right),g_{140}=\left(\frac{g_{52}g_{18}}{r_\mu}+g_{53}C_\mu g_{18}\right),g_{141}=\left(\frac{g_{53}g_{18}}{r_\mu}\right)$$
$$g_{142}=\left(\left(C_3+C_4\right)R_6g_1r_b\right),g_{143}=\left(g_1r_b-\left(C_3+C_4\right)R_6g_2r_b\right)$$
$$g_{144}=\left(\left(C_3+C_4\right)R_6a_{52}r_b+g_2r_b\right),g_{145}=a_{52}r_b$$
$$g_{146}=\left(g_{62}g_{11}r_b\right),g_{147}=\left(g_{62}g_{12}r_b+g_{63}g_{11}r_b\right)$$
$$g_{148}=\left(g_{62}g_{13}r_b+g_{63}g_{12}r_b+g_{64}g_{11}r_b\right)$$
$$g_{149}=\left(g_{62}g_{14}r_b+g_{63}g_{13}r_b+g_{64}g_{12}r_b+g_{65}g_{11}r_b\right)$$
$$g_{150}=\left(g_{63}g_{14}r_b+g_{64}g_{13}r_b+g_{65}g_{12}r_b+g_{66}g_{11}r_b\right)$$
$$g_{151}=\left(g_{64}g_{14}r_b+g_{65}g_{13}r_b+g_{66}g_{12}r_b+g_{67}g_{11}r_b\right)$$
$$g_{152}=\left(g_{65}g_{14}r_b+g_{66}g_{13}r_b+g_{67}g_{12}r_b+g_{68}g_{11}r_b\right)$$
$$g_{153}=\left(g_{66}g_{14}r_b+g_{67}g_{13}r_b+g_{68}g_{12}r_b+g_{69}g_{11}r_b\right)$$
$$g_{154}=\left(g_{67}g_{14}r_b+g_{68}g_{13}r_b+g_{69}g_{12}r_b\right)$$
$$g_{155}=\left(g_{68}g_{14}r_b+g_{69}g_{13}r_b\right),g_{156}=\left(g_{69}g_{14}r_b\right)$$
$$g_{157}=\left(g_{146}g_{47}\right),g_{158}=\left(g_{146}g_{48}+g_{147}g_{47}\right)$$
$$g_{159}=\left(g_{146}g_{49}+g_{147}g_{48}+g_{148}g_{47}\right)$$
$$g_{160}=\left(-g_{146}g_{50}+g_{147}g_{49}+g_{148}g_{48}+g_{149}g_{47}\right)$$

(8.12)

$$g_{161}=\left(-g_{146}g_{51}-g_{147}g_{50}+g_{148}g_{49}+g_{149}g_{48}+g_{150}g_{47}\right)$$
$$g_{162}=\left(-g_{147}g_{51}-g_{148}g_{50}+g_{149}g_{49}+g_{150}g_{48}+g_{151}g_{47}-\left(g_{139}g_{142}\right)\right)$$
$$g_{163}=\left(-g_{148}g_{51}-g_{149}g_{50}+g_{150}g_{49}+g_{151}g_{48}+g_{152}g_{47}-\left(g_{139}g_{143}+g_{140}g_{142}\right)\right)$$
$$g_{164}=\left(-g_{149}g_{51}-g_{150}g_{50}+g_{151}g_{49}+g_{152}g_{48}+g_{153}g_{47}-\left(g_{141}g_{142}+g_{140}g_{143}-g_{139}g_{144}\right)\right)$$
$$g_{165}=\left(-g_{150}g_{51}-g_{151}g_{50}+g_{152}g_{49}+g_{153}g_{48}+g_{154}g_{47}-\left(-g_{139}g_{145}-g_{140}g_{144}+g_{141}g_{143}\right)\right)$$
$$g_{166}=\left(-g_{151}g_{51}-g_{152}g_{50}+g_{153}g_{49}+g_{154}g_{48}+g_{155}g_{47}-\left(-g_{140}g_{145}-g_{141}g_{144}\right)\right)$$
$$g_{167}=\left(-g_{152}g_{51}-g_{153}g_{50}+g_{154}g_{49}+g_{155}g_{48}+g_{156}g_{47}+\left(g_{141}g_{145}\right)\right)$$
$$g_{168}=\left(-g_{153}g_{51}-g_{154}g_{50}+g_{155}g_{49}+g_{156}g_{48}\right)$$
$$g_{169}=\left(-g_{154}g_{51}-g_{155}g_{50}+g_{156}g_{49}\right)$$
$$g_{170}=\left(-g_{155}g_{51}-g_{156}g_{50}\right),g_{171}=\left(g_{156}g_{51}\right)$$

(8.13)

$$f_{12}=\left(\begin{array}{l}\left(\begin{array}{l}-s^{10}g_{179}-s^9g_{180}+s^8g_{189}+s^7g_{190}+s^6g_{191}\\+s^5g_{192}+s^4g_{193}+s^3g_{194}-s^2g_{187}+sg_{188}\end{array}\right)\\\left(s^3g_{11}r_b+s^2g_{12}r_b+sg_{13}r_b+g_{14}r_b\right)\\\times\left[s^4g_{47}+s^3g_{48}+s^2g_{49}-sg_{50}-g_{51}\right]\\\times\left[s\left(C_3+C_4\right)R_6+1\right]\left(s^2g_1-s\left(g_2\right)+\left(a_{52}\right)\right)\end{array}\right)$$
$$g_{172}=\left(g_{54}C_\mu g_{18}\right),g_{173}=\left(\frac{g_{54}g_{18}}{r_\mu}+g_{55}C_\mu g_{18}\right)$$
$$g_{174}=\left(\frac{g_{55}g_{18}}{r_\mu}\right),g_{175}=\left(\left(C_3+C_4\right)R_6+1\right)g_1$$
$$g_{176}=\left(g_1-\left(C_3+C_4\right)R_6g_2\right),g_{177}=\left(\left(C_3+C_4\right)R_6a_{52}-g_2\right)$$
$$g_{178}=a_{52}=\left(\frac{1}{R_1}+\frac{1}{R_2}+\frac{1}{r_b}\right)$$
$$g_{179}=\left(g_{56}g_{47}\right),g_{180}=\left(g_{57}g_{47}-g_{56}g_{48}\right)$$
$$g_{181}=\left(g_{57}g_{48}+g_{58}g_{47}-g_{56}g_{49}\right)$$
$$g_{182}=\left(g_{57}g_{49}+g_{58}g_{48}+g_{59}g_{47}+g_{56}g_{50}\right)$$
$$g_{183}=\left(g_{56}g_{51}-g_{57}g_{50}+g_{58}g_{49}+g_{59}g_{48}+g_{60}g_{47}\right)$$
$$g_{184}=\left(-g_{57}g_{51}-g_{58}g_{50}+g_{59}g_{49}+g_{60}g_{48}+g_{61}g_{47}\right)$$
$$g_{185}=\left(-g_{58}g_{51}-g_{59}g_{50}+g_{60}g_{49}+g_{61}g_{48}\right)$$
$$g_{186}=\left(-g_{59}g_{51}-g_{60}g_{50}+g_{61}g_{49}\right)$$
$$g_{187}=\left(-g_{60}g_{51}-g_{61}g_{50}\right),g_{188}=\left(g_{61}g_{51}\right)$$
$$g_{189}=\left(g_{172}g_{175}-g_{181}\right),g_{190}=\left(g_{172}g_{176}+g_{173}g_{175}-g_{182}\right)$$
$$g_{191}=\left(g_{172}g_{177}+g_{173}g_{176}+g_{174}g_{175}-g_{183}\right)$$
$$g_{192}=\left(g_{172}g_{178}+g_{173}g_{177}+g_{174}g_{176}-g_{184}\right)$$
$$g_{193}=\left(g_{173}g_{178}+g_{174}g_{177}-g_{185}\right),g_{194}=\left(g_{174}g_{178}-g_{186}\right)$$

(8.14)

$$f_{13}=\frac{\left[\begin{array}{l}s^{15}g_{195}+s^{14}g_{196}+s^{13}g_{197}+s^{12}g_{221}+s^{11}g_{222}+s^{10}g_{223}+s^9g_{224}+s^8g_{225}\\+s^7g_{226}+s^6g_{227}+s^5g_{228}+s^4g_{229}+s^3g_{207}+s^2g_{208}+sg_{209}+g_{210}\end{array}\right]}{\left[\begin{array}{l}\left[s^2g_1r_b^2-\left(sg_2r_b^2+a_{52}r_b^2\right)\right]\left[s^3g_{11}+s^2g_{12}+sg_{13}+g_{14}\right]\\\times\left[s^4g_{47}r_b+s^3g_{48}r_b+s^2g_{49}r_b-sg_{50}r_b-g_{51}r_b\right]\left[\begin{array}{l}s^6k_1r_b+s^5k_2r_b+s^4k_3r_b+s^3k_4r_b\\+s^2k_5r_b-sk_6r_b-k_7r_b\end{array}\right]\end{array}\right]}$$

(8.15)

$$g_{195}=\left(g_{70}r_bk_1r_b\right),g_{196}=\left(g_{70}r_bk_2r_b+g_{71}r_bk_1r_b\right),g_{197}=\left(g_{70}r_bk_3r_b+g_{71}r_bk_2r_b+g_{72}r_bk_1r_b\right)$$
$$g_{198}=\left(g_{70}r_bk_4r_b+g_{71}r_bk_3r_b+g_{72}r_bk_2r_b+g_{73}r_bk_1r_b\right),g_{199}=\left(g_{70}r_bk_5r_b+g_{71}r_bk_4r_b+g_{72}r_bk_3r_b+g_{73}r_bk_2r_b+g_{74}r_bk_1r_b\right)$$
$$g_{200}=\left(-g_{70}r_bk_6r_b+g_{71}r_bk_5r_b+g_{72}r_bk_4r_b+g_{73}r_bk_3r_b+g_{74}r_bk_2r_b+g_{75}r_bk_1r_b\right)$$
$$g_{201}=\left(-g_{70}r_bk_7r_b-g_{71}r_bk_6r_b+g_{72}r_bk_5r_b+g_{73}r_bk_4r_b+g_{74}r_bk_3r_b+g_{75}r_bk_2r_b+g_{76}r_bk_1r_b\right)$$
$$g_{202}=\left(-g_{71}r_bk_7r_b-g_{72}r_bk_6r_b+g_{73}r_bk_5r_b+g_{74}r_bk_4r_b+g_{75}r_bk_3r_b+g_{76}r_bk_2r_b+g_{77}r_bk_1r_b\right)$$
$$g_{203}=\left(-g_{72}r_bk_7r_b-g_{73}r_bk_6r_b+g_{74}r_bk_5r_b+g_{75}r_bk_4r_b+g_{76}r_bk_3r_b+g_{77}r_bk_2r_b+g_{78}r_bk_1r_b\right)$$
$$g_{204}=\left(-g_{73}r_bk_7r_b-g_{74}r_bk_6r_b+g_{75}r_bk_5r_b+g_{76}r_bk_4r_b+g_{77}r_bk_3r_b+g_{78}r_bk_2r_b-g_{79}r_bk_1r_b\right)$$
$$g_{205}=\left(-g_{74}r_bk_7r_b-g_{75}r_bk_6r_b+g_{76}r_bk_5r_b+g_{77}r_bk_4r_b+g_{78}r_bk_3r_b-g_{79}r_bk_2r_b\right)$$
$$g_{206}=\left(-g_{75}r_bk_7r_b-g_{76}r_bk_6r_b+g_{77}r_bk_5r_b+g_{78}r_bk_4r_b-g_{79}r_bk_3r_b\right)$$
$$g_{207}=\left(-g_{76}r_bk_7r_b-g_{77}r_bk_6r_b+g_{78}r_bk_5r_b-g_{79}r_bk_4r_b\right)$$
$$g_{208}=\left(-g_{77}r_bk_7r_b-g_{78}r_bk_6r_b-g_{79}r_bk_5r_b\right),g_{209}=\left(-g_{78}r_bk_7r_b+g_{79}r_bk_6r_b\right),g_{210}=\left(g_{79}r_bk_7r_b\right)$$
$$g_{211}=\left(g_{54}C_1^2g_{30}\right),g_{212}=\left(g_{54}C_1^2g_{31}+g_{55}C_1^2g_{30}\right),g_{213}=\left(g_{54}C_1^2g_{32}+g_{55}C_1^2g_{31}\right)$$
$$g_{214}=\left(g_{55}C_1^2g_{32}\right),g_{215}=\left(g_1r_b^2g_{11}\right),g_{216}=\left(g_1r_b^2g_{12}-g_2r_b^2g_{11}\right),g_{217}=\left(g_1r_b^2g_{13}-g_2r_b^2g_{12}-a_{52}r_b^2g_{11}\right)$$
$$g_{218}=\left(g_1r_b^2g_{14}-g_2r_b^2g_{13}-a_{52}r_b^2g_{12}\right),g_{219}=\left(-g_2r_b^2g_{14}-a_{52}r_b^2g_{13}\right),g_{220}=\left(a_{52}r_b^2g_{14}\right)$$
$$g_{221}=\left(g_{198}+\left(g_{211}g_{215}\right)\right),g_{222}=\left(g_{199}+\left(g_{211}g_{216}+g_{212}g_{215}\right)\right),g_{223}=\left(g_{200}+\left(g_{211}g_{217}+g_{212}g_{216}+g_{213}g_{215}\right)\right)$$
$$g_{224}=\left(g_{201}+\left(g_{211}g_{218}+g_{212}g_{217}+g_{213}g_{216}+g_{214}g_{215}\right)\right),g_{225}=\left(g_{202}+\left(g_{211}g_{219}+g_{212}g_{218}+g_{213}g_{217}+g_{214}g_{216}\right)\right)$$
$$g_{226}=\left(g_{203}+\left(-g_{211}g_{220}+g_{212}g_{219}+g_{213}g_{218}+g_{214}g_{217}\right)\right),g_{227}=\left(g_{204}+\left(-g_{212}g_{220}+g_{213}g_{219}+g_{214}g_{218}\right)\right)$$
$$g_{228}=\left(g_{205}+\left(-g_{213}g_{220}+g_{214}g_{219}\right)\right),g_{229}=\left(g_{206}-\left(g_{214}g_{220}\right)\right)$$

(8.16)

$$f_{14}=\left[\frac{\begin{bmatrix}-s^{16}(g_{230})-s^{15}(g_{231})-s^{14}(g_{259})-s^{13}(g_{260})-s^{12}(g_{261})+s^{11}(g_{262})+s^{10}(g_{263})+s^{9}(g_{264})\\+s^{8}(g_{265})+s^{7}(g_{266})+s^{6}(g_{267})+s^{5}(g_{268})+s^{4}(g_{269})+s^{3}(g_{270})+s^{2}g_{244}+sg_{245}\end{bmatrix}}{\left(\begin{bmatrix}s^{4}g_{47}r_b+s^{3}g_{48}r_b+s^{2}g_{49}r_b\\-sg_{50}r_b-g_{51}r_b\end{bmatrix}\left(s^{3}g_{11}r_b+s^{2}g_{12}r_b+sg_{13}r_b+g_{14}r_b\right)\times\left(s^{2}g_1-(sg_2+a_{52})\right)\begin{bmatrix}s^{6}k_1r_b+s^{5}k_2r_b+s^{4}k_3r_b+s^{3}k_4r_b\\+s^{2}k_5r_b-sk_6r_b-k_7r_b\end{bmatrix}\right)}\right]$$

$g_{230}=(g_{80}k_1r_b),g_{231}=(g_{80}k_2r_b+g_{81}k_1r_b),g_{232}=(g_{80}k_3r_b+g_{81}k_2r_b+g_{82}k_1r_b)$
$g_{233}=(g_{80}k_4r_b+g_{81}k_3r_b+g_{82}k_2r_b-g_{83}k_1r_b),g_{234}=(g_{80}k_5r_b+g_{81}k_4r_b+g_{82}k_3r_b-g_{83}k_2r_b-g_{84}k_1r_b)$
$g_{235}=(g_{80}k_6r_b-g_{81}k_5r_b-g_{82}k_4r_b+g_{83}k_3r_b+g_{84}k_2r_b+g_{85}k_1r_b)$
$g_{236}=(g_{80}k_7r_b+g_{81}k_6r_b-g_{82}k_5r_b+g_{83}k_4r_b+g_{84}k_3r_b+g_{85}k_2r_b+g_{86}k_1r_b)$
$g_{237}=(g_{81}k_7r_b-g_{82}k_6r_b+g_{83}k_5r_b+g_{84}k_4r_b+g_{85}k_3r_b+g_{86}k_2r_b-g_{87}k_1r_b)$
$g_{238}=(g_{82}k_7r_b-g_{83}k_6r_b+g_{84}k_5r_b+g_{85}k_4r_b+g_{86}k_3r_b-g_{87}k_2r_b-g_{88}k_1r_b)$
$g_{239}=(-g_{83}k_7r_b-g_{84}k_6r_b+g_{85}k_5r_b+g_{86}k_4r_b-g_{87}k_3r_b-g_{88}k_2r_b-g_{89}k_1r_b)$
$g_{240}=(-g_{84}k_7r_b-g_{85}k_6r_b+g_{86}k_5r_b-g_{87}k_4r_b-g_{88}k_3r_b-g_{89}k_2r_b)$
$g_{241}=(-g_{85}k_7r_b-g_{86}k_6r_b-g_{87}k_5r_b-g_{88}k_4r_b-g_{80}k_3r_b)$
$g_{242}=(-g_{86}k_7r_b+g_{87}k_6r_b-g_{88}k_5r_b-g_{89}k_4r_b)$
$g_{243}=(-g_{87}k_7r_b+g_{88}k_6r_b-g_{89}k_5r_b),g_{244}=(g_{88}k_7r_b+g_{89}k_6r_b),g_{245}=(g_{89}k_7r_b)$
$g_{246}=(g_{129}g_{30}C_1),g_{247}=(g_{129}g_{31}C_1+g_{130}g_{30}C_1),g_{248}=(g_{129}g_{32}C_1+g_{130}g_{31}C_1+g_{131}g_{30}C_1)$
$g_{249}=(g_{130}g_{32}C_1+g_{131}g_{31}C_1-g_{132}g_{30}C_1),g_{250}=(g_{131}g_{32}C_1-g_{132}g_{31}C_1-g_{133}g_{30}C_1)$
$g_{251}=(-g_{132}g_{32}C_1-g_{133}g_{31}C_1),g_{252}=(g_{133}g_{32}C_1)$
$g_{253}=(g_{11}r_bg_1),g_{254}=(g_{12}r_bg_1-g_{11}r_bg_2),g_{255}=(-g_{11}r_ba_{52}-g_{12}r_bg_2+g_{13}r_bg_1)$
$g_{256}=(-g_{12}r_ba_{52}-g_{13}r_bg_2+g_{14}r_bg_1),g_{257}=(-g_{13}r_ba_{52}-g_{14}r_bg_2),g_{258}=(g_{14}r_ba_{52})$
$g_{259}=g_{232}+(g_{246}g_{253}),g_{260}=g_{233}+(g_{246}g_{254}+g_{247}g_{253}),g_{261}=g_{234}+(g_{246}g_{255}+g_{247}g_{254}+g_{248}g_{253})$
$g_{262}=g_{235}-(g_{246}g_{256}+g_{247}g_{255}+g_{248}g_{254}+g_{249}g_{253})$
$g_{263}=g_{236}-(g_{246}g_{257}+g_{247}g_{256}+g_{248}g_{255}+g_{249}g_{254}+g_{250}g_{253})$
$g_{264}=g_{237}-(-g_{246}g_{258}+g_{247}g_{257}+g_{248}g_{256}+g_{249}g_{255}+g_{250}g_{254}+g_{251}g_{253})$
$g_{265}=g_{238}-(-g_{247}g_{258}+g_{248}g_{257}+g_{249}g_{256}+g_{250}g_{255}+g_{251}g_{254}-g_{252}g_{253})$
$g_{266}=g_{239}-(-g_{248}g_{258}+g_{249}g_{257}+g_{250}g_{256}+g_{251}g_{255}-g_{252}g_{254})$
$g_{267}=g_{240}-(-g_{249}g_{258}+g_{250}g_{257}+g_{251}g_{256}-g_{252}g_{255})$
$g_{268}=g_{241}-(-g_{250}g_{258}+g_{251}g_{257}-g_{252}g_{256})$
$g_{269}=g_{242}-(g_{251}g_{258}-g_{252}g_{257}),g_{270}=g_{243}-(g_{252}g_{258})$

(8.17)

$$f_{15}=\left[\frac{\begin{bmatrix}+\begin{bmatrix}s^{20}g_{285}+s^{19}g_{286}+s^{18}g_{287}+s^{17}g_{288}+s^{16}g_{334}+s^{15}g_{335}+s^{14}g_{336}+s^{13}g_{337}+s^{12}g_{338}+s^{11}g_{339}\\+s^{10}g_{340}+s^{9}g_{341}+s^{8}g_{342}+s^{7}g_{343}+s^{6}g_{344}+s^{5}g_{345}+s^{4}g_{346}+s^{3}g_{347}+s^{2}g_{348}+sg_{304}+g_{303}\end{bmatrix}\end{bmatrix}}{\begin{bmatrix}\left(s^{3}g_{11}r_b+s^{2}g_{12}r_b+sg_{13}r_b+g_{14}r_b\right)\left[s^{4}g_{47}r_b+s^{3}g_{48}r_b+s^{2}g_{49}r_b-sg_{50}r_b-g_{51}r_b\right]\\\times\left[s\left(C_3+C_4\right)R_6+1\right]\left(s^{2}g_1r_b-\left(sg_2r_b+a_{52}r_b\right)\right)\times\left[s^{6}k_1+s^{5}k_2+s^{4}k_3+s^{3}k_4+s^{2}k_5-sk_6-k_7\right]\end{bmatrix}}\right]$$

$g_{271}=(g_{129}g_{134}),g_{272}=(g_{129}g_{135}+g_{130}g_{134}),g_{273}=(g_{129}g_{136}+g_{130}g_{135}+g_{131}g_{134})$
$g_{274}=(-g_{129}g_{137}+g_{130}g_{136}+g_{131}g_{135}-g_{132}g_{134}),g_{275}=(-g_{129}g_{138}-g_{130}g_{137}+g_{131}g_{136}-g_{132}g_{135}-g_{133}g_{134})$
$g_{276}=(-g_{130}g_{138}-g_{131}g_{137}-g_{132}g_{136}-g_{133}g_{135}),g_{277}=(-g_{131}g_{138}+g_{132}g_{137}-g_{133}g_{136})$
$g_{278}=(g_{132}g_{138}+g_{133}g_{137}),g_{279}=(g_{133}g_{138})$
$g_{280}=\left((g_{11}r_b)\left(C_3+C_4\right)R_6\right),g_{281}=\left(g_{11}r_b+\left(g_{12}r_b\left(C_3+C_4\right)R_6\right)\right),g_{282}=\left(g_{12}r_b+g_{13}r_b\left(C_3+C_4\right)R_6\right)$
$g_{283}=\left(g_{13}r_b+g_{14}r_b\left(C_3+C_4\right)R_6\right),g_{284}=\left(g_{14}r_b\right)$
$g_{285}=(g_{157}k_1),g_{286}=(g_{157}k_2+g_{158}k_1),g_{287}=(g_{157}k_3+g_{158}k_2+g_{159}k_1),g_{288}=(g_{157}k_4+g_{158}k_3+g_{159}k_2+g_{160}k_1)$
$g_{289}=(g_{157}k_5+g_{158}k_4+g_{159}k_3+g_{160}k_2+g_{161}k_1),g_{290}=(-g_{157}k_6+g_{158}k_5+g_{159}k_4+g_{160}k_3+g_{161}k_2+g_{162}k_1)$
$g_{291}=(-g_{157}k_7-g_{158}k_6+g_{159}k_5+g_{160}k_4+g_{161}k_3+g_{162}k_2+g_{163}k_1)$
$g_{292}=(-g_{158}k_7-g_{159}k_6+g_{160}k_5+g_{161}k_4+g_{162}k_3+g_{163}k_2+g_{164}k_1)$
$g_{293}=(-g_{159}k_7-g_{160}k_6+g_{161}k_5+g_{162}k_4+g_{163}k_3+g_{164}k_2+g_{165}k_1)$
$g_{294}=(-g_{160}k_7-g_{161}k_6+g_{162}k_5+g_{163}k_4+g_{164}k_3+g_{165}k_2+g_{166}k_1)$
$g_{295}=(-g_{161}k_7-g_{162}k_6+g_{163}k_5+g_{164}k_4+g_{165}k_3+g_{166}k_2+g_{167}k_1)$
$g_{296}=(-g_{162}k_7-g_{163}k_6+g_{164}k_5+g_{165}k_4+g_{166}k_3+g_{167}k_2+g_{168}k_1)$
$g_{297}=(-g_{163}k_7-g_{164}k_6+g_{165}k_5+g_{166}k_4+g_{167}k_3+g_{168}k_2+g_{169}k_1)$
$g_{298}=(-g_{164}k_7-g_{165}k_6+g_{166}k_5+g_{167}k_4+g_{168}k_3+g_{169}k_2+g_{170}k_1)$
$g_{299}=(-g_{165}k_7-g_{166}k_6+g_{167}k_5+g_{168}k_4+g_{169}k_3+g_{170}k_2-g_{170}k_1)$
$g_{300}=(-g_{166}k_7-g_{167}k_6+g_{168}k_5+g_{169}k_4+g_{170}k_3-g_{171}k_2)$
$g_{301}=(-g_{167}k_7-g_{168}k_6+g_{169}k_5+g_{170}k_4-g_{171}k_3)$
$g_{302}=(-g_{168}k_7-g_{169}k_6+g_{170}k_5-g_{171}k_4)$
$g_{303}=(-g_{169}k_7-g_{170}k_6-g_{171}k_5),g_{304}=(-g_{170}k_7+g_{171}k_6),g_{305}=(g_{171}k_7)$
$g_{306}=(g_{271}g_{280}),g_{307}=(g_{271}g_{281}+g_{272}g_{280}),g_{308}=(g_{271}g_{282}+g_{272}g_{281}+g_{273}g_{280})$
$g_{309}=(g_{271}g_{283}+g_{272}g_{282}+g_{273}g_{281}+g_{274}g_{280})$
$g_{310}=(g_{271}g_{284}+g_{272}g_{283}+g_{273}g_{282}+g_{274}g_{281}+g_{275}g_{280})$
$g_{311}=(g_{272}g_{284}+g_{273}g_{283}+g_{274}g_{282}+g_{275}g_{281}+g_{276}g_{280})$
$g_{312}=(g_{273}g_{284}+g_{274}g_{283}+g_{275}g_{282}+g_{276}g_{281}+g_{277}g_{280})$
$g_{313}=(g_{274}g_{284}+g_{275}g_{283}+g_{276}g_{282}+g_{277}g_{281}+g_{278}g_{280})$
$g_{314}=(g_{275}g_{284}+g_{276}g_{283}+g_{277}g_{282}+g_{278}g_{281}+g_{279}g_{280})$
$g_{315}=(g_{276}g_{284}+g_{277}g_{283}+g_{278}g_{282}+g_{279}g_{281})$
$g_{316}=(g_{277}g_{284}+g_{278}g_{283}+g_{279}g_{282}),g_{317}=(g_{278}g_{284}+g_{279}g_{283}),g_{318}=(g_{279}g_{284})$

(8.18)

$g_{319}=(g_{306}g_1r_b),g_{320}=(g_{307}g_1r_b-g_{306}g_2r_b),g_{321}=(g_{308}g_1r_b-g_{307}g_2r_b-g_{306}a_{52}r_b)$
$g_{322}=(g_{309}g_1r_b-g_{308}g_2r_b-g_{307}a_{52}r_b),g_{323}=(g_{310}g_1r_b-g_{309}g_2r_b-g_{308}a_{52}r_b)$
$g_{324}=(g_{311}g_1r_b-g_{310}g_2r_b-g_{309}a_{52}r_b),g_{325}=(g_{312}g_1r_b-g_{311}g_2r_b-g_{310}a_{52}r_b)$
$g_{326}=(g_{313}g_1r_b-g_{312}g_2r_b-g_{311}a_{52}r_b),g_{327}=(g_{314}g_1r_b-g_{313}g_2r_b-g_{312}a_{52}r_b)$
$g_{328}=(g_{315}g_1r_b-g_{314}g_2r_b-g_{313}a_{52}r_b),g_{329}=(g_{316}g_1r_b-g_{315}g_2r_b-g_{314}a_{52}r_b)$
$g_{330}=(g_{317}g_1r_b-g_{316}g_2r_b-g_{315}a_{52}r_b),g_{331}=(g_{318}g_1r_b-g_{317}g_2r_b-g_{316}a_{52}r_b)$
$g_{332}=(-g_{318}g_1r_b-g_{317}a_{52}r_b),g_{333}=(-g_{318}a_{52}r_b)$
$g_{334}=(g_{289}+g_{319}),g_{335}=(g_{290}+g_{320}),g_{336}=(g_{291}+g_{321}),g_{337}=(g_{292}+g_{322})$
$g_{338}=(g_{293}+g_{323}),g_{339}=(g_{294}+g_{324}),g_{340}=(g_{295}+g_{325}),g_{341}=(g_{296}+g_{326})$
$g_{342}=(g_{297}+g_{327}),g_{343}=(g_{298}+g_{328}),g_{344}=(g_{299}+g_{329}),g_{345}=(g_{300}+g_{330})$
$g_{346}=(g_{301}+g_{331}),g_{347}=(g_{302}+g_{332}),g_{348}=(g_{303}+g_{333})$

(8.19)

$$f_{16}=\left(\frac{\begin{bmatrix}-s^{16}g_{349}-s^{15}g_{350}-s^{14}g_{398}-s^{13}g_{399}-s^{12}g_{400}+s^{11}g_{401}+s^{10}g_{402}+s^{9}g_{403}\\+s^{8}g_{404}+s^{7}g_{405}+s^{6}g_{406}+s^{5}g_{407}+s^{4}g_{408}+s^{3}g_{409}+s^{2}g_{363}-sg_{364}\end{bmatrix}}{\begin{bmatrix}\left(s^{3}g_{11}r_b+s^{2}g_{12}r_b+sg_{13}r_b+g_{14}r_b\right)\left[s^{4}g_{47}r_b+s^{3}g_{48}r_b+s^{2}g_{49}r_b-sg_{50}r_b-g_{51}r_b\right]\\\times\left[s\left(C_3+C_4\right)R_6+1\right]\left(s^{2}g_1-s\left(g_2\right)+\left(a_{52}\right)\right)\left[s^{6}k_1+s^{5}k_2+s^{4}k_3+s^{3}k_4+s^{2}k_5-sk_6-k_7\right]\end{bmatrix}}\right)$$

$g_{349}=(g_{179}k_1r_b),g_{350}=(g_{179}k_2r_b+g_{180}k_1r_b),g_{351}=(g_{179}k_3r_b+g_{180}k_2r_b-g_{189}k_1r_b)$
$g_{352}=(g_{179}k_4r_b+g_{180}k_3r_b-g_{189}k_2r_b-g_{190}k_1r_b)$
$g_{353}=(-g_{179}k_5r_b-g_{180}k_4r_b+g_{189}k_3r_b+g_{190}k_2r_b+g_{191}k_1r_b)$
$g_{354}=(g_{179}k_6r_b-g_{180}k_5r_b+g_{189}k_4r_b+g_{190}k_3r_b+g_{191}k_2r_b+g_{192}k_1r_b)$
$g_{355}=(g_{179}k_7r_b-g_{180}k_6r_b+g_{189}k_5r_b+g_{190}k_4r_b+g_{191}k_3r_b+g_{192}k_2r_b+g_{193}k_1r_b)$
$g_{356}=(g_{180}k_7r_b-g_{189}k_6r_b+g_{190}k_5r_b+g_{191}k_4r_b+g_{192}k_3r_b+g_{193}k_2r_b+g_{194}k_1r_b)$
$g_{357}=(-g_{189}k_7r_b-g_{190}k_6r_b+g_{191}k_5r_b+g_{192}k_4r_b+g_{193}k_3r_b+g_{194}k_2r_b-g_{187}k_1r_b)$
$g_{358}=(-g_{190}k_7r_b-g_{191}k_6r_b+g_{192}k_5r_b+g_{193}k_4r_b+g_{194}k_3r_b-g_{187}k_2r_b+g_{188}k_1r_b)$
$g_{359}=(-g_{191}k_7r_b-g_{192}k_6r_b+g_{193}k_5r_b+g_{194}k_4r_b-g_{187}k_3r_b+g_{188}k_2r_b)$
$g_{360}=(-g_{192}k_7r_b-g_{193}k_6r_b+g_{194}k_5r_b-g_{187}k_4r_b+g_{188}k_3r_b)$
$g_{361}=(-g_{193}k_7r_b-g_{194}k_6r_b-g_{187}k_5r_b+g_{188}k_4r_b)$
$g_{362}=(-g_{194}k_7r_b+g_{187}k_6r_b+g_{188}k_5r_b),g_{363}=(g_{187}k_7r_b-g_{188}k_6r_b),g_{364}=(-g_{188}k_7r_b)$
$g_{365}=(g_{54}C_1g_{134}),g_{366}=(g_{54}C_1g_{135}+g_{55}C_1g_{134}),g_{367}=(g_{54}C_1g_{136}+g_{55}C_1g_{135})$
$g_{368}=(g_{54}C_1g_{134}+g_{55}C_1g_{136}),g_{369}=(-g_{54}C_1g_{138}-g_{55}C_1g_{137}),g_{370}=(g_{55}C_1g_{138})$
$g_{371}=\left(g_{11}r_b\left(C_3+C_4\right)R_6\right),g_{372}=\left(g_{12}r_b\left(C_3+C_4\right)R_6+g_{11}r_b\right)$
$g_{373}=\left(g_{13}r_b\left(C_3+C_4\right)R_6+g_{12}r_b\right),g_{374}=\left(g_{14}r_b\left(C_3+C_4\right)R_6+g_{13}r_b\right),g_{375}=\left(g_{14}r_b\right)$
$g_{376}=(g_{365}g_{371}),g_{377}=(g_{365}g_{372}+g_{366}g_{371}),g_{378}=(g_{365}g_{373}+g_{366}g_{372}+g_{367}g_{371})$
$g_{379}=(g_{365}g_{374}+g_{366}g_{373}+g_{367}g_{372}+g_{368}g_{371})$
$g_{380}=(g_{365}g_{375}+g_{366}g_{374}+g_{367}g_{373}+g_{368}g_{372}+g_{369}g_{371})$
$g_{381}=(g_{366}g_{375}+g_{367}g_{374}+g_{368}g_{373}+g_{369}g_{372}-g_{370}g_{371})$
$g_{382}=(g_{367}g_{375}+g_{368}g_{374}+g_{369}g_{373}-g_{370}g_{372})$
$g_{383}=(g_{368}g_{375}+g_{369}g_{374}-g_{370}g_{373}),g_{384}=(g_{369}g_{375}-g_{370}g_{374}),g_{385}=(g_{370}g_{375})$
$g_{386}=(g_{376}g_1),g_{387}=(g_{377}g_1-g_{376}g_2),g_{388}=(g_{376}a_{52}-g_{377}g_2+g_{378}g_1)$
$g_{389}=(g_{377}a_{52}-g_{378}g_2+g_{379}g_1),g_{390}=(g_{378}a_{52}-g_{379}g_2+g_{380}g_1)$
$g_{391}=(g_{379}a_{52}-g_{380}g_2+g_{381}g_1),g_{392}=(g_{380}a_{52}-g_{381}g_2+g_{382}g_1)$
$g_{393}=(g_{381}a_{52}-g_{382}g_2+g_{383}g_1),g_{394}=(g_{382}a_{52}-g_{383}g_2+g_{384}g_1)$
$g_{395}=(g_{383}a_{52}-g_{384}g_2-g_{385}g_1),g_{396}=(g_{384}a_{52}+g_{385}g_2),g_{397}=(g_{385}a_{52})$
$g_{398}=(g_{351}+g_{386}),g_{399}=(g_{352}+g_{387}),g_{400}=(g_{353}+g_{388}),g_{401}=(g_{354}-g_{389})$
$g_{402}=(g_{355}-g_{390}),g_{403}=(g_{356}-g_{391}),g_{404}=(g_{357}-g_{392}),g_{405}=(g_{358}-g_{393})$
$g_{406}=(g_{359}-g_{394}),g_{407}=(g_{360}-g_{395}),g_{408}=(g_{361}-g_{396}),g_{409}=(g_{362}-g_{397})$

(8.20)

$$f_{17}=\left[\begin{array}{c}\begin{bmatrix}s^{35}h_1+s^{34}h_2+s^{33}h_3+s^{32}h_{68}+s^{31}h_{69}\\+s^{30}h_{70}+s^{29}h_{71}+s^{28}h_{72}+s^{27}h_{73}+s^{26}h_{74}\\+s^{25}h_{75}+s^{24}h_{76}+s^{23}h_{77}+s^{22}h_{78}+s^{21}h_{79}\\+s^{20}h_{80}+s^{19}h_{81}+s^{18}h_{82}+s^{17}h_{83}+s^{16}h_{84}\\+s^{15}h_{85}+s^{14}h_{86}+s^{13}h_{87}+s^{12}h_{88}+s^{11}h_{89}\\+s^{10}h_{90}+s^{9}h_{91}+s^{8}h_{92}+s^{7}h_{93}+s^{6}h_{94}\\+s^{5}h_{95}+s^{4}h_{96}+s^{3}h_{97}+s^{2}h_{98}+sh_{35}+h_{36}\end{bmatrix}\\\hline\begin{bmatrix}s^{15}h_{116}+s^{14}h_{117}+s^{13}h_{118}+s^{12}h_{119}\\+s^{11}h_{120}+s^{10}h_{121}+s^{9}h_{122}+s^{8}h_{123}\\+s^{7}h_{124}+s^{6}h_{125}+s^{5}h_{126}+s^{4}h_{127}\\+s^{3}h_{128}+s^{2}h_{129}+sh_{130}-h_{131}\end{bmatrix}\begin{bmatrix}s^{20}g_{285}+s^{19}g_{286}+s^{18}g_{287}+s^{17}g_{288}\\+s^{16}g_{334}+s^{15}g_{335}+s^{14}g_{336}+s^{13}g_{337}\\+s^{12}g_{338}+s^{11}g_{339}+s^{10}g_{340}+s^{9}g_{341}\\+s^{8}g_{342}+s^{7}g_{343}+s^{6}g_{344}+s^{5}g_{345}\\+s^{4}g_{346}+s^{3}g_{347}+s^{2}g_{348}+sg_{304}\\+g_{303}\end{bmatrix}\end{array}\right]$$

$$\begin{aligned}
&h_{116}=\left(h_{99}h_{105}\right),h_{117}=\left(h_{99}h_{106}+h_{100}h_{105}\right),h_{118}=\left(h_{99}h_{107}+h_{100}h_{106}+h_{101}h_{105}\right)\\
&h_{119}=\left(h_{99}h_{108}+h_{100}h_{107}+h_{101}h_{106}+h_{102}h_{105}\right)\\
&h_{120}=\left(h_{99}h_{109}+h_{100}h_{108}+h_{101}h_{107}+h_{102}h_{106}+h_{103}h_{105}\right)\\
&h_{121}=\left(h_{99}h_{110}+h_{100}h_{109}+h_{101}h_{108}+h_{102}h_{107}+h_{103}h_{106}-h_{104}h_{105}\right)\\
&h_{122}=\left(h_{99}h_{111}+h_{100}h_{110}+h_{101}h_{109}+h_{102}h_{108}+h_{103}h_{107}-h_{104}h_{106}\right)\\
&h_{123}=\left(h_{99}h_{112}+h_{100}h_{111}+h_{101}h_{110}+h_{102}h_{109}+h_{103}h_{108}-h_{104}h_{107}\right)\\
&h_{124}=\left(h_{99}h_{113}+h_{100}h_{112}+h_{101}h_{111}+h_{102}h_{110}+h_{103}h_{109}-h_{104}h_{108}\right)\\
&h_{125}=\left(h_{99}h_{114}+h_{100}h_{113}+h_{101}h_{112}+h_{102}h_{111}+h_{103}h_{110}-h_{104}h_{109}\right)\\
&h_{126}=\left(h_{99}h_{115}+h_{100}h_{114}+h_{101}h_{113}+h_{102}h_{112}+h_{103}h_{111}-h_{104}h_{110}\right)\\
&h_{127}=\left(h_{100}h_{115}+h_{101}h_{114}+h_{102}h_{113}+h_{103}h_{112}-h_{104}h_{111}\right)\\
&h_{128}=\left(h_{101}h_{115}+h_{102}h_{114}+h_{103}h_{113}-h_{104}h_{112}\right)\\
&h_{129}=\left(h_{102}h_{115}+h_{103}h_{114}-h_{104}h_{113}\right)\\
&h_{130}=\left(h_{103}h_{115}-h_{104}h_{114}\right)\\
&h_{131}=\left(h_{104}h_{115}\right)
\end{aligned}\qquad(8.21)$$

$$\begin{aligned}
&h_1=\left(g_{195}g_{285}\right),h_2=\left(g_{195}g_{286}+g_{196}g_{285}\right)\\
&h_3=\left(g_{195}g_{287}+g_{196}g_{286}+g_{197}g_{285}\right)\\
&h_4=\left(g_{195}g_{288}+g_{196}g_{287}+g_{197}g_{286}+g_{221}g_{285}\right)\\
&h_5=\left(g_{195}g_{334}+g_{196}g_{288}+g_{197}g_{287}+g_{221}g_{286}+g_{222}g_{285}\right)\\
&h_6=\left(g_{195}g_{335}+g_{196}g_{334}+g_{197}g_{288}+g_{221}g_{287}+g_{222}g_{286}+g_{223}g_{285}\right)\\
&h_7=\begin{pmatrix}g_{195}g_{336}+g_{196}g_{335}+g_{197}g_{334}+g_{221}g_{288}+g_{222}g_{287}\\+g_{223}g_{286}+g_{224}g_{285}\end{pmatrix}\\
&h_8=\begin{pmatrix}g_{195}g_{337}+g_{196}g_{336}+g_{197}g_{335}+g_{221}g_{334}+g_{222}g_{288}\\+g_{223}g_{287}+g_{224}g_{286}+g_{225}g_{285}\end{pmatrix}\\
&h_9=\begin{pmatrix}g_{195}g_{338}+g_{196}g_{337}+g_{197}g_{336}+g_{221}g_{335}+g_{222}g_{334}\\+g_{223}g_{288}+g_{224}g_{287}+g_{225}g_{286}+g_{226}g_{285}\end{pmatrix}\\
&h_{10}=\begin{pmatrix}g_{195}g_{339}+g_{196}g_{338}+g_{197}g_{337}+g_{221}g_{336}+g_{222}g_{335}\\+g_{223}g_{334}+g_{224}g_{288}+g_{225}g_{287}+g_{226}g_{286}+g_{227}g_{285}\end{pmatrix}\\
&h_{11}=\begin{pmatrix}g_{195}g_{340}+g_{196}g_{339}+g_{197}g_{338}+g_{221}g_{337}+g_{222}g_{336}\\+g_{223}g_{335}+g_{224}g_{334}+g_{225}g_{288}+g_{226}g_{287}+g_{227}g_{286}\\+g_{228}g_{285}\end{pmatrix}\\
&h_{12}=\begin{pmatrix}g_{195}g_{341}+g_{196}g_{340}+g_{197}g_{339}+g_{221}g_{338}+g_{222}g_{337}\\+g_{223}g_{336}+g_{224}g_{335}+g_{225}g_{334}+g_{226}g_{288}+g_{227}g_{287}\\+g_{228}g_{286}+g_{229}g_{285}\end{pmatrix}\\
&h_{13}=\begin{pmatrix}g_{195}g_{342}+g_{196}g_{341}+g_{197}g_{340}+g_{221}g_{339}+g_{222}g_{338}\\+g_{223}g_{337}+g_{224}g_{336}+g_{225}g_{335}+g_{226}g_{334}+g_{227}g_{288}\\+g_{228}g_{287}+g_{229}g_{286}+g_{207}g_{285}\end{pmatrix}
\end{aligned}\qquad(8.22a)$$

$$\begin{aligned}
h_{14}&=\begin{pmatrix}g_{195}g_{343}+g_{196}g_{342}+g_{197}g_{341}+g_{221}g_{340}+g_{222}g_{339}\\+g_{223}g_{338}+g_{224}g_{337}+g_{225}g_{336}+g_{226}g_{335}+g_{227}g_{334}\\+g_{228}g_{288}+g_{229}g_{287}+g_{207}g_{286}+g_{208}g_{285}\end{pmatrix}\\
h_{15}&=\begin{pmatrix}g_{195}g_{344}+g_{196}g_{343}+g_{197}g_{342}+g_{221}g_{341}+g_{222}g_{340}\\+g_{223}g_{339}+g_{224}g_{338}+g_{225}g_{337}+g_{226}g_{336}+g_{227}g_{335}\\+g_{228}g_{334}+g_{229}g_{288}+g_{207}g_{287}+g_{208}g_{286}+g_{209}g_{285}\end{pmatrix}\\
h_{16}&=\begin{pmatrix}g_{195}g_{345}+g_{196}g_{344}+g_{197}g_{343}+g_{221}g_{342}+g_{222}g_{341}\\+g_{223}g_{340}+g_{224}g_{339}+g_{225}g_{338}+g_{226}g_{337}+g_{227}g_{336}\\+g_{228}g_{335}+g_{229}g_{334}+g_{207}g_{288}+g_{208}g_{287}+g_{209}g_{286}+g_{210}g_{285}\end{pmatrix}\\
h_{17}&=\begin{pmatrix}g_{195}g_{346}+g_{196}g_{345}+g_{197}g_{344}+g_{221}g_{343}+g_{222}g_{342}\\+g_{223}g_{341}+g_{224}g_{340}+g_{225}g_{339}+g_{226}g_{338}+g_{227}g_{337}\\+g_{228}g_{336}+g_{229}g_{335}+g_{207}g_{334}+g_{208}g_{288}+g_{209}g_{287}+g_{210}g_{286}\end{pmatrix}\\
h_{18}&=\begin{pmatrix}g_{195}g_{347}+g_{196}g_{346}+g_{197}g_{345}+g_{221}g_{344}+g_{222}g_{343}\\+g_{223}g_{342}+g_{224}g_{341}+g_{225}g_{340}+g_{226}g_{339}+g_{227}g_{338}\\+g_{228}g_{337}+g_{229}g_{336}+g_{207}g_{335}+g_{208}g_{334}+g_{209}g_{288}+g_{210}g_{287}\end{pmatrix}\\
h_{19}&=\begin{pmatrix}g_{195}g_{348}+g_{196}g_{347}+g_{197}g_{346}+g_{221}g_{345}+g_{222}g_{344}\\+g_{223}g_{343}+g_{224}g_{342}+g_{225}g_{341}+g_{226}g_{340}+g_{227}g_{339}\\+g_{228}g_{338}+g_{229}g_{337}+g_{207}g_{336}+g_{208}g_{335}+g_{209}g_{334}+g_{210}g_{288}\end{pmatrix}\\
h_{20}&=\begin{pmatrix}g_{195}g_{304}+g_{196}g_{348}+g_{197}g_{347}+g_{221}g_{346}+g_{222}g_{345}\\+g_{223}g_{344}+g_{224}g_{343}+g_{225}g_{342}+g_{226}g_{341}+g_{227}g_{340}\\+g_{228}g_{339}+g_{229}g_{338}+g_{207}g_{337}+g_{208}g_{336}+g_{209}g_{335}+g_{210}g_{334}\end{pmatrix}
\end{aligned}\qquad(8.22b)$$

$$\begin{aligned}
h_{21}&=\begin{pmatrix}g_{195}g_{303}+g_{196}g_{304}+g_{197}g_{348}+g_{221}g_{347}+g_{222}g_{346}\\+g_{223}g_{345}+g_{224}g_{344}+g_{225}g_{343}+g_{226}g_{342}+g_{227}g_{341}\\+g_{228}g_{340}+g_{229}g_{339}+g_{207}g_{338}+g_{208}g_{337}+g_{209}g_{336}+g_{210}g_{335}\end{pmatrix}\\
h_{22}&=\begin{pmatrix}g_{196}g_{303}+g_{197}g_{304}+g_{221}g_{348}+g_{222}g_{347}+g_{223}g_{346}\\+g_{224}g_{345}+g_{225}g_{344}+g_{226}g_{343}+g_{227}g_{342}+g_{228}g_{341}\\+g_{229}g_{340}+g_{207}g_{339}+g_{208}g_{338}+g_{209}g_{337}+g_{210}g_{336}\end{pmatrix}\\
h_{23}&=\begin{pmatrix}g_{197}g_{303}+g_{221}g_{304}+g_{222}g_{348}+g_{223}g_{347}+g_{224}g_{346}\\+g_{225}g_{345}+g_{226}g_{344}+g_{227}g_{343}+g_{228}g_{342}+g_{229}g_{341}\\+g_{207}g_{340}+g_{208}g_{339}+g_{209}g_{338}+g_{210}g_{337}\end{pmatrix}\\
h_{24}&=\begin{pmatrix}g_{221}g_{303}+g_{222}g_{304}+g_{223}g_{348}+g_{224}g_{347}+g_{225}g_{346}\\+g_{226}g_{345}+g_{227}g_{344}+g_{228}g_{343}+g_{229}g_{342}+g_{207}g_{341}\\+g_{208}g_{340}+g_{209}g_{339}+g_{210}g_{338}\end{pmatrix}\\
h_{25}&=\begin{pmatrix}g_{222}g_{303}+g_{223}g_{304}+g_{224}g_{348}+g_{225}g_{347}+g_{226}g_{346}\\+g_{227}g_{345}+g_{228}g_{344}+g_{229}g_{343}+g_{207}g_{342}+g_{208}g_{341}\\+g_{209}g_{340}+g_{210}g_{339}\end{pmatrix}\\
h_{26}&=\begin{pmatrix}g_{223}g_{303}+g_{224}g_{304}+g_{225}g_{348}+g_{226}g_{347}+g_{227}g_{346}\\+g_{228}g_{345}+g_{229}g_{344}+g_{207}g_{343}+g_{208}g_{342}+g_{209}g_{341}+g_{210}g_{340}\end{pmatrix}\\
h_{27}&=\begin{pmatrix}g_{224}g_{303}+g_{225}g_{304}+g_{226}g_{348}+g_{227}g_{347}+g_{228}g_{346}\\+g_{229}g_{345}+g_{207}g_{344}+g_{208}g_{343}+g_{209}g_{342}+g_{210}g_{341}\end{pmatrix}\\
h_{28}&=\begin{pmatrix}g_{225}g_{303}+g_{226}g_{304}+g_{227}g_{348}+g_{228}g_{347}+g_{229}g_{346}\\+g_{207}g_{345}+g_{208}g_{344}+g_{209}g_{343}+g_{210}g_{342}\end{pmatrix}\\
h_{29}&=\left(g_{226}g_{303}+g_{227}g_{304}+g_{228}g_{348}+g_{229}g_{347}+g_{207}g_{346}+g_{208}g_{345}+g_{209}g_{344}+g_{210}g_{343}\right)\\
h_{30}&=\left(g_{227}g_{303}+g_{228}g_{304}+g_{229}g_{348}+g_{207}g_{347}+g_{208}g_{346}+g_{209}g_{345}+g_{210}g_{344}\right)\\
h_{31}&=\left(g_{228}g_{303}+g_{229}g_{304}+g_{207}g_{348}+g_{208}g_{347}+g_{209}g_{346}+g_{210}g_{345}\right)\\
h_{32}&=\left(g_{229}g_{303}+g_{207}g_{304}+g_{208}g_{348}+g_{209}g_{347}+g_{210}g_{346}\right)\\
h_{33}&=\left(g_{207}g_{303}+g_{208}g_{304}+g_{209}g_{348}+g_{210}g_{347}\right)\\
h_{34}&=\left(g_{208}g_{303}+g_{209}g_{304}+g_{210}g_{348}\right)\\
h_{35}&=\left(g_{209}g_{303}+g_{210}g_{304}\right),h_{36}=\left(g_{210}g_{303}\right)
\end{aligned}\qquad(8.23)$$

$$
\begin{aligned}
&h_{37}=\left(g_{349}g_{230}r_b^2\right),h_{38}=\left(g_{349}g_{231}r_b^2+g_{350}g_{230}r_b^2\right)\\
&h_{39}=\left(g_{349}g_{259}r_b^2+g_{350}g_{231}r_b^2+g_{398}g_{230}r_b^2\right)\\
&h_{40}=\left(g_{349}g_{260}r_b^2+g_{350}g_{259}r_b^2+g_{398}g_{231}r_b^2+g_{399}g_{230}r_b^2\right)\\
&h_{41}=\left(g_{349}g_{261}r_b^2+g_{350}g_{260}r_b^2+g_{398}g_{259}r_b^2+g_{399}g_{231}r_b^2+g_{400}g_{230}r_b^2\right)\\
&h_{42}=\left(-g_{349}g_{262}r_b^2+g_{350}g_{261}r_b^2+g_{398}g_{260}r_b^2+g_{399}g_{259}r_b^2+g_{400}g_{231}r_b^2-g_{401}g_{230}r_b^2\right)\\
&h_{43}=\begin{pmatrix}-g_{349}g_{263}r_b^2-g_{350}g_{262}r_b^2+g_{398}g_{261}r_b^2+g_{399}g_{260}r_b^2+g_{400}g_{259}r_b^2\\-g_{401}g_{231}r_b^2-g_{402}g_{230}r_b^2\end{pmatrix}\\
&h_{44}=\begin{pmatrix}-g_{349}g_{264}r_b^2-g_{350}g_{263}r_b^2-g_{398}g_{262}r_b^2+g_{399}g_{261}r_b^2+g_{400}g_{260}r_b^2\\-g_{401}g_{259}r_b^2-g_{402}g_{231}r_b^2-g_{403}g_{230}r_b^2\end{pmatrix}\\
&h_{45}=\begin{pmatrix}-g_{349}g_{265}r_b^2-g_{350}g_{264}r_b^2-g_{398}g_{263}r_b^2-g_{399}g_{262}r_b^2+g_{400}g_{261}r_b^2\\-g_{401}g_{260}r_b^2-g_{402}g_{259}r_b^2-g_{403}g_{231}r_b^2-g_{404}g_{230}r_b^2\end{pmatrix}\\
&h_{46}=\begin{pmatrix}-g_{349}g_{266}r_b^2-g_{350}g_{265}r_b^2-g_{398}g_{264}r_b^2-g_{399}g_{263}r_b^2-g_{400}g_{262}r_b^2\\-g_{401}g_{261}r_b^2-g_{402}g_{260}r_b^2-g_{403}g_{259}r_b^2-g_{404}g_{231}r_b^2-g_{405}g_{230}r_b^2\end{pmatrix}\\
&h_{47}=\begin{pmatrix}-g_{349}g_{267}r_b^2-g_{350}g_{266}r_b^2-g_{398}g_{265}r_b^2-g_{399}g_{264}r_b^2-g_{400}g_{263}r_b^2\\+g_{401}g_{262}r_b^2-g_{402}g_{261}r_b^2-g_{403}g_{260}r_b^2-g_{404}g_{259}r_b^2-g_{405}g_{231}r_b^2-g_{406}g_{230}r_b^2\end{pmatrix}\\
&h_{48}=\begin{pmatrix}-g_{349}g_{268}r_b^2-g_{350}g_{267}r_b^2-g_{398}g_{266}r_b^2-g_{399}g_{265}r_b^2-g_{400}g_{264}r_b^2+g_{401}g_{263}r_b^2\\+g_{402}g_{262}r_b^2-g_{403}g_{261}r_b^2-g_{404}g_{260}r_b^2-g_{405}g_{259}r_b^2-g_{406}g_{231}r_b^2-g_{407}g_{230}r_b^2\end{pmatrix}\\
&h_{49}=\begin{pmatrix}-g_{349}g_{269}r_b^2-g_{350}g_{268}r_b^2-g_{398}g_{267}r_b^2-g_{399}g_{266}r_b^2-g_{400}g_{265}r_b^2+g_{401}g_{264}r_b^2\\+g_{402}g_{263}r_b^2+g_{403}g_{262}r_b^2-g_{404}g_{261}r_b^2-g_{405}g_{260}r_b^2\\-g_{406}g_{259}r_b^2-g_{407}g_{231}r_b^2-g_{408}g_{230}r_b^2\end{pmatrix}\\
&h_{50}=\begin{pmatrix}-g_{349}g_{270}r_b^2-g_{350}g_{269}r_b^2-g_{398}g_{268}r_b^2-g_{399}g_{267}r_b^2-g_{400}g_{266}r_b^2+g_{401}g_{265}r_b^2\\+g_{402}g_{264}r_b^2+g_{403}g_{263}r_b^2+g_{404}g_{262}r_b^2-g_{405}g_{261}r_b^2\\-g_{406}g_{260}r_b^2-g_{407}g_{259}r_b^2-g_{408}g_{231}r_b^2-g_{409}g_{230}r_b^2\end{pmatrix}
\end{aligned}
\tag{8.24}
$$

$$
\begin{aligned}
&h_{99}=\left(g_1r_b^2g_{11}\right),h_{100}=\left(g_1r_b^2g_{12}-g_2r_b^2g_{12}\right)\\
&h_{101}=\left(g_1r_b^2g_{13}-g_2r_b^2g_{12}-a_{52}r_b^2g_{11}\right)\\
&h_{102}=\left(g_1r_b^2g_{14}-g_2r_b^2g_{13}-a_{52}r_b^2g_{12}\right)\\
&h_{103}=\left(-g_2r_b^2g_{14}-a_{52}r_b^2g_{13}\right),h_{104}=\left(a_{52}r_b^2g_{13}g_{14}\right)\\
&h_{105}=\left(g_{47}r_bk_1r_b\right),h_{106}=\left(g_{47}r_bk_2r_b+g_{48}r_bk_1r_b\right)\\
&h_{107}=\left(g_{47}r_bk_3r_b+g_{48}r_bk_2r_b+g_{49}r_bk_1r_b\right)\\
&h_{108}=\left(g_{47}r_bk_4r_b+g_{48}r_bk_3r_b+g_{49}r_bk_2r_b-g_{50}r_bk_1r_b\right)\\
&h_{109}=\left(g_{47}r_bk_5r_b+g_{48}r_bk_4r_b+g_{49}r_bk_3r_b-g_{50}r_bk_2r_b-g_{51}r_bk_1r_b\right)\\
&h_{110}=\left(-g_{47}r_bk_6r_b+g_{48}r_bk_5r_b+g_{49}r_bk_4r_b-g_{50}r_bk_3r_b-g_{51}r_bk_2r_b\right)\\
&h_{111}=\left(-g_{47}r_bk_7r_b-g_{48}r_bk_6r_b+g_{49}r_bk_5r_b-g_{50}r_bk_4r_b-g_{51}r_bk_3r_b\right)\\
&h_{112}=\left(-g_{48}r_bk_7r_b-g_{49}r_bk_6r_b-g_{50}r_bk_5r_b-g_{51}r_bk_4r_b\right)\\
&h_{113}=\left(-g_{49}r_bk_7r_b+g_{50}r_bk_6r_b-g_{51}r_bk_5r_b\right)\\
&h_{114}=\left(g_{50}r_bk_7r_b+g_{51}r_bk_6r_b\right),h_{115}=\left(g_{51}r_bk_7r_b\right)
\end{aligned}
\tag{8.28}
$$

$$
\begin{aligned}
&h_{51}=\begin{pmatrix}-g_{349}g_{244}r_b^2-g_{350}g_{270}r_b^2-g_{398}g_{269}r_b^2-g_{399}g_{268}r_b^2-g_{400}g_{267}r_b^2+g_{401}g_{266}r_b^2+g_{402}g_{265}r_b^2+g_{403}g_{264}r_b^2+g_{404}g_{263}r_b^2+g_{405}g_{262}r_b^2\\-g_{406}g_{261}r_b^2-g_{407}g_{260}r_b^2-g_{408}g_{259}r_b^2-g_{409}g_{231}r_b^2-g_{363}g_{230}r_b^2\end{pmatrix}\\
&h_{52}=\begin{pmatrix}-g_{349}g_{245}r_b^2-g_{350}g_{244}r_b^2-g_{398}g_{270}r_b^2-g_{399}g_{269}r_b^2-g_{400}g_{268}r_b^2+g_{401}g_{267}r_b^2+g_{402}g_{266}r_b^2+g_{403}g_{265}r_b^2+g_{404}g_{264}r_b^2+g_{405}g_{263}r_b^2\\+g_{406}g_{262}r_b^2-g_{407}g_{261}r_b^2-g_{408}g_{260}r_b^2-g_{409}g_{259}r_b^2-g_{363}g_{231}r_b^2+g_{364}g_{230}r_b^2\end{pmatrix}\\
&h_{53}=\begin{pmatrix}-g_{350}g_{245}r_b^2-g_{398}g_{244}r_b^2-g_{399}g_{270}r_b^2-g_{400}g_{269}r_b^2+g_{401}g_{268}r_b^2+g_{402}g_{267}r_b^2+g_{403}g_{266}r_b^2+g_{404}g_{265}r_b^2+g_{405}g_{264}r_b^2+g_{406}g_{263}r_b^2\\+g_{407}g_{262}r_b^2-g_{408}g_{261}r_b^2-g_{409}g_{260}r_b^2-g_{363}g_{259}r_b^2+g_{364}g_{231}r_b^2\end{pmatrix}\\
&h_{54}=\begin{pmatrix}-g_{398}g_{245}r_b^2-g_{399}g_{244}r_b^2-g_{400}g_{270}r_b^2-g_{401}g_{269}r_b^2+g_{402}g_{268}r_b^2+g_{403}g_{267}r_b^2+g_{404}g_{266}r_b^2+g_{405}g_{265}r_b^2+g_{406}g_{264}r_b^2+g_{407}g_{263}r_b^2\\+g_{408}g_{262}r_b^2-g_{409}g_{261}r_b^2-g_{363}g_{260}r_b^2+g_{364}g_{259}r_b^2\end{pmatrix}
\end{aligned}
\tag{8.25}
$$

$$
f_{17}=\frac{\begin{bmatrix}s^{35}h_1+s^{34}h_2+s^{33}h_3+s^{32}h_{68}+s^{31}h_{69}+s^{30}h_{70}\\+s^{29}h_{71}+s^{28}h_{72}+s^{27}h_{73}+s^{26}h_{74}+s^{25}h_{75}+s^{24}h_{76}\\+s^{23}h_{77}+s^{22}h_{78}+s^{21}h_{79}+s^{20}h_{80}+s^{19}h_{81}+s^{18}h_{82}\\+s^{17}h_{83}+s^{16}h_{84}+s^{15}h_{85}+s^{14}h_{86}+s^{13}h_{87}+s^{12}h_{88}\\+s^{11}h_{89}+s^{10}h_{90}+s^9h_{91}+s^8h_{92}+s^7h_{93}+s^6h_{94}\\+s^5h_{95}+s^4h_{96}+s^3h_{97}+s^2h_{98}+sh_{35}+h_{36}\end{bmatrix}}{\begin{bmatrix}s^{35}h_{132}+s^{34}h_{133}+s^{33}h_{134}+s^{32}h_{135}+s^{31}h_{136}+s^{30}h_{137}\\+s^{29}h_{138}+s^{28}h_{139}+s^{27}h_{140}+s^{26}h_{141}+s^{25}h_{142}+s^{24}h_{143}\\+s^{23}h_{144}+s^{22}h_{145}+s^{21}h_{146}+s^{20}h_{147}+s^{19}h_{148}+s^{18}h_{149}\\+s^{17}h_{150}+s^{16}h_{151}+s^{15}h_{152}+s^{14}h_{153}+s^{13}h_{154}+s^{12}h_{155}\\+s^{11}h_{156}+s^{10}h_{157}+s^9h_{158}+s^8h_{159}+s^7h_{160}+s^6h_{161}\\+s^5h_{162}+s^4h_{163}+s^3h_{164}+s^2h_{165}+sh_{166}+h_{167}\end{bmatrix}}
$$

$$
\begin{aligned}
&h_{161}=\left(h_{125}g_{303}+h_{126}g_{304}+h_{127}g_{348}+h_{128}g_{347}+h_{129}g_{346}+h_{130}g_{345}-h_{131}g_{344}\right)\\
&h_{162}=\left(h_{126}g_{303}+h_{127}g_{304}+h_{128}g_{348}+h_{129}g_{347}+h_{130}g_{346}-h_{131}g_{345}\right)\\
&h_{163}=\left(h_{127}g_{303}+h_{128}g_{304}+h_{129}g_{348}+h_{130}g_{347}-h_{131}g_{346}\right)\\
&h_{164}=\left(h_{128}g_{303}+h_{129}g_{304}+h_{130}g_{348}-h_{131}g_{347}\right)\\
&h_{165}=\left(h_{129}g_{303}+h_{130}g_{304}-h_{131}g_{348}\right),h_{166}=\left(h_{130}g_{303}-h_{131}g_{304}\right),h_{167}=\left(h_{131}g_{303}\right)
\end{aligned}
\tag{8.29}
$$

$$
\begin{aligned}
&h_{55}=\begin{pmatrix}-g_{399}g_{245}r_b^2-g_{400}g_{244}r_b^2+g_{401}g_{270}r_b^2+g_{402}g_{269}r_b^2+g_{403}g_{268}r_b^2\\+g_{404}g_{267}r_b^2+g_{405}g_{266}r_b^2+g_{406}g_{265}r_b^2+g_{407}g_{264}r_b^2+g_{408}g_{263}r_b^2\\+g_{409}g_{362}r_b^2-g_{363}g_{231}r_b^2+g_{364}g_{390}r_b^2\end{pmatrix}\\
&h_{56}=\begin{pmatrix}-g_{400}g_{245}r_b^2+g_{401}g_{244}r_b^2+g_{402}g_{270}r_b^2+g_{403}g_{269}r_b^2+g_{404}g_{268}r_b^2\\+g_{405}g_{267}r_b^2+g_{406}g_{266}r_b^2+g_{407}g_{265}r_b^2+g_{408}g_{264}r_b^2+g_{409}g_{263}r_b^2\\+g_{363}g_{362}r_b^2+g_{364}g_{231}r_b^2\end{pmatrix}\\
&h_{57}=\begin{pmatrix}g_{401}g_{245}r_b^2+g_{402}g_{244}r_b^2+g_{403}g_{270}r_b^2+g_{404}g_{390}r_b^2+g_{405}g_{268}r_b^2\\+g_{406}g_{267}r_b^2+g_{407}g_{266}r_b^2+g_{408}g_{265}r_b^2+g_{409}g_{264}r_b^2+g_{363}g_{263}r_b^2\\-g_{364}g_{262}r_b^2\end{pmatrix}\\
&h_{58}=\begin{pmatrix}g_{402}g_{245}r_b^2+g_{403}g_{244}r_b^2+g_{404}g_{270}r_b^2+g_{405}g_{390}r_b^2+g_{406}g_{264}r_b^2\\+g_{407}g_{267}r_b^2+g_{408}g_{266}r_b^2+g_{409}g_{265}r_b^2+g_{363}g_{264}r_b^2-g_{364}g_{263}r_b^2\end{pmatrix}\\
&h_{59}=\begin{pmatrix}g_{403}g_{245}r_b^2+g_{404}g_{244}r_b^2+g_{405}g_{270}r_b^2+g_{406}g_{390}r_b^2+g_{407}g_{268}r_b^2\\+g_{408}g_{267}r_b^2+g_{409}g_{266}r_b^2+g_{363}g_{265}r_b^2-g_{364}g_{264}r_b^2\end{pmatrix}\\
&h_{60}=\begin{pmatrix}g_{404}g_{245}r_b^2+g_{405}g_{244}r_b^2+g_{406}g_{270}r_b^2+g_{407}g_{390}r_b^2+g_{408}g_{268}r_b^2\\+g_{409}g_{267}r_b^2+g_{363}g_{266}r_b^2-g_{364}g_{265}r_b^2\end{pmatrix}\\
&h_{61}=\begin{pmatrix}g_{405}g_{245}r_b^2+g_{406}g_{244}r_b^2+g_{407}g_{270}r_b^2+g_{408}g_{390}r_b^2+g_{409}g_{268}r_b^2\\+g_{363}g_{267}r_b^2-g_{364}g_{266}r_b^2\end{pmatrix}\\
&h_{62}=\left(g_{406}g_{245}r_b^2+g_{407}g_{244}r_b^2+g_{408}g_{270}r_b^2+g_{409}g_{390}r_b^2+g_{363}g_{268}r_b^2-g_{364}g_{390}r_b^2\right)\\
&h_{63}=\left(g_{407}g_{245}r_b^2+g_{408}g_{244}r_b^2+g_{409}g_{270}r_b^2+g_{363}g_{390}r_b^2-g_{364}g_{268}r_b^2\right)\\
&h_{64}=\left(g_{408}g_{245}r_b^2+g_{409}g_{244}r_b^2+g_{363}g_{270}r_b^2-g_{364}g_{390}r_b^2\right)\\
&h_{65}=\left(g_{409}g_{245}r_b^2+g_{363}g_{244}r_b^2-g_{364}g_{270}r_b^2\right)\\
&h_{66}=\left(g_{363}g_{245}r_b^2-g_{364}g_{244}r_b^2\right),h_{67}=\left(g_{364}g_{245}r_b^2\right)
\end{aligned}
\tag{8.26}
$$

$$
\begin{aligned}
&h_{68}=\left(h_4-h_{37}\right),h_{69}=\left(h_5-h_{38}\right),h_{70}=\left(h_6-h_{39}\right),h_{71}=\left(h_7-h_{40}\right),h_{72}=\left(h_8-h_{41}\right),h_{73}=\left(h_9-h_{42}\right),h_{74}=\left(h_{10}-h_{43}\right)\\
&h_{75}=\left(h_{11}-h_{44}\right),h_{76}=\left(h_{12}-h_{45}\right),h_{77}=\left(h_{13}-h_{46}\right),h_{78}=\left(h_{14}-h_{47}\right),h_{79}=\left(h_{15}-h_{48}\right),h_{80}=\left(h_{16}-h_{49}\right)\\
&h_{81}=\left(h_{17}-h_{50}\right),h_{82}=\left(h_{18}-h_{51}\right),h_{83}=\left(h_{19}-h_{52}\right),h_{84}=\left(h_{20}-h_{53}\right),h_{85}=\left(h_{21}-h_{54}\right),h_{86}=\left(h_{22}-h_{55}\right)\\
&h_{87}=\left(h_{23}-h_{56}\right),h_{88}=\left(h_{24}-h_{57}\right),h_{89}=\left(h_{25}-h_{58}\right),h_{90}=\left(h_{26}-h_{59}\right),h_{91}=\left(h_{27}-h_{60}\right),h_{92}=\left(h_{28}-h_{61}\right)\\
&h_{93}=\left(h_{29}-h_{62}\right),h_{94}=\left(h_{30}-h_{63}\right),h_{95}=\left(h_{31}-h_{64}\right),h_{96}=\left(h_{32}-h_{65}\right),h_{97}=\left(h_{33}-h_{66}\right),h_{98}=\left(h_{34}+h_{67}\right)
\end{aligned}
\tag{8.27}
$$

IV. A Simulation of input impedance graph of a BJT phase shift oscillator topology with MATLAB

All of the necessary equations which are defined and typed in text file inside MATLAB platform so that the polynomial form of the input impedance function of the BJT phase shift amplifier. The BJT phase shift amplifier dc operating point can be designed by setting the collector current consumption for 1mA, 5mA and 10mA so that three values of the biasing resistor can be computed by using Kirchoff's current law at the base terminal of the figure1. Base current can be computed by dividing the collector current by a dc current gain which can be seen from data sheet of the transistor at a typical value of the operating temperature. If the feasible room temperature is 40 degree Celcius because the room has no air conditioning. The thermal voltage can be computed by Boltzmann's constant multiplied by temperature and divide by electron charge. The base emitter voltage can be computed by multiplied thermal voltage by natural logarithm of the ratio of the collector current and saturation current. Saturation current can be seen from SPICE model of the transistor data sheet. For the circuit diagram of the phase shift amplifier the emitter terminal is not connected with other passive elements because it is connected with ground plane.

The other passive components in the phase shift network which are three resistors and four capacitors can be designed by equate with numerical value. So that if the input impedance of the phase shift amplifier are defined with all of the coefficients which are derived in the report. Thus, all of the numerical values are defined by basic programming. It means something similar with the first group of coefficient, second group until the last group which are a function of the small signal parameters and all passive components in the circuit diagram. The magnitude and phase response at various current consumption can be plotted as shown in figure2.

The magnitude response can be described as following, the magnitude response is increased at the frequency higher than 10 kilo Hertz until it is reached the first peak of the magnitude response around 600 kilo Hertz at current consumption of 1 milli ampere. Then, the magnitude response is decreased after it pass the first peak. The highest peak of the magnitude response is around 16 gigahertz. Different current consumption has some different magnitude response such as maximum magnitude response from the 3 values of current consumption should be 10 milli ampere approximately 700 dB.

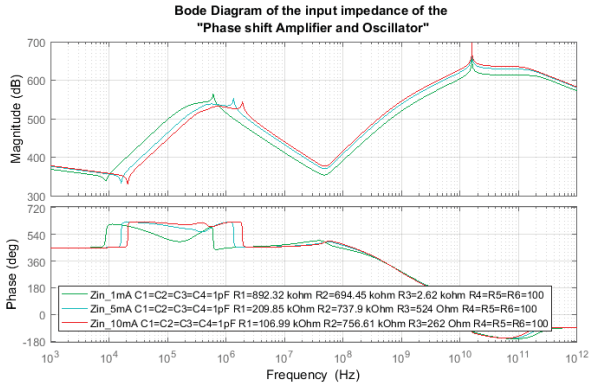

FIGURE 2. A BJT Phase Shift Amplifier magnitude and phase response as a function of current consumption

(a) Input impedance for 1 milliamp

(b) Input impedance for 5 milliamp

(c) Input impedance for 10 milliamp

VII. CONCLUSION

According to the theory of the root locus of complex poles of the denominator polynomial after factorization of the input impedance in the frequency domain. If it is impossible for poles to move from complex poles to imaginary pole in the complex poles plot. It means that the phase shift oscillator may not practical without input impedance matching. In microwave oscillator theory, it is possible that any transistor network can be oscillate as a periodic function if it is matched with impedance matching network so that its denominator polynomial input impedance can be factorized to have the real parts less than or approximately zero ohm.

REFERENCES

[1] E. L. Ginzton, L. M. Hollingsworth, "Phase Shift Oscillators", Proceedings of the I. R. E, February 1941, pp. 43-49

[2] R. W. Johnson, " Extending the Frequency Range of The Phase Shift Oscillator", Proceedings of the I. R. E, September 1945, pp. 597-603

[3] S. Sherr, " Generalized Equations for RC Phase-Shift Oscillator", Proceedings of the I.R.E, July 1954, pp. 1169-1172

[4] W. M. Locke, V. M. Moore, W. W. Happ, " A New Analysis of the Transistor Phase-Shift Oscillator", Journal Brit. I. R. E, February 1963, pp. 145-153

[5] K. Tripetch, N. Nakano, "A Design of Cross Couple Oscillator with Root Locus by using current consumption", Journal of Electrical Engineering and Electronic Technology, Volume 7, Issue 2, 1000158, pp. 1-6

Kittipong Tripetch (M'02) received the Bachelor of Engineering degree in Telecommunication Engineering since 1996 from Mahanakorn University of Technology. He received the Master of Engineering in Microelectronic Engineering since 2002 from Mahanakorn University of Technology. He have been employed by Rajamangala University of technology Suvarnabhumi, Nonthaburi Campus since 2004 as a lecturer. Since April 2014, he studied with associate professor Dr. Nobuhiko Nakano so that he can design a circuit diagram according to the function and specification of the block diagram with linear algebra, calculus, Laplace's transform and inverse Laplace's transform, symbolic partial fraction expansion without a limit theorem and a high order symbolic factorization which teach how a pole frequency of the denominator polynomial can be written as a function of the coefficient of the denominator polynomial by solving a linear algebra problem. He have been received a Ph.D degree from Graduate School of Science and Technology, Department of Electrical and electronic engineering, with a major in integrated design engineering, Keio University since 28 March 2019, his Supervisor is Associate Prof. Dr. Nobuhiko Nakano, his three co-supervisors are Prof. Dr. Hiroki Ishikuro, Prof. Dr. Hiroyasu Izeki, Assoc. Prof. Dr. Ryogo Kubo. He is a member of IEEE since 2002.

Production and Evaluation of Activated Carbon from Oil Palm Kernel Shell in the Removal of Paraquat Diluted in Water

Sonia L. Rincón Prat, Oscar F. Alvarez Alvarez, Daniel M. Alvarez Villanueva

***Abstract*—**Oil Palm Kernel Shell (OPKS) is a residue of the palm oil extraction process, which has good characteristics for the production of activated carbon (AC). Colombia ranks fourth in the world in palm oil production and it is estimated that in 2018 the amount produced of OPKS was approximately 350,000 tons per year.

Within the contaminants of surface waters, the pesticide Paraquat is identified as one of the most dangerous for human health and most used in agriculture in Colombia.

Oil palm kernel shells were first carbonized in a horizontal oven under N_2 atmosphere until 850 °C for 30 min. After that, three batches, each of 300 g of the carbonized OPKS (C- OPKS) were activated in the same horizontal reactor by means of partial gasification using H_2O as reaction agent. The activation process starts with a heating stage by raising the temperature from 20 °C to 850 °C in approximately 280 minutes under a flow of 0.481 l/min N_2 at standard conditions. Subsequently in the activation stage the flow of N_2 is suspended and replaced by a flow of 4 ml/min steam (measurement in liquid state before going through the evaporation system) while maintaining the temperature at 850 ± 10 °C for another 310 minutes. Finally the flow of steam is changed to N_2 and the oven is cooled down until ambient temperature. As a result of the activation process (partial gasification), an activated carbon (AC-OPKS) with approximately 50 % degree of activation and a surface area of 1200 m^2/g were obtained.

The activated carbon is characterized by means of determination of pH, soluble water content, extractable acid content, iodine number, methylene blue index, phenol adsorption, BET surface area from N_2 adsorption and density.

The adsorption capacity of the AC-OPKS towards Paraquat is studied by measuring breakthrough curves in an adsorption column using initial concentrations of Paraquat between 600 µg / l and 5000 µg / l. A comparison is performed by using a commercial activated carbon CO-AC from the company Donau Carbon ref. Hydraffin. The determination of the concentration of Paraquat in water is made by voltammetry. This technique provides the necessary sensitivity, and is economical and accessible.

***Keywords*—**Activated carbon, Oil Palm Kernel Shell, Partial gasification, Removal of contaminants.

S. L. Rincón, Associate Professor - Universidad Nacional de Colombia – Sede Bogotá – Facultad de Ingeniería – Departamentos de Ingeniería Mecánica y Mecatrónica – Grupo de Investigación en Biomasa y Optimización Térmica de Procesos – BIOT - Carrera 30 Nº 45-03 Edificio 453 Of. 400, Bogotá, Colombia (e-mail: slrinconp@unal.edu.co).

O. F. Alvarez Alvarez., Student Masters Degree in Mechanical Engieering Universidad Nacional de Colombia – Sede Bogotá – Facultad de Ingeniería – Departamentos de Ingeniería Mecánica y Mecatrónica – Grupo de Investigación en Biomasa y Optimización Térmica de Procesos – BIOT - Carrera 30 Nº 45-03 Edificio 453 Of. 400, Bogotá, Colombia (e-mail: ofalvareza@ unal.edu.co).

D. M. Alvarez Villanueva., Student Masters Degree in Materials and Manufacturing Processes - Universidad Nacional de Colombia – Sede Bogotá – Facultad de Ingeniería – Departamentos de Ingeniería Mecánica y Mecatrónica – Grupo de Investigación en Biomasa y Optimización Térmica de Procesos – BIOT - Carrera 30 Nº 45-03 Edificio 453 Of. 400, Bogotá, Colombia (e-mail: dmalvarezvi@ unal.edu.co).

Commissioning, Test and Characterization of Low-Tar Biomass (LTB) Gasifier for Rural Applications and Small-Scale Plant

Md Mashiur Rahman, Ulrik Birk Henriksen, Jesper Ahrenfeldt, Maria Puig Arnavat

Abstract**—**Using biomass gasification to make producer gas is one of the promising sustainable energy options available for small scale plant and rural applications for power and Electricity. Tar content in producer gas is the main problem if it is used directly as a fuel. A low-tar biomass (LTB) gasifier of approximately 30 kW capacity has been developed to solve this. Moving bed gasifier with internal recirculation of pyrolysis gas has been the basic principle of the LTB gasifier. The gasifier focuses on the concept of mixing the pyrolysis gases with gasifying air and burning the mixture in separate combustion chamber. Five tests were carried out with the use of wood pellets and wood chips separately, with moisture content of 9-34%. The LTB gasifier offers excellent opportunities for handling extremely low-tar in the producer gas. The gasifiers producer gas had an extremely low tar content of 21.2 mg/Nm^3 (avg.) and an average lower heating value (LHV) of 4.69 MJ/Nm^3. Tar content found in different tests in the ranges of 10.6-29.8 mg/Nm^3. This low tar content makes the producer gas suitable for direct use in internal combustion engine. Using mass and energy balances, the average gasifier capacity and cold gas efficiency (CGE) observed 23.1 kW and 82.7% for wood chips, and 33.1 kW and 60.5% for wood pellets, respectively. Average heat loss in term of higher heating value (HHV) observed 3.2% of thermal input for wood chips and 1% for wood pellets, where heat loss was found 1% of thermal input in term of enthalpy. Thus, the LTB gasifier performs better compared to typical gasifiers in term of heat loss. Equivalence ratio (ER) in the range of 0.29 to 0.41 gives better performance in terms of heating value and CGE. The specific gas production yields at the above ER range were in the range of 2.1-3.2 Nm^3/kg. Heating value and CGE changes proportionally with the producer gas yield. The average gas compositions (H_2-19%, CO-19%, CO_2-10%, CH_4-0.7% and N_2-51%) obtained for wood chips are higher than the typical producer gas composition. Again, the temperature profile of the LTB gasifier observed relatively low temperature compared to typical moving bed gasifier. The average partial oxidation zone temperature of 970°C observed for wood chips. The use of separate combustor in the partial oxidation zone substantially lowers the bed temperature to 750°C. During the test, the engine was started and operated completely with the producer gas. The engine operated well on the produced gas, and no deposits were observed in the engine afterwards. Part of the producer gas flow was used for engine operation and corresponding electrical power was found to be 1.5 kW continuously, and maximum power of 2.5 kW was also observed, while maximum generator capacity is 3 kW. A thermodynamic equilibrium model is good agreement with the experimental results and correctly predicts the equilibrium bed temperature, gas composition, LHV of the producer gas and ER with the experimental data, when the heat loss of 4% of the energy input is considered.

Keywords**—**Gasification, Biomass, Low-tar, Moving bed gasifier, tar reduction process, Engine, Deposits, Condensate.

MD Mashiur Rahman is with the Regional Agricultural Research Station, Bangladesh Agricultural Research Institute, Bangladesh (phone: +8801717094587; e-mail: mashi.fpm84@gmail.com).

Ulrik Birk Henriksen, Senior Researcher, is with the Department of chemical Engineering, Technical University of Denmark, Denmark (e-mail: ubhe@kt.dtu.dk).

Jesper Ahrenfeldt, Senior Researcher, is with the Department of chemical Engineering, Technical University of Denmark, Denmark (e-mail: jeah@kt.dtu.dk).

Maria Puig Arnavat, Researcher is with the Department of chemical Engineering, Technical University of Denmark, Denmark (e-mail: mpar@kt.dtu.dk).

Groundwater Fluoride Status and Its Effects on the People of the Rural Areas of Guntur District, Andhra Pradesh

Babu Rao Gudipudi

Abstract—Fluoride in groundwater is considered to be a toxilogical geo-environment issue when it is present in excess or deficient. In view of this Nuzendla mandal of Guntur District is carefully chosen for the present study. The study intends to identify the groundwater fluoride levels in and its impact on people living in the study area. Fifty groundwater and urine samples from the study area were collected and dental survey was also conducted in selected five villages of the study area. About 64% and 72 % of the total groundwater samples during pre-and post-monsoon periods are exceeding the safe limit of F- (1.5 mg/L). Dental survey indicates four out of five villages are exhibiting higher Community Fluorosis Index value (> 0.6) may causes public health problem. Urine sample survey suggests that urine F− content in most of the locations is exceeding the acceptable concentration of 1.0 mg/L. This shows that the groundwater consumed by the individual itself is main causative factor for fluorosis hazard in the study area.

Keywords—Groundwater, Fluoride, Dental survey, fluorosis hazard.

Dr. Babu Rao Gudipudi, Associate Professor, Department of Civil Engineering, Narasaraopeta Engineering College, Kottapakonda Road, Yallamanda (P), Narasaraopet-522 601 (e-mail: gudipudi.br@gmail.com).

Analyzing Sun Valley Music Pavilion *Idaho, USA, 2008* in Relation Flexibility and Adaptability

Ola Haj Saleh

***Abstract*—**This study of a contemporary building attempts to identify how a building can reflect its presence within its community. The example of the pavilion is discussed here with references to adaptability & flexibility theories. The analytical methodology of the Sun Valley Pavilion discovers to what extent a public space can be flexible and adaptable to several conditions. Furthermore, redefine an existing public building in an urban landscape context, becomes more than an important place for its community as a music pavilion for the arts, it is even for the interactivity wedding parties. Thus, the Sun Valley Pavilion can have an obvious role in a community gathering place in a result that flexibility and adaptability are more economical in the long term.

***Keywords*—**Adaptability, flexibility, pavilion, tensile.

Ola Haj Saleh is with Eastern Mediterranean University, Cyprus (e-mail: olamajed91@gmail.com).

Omni: Data Science Platform for Evaluate Performance of a LoRaWAN Network

Emanuele A. Solagna, Ricardo S, Tozetto and Roberto dos S. Rabello,

Abstract—Nowadays, physical processes are becoming digitized by the evolution of communication, sensing and storage technologies which promote the development of smart cities. These technology's evolution has generated multiple challenges related to the generation of big data and the active participation of electronic devices in society. Thus, devices can send information that is captured and processed over large areas, but there is no guarantee that all the obtained data amount will be effectively stored and correctly persisted. Because, depending on the technology which is used, there are parameters that has huge influence on the full delivery of information. This article aims to characterize the project, currently under development, of a platform that based on data science will perform a performance and effectiveness evaluation of an industrial network that implements LoRaWAN technology considering its main parameters configuration relating this parameters to the information loss.

Keywords—Internet of Things, LoRa, LoRaWAN, Smart Cities

I. Introduction

IN the context of Smart Cities, the Internet of Things has promoted the experimentation and analysis of urban infrastructures that allow innovation [1], enabling the emergence of new data communication technologies. These new technologies are usually composed of devices that have sensing, processing and communication capabilities with other devices. They can perform tasks, automate processes, which enable them to learn common behaviors and identify eventualities across many types of systems and infrastructures. These devices can be called Smart Objects [2]. However, such objects have recurrent processing and energy limitations, making wireless communication a major challenge.

LoRaWAN networks aim to solve this challenge by being a Low Power Wide Area Network (LPWAN), a low power and long range network. They are implemented using LoRa (Long-Range) technology, a radio-frequency technology that enables low power long-distance communication [3]. In addition, LoRa devices configuration comprises a few main parameters, one of them, which is the radio signal modulation technique, called Spread Spectrum Modulation (SSM) [4]. In this technique, the original signal is spread in the frequency field, increasing the signal robustness. In the LoRa specification, the SSM is related to a parameter called *Spreading Factor*(SF).

The SF can be set as six different values, from SF7 to SF12 [5]. Each value causes variation between the robustness of interference modulation and the bit rate. On the one hand, depending on the configured value, the transmission rate may increase, which also increases the communication flow rate. However, on the other hand, the value of the parameter may imply loss of resistance to interference, which induces packet loss and decreases the flow.

Because LoRa technology is relatively new, little is known about the impact of SF value configuration, assuming that this parameter is one of the main factors that directly affect network performance and effectiveness. Thus, this paper proposes to present the project, under development, of the development of a web platform to perform an evaluation of the performance and communication effectiveness of LoRa technology. The analysis will be performed according to the Spreading Factor parameter, since this is a particularity of the technology, its value is configurable via software and because it is a parameter that significantly implies the network performance. The parameters of signal strength, gateway latency, packet loss rate, and communication flow rate will be analyzed to evaluate the efficiency of the defined spreading factor.

The network to be evaluated will be an industrial network using LoRaWAN technology, which was built by OPTIM, a customized hardware/firmware developer company, integrate at UPF Planalto Mdio Science and Technology Park, at University of Passo Fundo (UPF), located in the city of Passo Fundo - Rio grande do Sul, Brazil. The company has the demand to obtain a performance and effectiveness assessment of its network, aiming to use the maximum capacity and efficiency of the devices that are in operation. Thus, was proposed the development of a web platform for data collection regarding packet traffic on the network and the use of Data Science (interdisciplinary area focused on study and data analysis), aiming at the extraction of knowledge or insights, based on the data that will be obtained.

II. Scientific Foundation

Since 3,000 B.C., cities have developed as a means for the strengthening of human life and housing. The emergence of cities was a natural response to life circumstances, but they also had a profound and lasting impact on the evolution of the human species as a whole [6].

Currently, cities are challenged with issues related to economic development, social inclusion, security, sustainability, infrastructure, transportation, housing, etc. At the same time, the advent of new information and communication technologies has allowed the democratization of the production capacity of citizens, who are empowered to participate in the innovation dynamics of their cities [7]. Thus, they can be conceptualized as complex ecosystems, where different

E. A. Solagna and R. dos S. Rabello are with the Institute of Exact Sciences and Geosciences - University of Passo Fundo (UPF), Passo Fundo, RS, BRAZIL e-mail: 175478, roberto.rabello@upf.br

R. S. Tozetto is with the Faculty of Engineering and Architecture - University of Passo Fundo (UPF)

actors with different interests collaborate with each other. And from the emergence of new media *Information and Communication Technologies* (ICTs), performance indicators such as knowledge-based social capital gained ground [8] and concepts such as *smart cities* were developed and put into practice.

Smart cities are generally characterized by the widespread use of ICTs in traditional infrastructures, as well as to enhance the active participation of human and social capital [7], [9]. This technology-based approach is considered capable of dealing with different problems[10], [11], while ensuring the quality of the urban environment and the sustainability of its development. Thus, a smart city can be described as a city that uses ICTs to improve the quality of life of its population [7]. The formation of smart cities, widely connected to the Internet, makes use of the Internet of Things to transform the life and work of the community.

For the use of IoT solutions, technologies with long battery life and communication over long distances are required as shown in Figure 1.

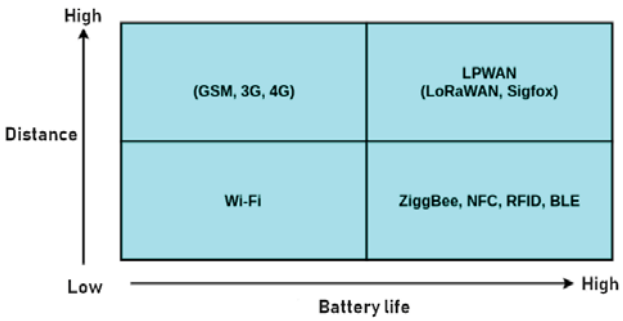

Fig. 1. Communication distance x battery life of each communication technology [12]

A promising solution is low power long range networks (LPWAN). They where created specifically focused on low-level IoT applications, in other words, low cost devices, long battery life and low transmission rates [13]. Devices on the LPWAN network use LoRa technology, which is a radio frequency technology that enables long distance communication with minimal power consumption and follows the Internet of Things paradigm.

LoRa technology defines a physical layer, which seeks to attempt the low power requirements of Smart Objects and is used to implement the LoRaWAN protocol. LoRaWAN is the protocol that defines system architecture and communication and access parameters. The protocol also defines the rates of data transmission speed, support for two-way communication and provision of mobility services and location of network devices.

The LoRaWAN network consists of four components: end-devices, gateways, network server and application server. End-devices are the Smart Objects, usually with energy restrictions, they can be sensors or other types of smart devices. Gateways act as relays that forward messages sent by any end device to the network server, after adding some reception quality information. The Network Server is responsible for filtering out unwanted and duplicate packets and responding to an end device by choosing a particular gateway according to the quality of the [14] radio connection. End devices are associated with the network server, so they can ”move” along the network being served by different gateways [4], [15]. Application servers are specific programs that receive (via request or automatically) packets from network servers and according to the information perform one or more specific actions.

The LoRaWAN protocol uses authentication, data integrity and packet duplication mechanisms characterized as MAC (Media Access Control). Thus, every packet of information that circulates on a LoRaWAN network is protected with Advanced Encryption Standard (AES) cite Singh encryption. In the physical layer, LoRa technology has chirps-based modulation, which are signal frequency changes at predefined times. These chirps can be separated between base-chirps and down-chirps, depending on whether the frequency ranges from $f_{min} = \frac{-BW}{2}$ to $f_{max} = \frac{+BW}{2}$ for base-chirps and $f_{max} = \frac{+BW}{2}$ up to $f_{min} = \frac{-BW}{2}$ for down-chirps , assuming that BW (Bandwidth) is the signal bandwidth. Thus, for different digital signal inputs for modulation different chirps with different time offsets are produced. In addition, for signal demodulation to occur, there must be alignment of time references between the transmitter and the receiver. From there, the demodulator determines the displacement of each chirp by multiplying it by itself and searching for the Fast Fourier Transform (FFT) of the result, and in this power spectral diagram performing a search for the maximum signal, thus determining The demodulated digital symbol. Another important feature of this modulation is the SF (Spreading Factor) which is given by $\log N$, where N is chirp length, considering that there may be different cyclic changes in this value and characterizing the factor. spreading communication [16]. Also, we can mention the Symbol Rate (SR) and Data Rate (DR) that depend directly on the Spreading Factor and determine the transmission rate of the communication system. The Figure 2presents the spectrum of a LoRa packet.

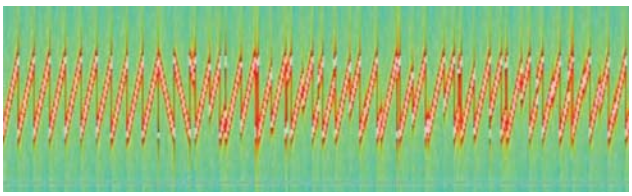

Fig. 2. Power spectral density of a LoRa packet (Adapted from [16].

As for topology, LoRaWAN networks are typically defined as tree cluster topology, as can be seen in Figure 3. Gateways are connected to the network server over an Internet Protocol (IP) connection, while end devices connect to one or more gateways using single hop communication. As shown, the proposed platform lies between the network server and the [15] application server.

The LoRaWAN network specification defines three classes of end devices in its architecture to achieve different types of service: class A, class B, and class C [15]. On Class

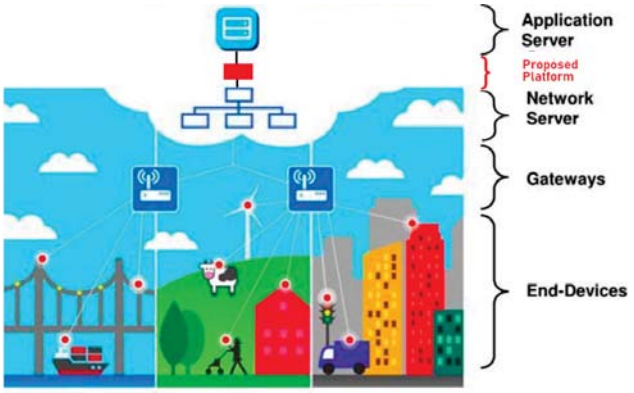

Fig. 3. LPWAN network architecture, where devices, gateways, network server, and application servers are present (Adapted from [4]).

A devices, they can send messages to the gateway at any time. However, they are only available for reception during time windows called reception windows. During these windows, the gateway can send messages to devices. A class A device initiates communication with the gateway and, after transmission, initiates a receive window, waits for a certain amount of time, and initiates a second receive window. A new receive window will only open after a new transmission from the same class A device. This mode of operation must be implemented by all LoRa devices. On class B devices, the process is similar. The class B device also opens two receive windows after performing a transmission. However, additionally, Class B devices open reception windows with scheduled times, configured through messages issued by the gateway. On class C devices, terminal devices are always available for receiving [14] messages.

III. Material and Methods

The execution of this project aims to achieve as a final result the implementation of a web platform, integrated with the LoRaWAN telemetry [1] network developed by OPTIM. And based on this integration, apply data science concepts and perform an evaluation of performance and effectiveness of the LoRaWAN network.

The project development is divided into phases, which are: research, platform development, data collection and analysis, which are further subdivided into smaller steps. Figure 4 gives an overview of the phases and their activities:

The project began with a literature review and study of the general topics covered, smart cities, communication technologies (LPWAN, LoRa and LoRaWAN) and data science, including books, journal and congress articles and the study of the network, its platforms and integration APIs.

The functional structure of the platform, already implemented, is divided into four layers: Data Source, Data Collection, Web Layer and Interaction forms. Figure 5 shows the schematic diagram of the developed architecture.

[1] Automated communication process in which measurements are taken and other data is also collected at remote or mobile points where there is usually difficult to access, or impossible to establish cabling.

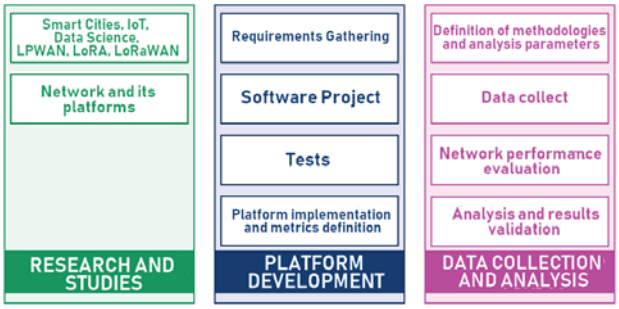

Fig. 4. Phases and activities that are being followed to complete the project, which is currently in the data collection (AUTHOR).

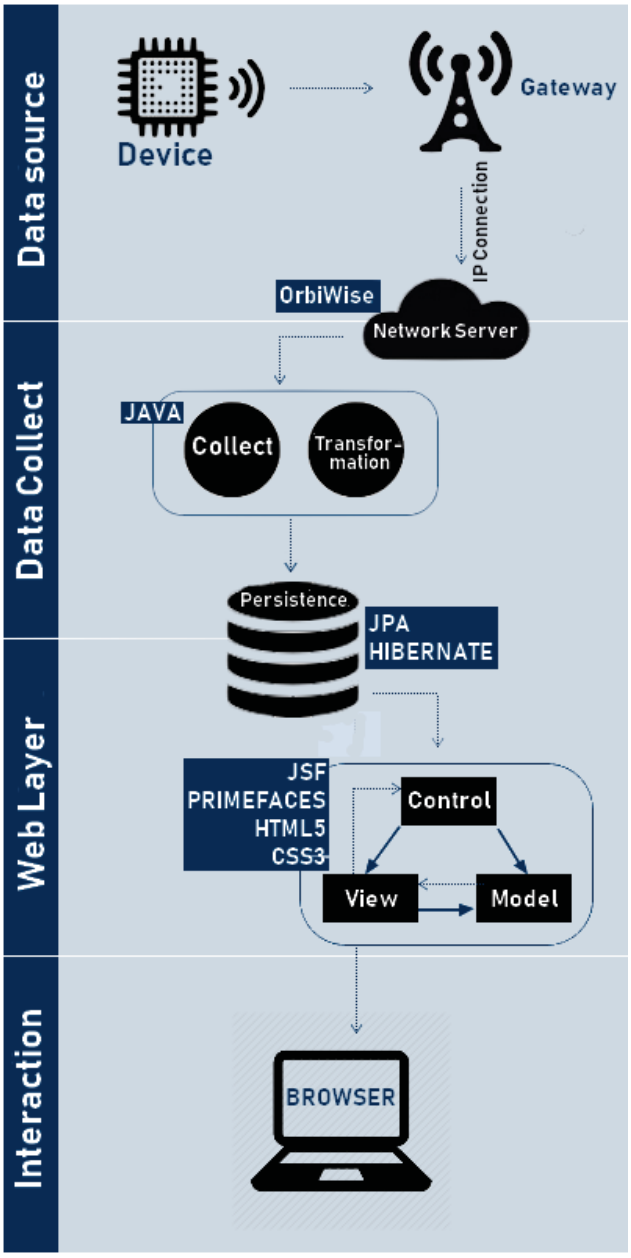

Fig. 5. Developed subdivided platform architecture (AUTHOR).

The first layer is the data source layer, basically the LoRaWAN network where end devices collect and send data obtained from their sensing to a gateway. Data is temporarily stored by *Orbiwise* [2], Which was OPTIM's own chosen network server.

At this point, the data set stored on the network server is considered to be in JSON document format. JSON is an acronym for "JavaScript Object Notation", it is a compact format for fast and simple data exchange between open standard systems, independent of the JavaScript [17] derived programming language. This format has unique specifications that need to be considered while handling.

The second layer is the Data Collection layer, where JSON documents are "harvested", modeled on a Java object (language chosen by the company for platform development) and, using the Java Persistence API (JPA) with Hibernate 4, the data will be persisted into the database. Both technologies were chosen to compose the project because they are already consolidated technologies and have a satisfactory performance.

Once stored, the data is available for use by the Web Layer. In this layer, the repository built by the Data Collection step will be mined using data science technology, which will still be chosen. In order to extract information about the collected packages, which will be presented as dynamic dashboards in the platform. In addition, the Web layer is also responsible for all navigation and interactivity logic devised for the tool. Several technologies were necessary to build the Web layer, the main ones being the Java Server Faces (JSF) frameworks with PrimeFaces and the HTML5, Javascript and CSS3 technologies. And finally, the Interaction Layer is where access to the platform's web layer is provided via the web browser.

Methodologically the tests and evaluations performed will be based on the Ishikawa Diagram, also known as Cause and Effect Diagram, presented in Figure 6. A tool that helps to root out the root causes of a problem by analyzing all the factors surrounding the process execution.

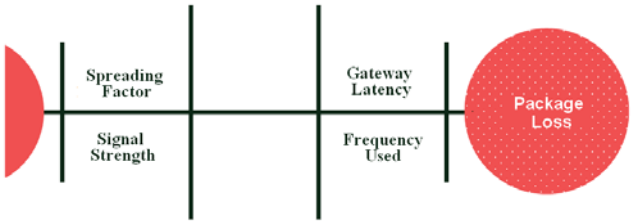

Fig. 6. Ishikawa diagram presents the possible causes for packet loss on the network.

In the case of this project, as already commented, the following parameters will be considered: Spreading factor, Gateway latency, signal strength and frequency. The purpose of using this methodology is to find out what is the influence of these parameters on the packet losses that happen in the network and which one of them have more action in this problem.

Currently the project is in the last phase, this happens the data collection, cleaning them so that the performance and effectiveness of the network can be performed considering the previously defined metrics, analysis and validation of the results obtained. The necessary cleaning of the 112.000 stored packages is currently being carried out. Since the network has 40 devices in operation, with standard communication every 1 hour from April 23, 2019 and data collection was done until August 21, 2019 (120 days), that was the amount expected packets that would be received.

Figure 7 presents the packages at the platform and with some storaged parameters. In addition to the presented parameters, gateway latency data, SF used for each packet, other signal strength data, and standard data provided by the LoRaWAN protocol are also being stored.

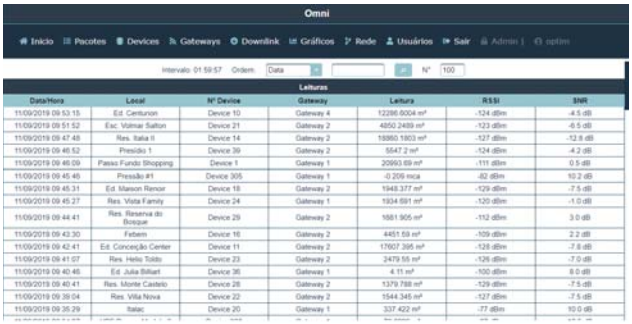

Fig. 7. The platform that was called Omni Platform shows already stored packages and displaying some values from each package.

IV. Final Considerations

This paper aimed to present the project of developing a web platform to evaluate the functionality and effectiveness of a LoRaWAN industrial network. The project was based on OPTIM's need for a performance appraisal of its LoRaWAN network. It was discussed about the spreading factor, a parameter defined as the basis for the network evaluation to be performed, which is a very important factor in the network configuration. The idea of measuring packet loss rate and communication flow was established in order to evaluate the efficiency of the spreading factor defined for the network in question.

The steps and phases that divide the project were exposed, so that the proposed objectives can be successfully achieved. And currently the project is at the end of the data collection stage, which will be used to start the performance and effectiveness analysis of the network.

From this project it is expected to demonstrate that LoRaWAN technology meets the expectations of being a solution with good performance and significant effectiveness, proving to be reliable for use in the context of smart cities.

[2]Swiss network company that develops advanced technologies for the IoT industry. It has a network server (Orbiwan) for networks based on LoRa technology.

References

[1] N. Schaffers, H.and Komnimos and M. e. a. Pallot, "Smart cities and the future internet: Towards cooperation frameworks for open innovation,"

In: The Future Internet: Future Internet Assembly 2011: Achievements and Technological Promises, Springer Berlin Heidelberg, no. 31, p. 431446, 2011.

[2] V. Rozsa, M. Dutra, A. Pinto, and E. Muriel-Torrado, "O paradigma tecnolgico da internet das coisas e sua relao com a ciŁncia da informao," vol. 27, no. 3, p. 255266, 2017.

[3] L. Alliance, "Lorawan specification v1.0.2," *LoRa Alliance*, 2019.

[4] C. SEMTECH, "Loratm modulation basics an1200.22," Tech. Rep., 2015. [Online]. Available: https://www.semtech.com/uploads/documents/

[5] L. Alliance, "Lorawan regional parameters," *LoRa Alliance*, 2019.

[6] D. Schuurman, B. Baccarne, and L. D. Marez, "Smart ideas for smart cities: Investigating crowdsourcing for generating and selecting ideas for ICT innovation in a city context," *Journal of theoretical and applied electronic commerce research*, vol. 7, no. 34, pp. 11–124, 2012.

[7] I. Capdevila and M. I. Zarlenga, "Smart city or smart citizens? the barcelona case," *Journal of Strategy and Management*, vol. 8, no. 3, pp. 266–282, 2015.

[8] A. Caragliu, C. Del Bo, and P. Nijkamp, "Smart cities in europe," Thought Technology Ltd., Amsterdam, Tech. Rep., 2009.

[9] R. Dameri, "Searching for smart city definition: a comprehensive proposal," *International Journal of Computers & Technology*, vol. 11, pp. 2544–2551, 2013.

[10] M. Batty, K. Axhausen, F. Giannott, A. Pozdnoukhov, A. Bazzani, M. Wachowicz, G. Ouzounis, and Y. Portugali, "Smart cities of the future," *The European Physical Journal Special Topics*, vol. 214, no. 1, pp. 481–518, 2012.

[11] J. H. Lee, R. Phaal, and S.-H. Lee, "An integrated service-device-technology roadmap for smart city development," *Technological Forecasting and Social Change*, vol. 80, no. 2, pp. 286–306, 2013.

[12] L. Saraiva, "Projeto de hardware e software para dispositivos finais em uma rede LoRaWAN," 2017, engenharia de Telecomunicaes - Instituto Federal de Santa Catarina (IFSC), So Jos SC.

[13] M. R. Palattella, M. Dohler, A. Grieco, G. Rizzo, J. Torsner, T. Engel, and L. Ladid, "Internet of things in the 5g era: Enablers, architecture, and business models," *IEEE Journal on Selected Areas in Communications*, vol. 34, no. 3, pp. 510–527, Mar 2016.

[14] M. Bor, J. Vidler, and U. Roedig, "International conference on embedded wireless systems and networks, ewsn 16," in *Lora for the internet of things*. Junction Publishing, Out 2016, p. 361366.

[15] M. Centenaro, L. Vangelista, A. Zanella, and M. Zorzi, "Long-range communications in unlicensed bands: the rising stars in the iot and smart city scenarios," *IEEE Wireless Communications*, vol. 23, no. 5, pp. 60–67, Out 2016.

[16] J. Haxhibeqiri, E. D. Poorter, I. Moerman, and J. Hoebeke, "A survey of LoRaWAN for IoT: From technology to application," *Sensors*, vol. 18, no. 11, p. 3995, nov 2018. [Online]. Available: https://doi.org/10.3390/s18113995

[17] JSON, "Json documentation," *JSON Org*, 2019.

Evaluation of the Quality of Groundwater in the Zone of the Irrigated Perimeter Guelma-Bouchegouf, Northeast of Algeria

M. Benhamza, M. Touati, M. Aissaoui

***Abstract*—**The Guelma-Bouchegouf irrigated area is located in the north-east of the country, it extends about 80 km. It was commissioned in 1996, with an irrigable area of 9250 ha, it spreads on both banks of the Seybouse Wadi and it is subdivided into five autonomous distribution sectors.

In order to assess the state of groundwater quality, physico-chemical and organic analyzes were carried out during the low water period in November 2017, at the level of fourteen wells in the Guelma-Bouchegouf irrigation area.

The interpretation of the results of the chemical analyzes shows that the waters of the study area belong to two dominant chemical facies: sulphated-chlorinated-calcium and Sulfated-chlorinated-sodium.

The mineral quality of the groundwater in the study area shows that Ca^{2+}, Cl^{-} and SO_4^{2-} indicate little to significant pollution, Na^{+} and Mg^{2+} show moderate to significant mineralization of water, closely correlated with very high conductivities. NO_3^{-} and NH_4^{+} show little to significant pollution throughout the study area.

Phosphate represents a significant pollution, with excessive values exceeding the allowable standard. Phosphate concentrations indicate pollution caused by agricultural practices in the irrigated area, following the use of phosphates in the form of chemical fertilizers or pesticides.

***Keywords*—**Algeria, Groundwater, irrigated perimeter, Pollution.

M. Benhamza, M. Touati, M. Aissaoui are with Department of Geology, University of Badji Mokhtar Annaba, Laboratory of Geodynamic and Natural Resources (LGRN) BP 12 - 23000 - Annaba, Algeria (e-mail: moussa_benhamza@yahoo.fr, touati.mounira24@gmail.com, marwaaissaoui8@gmail.com).

The Regional Geology of the Northwestern Edge of the Sirt Basin

Elhadi Nasr, Hussein Abushaina

Harouge Oil Operations Company, Libya (e-mail: hadisaido@yahoo.com)

Introduction:

Recent regional geological work has been integrated with seismic investigations on the north western edge of the Sirt Basin and its overlap with the Ghadames Basin. The primary aim has been to prove the existence of a local petroleum system in this area with the presence of hydrocarbon source rocks, reservoir and seal.

The study area lies in the Northwestern Sirt Basin and is centred on Harouge Oil Operations Concession 10, this Concession is 10kms due east of the town of Sirt. Although it is mainly onshore a portion of the block also extends into the present day offshore.

Two wells have been drilled on the Concession, A1-10 drilled in 1959 and B1-10 that was drilled in 1994. The A1-10 well had only minor oil shows (poor fluorescence) that were recorded from near to the top of the Kalash Formation; the B1-10 well tested oil at 70 BOPD from a Kalash Formation reservoir.

Methodology:

Geochemical studies have been undertaken on samples from six wells in the study area.

Seismic interpretations and geological correlation's were used in this study .

Following the discovery of oil in the B1-10 well a local regional geological study was initiated. High resolution biostratigraphical analyses were undertaken including palynological, foraminiferal and calcareous nannofossil work to aid in the understanding of the stratigraphy and of the geological and structural relationships in the area , also identify and locate the hydrocarbon source for the B1-10 oil.

In an assessment of the Kalash Formation hydrocarbon reservoir a petrographical study was also undertaken on the B1-10 well.

Interpretation and Results:

Geochemical studies have been undertaken on samples from six wells in the study area. Results proved the presence of good quality source rocks for gas and light oil. Oil to source correlation's suggest that the Sirt Shale Formation is a preferred hydrocarbon source on isotopes and the Etel Formation on biomarkers. A generated thermal maturity trend indicates that early maturity is reached below a depth of approximately 7000'.

Seismic interpretations and geological correlation's confirm that there is an offshore extension of the Hagfa Trough where the Late Cretaceous section appears to thicken northwestwards, this is expected to have provided the hydrocarbon source for local recovered oil.

The Kalash Formation is recognised as the main hydrocarbon reservoir in the area. Lithologies are represented by very fine grained chalky and bioclastic limestones.

Recent biostratigraphical work on eight wells in the area indicates that the Kalash Formation is of Late Cretaceous, Early to Late Maastrichtian in age, it was deposited in a marine, low energy inner to outer shelf palaeoenvironment.

A probable hiatus / unconformity separates the Palaeocene section from the Kalash Formation. Petrographical analyses suggest that secondary carbonate dissolution associated with this stratigraphical break may have improved the porosities of the Kalash reservoir.

Conclusion:

The integrated multidisciplinary approach taken by this study has advanced our understanding of some of the geological relationships and the hydrocarbon prospectivity of the Northwest Sirt Basin and the area where it overlaps the eastern Ghadames Basin.

Recent identification of Late Cretaceous source rocks in the present day offshore indicate the Hagfa Trough extended Northwest through the An Nawfaliyah High area. It is possible source rock presence, quality and preservation exist and may improve within the trough to the Northwest where they are buried deep enough to have provided the oil for this newly recognised and underexplored petroleum system.

References:

ELAND, H.B. (1991). The Palynology and Thermal Maturity of seven core samples from the interval 6136' to 10,484' in the A1-10 well, onshore Libya. Petroleum Research Center, Tripoli, Libya. Unpublished Report for Veba Oil Operations.

GEOCHEM GROUP LIMITED (1989). A Biostratigraphical Evaluation of the Mobil F1-11 Well, Sirte Basin, Libya. Unpublished Report for Mobil Oil Libya Limited.

GEOCHEM GROUP LIMITED (1996a). A Biostratigraphical Analysis of the Interval 3650' - 4650' from the B1-10 well, Libya. Unpublished Report for Veba Oil Operations.

GEOCHEM GROUP LIMITED (1996b). Geochemical Evaluation of Wells A1-10 and B1-10, Northern Libya. Unpublished Report for Veba Oil Operations.
GEOCHEM GROUP LIMITED (1997a). A Biostratigraphical Study of the D1-87 Well, Libya. Unpublished Report for Veba Oil Operations.
GEOCHEM GROUP LIMITED (1997b). Geochemical Evaluation of the Offshore B1-87, C1-87 and D1-87 Wells as Source for the B1-10 Crude Oil. Unpublished Report for Veba Oil Operations.
GEOCHEM GROUP LIMITED (1999a). West Sirt Basin Regional Geological Study - Geochemistry. Unpublished Report for Veba Oil Operations.
GEOCHEM GROUP LIMITED (1999b). The Biostratigraphy of selected intervals from the wells B1-24, C1-86, C1-87 and H1-87 wells, Libya . Unpublished Report for Veba Oil Operations.
ROBERTSON GROUP PLC (1988). Petroleum Geochemical Evaluation of the Western Sirte Basin, Libya. **v.3**. Unpublished report for Mobil Oil Libya, Limited.

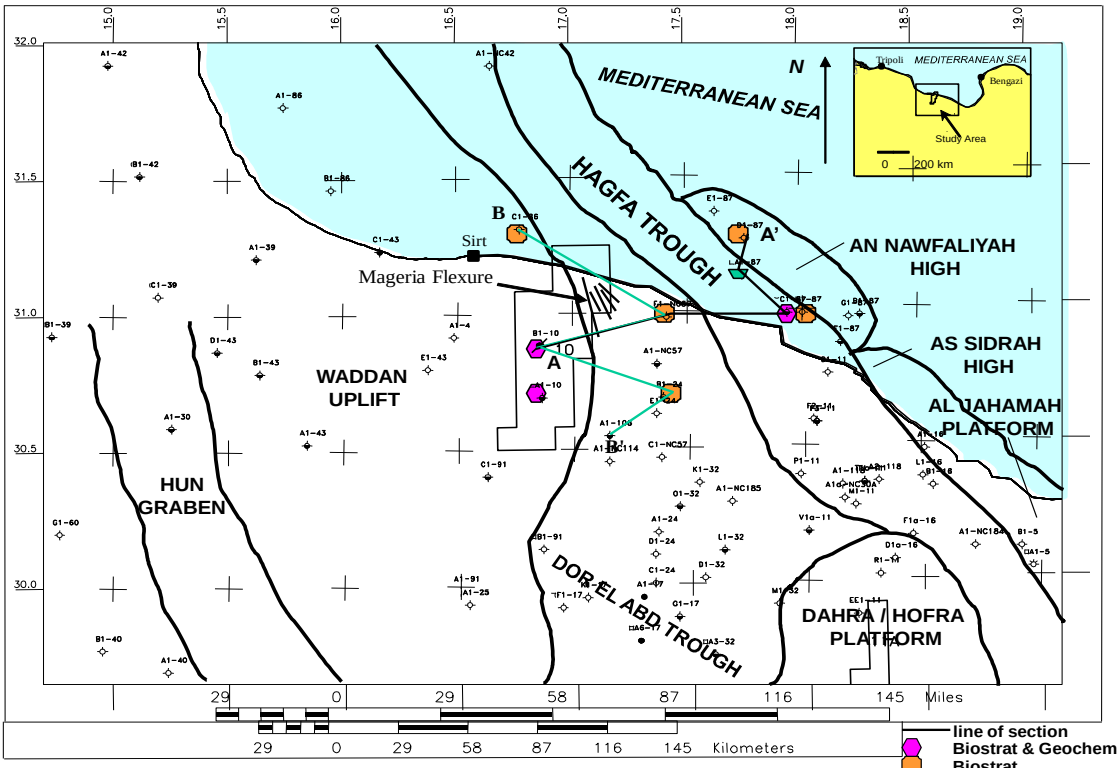

STUDY AREA LOCATION MAP AND MAIN TECTONIC FEATURES.

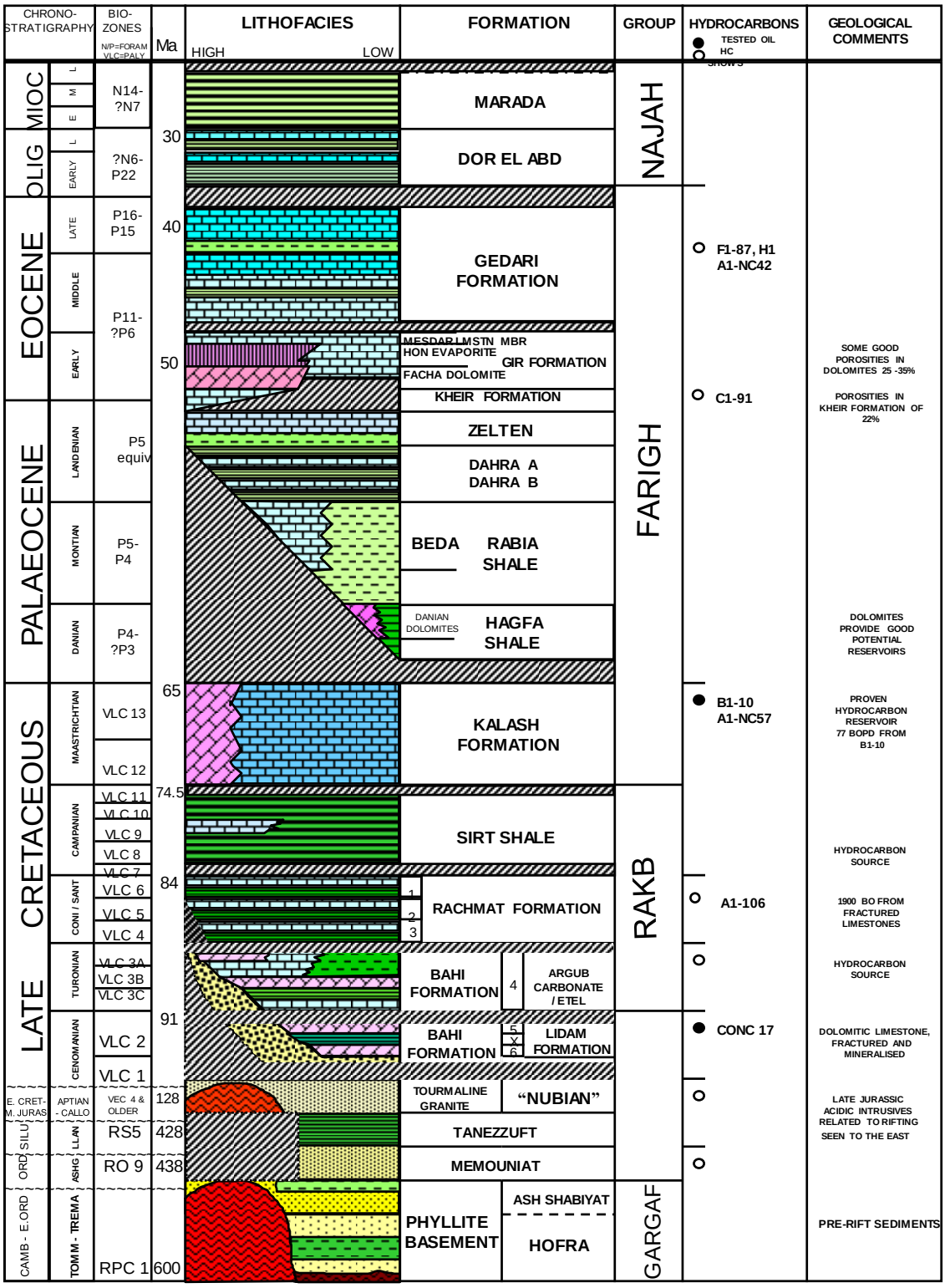

Composite Stratigraphical Column, Concession 10 Area, NW Sirt Basin

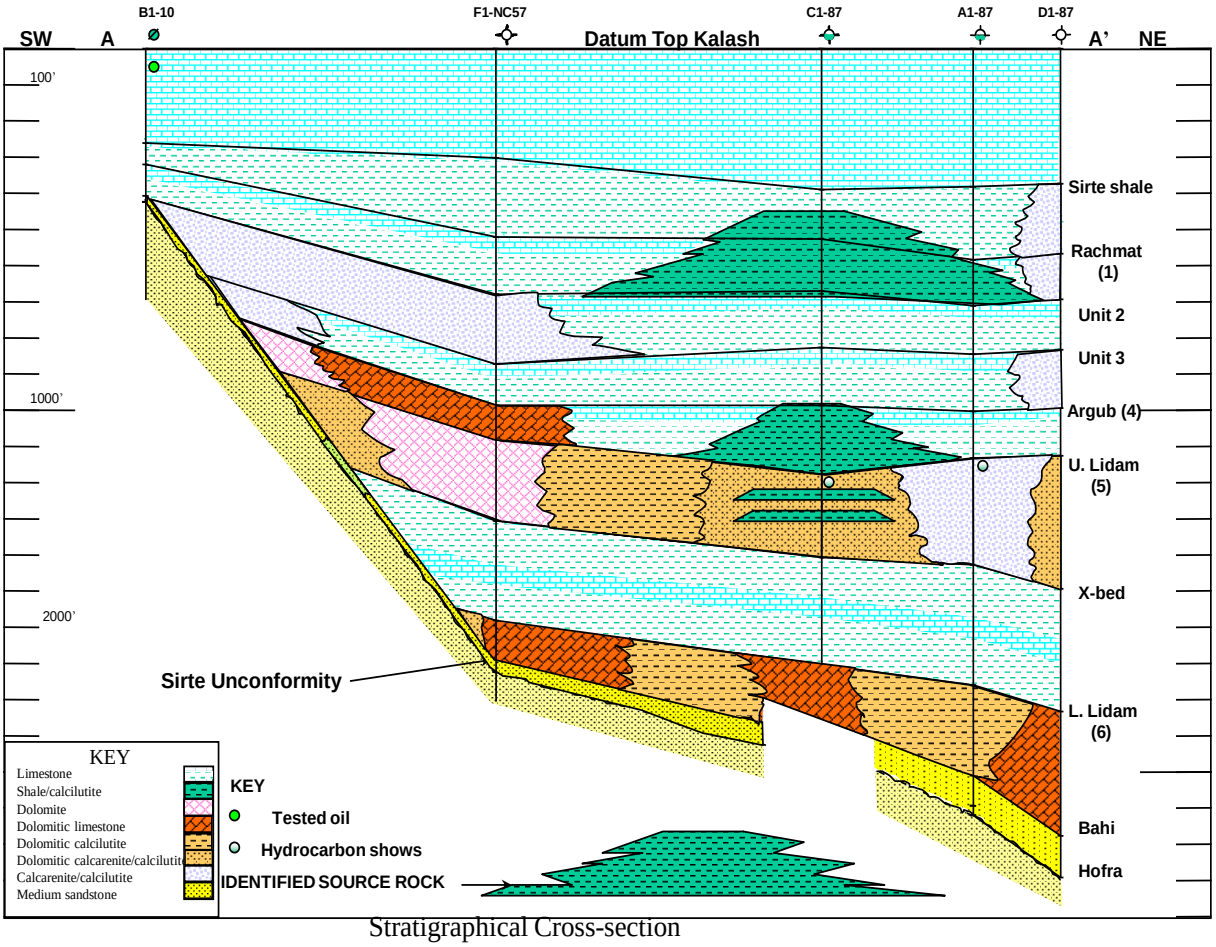

Stratigraphical Cross-section

Predicting Subseismic Carbonates Fracture Density and Orientation to Optimize Field Development Program in Tiaka Field, Sulawesi, Indonesia

Reza Armanda

Abstract**—**Fractured carbonate reservoir in Tiaka Field is dominated by tight shallow-water bioclastic platform limestones. Tomori Formation which is the main resevoir objective in this field, is controlled by low angle thrust fault as its structural trap. This field has 13 wells with 2 of them are sidetracks, but not all of them have good hydrocarbon production. In order to optimize the production of hydrocarbon, quantitative prediction of spatial and statistical properties of natural fractures are needed to give precise and wide prediction of fracture characteristic.

The elastic dislocation (ED) methodology was used to predict quantitative distribution of fractures in Tiaka Field by estimating strain and stress in the rock volume which has been derived from seismic interpretation. In ED theory, faults are represented as displacement discontinuities and the surrounding volume is modeled as a uniform elastic half space (Dee et al., 2007). ED forward modelling used magnitudes and orientations of the principal stresses that acting at each point in the rock volume to predict failure mode: shear or tensile, and also its orientation. Furthermore, the orientations of principal stresses also control the result of normal, reverse, or strike-slip fracturing. Maximum Coulomb Shear Stress (MCSS) has been used to define the deformation intensity as an indicator for relative of fracture density in Tiaka field, which is controlled by the degree to which shear stress exceed Mohr-Coulumb failure envelope (Freeman et al. 2015, Maerten et al., 2002, Bourne et al., 2001). Reliable ED forward modelling is also controlled by background strain and elastic properties of rock i.e Poisson's ratio and Young's modulus. Poisson's ratio governs the result in perturbed stress from the mechanical interaction between interacted faults.

Rock mechanical properties of Tomori Formation has been derived geomechanical analysis of Tiaka 7ST2A, at this case the only known information is Poisson ratio 0.24, 63 MPA for cohesive strength and 0.6 for coefficient internal friction. The orientation of simulated fractures network indicated that the dominant strike of simulated fractures is NW - SE with average dip for all predicted fractures has been confirmed by interpreted natural open fractures in image log. The high predicted fracture densities occur along the fault surface, especially at bends, which are the concentration of perturbed stress on the deformation surface, the highest densities also present at faults which have high dip-slip values. The ultimate proof to the validity is to get matched between fracture models with pressure transient analysis. Furthermore the result of this study will be utilized in Tiaka development strategy to reach IRR more than 15% and positive NPV.

Keywords**—**Fracture, fault elastic dislocation, rock failure, development strategy.

Reza Armanda is with PT Pertamina (Persero), Indonesia (e-mail: reza.armanda@pertamina.com).

Generation and Migration of CO_2 in the Bahi Sandstone Reservior within the En Naga Sub Basin

M. Gdara

Harouge Oil Operations / Petroleum Engineering Department Tripoli, Libya (e-mail: Moawia.Ghadara@harouge.com)

Abstract

The Lower Cretaceous Bahi Sandstone is the result of deposition that occurred between the start of the Cretaceous rifting that formed the area's Horsts, Grabens and Cenomanian marine transgression .Bahi sediments were derived mainly from those Nubian sediments exposed on the structurally higher blocks ,transported short distances into newly forming depocenters such as the En Naga Sub-basin and were deposited by continental processes over the Sirte Unconformity (pre-Late Cretaceous surface)

Bahi Sandstone facies are recognized in the En Naga Sub-basin within different lithofacies distribution over this subbase.

One of the two lithofacies recognized in the Bahi is a very fine to very coarse, subangular to angular, pebbly and occasionally conglomeratic, quartz sandstone, which is commonly described as being compacted but friable. This sandstone may contain pyrite, minor kaolinite .This facies was encountered at 11,042 feet in F1-72 well, and at 9,233 feet in L1-72.Good, reservoir quality sandstones are associated with paleotopographic highs within the sub-basin and around its margins where winnowing and / or deflationary processes occurred.

The second Bahi Lithofacies is a thinly bedded sequence dominated by shales and siltstones with subordinate sandstones and carbonates. The sandstones become more abundant with depth.This facies was encountered at 12,580 feet in P1 -72 and at 11,850 feet in G1a -72. This argillaceous sequence is likely the Bahi sandstone's lateral facies equivalent deposited in paleotopographic lows, which received finer grained material.

The Bahi sandstones are generally described as a good reservoir rock, which after prolific production tests for the drilled wells that makes Bahi sandstones the principle reservoir rocks for CO_2 where large volumes of CO_2 gas have been discovered in the Bahi Formation on and near EPSA 120/136, (conc 72).

CO_2 occurs in this area as a result of the igneous activity of the Al Harouge Al Aswad complex .Igneous extrusive have been pierced in the subsurface are exposed at the surface.

Bahi CO_2 prospectivity is thought to be excellent in the central to western areas of EPSA 120/136 (CONC 72) where there are better reservoir quality sandstones associated with Paleostructural highs. Condensate and gas prospectivity increases to the east as the CO_2 prospectivity decreases with distance away from the Al Haruj Al Aswad igneous complex.

To date, it has not been possible to accurately determine the volume of these strategically valuable reserves although there are positive indications that they are very large.

The Bahi is prospective for oil on the Khalifa High, where the best oil shows attributed to the Bahi are in N1-72 on the high flank of the Khalifah High The lower cretaceous Bahi Sandstone is considered as one of the deep reservoirs for hydrocarbon and non-hydrocarbon potential and it reflects a good example of deep over pressured reservoirs in the En Naga Sub – Basin.

Three main structures (Barrut I, En Naga A and En Naga O) are thought to be prospective for the lower Cretaceous Bahi sandstone development. These leads are the most attractive on EPSA 120/136 for the deep potential.

1) INTRODUCTION

In the Lower Cretaceous Bahi Sandstones, the presence of trapped carbon dioxide is proven within the En Naga Sub-basin. This makes it unique in providing an abundance of CO_2 gas reservoirs with almost pure magmatic CO_2, which can be easily sampled. Huge amounts of CO_2 exist in the Lower Cretaceous Bahi Sandstones in the En-Naga sub-basin where the economic value of CO_2 is related to its use for enhanced oil recovery (EOR). CO_2 considered flooding is a proven EOR process, which can be applied by miscible and/or immiscible displacement mechanisms to a wide variety of reservoir rocks and oil types.

En Naga Sub – basin have likely been point-sourced of CO_2 accumulations during the last 7 million years from local satellite intrusives associated with the Haruj Al Aswad igneous complex. CO_2 in the En Naga Sub-basin is thought to occur most dominantly because of the Al Haruj Al Aswad's igneous complex. The lower Cretaceous Bahi Sandstones are the principal reservoir rocks for CO_2. These sandstones are best developed when they are associated with paleostructures highs within the sub-basin or around its margins. In addition, the Bahi may be prospective for oil in the northeast part of the area.

In the En -Naga sub - basin, three main developed structures (Barrut I, En Naga A and En Naga O) are thought to be prospective for the lower Cretaceous Bahi sandstone reservoir. These structures represents a good example for the deep over pressure potential in EPSA 120/136 (CONC72). The very high pressures assumed associated

with local igneous intrusives may account for the abnormally high Bahi (and Lidam) reservoir pressures.

The CO_2 tested at F1-72 (Barrut I structure) as 98% overpressured. At U1-72 (En Naga O structure), a significant CO_2 gas kick occurred at 11,971 feet and quickly led to blowout conditions due to uncontrollable leaks in the surface equipment.

Unknown CO2 source locations and stratigraphic entry points, variable emanation parameters and limited existing data, combine to make predictions of CO2 presence within undrilled Bahi closures. For example, Q1-72's Facha closure within the En Naga (A). This structure contains black oil whose low volume gas contains 22% CO_2 whereas it did not reached the Bahi reservoir in this well.
The purpose of this work attempts to address EPSA120/136 (CONC 72) tectonic setting and depositional environment particularly as they relate to the Bahi Formation's sandstone distribution and prospectivity Within the En Naga Sub – basin.

Integrating all of the available date (biostratigraphical data, lithologies, wireline logs, and petrographical, paleoenvironmental, and seismic information to study the Bahi sandstones will provide the following :

1) Stratigraphic interpretation of the Lower cretaceous section of the En Naga sub-basin.
2) Geological settings of the En-Naga sub-basin.
3) Facies maps showing distribution of Bahi sandstones in the En Naga Sub-basin
4) Generation and migration of the CO_2 in the En Naga sub-basin.
5) Presence and Origin and of the CO_2
6) Economic Value of the CO_2
7) Apply all of the above data to precisely determine CO_2 source locations in the En-Naga Sub - basin.
8) Support future exploration and development interpretation.

- **Geographic and Geological Settings.**

EPSA120/136 (CONC 72) is located 280km south of Ras Lanuf. It is the most southern of the concessions in the Sirte Basin operated by Harouge oil Operations (Figure1).

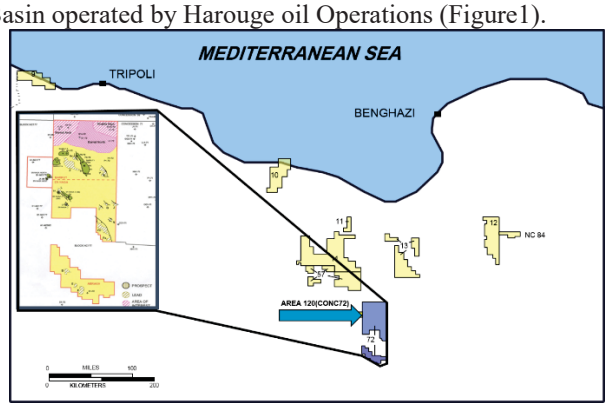

Figure 1: Location map shows Harouge Oil Operations Concessions including area 120/136(CONC72)

The concession was acquired on 18 December 1957 and had an original area of 11,000km^2. After partial relinquishments in 1967, 5000 kms remain. This area is split between three blocks along the 30 minute-latitude line that are named from north to south as Barrut, En Naga and Abragh. The En Naga part of EPSA120/136 C72 contains the En Naga A discovery and should not be confused with the producing En Naga Field in the neighboring NC177 to the west.

EPSA120/136 (Conc72) northern boundary is 20kms south-west of the Samah, Balat and Belhaden Fields, 12 kms south of the Khalifa Fields and 45kms southeast of the Sabah Field. The En Naga part of Conc 72 contains the En Naga A discovery and should not be confused with the producing En Naga Field in the neighboring NC177 to the west.

Geologically it is located over the En Naga sub –basin .this sub-basin is the most southern in a series of sub-basins that form with the northwest trending Zella Trough (Figure 2). The Zella Trough is a major western component of the regional horst and graben structural fabric of the Sirte Basin. The Zella Trough has a number of sub-basins of which the En Naga sub-basin covers most of EPSA120/136. The Khalifa high and Eastern Platform, both of which are westerly extensions of the Beda Platform, bound it to the northeast and east. To the west, the Bessaud Ridge and the Abragh Slope bound the En Naga Sub-basin. During the late Cretaceous and early Tertiary, the En Naga Sub-basin was open to the rest of the Zella Trough to the north-west.

The first major phase of extensional faulting to affect the En Naga Sub-basin was during the Late Cretaceous period, when intra-basinal features such as the Barrut I structure were formed. Pre-rift basement was eroded and deposited into the basin during a major Cenomanian marine transgression.

A further phase of late Cretaceous (end Etel Formation) faulting deepened the graben particularly towards in the western En Naga Sub-basin and to the north of EPSA120/136. The Cretaceous ended with a further episode of fault activity (end Kalash Formation) in which the margins of the En Naga Sub-basin were eroded.

During the Paleocene, the Barrut arch started to uplift and the En Naga Sub-basin became increasingly structurally isolated. By the Eocene, the sub-basin was marginal to the central area of subsidence and minor faulting episodes that centered on the central Sirte Basin. In EPSA120/136, uplift of the Barrut arch and associated faulting continued into the Oligocene.

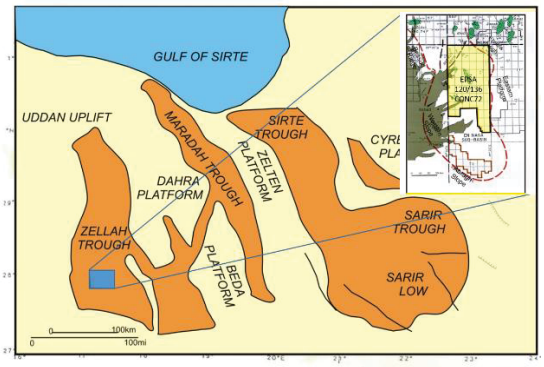

Figure 2: Tectonic elements of the Sirte Basin Showing location of the En Naga Sub Basin at the southern end of the Zella Trough graben (after Gumi and Naurin 1970).

2) STRATIGRAPHIC FRAMEWORK OF PRE-TERTIARY WITHIN THE EN NAGA SUB-BASIN

The following section describing the sedimentary sequence deposited in the En Naga Sub-basin during the structural activity period including the character and reservoir potential of the EPSA 120 (CONC72).

The stratigraphic framework of the pre - tertiary formations is comprised of the Hofra, Nubian, Bahi, Lidam, Etel, Rachmat, Rakb and Kalash (figure3)

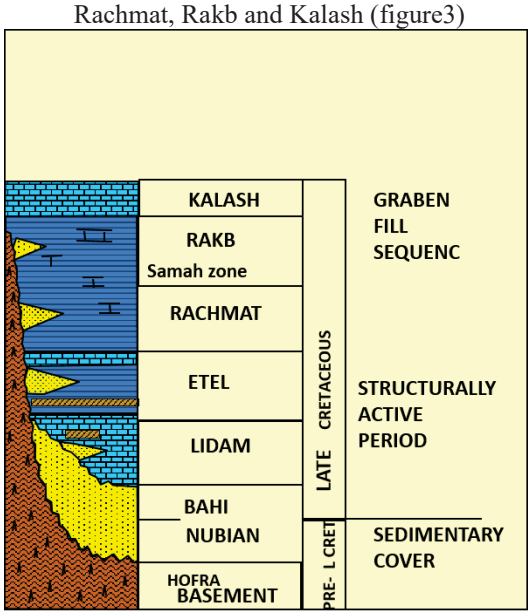

Figure 3: Simplified pre-tertiary lithostratigraphy of the En-Naga Sub Basin. Libya

Hofra Formation

The Cambro-Ordovician Hofra Formation is the oldest preserved part of the sedimentary sequence that once covered metamorphic and igneous basement in this area (Figure 4). The Hofra Formation is composed of relatively clean, fine to course grained sandstones, which are commonly well cemented with silica. Fractured Hofra quartzite reservoirs produce oil at the Samah, Bel Hedan and Balat fields on the Khalifah High (Beda High) northeast of Concession 72, and at GG1-71.

Nubian Formation

The Early Cretaceous Nubian Formation is generally a widespread continental sequence whose upper contact is the Sirte Unconformity and therefore, its youngest age, is Early Cretaceous. Nubian sandstones are likely to be present on EPSA 120/136 (CONC72) but have not been recognized because of the lack of Early Cretaceous age-specific data and its lithology similarity to the overlying Bahi sandstones. At this stage of the exploration of the area, it is unnecessary to differentiate Bahi from Nubian sandstones

Sirte Unconformity

The Sirte Unconformity contact is placed at the top of pre – Late Cretaceous rock. The dominant characteristic of this unconformity is that it is regionally extensive. In the area of EPSA 120 (CONC72) the unconformity is picked at the top of the Hofra quartzites, or the metamorphic or igneous rock around the higher margins of the En Naga Sub –basin. The unconformity is overlain by the Bahi Formation in the deeper parts of the Late Cretaceous sub – basin, and progressively younger rocks, up to those of Maastrichtian age, over the sub-basinal margins.

3.2) Syn-rift Stratigraphy (Late Cretaceous)

Bahi Formation

The Bahi Formation is the result of deposition that occurred between the start of the Cretaceous rifting that formed the area's Horst and Graben during the Cenomanian marine transgression and was derived mainly from those Nubian sediments exposed on the structurally higher blocks, transported short distances into the newly forming depocenters such as the En Naga sub- basin .

The Bahi sandstones are commonly described as being compacted but poorly cemented and friable, very fine to very coarse, subangular to subrounded, pebbly and occasionally conglomeratic especially near its base. Bahi sandstones are frequently described as being good reservoir rock. Intergranular porosities and permeabilities are highly variable and can exceed 25% and 100 md.

It was penetrated in P1-72, G1a-72, F1-72 and L1-72 and has good reservoir potential (porosities can be >25% and permeabilities >100md). Oil has been found in the Bahi along the flank of the Khalifa High (N1-72 and J1-72, while CO_2 gas has been produced in Barrut I and G1a-72.

The Bahi Unconformity

The Bahi Unconformity locally occurs at the top of the Bahi Formation and is often well developed along the margins of the Sub-Basin and associated with Intrabasinal paleo-highs.

Lidam Formation

The late Cenomanian Lidam Formation is the earliest dominantly marine deposit in the En Naga Sub-basin. The Lidam is composed of dolomites, calcarenite and argillaceous limestones deposited in generally shallow marine depositional environments.

Lidam prospectivity is best over structurally high areas where shoaling conditions may have concentrated calcarenite, oolites and fossil debris. The best Concession 72 example of reservoir quality Lidam is on the Khalifah High at 8,380 feet in J1-72 This 35 feet dolomite has intervals of intercrystalline and vuggy porosity, and overlies a porous and permeable 30 feet Bahi sandstone.

Etel Formation

The Etel Formation represents a marginal marine clastic succession made up of alternating carbonates and anhydrites and rare sandstones. Within the En Naga Sub-basin, the Etel

Formation is a thinly bedded sequence of shales, carbonates, anhydrites, siltstones and sandstones. The Etel's prospectivity becomes more clastic-prone at the southern end of the En Naga Sub-basin. The Etel Formation is penetrated in F1-72, P1-72 and H1-72. Condensate-cut and gas cut mud was recovered from a test of the Etel in F1-72, while an Etel equivalent flowed water in D1-72.

Rachmat Formation

The Rachmat Formation is a transgressive shale sequence. It was deposited in a mainly deepening marine environment where preservation of organic material was moderate to good. The upper portion of the Rachmat shales have been effective oil-prone source rocks in the deeper northern and central parts of the En Naga Sub-basin. Further, south, these shales are closer to the Sirt Basin's southern shoreline that likely made them more gas prone. The Rachmat's upper contact is marked by a marine regression and the Samah (Santonian) Unconformity.

The Rachmat shale sequence is not a reservoir target on EPSA 120 and considered more of a seal than a zone of interest.

The Samah Unconformity

The Samah unconformity separates the Rakb shales from the Rachmat shales through the En Naga Sub-basin. It represents a relative fall in sea level, which exposed the intrabasinal highs and the basin flanks. As with the Bahi Unconformity, it converges with the Sirte Unconformity at the basin margin.

Rakb Group: Sirt Shale

Rakb Formation

The Rakb Formation (or Sirt Shale) is a Campanian shale sequence that occurs between the Rachmat and Kalash formations. Sirt shales have been effective oil-prone source rocks in the deeper northern and central parts of the En Naga Sub-basin, and are more gas prone to the south. Relatively thin Sirt and Rachmat shale sequences occur at Q1-72 and S1-72. Sandstone having elevated gas readings and DOS occurs at 10,370 feet in Q1-72 but is less well developed and has no staining at 10,020 feet in S1-72. At the proposed well location, the Samah Zone is considered a zone of interest having very high exploration risk because of its unpredictable nature and lateral continuity. The top of the Rakb is marked by the base of the carbonates of the Kalash Formation and can be Maastrichtian to Campanian in age.

Kalash Formation.

The Maastrichtian Kalash Formation within the En Naga Sub-basin grades southwestward from a 220 feet marine limestone in the north as at 7850 feet in N1-72; to a thicker sequence of more argillaceous, nearshore carbonates with anhydrites and shales in F3a-72; to a thickly bedded limestone.

The Maastrichtian interval is 545 feet thick in Q1-72 (9740 feet-10,285 feet) and 495 feet thick in S1-72 (9455feet-9950 feet). This interval is almost entirely shale and has been called the "Kalash Shale Member" in recent analytical biostratigraphic reports commissioned by HOO.

The Maastrichtian shale interval is not considered prospective over much of En Naga A because of its nature at Q1-72 and S1-72. It is possible, however, for sandstone beds to occur in this interval at more southern locations such as at the proposed location.

Kalash Unconformity

A Kalash Unconformity has been interpreted over the Khalifa high where Palaeocene Hagfa shales rest on Campanian Rakb Formation shales (eg. J1-72). A similar conclusion has been drawn from areas adjacent to C72 the northwest, over the Bessaud ridge west and to the south of the Abragh block.

3) THE EN - NAGA SUB- BASIN BOUNDARIES AND BAHI SANDSTONE FACIES DISTRIBUTION

With the start of the formation of the Sirte Basin's Horsts and grabens near the beginning of the Late Cretaceous, depocenters formed within the Grabens, the marine circulation was restricted to the Grabens, deposits that have a character and terrestrial influences were often pronounced. The En-Naga Sub – basin was a depocenter and is located at the southern end of the Zella Trough graben.

This Sub – basin was open to the northwest, north and northeast but was adjacent to the southern margin of the Sirte Basin As sedimentary processes infilled the Sub – basin with detritus from the higher flanking areas or with the marine deposits, faulting episodes and differential compaction continued to enhance the Sub – basinal margin. The boundaries of the En Naga Sub-basin were fixed during Cretaceous time by the normally faulted at the Khalifa High in the northeast, the Eastern Platform,

the Bessaud Ridge to the west and the Abragh Slope to the south (Figure4)

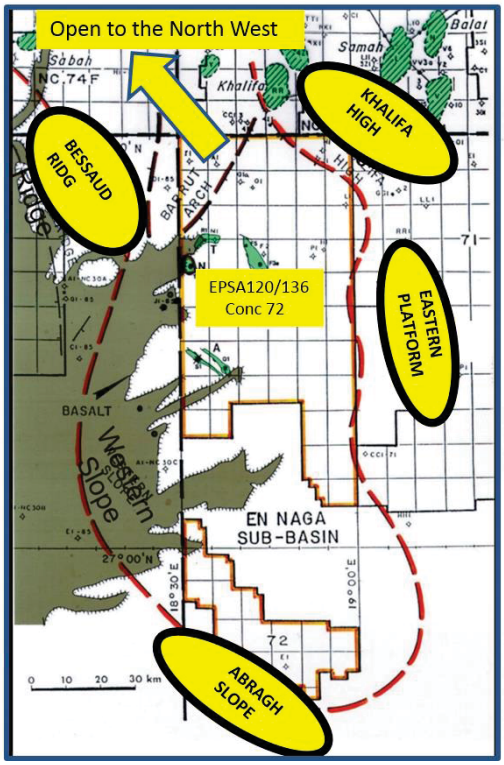

Figure 4: Location map showing Cretaceous Boundaries and major structural Features of the En-Naga Sub-

Three **Bahi facies** are recognised in the En Naga Sub-basin. They result from the influence of paleotopography on the processes associated with continental deposition over the Sirt Unconformity and the Cenomanian marine transgression (Figure 5). The Bahi sandstones tend to concentrate and thicken on the flanks of pre-existing structural highs around the margins and within the sub-basin such as at Barrut (I)

And En Naga (A)

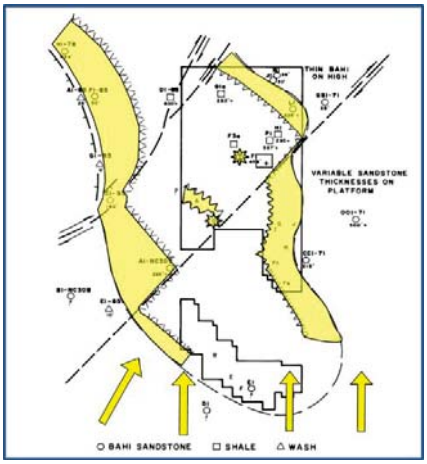

Figure 5: Shows the distribution of the Bahi Formation's facies within the En Naga Sub-basin. The Bahi sandstones (Sandstones highlighted in bright yellow)

i. Bahi sandstone: a very fine to very coarse, subangular to subrounded, pebbly and occasionally conglomeratic sandstone – a subarkosic quartz arenite commonly described as being compacted but friable. These sandstones contain some silica cement, pyrite, clay and beds of red to purple shale. The presence of glauconite and calcareous cement near the top of the Bahi respectively indicate the nearshore marine influences associated with the Cenomanian transgression and subsequent deposition of Lidam carbonates. Examples of this facies are at 11,042feetin F1-72 and at 9233 feet in L1-72 (Figure 3). The Bahi sandstone is interpreted to have been deposited on or adjacent to paleotopographic highs as a lateral facies equivalent to the Bahi shales or a proximal lateral facies equivalent to the Lidam carbonates.
The best gas tests from this facies are at F1-72 on the Barrut I structure from part of a 458 feet+ section having an estimated CO_2 flow rate of 22-39 MMCF/D.

ii. Bahi shale: a thinly bedded, generally thick sequence dominated by shales and siltstones with subordinate sandstones and carbonates. Sandstones become more abundant with depth. This facies occurs at 11,795 feet in H1-72 and at 11,850 feet in G1a-72. The upper contact of this facies is conformable and transitional to thick argillaceous Lidam carbonates. The Bahi shale is interpreted to have been deposited in paleotopographic lows as a nonreservoir, lateral facies equivalent to the Bahi sandstones.

iii. Bahi wash: a thin argillaceous sandstone as at 5114 feet in A1-85 and at 7276' in E1-85. This facies is of indeterminate Late Cretaceous age and is interpreted to be a local detrital basement covering. It is distinguished from the other Bahi sandstones by its nonfriable nature and its stratigraphic isolation by unconformities on paleohighs. This facies may have hydrocarbon potential but it is not considered to be a prospective target because of its unpredictable lateral continuity and lack of shows to date.

4) Main Structures associated within the En-Naga Sub basin area.

Bahi sandstone distribution in the En Naga Sub-basin is very closely associated with positive paleostructures that existed in the early Cenomanian. This association reflects the higher depositional and reworking energies available in these high areas to clean and concentrate sands regardless of whether their provenance was local or not. Three main Structures of sandstone distribution sites are observed (Figure 6)

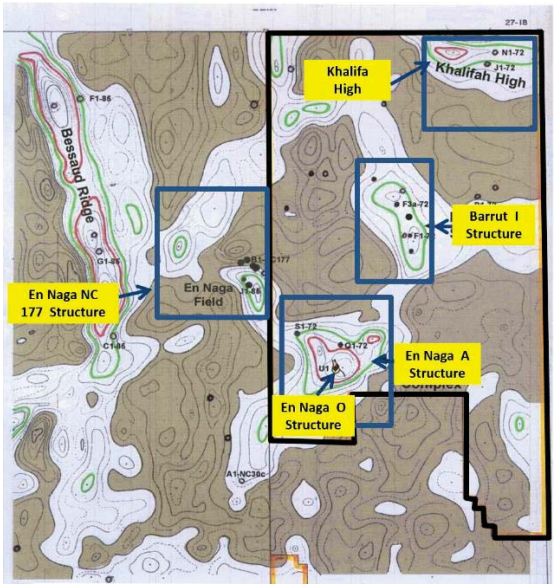

Figure 6: Residual gravity showing highs conform to oil fields in the En Naga sub-Basin

i. Intrabasinal Paleostructures (Barrut I and En Naga A Structures)

Barrut I appears to be an Intrabasinal paleostructure formed prior to the Late Cretaceous. F1-72 penetrated a 104 feet Lidam carbonate cover and a 458 feet section of Bahi sandstones without Nubian, Hofra or Basement rock being recognised. Barrut I's paleotopography is thought to have been high (as indicated by thick Bahi sandstones and thin Lidam carbonates at F1-72) and somewhat laterally limited (F3a-72 encountered a thick Bahi/Lidam - equivalent Bahi shale facies).

En Naga A located SE of the Barrut I may have been the southern end of the Gattar High in the early Cenomanian. It remained structurally high during the Turonian but strike-slip fault displacement made it intrabasinal. S1-72 penetrated thin Etel sandstone beds, which increase in thickness and quality with depth. This suggests the structure may not have been fully covered by Lidam carbonates and exposed older sandstones were locally eroded and redeposited. En Naga A's Lidam and Bahi formations have yet to be drilled.

ii. Sub-basinal flanking margins (Khalifa High Structure)

The Khalifa high is located in the northeast corner of EPSA 120/1369(C72) and has been a Paleostructural high throughout much of the En Naga Sub-basin's structural and depositional history. The Khalifa high area is considered to be on a primary oil migration path. It has staked potential pay intervals for the best oil show in the porous rock. Bahi is on the flank of the Khalifa High at N1-72 where the interval had live, light brown oil staining, gold fluorescence excellent streaming cut and tested 350 feet of OCM. Nearby at J1-72, DST # 1 Recovered 520'feet of OGCM (10% oil) and 400 OGCSW from a lower Etel, Lidam. An unconformity has been recognised at the top of the Bahi sandstones associated with contemporaneous structural highs. The sandstones' upper contact is interpreted to be the Cenomanian's transgressive surface. Deposition of the Lidam carbonates first occurred in the lows and then with time on lapped Bhai's sandstone surface.(figur7)

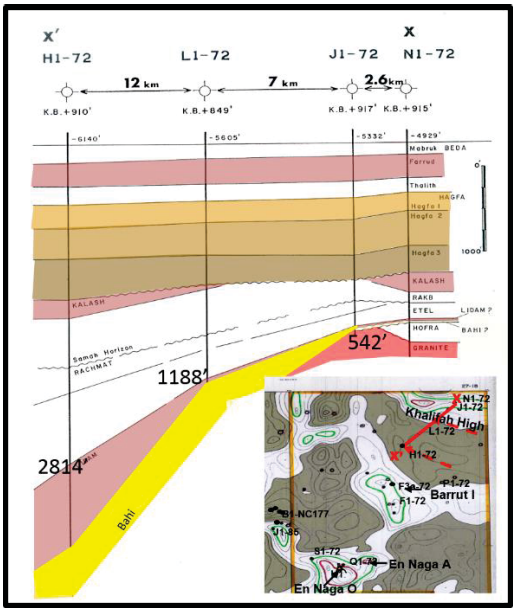

Figure 7: STRATIGRAPHIC CROSS-SECTION X – X'SHOW FLANK OF KHALIFA HIGH,

EN NAGA SUB-BASIN (Bahi and Hofra sediments have to be recognised in the En Naga Sub-basin, except at N1-72. This suggests that this area was structurally high and subjected to more erosion than occurred to the north and east.)

It appears that the up dip zero edge of the Bahi sandstones approximates the position of the Lidam carbonate edge. Bahi and Hofra sediments have to be recognised in the Khalifa High, except at N1-72. This suggests the Bahi sands structurally high on the flanks and subjected to more erosion and Bahi Sands were eroded away.

iii. Southern shoreline

The En Naga Sub-basin's Late Cretaceous southern limits are likely related to the southern collapse limit of the Tibisti-Sirt Uplift. The sub-basin's southwestern margin (Abragh Slope), its floor and its southeastern margin (southern Eastern Platform) appear to ramp up to the south. This area was exposed to some erosion (a Bahi wash was identified in H1-85), but generally it funneled clastic sediments north. Cenomanian Bahi sandstones in this area are now part of the Sirt Basin's Late Cretaceous southern shoreline.

5) PRESENCE AND ORIGINE OF CO_2 IN THE EN-NAGA SUB-BASIN

CO_2 is considered as one of Libya's prime and most valuable assets. By using CO_2 as a tertiary recovery agent in declining suitable oil fields (and HOO has a good number) an additional 15% of the original oil –in-place may be recovered rather than left behind. This huge amount of additional CO_2 has essentially no risk or cost since the fields have already been discovered, and it is worth many billions of dollars.

Large volumes of CO2 have been discovered in the Bahi Formation within and around EPSA 120/136 in the En Naga Sub-basin.CO_2 in the En Naga Sub-basin is thought to occur most dominantly as a result of the Al Haruj Al Aswad's igneous complex (Figure8) The Al Aswad igneous complex is thought to be the major source for the CO_2 in this area.

Figure 8: This Figure shows the eastern edge of the Al Haruj Al Aswad lava flows

This complex is the likely origin of mantle-derived CO_2 emanations and/or the heat source necessary for inorganic crust-derived CO_2 (disassociated from argillaceous calcium carbonate at elevated temperatures). Intrusives have been mapped at the surface in Concession EPSA126/130,(Figure 9).

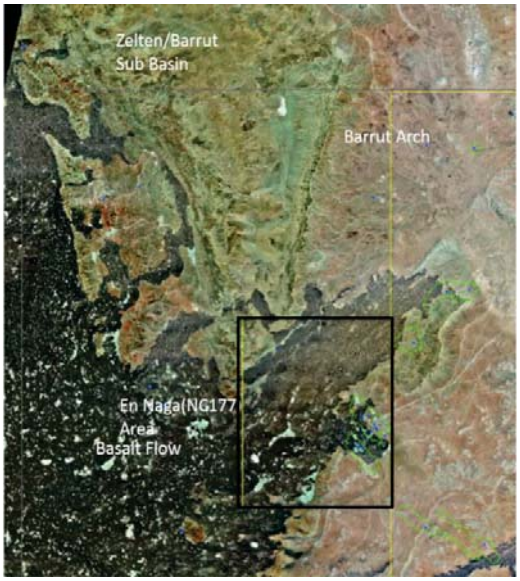

Figure 9: Satellite image showing the association of the lava flow with the En Naga Sub Basin

Seismically interpreted in the subsurface in NC74F (Blinn and Johnson, 1988), and pierced in the subsurface by A1-72, F1-72, I1-72 and P1-72. Basaltic extrusives now cover much of the En Naga Sub-basin's western margin.

Although the volumetric proportions of **inorganic** mantle-derived CO_2 and **organic** crust-derived CO_2 in this area are presently unknown, the potential CO_2 generating capacity of either origin is immense. CO_2 is second in volume only to water vapor in volcanic gas emanations (Some of the water vapor may be sourced from the formation water contained in strata penetrated by the intrusives). Potential CO_2 volumes generated by contact and regional metamorphism may be in the order of trillions of cubic feet (Brown, 1984). The primary CO_2 (mantle derived) the heat source necessary for any metamorphically derived CO_2 (disassociated from argillaceous calcium carbonate at elevated temperatures). Although the relative contribution of each source mechanism in this area is unknown, the potential of each is immense. CO_2 is second in volume only in water vapor in volcanic gas emanations.

Until isotopic analyses are made of the CO_2 occurrences in the En Naga Sub-basin and serve to determine their origin(s), this interpretation will favor an inorganic mantle-derived (igneous emanation) origin for the CO_2 in this area for the following reasons:

1) The Al Haruj Al Aswad igneous complex has a notable presence, particularly in regard to its intrusive bodies that have penetrated the En Naga Sub-basin beyond the perimeter of the lava fields. These intrusives may have served as point sources for CO_2 injection into the stratigraphic record.
2) CO_2 is expected to be the most voluminous gas after water vapor emanating from this complex.
3) The very high CO_2 content (98 %+) in the gas mixture trapped in the Bahi (and Lidam) reservoirs strongly indicates an inorganic origin.

4) The very high CO_2 content in the Bahi reservoirs, the lowest reservoir rocks in the sub- basin, suggest primary emplacement from below. The more varied and lesser CO_2 content in some of the overlying rocks suggest secondary CO_2 migration.
5) The very high pressures assumed associated with local igneous intrusives may account for the abnormally high Bahi (and Lidam) reservoir pressures at F1-72 and U1-72, and also suggest primary CO_2 emplacement from below. The CO_2 tested at F1-72 (Barrut I structure) was overpressured. The CO_2 encountered at U1-72 (En Naga A structure) was overpressured. These porous and permeable reservoirs are not in a geological situation susceptible to compaction- or structurally-induced overpressuring. Normal pressures were observed in Bahi reservoirs elsewhere in the sub-basin.

6) Bahi Sandstone Prospectivity within the En- Naga Sub-basin

- **Barrut (I) structure**

The Bahi sandstone reservoir associated with the Intrabasinal Barrut I structure is saturated with over-pressured CO2 gas. The Barrut I structure has a thick Bahi sandstone over-pressured with gas that is 98% CO2. Six wells were drilled in the Barrut I structure (F1 to F6) only two wells (F1 & F3) were penetrated Bahi Sandstones.

F1-72 well was drilled in 1966 penetrated 458 feet. Of friable, fine to very coarse, porous and permeable sandstones generally described as being a good to excellent reservoir rock. Mechanical logs were limited to the top 50 ft. of this interval.

DST (10,975'-11,100') covers the uppermost 58 feet of this sandstone and tested an overpressured, 98% pure CO_2 gas, which flowed at unmeasured rates estimated to be in the 22-39 MMSCF/D range. Analyses of gas samples taken from F1-72 and indicate a CO2 content in excess of 98%. Methane, nitrogen and ethane are also present. G1a-72 produced during drillstem testing a colorless, odorless and nonflammable gas thought to be CO2. Seismic indicated the 458 feet of sandstone drilled by F1-72 is on the downthrown side of a deep –seated fault scarp that occurs between the F1-72 and B1-72 well locations. Seismic data shows this scrap plunges to the north and south.

F3-72 well located 6 km north to the F1-72, the well was drilled in 1992 and penetrated total depth of 13,000 ft. Electric logs and samples shows facies change where a thinly bedded, generally thick sequence dominated by shales and siltstones with subordinate sandstones and carbonates .(figure 10)

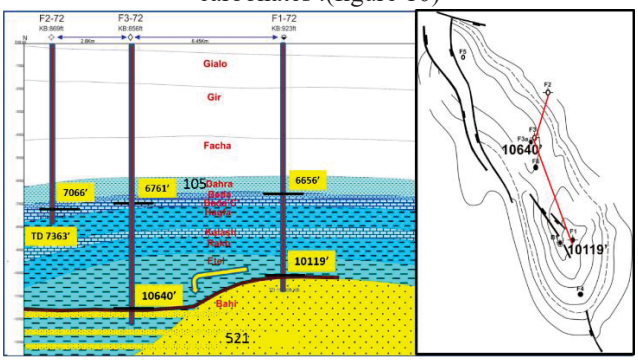

Figure 10: Cross Section shows the variation of Sandstone Lithology from Sandstone in F1 well to Sand Shale in F3 well.

. This Bahi shale is interpreted to have been deposited in paleotopographic lows as a nonreservoir, lateral facies equivalent to the Bahi sandstones. DST (11,075 feet – 13,000 feet) recovered weak air blow, no indication of gas or CO2 at surface. The Bahi reservoir in the Barrut I structure is estimated to contain 10 TCF of overpressured, highly speculative recoverable CO_2 reserves. An emanation CO_2 source could account for the pool's approximately 2,400 psi overpressuring. These reserve estimates are speculative because the areal extent, average reservoir parameter values and average effective pay thickness could not be identified yet. If the Bahi reservoir facies is evenly distributed over the areal extent of Barrut I as mapped seismically at the above levels Ex; Beda, Facha , make an estimated values of CO_2 reserves is considered reasonable.

- **EN-Naga(O)structure**

U1a-72 well drilled later in 2004 located South the crest of the En Naga A structure named (En-Naga O) one of the most prominent features defined by positive magnetic and gravity anomalies in the En Naga Sub-basin A(3-D) seismic survey covers most of the En Naga A complex but does not fully cover the En Naga O area. Interpretation of this survey

(IR 406) describes the En Naga (A) anticline as having a NW-trending faulted. At U1a -72 CO_2 was observed at 11,580 feet in dominantly shale section, then in a minor kick within the Lidam. Significant CO_2 gas kick occurred at 11,971feet and quickly led to blowout conditions due to uncontrollable leaks in the surface equipment. As there was no loss of circulation prior to the kick; the CO_2 reservoir discovered by U1a -72 is interpreted to be over-pressured. But for operation reasons the well was not logged. U1-72 discovered CO_2 in a sandy Lidam. Carbonate likely stratigraphically near to and in hydrodynamic communication with underlying Bahi sandstones. Bahi sandstones may occur beneath this Lidam.

- **<u>En Naga(A) structure</u>**

Q1-72 well (7.7 km north of the U1a-72 well) drilled to evaluate the potential of the lower Gir Formation and the Beda C Member of the Beda Formation. Q1-72 was deepened to 10,500 feet from the initial recommended total depth of 9250' to explore for any additional hydrocarbon accumulations. Apart from an untested 5 feet thick Rakb Group sandstone at 10,365 feet having dead oil staining and elevated gas readings, no zones of interest were encountered. Q1-72's Facha closure within the En Naga A structure contains black oil whose low volume gas contains 22% CO_2. The deeper Beda C closure contains a highly saturated oil whose gas has only 1.2% CO_2. This downward decrease in relative CO_2proportions precludes certainty that CO_2 is trapped deeper, and suggests these closures received their CO_2 charge by migration along strata cut by possible nonsealing faults and/or intrusives located somewhere outside of closure .

RESULTS

Known CO2 occurrences and estimated reserves in the En Naga Sub-basin are:

1. En Naga Structure, Recoverable Reserves:
   U1-72: Lidam / Bahi; over-pressured gas volume Is 83%+ CO2.
   Q1-72: Facha; black oil with low GOR (minor gas volume is 22% CO2),
   Beda C; volatile oil with high GOR (gas volume is 1.2% CO2).

2. Barrut I Structure, Recoverable Reserves: Up to 10TCF (ETM, October, 1994).
   F1-72: Bahi; over-pressured gas volume is 98% CO2.

3. Northeast Bessaud Flank, Recoverable Reserves: 3 to 17 TCF (IR 392).
   H1-78: Bahi; normally pressured gas volume Is 95% CO2.
   F1-85: Bahi; probably as for H1-78.

All of the Bahi wells drilled in the previous structures didn't complete the total Bahi interval and didn't reach the Basement. Additional drilling, more exploration and appraisal wells are required to complete the Bahi formation by reaching the Basement is required to establishing the full CO_2 potential of this area for the following reasons:

- The CO_2 saturated Bahi reservoir is over-pressured by approximately 2400 psi. The abnormally high pressure in this porous and permeable sandstone may indicate that the CO_2 "reserves" may be larger.
- Lateral permeability, porosity, pressure barriers, facies changes from the sandstone to the Bahi sandstone-shale sequence, and other factors that cannot be determined until the Bahi reservoir is fully drilled, logged and sampled.
- The Bahi's 10 TCF CO_2 "reserves" the estimate could be speculative because:

1. The average thickness of the reservoir gas pay is unknown.
2. The reservoir's average Petrophysical parameters are unknown.
3. The areal extent of the gas –fill reservoirs is not known.

7) Economic Value of the Carbon Dioxide.

The economic value of the CO_2 is related to its use for enhanced oil recovery (EOR). CO_2 flooding is a proven EOR process, which can be applied by miscible and /or immiscible displacement mechanisms to a wide variety of reservoir rocks and oil types.

Factors that contribute to the enhanced recovery of oil are:

1. CO_2's high solubility in (oil and water) which favorably reduces crude oil viscosity, swells crude oil volumes, and reduces interfacial tension in the reservoir.
2. CO_2's high compressibility which allows for high injection rates and can provide an internal solution gas drive
3. CO_2 beneficial miscibility properties, which can occur in certain situations.

The successful application of EOR techniques , CO_2 flooding in particular , to numerous selected Libyan oil fields can increase total recoverable reserves from a current 35% An estimated 50% of the original oil in place. This 15% increase in recovery is equivalent to about 20 billion barrels of oil (Misellati and Krekshi, 1990)

Conclusion

- Paleostructures highs within the Sub-basin and its margins are important features for the prospectivity of EPSA120/136 (conc 72). These are areas of positive topographic relief, which ultimately resulted in better reservoir quality rock. This association is particularly noticeable within the Bahi reservoir.
- The Lower Cretaceous BahiSandstones are the principal reservoir rocks for CO_2. These Sandstones are best developed when they are associated with Paleostructural highs within the sub-basin or around its margins. The Bahi may be prospective for oil in the northeast partof the EPSA 120/136(CONC 72).
- The CO_2 presence in this area is a relatively occurred and associated with the Al Haruj Al Aswad igneous complex. This work favorers an emanation source for the CO_2 in EPSA 120/136(CONC 72).
- The Barrut (I) is the most prospective gas in the En Naga Sub-basin where the Bahi

reservoir is estimated to contain 10 TCF of overpressure, 98% pure CO2.

- In the En Naga (O)Structure Bahi formation contains between 6 to 8 TCF of CO_2 based on 3D seismic, these estimated figures are still need to be evaluated due to bad seismic data.
- The existing 3D seismic was designed for Beda (C) reservoir (8,500 feet.), Lidam & Bahi formations (are at about 12,500 (feet.) which show badly seismic imaged (discontinuity and chaotic seismic horizons) especially on the well structure where we have CO_2 accumulation.
- EPSA 120/136 considered being a good candidate for implementing CO_2 miscible and immiscible flood for main three reasons; firstly, the relevant area is near to the CO_2 source and secondly there is already reservoir study conducted for CO_2 project, and finally any pilot project is preferable to be started in En Naga for above-mentioned Reasons.

ACKNOWLEDGEMENT

It is believed express my very special thanks to the management of the Harouge oil Operations for permission to release this paper.

References

MISELATI, A.A. and KREKSHI, F.M., 1990, Enhanced Oil Recovery in Libya: Petroleum Research Journal, V.2

JOHNSON, B. A. (1992). Geological evaluation of Concession 72. Internal report, LGM 192, Veba Oil Operations B. V.

JOHNSON, B. (2002). Concession 72: Structural analysis and Bahi prospectivity. Exploration Technical Meeting Booklet, May 2002, Veba Oil Operations B. V.

JOHNSON, B. (2004). Concession 72: Some aspects of hydrocarbon and CO_2 generation and migration within the En Naga Sub-basin. Exploration Technical Meeting Booklet, October 2004, Veba Oil Operations B. V.

JOHNSON, B. (2005). Concession 72: U1-72 well results and future work. Exploration Technical Meeting Booklet, May 2005, Veba Oil Operations B. V.

PINNEKAMP, H. (1998). Barrut I structure, Concession 72, Geophysical interpretation of the 1996 3-D survey. Internal report, IR 405, Veba Oil Operations B. V.

Biography

Mr. Moawia Gdara is a Chief Geologist with Harouge Oil operations in Libya. He holds a BSc in Geology from the University Of Tripoli, Libya.
M.Sc. 1996 From Oxford Brooks University, Oxford, United Kingdom, and The project is on concession 11 (Veba Oil Operations)
Detail hydrocarbon prospectivity of the Kalash Formation on Dahra Platform in Conc.11, Study sequence stratigraphy and oil potential.
Evaluate hydrocarbon potential in West- Sirt basin (Farrud, Facha Fm).
Interpret the Facies of Zelten formation and its extension over the En Naga NC177 and follow up if there is any change during major tectonic events in the history of the En Naga Sub Basina.
Study deep over pressured reservoirs around the area (Bahi, Lidam) for hydrocarbon and non – hydrocarbon potential & Investigate EOR Opportunities (such as CO_2) Injection.

Zeolite Origin within the Pliocene Sedimentary-Pyroclastic Deposits in the Southwestern Part of Syria

Abdulsalam Turkmani, Mohammed Khaled Yezbek, Farouk Al Imadi

Abstract—Geological surveys in the southwestern part of Syria showed the presence of sedimentary-pyroclastic deposits, volcanic tuff, to the age of the Upper Pliocene and contain the following minerals according petrographical study and X.R.D, SEM, X.R.F analysis and surface properties.

X-Ray diffraction results indicate the presence of analcime, phillipsite and chabazite in in all the studied localities. There are also amorphous materials and clay minerals such as illite and montmorillonite. The non-zeolite constituents include olivine, clinopyroxene orthopyroxene and spinel, and less of magnetite and feldspar.

Some major oxides were determined through XRF geochemical analyses which include SiO_2, Al_2O_3, K_2O, Fe_2O_3 and CaO for volcanic tuff and zeolite.

The formation of these depositions can be summarized in the following stages during the Pliocene:

- Volcanic activity at the edges of Al Rutba uplift and Jabal Al Arab depression was a rich by tuff bearing ultra basic and basic xenoliths plus second phase by scoria, during the early Pliocene.
- Volcanic calm with the activity of erosion and form lakes in which deposition of a set of wastes, including olivine resulting from the disintegration of xenoliths during the middle Pliocene.
- Zeolites minerals form later, which make up about 15-20% and increase and decrease in reverse relation with the olivine sand .
- Zeolite is formed from volcanic glass, and the results of SEM show that the zeolites minerals very well crystallized.

Keywords—Minerals, Origin, Pyroclastic, Zeolite.

Abdulsalam Turkmani, Geo Mining - Geological Studies and Consulting - Damascus – Syria (e-mail: abdulsalam.turkmani@gmail.com).

Mohammed Khaled Yezbek, Al Baath University - Faculty of Science - Department of Geology - Homs – Syria (e-mail: mkhyzbek@hotmail.com).

Farouk Al Imadi, Ministry of Petroleum & Minerals Resources – General Est.of Geology and Minerals resources. Damascus – Syria (e-mail: geo@net.sy).

Analysis of Pore Pressure Regime and Geomechanics in Banggai Foreland Basin: "No More Contractional Regime"

Reza Armanda, Agus Mochamad Ramdhan

Abstract**—**The study area is located in the Banggai Foreland Basin, Central Sulawesi, Indonesia. The stratigraphy of the Senoro Field consists of Tomori, Matindok, Minahaki, Mentawa, Poh, Kintom, and Biak formations which are Middle Miocene to Recent in age.

The purposes of this study are to determine of pore pressure regime, analysis of overpressure generating mechanism, and estimation of overpressure magnitude. Meanwhile, the geomechanic analysis comprises the determinations of horizontal stress direction, stress regime, and critical stress condition. The data processing were performed in 50 wells in Banggai Basi. Pore pressure regime determine by using wireline log data, well report, temperature data, pressure data, vitrinite reflectance data, and XRD data. The pore pressure regime characteristic was analyzed by observing pressure/stress profile through depth, wireline log respons through depth, sedimentation rate, sonic log- density log cross plot compared with XRD, and vitrinite reflectance depth plot. Geomechanic analysis performed using caliper and image log to identified in-situ stress regime and its associated rock strength. Drilling induced fracture can be used to give information of the maximum principal horizontal stress (SH Max) and borehole breakout occurence is used as minimum principal horizonal stress (Sh min).

Based on data processing and analysis, There are two distinct pore pressure regimes in the study area, i.e. hydrostatic pore pressure regime and slight overpressure regime from 1003–1519 psi. Slight overpressure regime caused by be loading mechanism due to burial of high sedimentation rate of syn-orogenic sediment (532-728 m/mY). The stress analysis reveals that stress regime in the study area is normal faulting, i.e. Sv > SHmax > Shmin. The horizontal stress is increasing systematically toward the northeastern part of the study area due to the different of tectonic feature. The critical stress analysis reveals that the stress state in the study area is still located below Coulomb failure lain. Therefore, it can be concluded that the area is stable area with respect to stress, meaning that differential stress between maximum and minimum stress is not high. The image log analysis reveals that the direction of the maximum horizontal stress is NW – SE, and the direction of minimum horizontal stress is perpendicular to the maximum horizontal stress, i.e. NE – SW.

Keywords**—**Banggai Basin, foreland basin, overpressure, stress magnitude.

Reza Armanda is with JOB Pertamina Medco E&P Tomori Sulawesi, Indonesia (e-mail: reza.armanda@pertamina.com).

Agus Mochamad Ramdhan is with Bandung Institute Technology.

Effect of Petrophysical and Sedimentological Properties on the Heterogeneity of Carbonate Reservoirs: Impact on Production Parameters

Rafik Baouche[1], K. Boutaleb[2], R. Chaouchi[3]

[1, 2, 3] Department of Geophysics, Laboratory of Ressources Minérales et Energétiques, Faculty of Sciences, M'Hamed Bougara University of Boumerdes, 35000. Boumerdes, Algeria
* Corresponding author: R_Baouche@yahoo.fr

Abstract
The carbonated reservoirs, concentrated mainly in the Middle East, contain about 50% of the world's hydrocarbon resources, where the considerable challenge they represent for the sustainable development of oil resources and the challenges posed by their production are commensurate with this potential. The characterization of these reservoirs through the control of their heterogeneities makes it possible to reduce the uncertainties on the quantification of their reserves in order to improve their productivity as well as their recovery rate.
The recovery rates obtained today on the main carbonated fields are mainly related to their sedimentary deposits and the very varied climatic conditions, resulting in a very heterogeneous geology and represent difficult challenges to overcome where the permeability is not the same, only condition for better production. This can vary from less than 10% to more than 40% on medium permeability deposits (10 to 100 md). To these parameters is added the diversity of recovery mechanisms and development patterns, on which the dynamic behavior of the deposit depends, which are far from being conditioned by the single permeability factor.
Currently, in Algeria, the valorization of carbonated reservoirs, mainly located at the level of South Eastern Constantinois reservoirs where most of these reserves remain unexploited, are among the strategic and priority objectives, because of their complexity.
Indeed, the study of stratigraphic heterogeneities, obtained from logging data and core studies, applied to South-Eastern Constantinois reservoirs (Algeria), shows that the results play an important role in the development of carbonate reservoirs production in this area.

Keywords: Well log data; Carbonated Reservoirs; Cenomanian-Turonian; Hierarchical Statistic; South Eastern Constantinois; Algeria.

1. Introduction

Carbonate reservoirs are notoriously heterogeneous at scales ranging from pore throats to deposition sequences (Kjonsvik et al., 1994, Palermo et al., 2010). The evaluation, prediction and exploitation of hydrocarbon resources in carbonate reservoirs commonly use reservoir modeling and flow simulation, but the range of complex deposits (Kjonsvik et al., 1994; Shekhar et al. ., 2014) and diagenetics (Shekhar et al., 2014) Heterogeneities complicate predictive modeling of reservoirs. The variability of these systems is controlled by a series of sedimentation and diagenetic factors, the influences of which can accurately predict the characteristics of the production (for example, the original oil in place [OOIP], the production rate cumulative production) that pose challenges (Fitch et al., 2014, Shekhar et al., 2014).

2. Sedimentologic and stratigraphic context

The geologic foundation from outcrops and reservoir analogs provide a framework for building the suite of simple, idealized geologic models. This suite of models attempts to capture the essence of the influence of geological parameters and develops broadly applicable understanding, without trying to reproduce one specific reservoir or outcrop analog. As such, the geologic models capture the range of variability of possible geologic heterogeneities. These heterogeneities are divided into three groups:
1) facies and stratigraphic geometry (e.g., clinoforms versus layer-cake geometries; variable facies-stacking patterns and stochastically distributed properties),
2) diagenesis, which impacts connectivity between ridge sets (e.g.,presence or absence of permeability barriers or conduits, and different properties among ridge sets), and
3) distribution of porosity and permeability within and among stratigraphic units. As all of these geological variables use a variety of realistic geological values, the models simulate a spectrum of geologically plausible scenarios that could exist in subsurface reservoirs.

3. Methodology Modeling Framework

A suite of 25 geologic models, built in Petrel, reflect different aspects of the conceptual model of carbonate shoreface deposits, and explicitly include several scales of potentially influential geologic heterogeneities. Construction of facies

models included several major iterative steps. The first step is creating a relatively deterministic framework, based on 36 facies- based pseudo-logs and predetermined surfaces. The second step is defining zones. Most models use three shingled clinoformal zones, constrained by surface inputs, mimicking three progradational ridge sets. Layering for clinoform-based models follows the base or top surface for each zone to honor the internal stratigraphic architecture of clinoform geometries. In addition to these clinoform models, other contrasting facies models are layer-cake with parallel horizontal layers.

Modeling Geologic Heterogeneities

This study models several scales of potentially influential geologic heterogeneities (Fig. 1):
1) depositional geometry, 2) stratal architecture, and 3) petrophysical property variance (Figure 2, 3). The various scenarios are derived from combinations of these heterogeneities, and in results are reported relative to a base case.

Depositional geometry

Depositional geometries for the majority of the facies models (Fig. 3) used low-angle clinoforms that simulate prograding ridge sets (Handford and Baria, 2007). Clinoform dimensions are 1 km long, 20 m high, and 1º inclined, and are laterally offset (with no topset aggradation; mimicking the outcrops). Within designated reservoir units, layering honors the inclined clinoform geometry, with an average layer thickness of 1 m. Other models used simple layer-cake geometry.

Facies architecture

Facies distribution was modeled using the TGSim algorithm because of the ordered shallowing-upward trend in shoreface facies associations (MacDonald & Aasen, 1994; Deutch, 2002; Handford and Baria, 2007; Rankey 2014; Figure 2, 3). From base to top, the three facies throughout the models include lower shoreface, upper shoreface, and foreshore. Facies proportions are represented in the modeling nomenclature as a three-digit ratio for the relative vertical distribution of the three reservoir facies (in order, foreshore:upper shoreface:lower shoreface). The majority of models, including the base model use a facies proportion of 1:1:3, whereas selected models use facies proportions of 1:2:2 and 1:3:1.
Select models exhibit a purely stochastic facies distribution using sequential Gaussian simulation (SGS). These models evaluate the general absence of geologic constraints. Facies proportions for these models are the same as the base model.

Diagenetic surfaces and bodies

Subaerial exposure surfaces are common in Pleistocene and older carbonate strata. These subaerial exposure surfaces represent periods of possible meteoric diagenesis during relative falls.

4. Results

1. Petrophysical variability

Distribution of reservoir petrophysical parameters commonly is controlled by facies; therefore, the models use a facies-based distribution of continuous properties (i.e., porosity and permeability) (e.g., Sahin et al., 1998; Eltom et al., 2012) (Fig. 3). Cells were populated with synthetic porosity and permeability values derived from analog reservoir values (Table 3) using sequential Gaussian simulation (SGS). Porosity distribution used a normal distribution, whereas permeability had a log-normal distribution, and, in Petrel, input parameters are simplified to mean and standard deviation values (Figure 2, 3). Values and ranges of analog reservoir petrophysical parameters are conditioned to the respective facies model. Several models used purely stochastic (not facies-based) property population. Note that inherent uncertainty related to facies modeling introduces additional uncertainty to porosity and permeability models (Eltom et al., 2012).

2. Flow Simulations and Uncertainty

A common method for evaluating and quantifying the efficiency of geologic models is to take them through reservoir flow simulations (e.g., Kjonsvik et al., 1994; Carrasco et al., 2001; Jackson et al., 2009; Fitch et al., 2014; Shekhar et al., 2014). Flow simulations enhance understanding and allow quantification of the role and relative impact of static geologic heterogeneities impact production on the dynamic behavior of fluid flow (Carrasco et al., 2001). This study evaluates the relative impact of heterogeneities from the series of geologic models using OOIP (static), production rates and cumulative production (dynamic) as metrics. Since this project is not simulating a particular reservoir or outcrop analog, engineering parameters are held constant to isolate the role of geologic variability on production. Twenty five modeled geologic scenarios were each taken through a set of 30 primary-recovery reservoir

5. Conclusions

Such geological controls as stratigraphy, facies, and diagenesis influence production trends of carbonate reservoirs. Designed to capture a spectrum of potential geological variability of carbonate shorefaces, a suite of simple geologic models carried through to reservoir simulation permitted systematic and quantitative assessment of the influence of these geological factors on initial production.
The data derived from these simulations illustrate how the influence of geologic factors range in nature and scope on both static and dynamic production metrics. For example, models with *stochastic facies distribution* (either with horizontal parallel [layer cake] zones or with clinoform bounding surfaces; mean porosity, facies proportions, etc. similar to a base model) have production rates and cumulative production that differs from the base clinoform model by < 2%. Analogously, *depositional geometries* (i.e., clinoforms versus layer cake) *alone* do not have a marked impact on OOIP or production rates. If associated with a continuous, impermeable barrier (e.g., cemented *subaerial exposure surface* or a flooding surface) that compartmentalizes the reservoir, however, these bounding surfaces impact production. Although OOIP is not impacted markedly (< 1% change), production rates and cumulative production can decrease in excess of 7% as a function of the impact of one thin zone alone. This influence can be emphasized if the impermeable barrier is linked to enhanced *diagenesis* (e.g., cementation that decreases porosity) to create a distinct stratigraphically constrained *diagenetic body* (e.g., clinoform with distinct porosity) in underlying deposits. Simulations suggest that this impact alone can result in decreases in OOIP (up to 36%), and corresponding declines in production rate (up to 33%), and cumulative production (up to 23%). Since facies include distinct petrophysical characteristics in the models, changing *facies proportions* impact OOIP, production rate,

and cumulative production; greater proportions of high-energy porous and permeable upper shoreface and foreshore strata result in increased OOIP and production

References

Aalto, K.R., and Dill, R.F., 1996, Late Pleistocene stratigraphy of a carbonate platform margin, Exumas, Bahamas: Sedimentary Geology, v. 103, p. 129-143.

Agada, S., Chen, F., Geiger, S., Toigulova, G., Agar, S., Shekhar, R., Benson, G., Hehmeyer, O., Amour, F., Mutti, M., Christ, N., and Immenhauser, A., 2014, Numerical simulation of fluid flow processes in a 3D high-resolution carbonate reservoir analogue: Petroleum Geoscience, v. 20, p. 125–142.

Agar, S.M., and Hampson, G.J., 2014, Fundamental controls on flow in carbonates: an introduction: Petroleum Geoscience, v. 20, p, 3–5.

Agar, S.M., Geiger-Boschung, S., Matthai, S.K., Always, R., Tomas, S., Immenhauser, A., Shekhar, R., Paul, J., Benson, G., Karcz, Z., and Kabiri, L., 2009, The impact of hierarchical fracture networks on flow partitioning in carbonate reservoirs: Examples based on a Jurassic carbonate analog from the High Atlas: OnePetro SPE #135135, 19 p.

Alsharhan, A., 1993, Asab Field--United Arab Emirates, Rub Al Khali Basin, Abu Dhabi, *in* Foster, N.H., and Beaumont, E.A., eds., Structural Traps VIII: AAPG Treatise of Petroleum Geology, Atlas of Oil and Gas Fields, p. 69–97.

Amour, F., Mutti, M., Christ, N., Immenhauser, A., Benson, G.S., Agar, S.M., Tomas, S., and Kabiri, L., 2012, Capturing and modeling metre-scale spatial facies heterogeneity in a Jurassic ramp setting (Central High Atlas, Morocco): Sedimentology, v. 59, p. 1158–1189.

Amour, F., Mutti, M., Christ, N. Immenhauser, A., Agar, S.M, Benson, G.S., Tomas, S., Alway, R., and Kabiri, L.,2013, Outcrop analog for an oolitic carbonate ramp reservoir: A scale- dependent geologic modelling approach based on stratigraphic hierarchy: AAPG Bulletin, v. 97, p. 845–871.

Arakel, A.V., 1982, Genesis of calcrete in Quaternary soil profiles, Hutt and Leeman Lagoons, Western Australia: Journal of Sedimentary Petrology, v. 52, p. 109-125.

Aurell, M., McNeill, D.F., Guyomard, T., and Kindler, P., 1995, Pleistocene shallowing-upward sequences in New Providence, Bahamas: Signature of high-frequency sea-level fluctuations in shallow carbonate platforms: Journal of Sedimentary Research, v. 65, p. 170–182.

Benson, D.J., and Mancini, E.A., 1982, Petrology and reservoir characteristics of the Smackover Formation, Hatter's Pond Field: implications for Smackover exploration in southwestern Alabama: Gulf Coast Association of Geological Societies Transactions, v. 32, p. 67–75.

Cao, R., Ma, Y.Z., Gomez, E., 2014. Geostatistical applications in petroleum reservoir modeling: Southern African Institute of Mining and Metallurgy, v. 114, p. 625–629.

Carew, J. L. and J. E. Mylroie, 1995, Depositional model and stratigraphy for the Quaternary geology of the Bahama Islands, *in* Curran, H.A., and White, B., eds., Terrestrial and

Shallow Marine Geology of the Bahamas and Bermuda: Geological Society of America, Special Paper No. 300, p. 5-32.

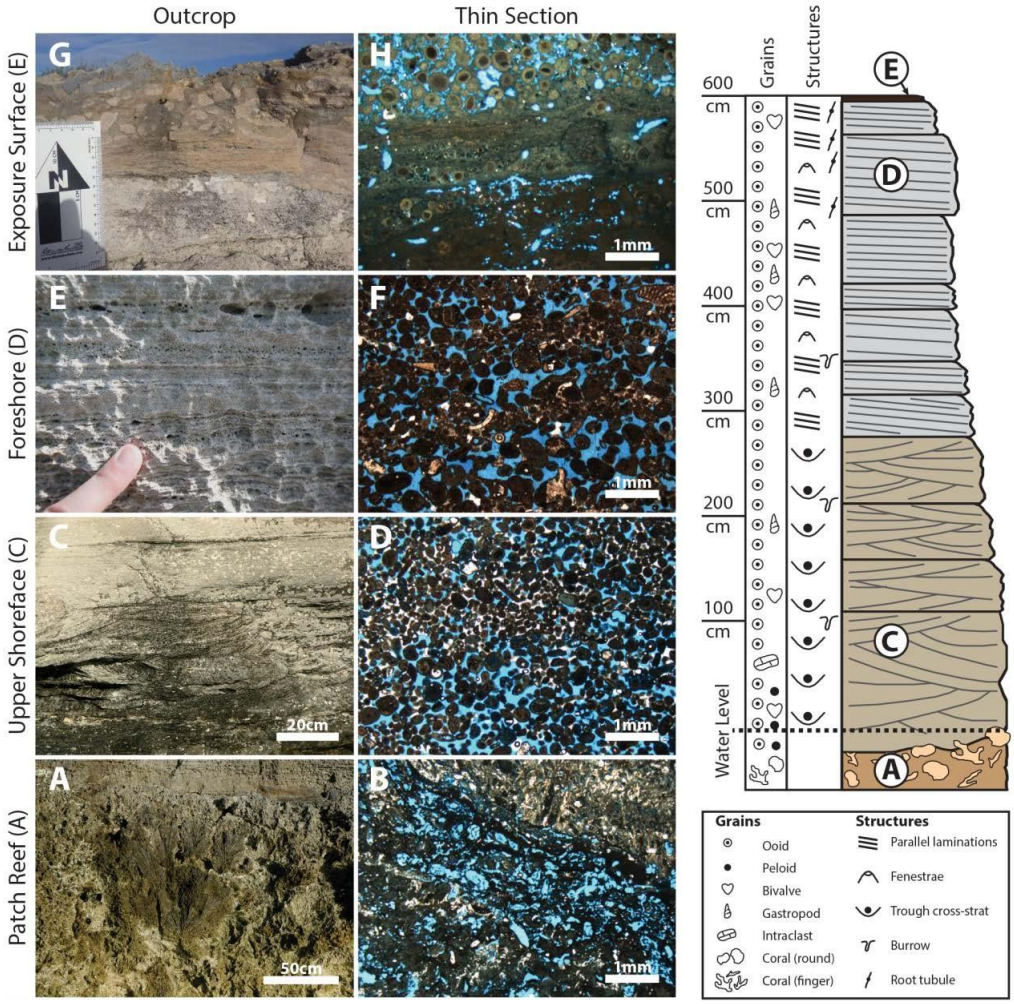
Outcrop
Thin Section
Exposure Surface (E)
Foreshore (D)
Upper Shoreface (C)
Patch Reef (A)
G
H
E
F
C
D
A
B
1mm
20cm
50cm
Grains
Structures
600 cm
500 cm
400 cm
300 cm
200 cm
100 cm
Water Level
Grains
Ooid
Peloid
Bivalve
Gastropod
Intraclast
Coral (round)
Coral (finger)
Structures
Parallel laminations
Fenestrae
Trough cross-strat
Burrow
Root tubule

Fig. 1

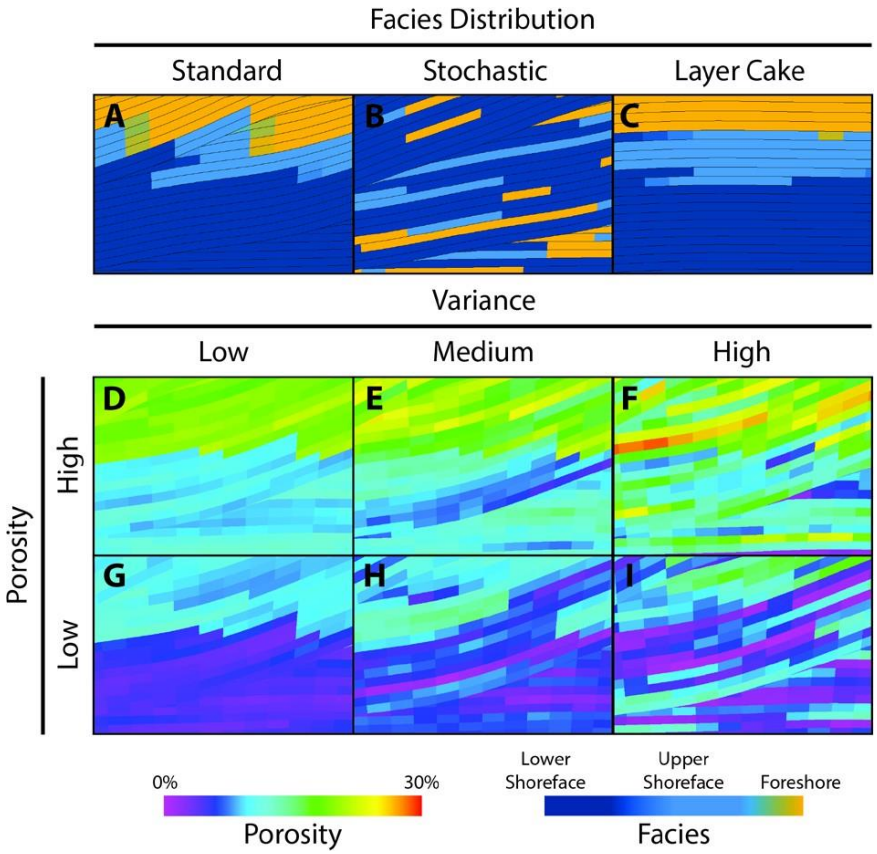
Facies Distribution
Standard
Stochastic
Layer Cake
A
B
C
Variance
Low
Medium
High
Porosity
High
Low
D
E
F
G
H
I
0%
30%
Porosity
Lower Shoreface
Upper Shoreface
Foreshore
Facies

Fig. 2

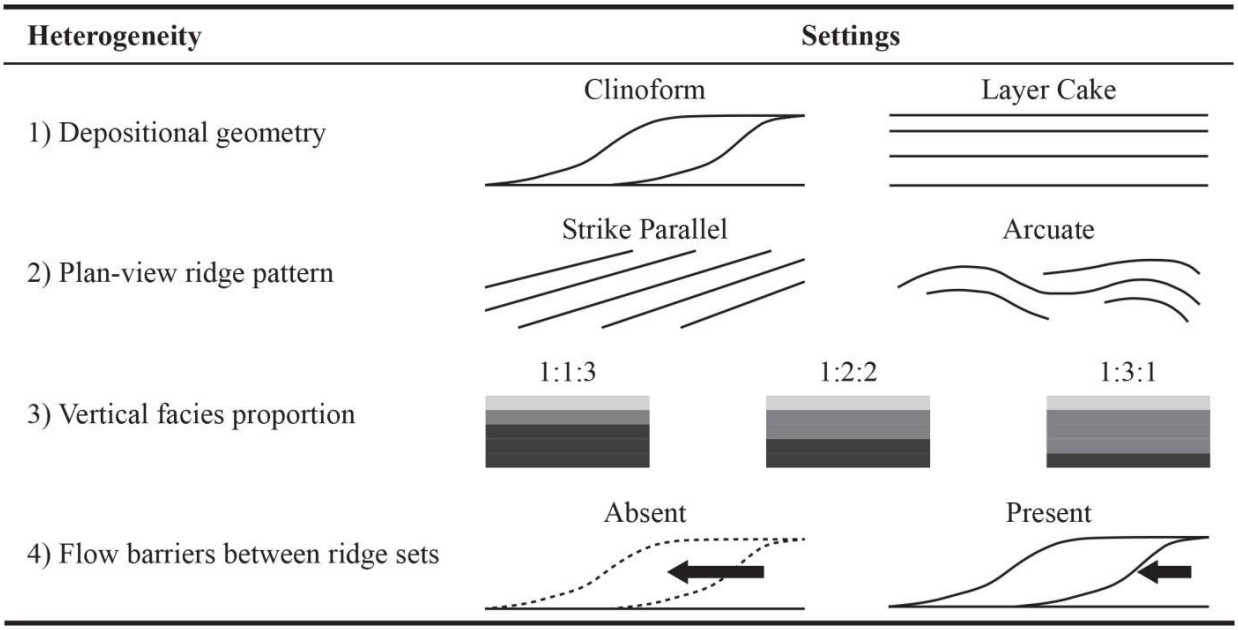
Heterogeneity
Settings
1) Depositional geometry
Clinoform
Layer Cake
2) Plan-view ridge pattern
Strike Parallel
Arcuate
3) Vertical facies proportion
1:1:3
1:2:2
1:3:1
4) Flow barriers between ridge sets
Absent
Present

Fig. 3

Removal of Cr(VI) and COD from Synthetic Wastewater by Electrocoagulation Process: Optimization Using Box–Behnken Design

Safia Lemdani, Aicha Bensmaili

Abstract—The need for water is increasing while the quantities released are high. The origins of water pollution are diverse and varied. Industrial water pollution is the most important both quantitatively and qualitatively. the treatment of metal wastewater is of great importance in the management of used industrial waste. Hydrocarbons, in a general way, are heavy metals in a particular way are considered hazardous waste that can have a significant negative impact on the environment The purpose of this study is to remove hexavalent chromium and COD from wastewater by electrocoagulation. The electrocoagulation process is based on the continuous in situ production of a coagulant in the contaminated water. Strictly speaking the pollutants are removed by sorption, co-precipitation or electrostatic attraction sorbents generated electrochemically. Anodic metal ions and hydroxide ions generated at the electrode surfaces react in wastewater. This technique does not require any supplementary addition of chemicals, reduces the volume of produced sludge, and first economical studies indicate also a financial advantage compared to the conventional methods. Hexavalent chromium Cr (VI) exists in various industrial effluents such as chrome plating, metal finishing, pigments and tanning. Cr (VI) is one of the toxic metal pollutants among all the heavy metals. The experiments were carried out in an electrochemical batch reactor for the treatment of aqueous solutions containing chromium hexavalent using iron sacrificial electrode. Electrocoagulation treatment conditions were optimized through response surface methodology (RSM). The Box–Behnken design (BBD) as was applied to investigate the effects of major operating variables and optimization conditions. The objective of the present study is to optimise the removal efficiency of COD for electrocoagulation process with minimum cost and time. RSM is statistical tool used to evaluate, analyse and optimise the process parameters. RSM has important application in the improvement of existing design. It defines the effect of the independent variables alone or in combination and also it generates a mathematical model which describes the processes interaction. Hence this study focussed on optimisation of three factors at three levels using Box Behnken design approach. The optimal operating conditions were determined and applied to the process. All the parameters were examined: the current density (I), the initial pH and the concentration of the electrolyte (NaCl), the results obtained allowed us to determine the optimal conditions to perform the reaction. the results obtained show that electrogulation (EC) using iron electrodes is a process that is perfectly applicable to the treatment of metallic (Cr (VI)) discharges, characterized by high stability and a high pollutant load, for optimal values of the operating parameters distance electrodes 2cm and 25 minutes of electrolysis), the reduction the COD is of the order of 94.41%, with a residual COD equal to 1450 mg O2 / L. These results reveal the applicability of electrocoagulation treatment to the wastewater as an alternative treatment method cleaning. Keywords: COD removal, electrocoagulation process, toxic metals , wastewater

Keywords—COD removal, electrocoagulation process, toxic metals, wastewater

Corresponding Author
Safia Lemdani from University of Science and Technology Houari Boumediene, Algeria
e-mail: lemdanisafia@yahoo.fr

Removal of Basic Yellow 28 Dye from Aqueous Solutions Using Plastic Wastes

Nadjib Dahdouh, Samira Amokrane, Elhadj Mekatel, Djamel Nibou

Abstract—The removal of Basic Yellow 28 (BY28) from aqueous solutions by plastic wastes PMMA was investigated. The characteristics of plastic wastes PMMA were determined by SEM, FTIR and chemical composition analysis. The effects of solution *pH*, initial Basic Yellow 28 (BY28) concentration *C*, solid/liquid ratio *R* and temperature *T* were studied in batch experiments. The Freundlich and the Langmuir models have been applied to the adsorption process and it was found that the equilibrium followed well Langmuir adsorption isotherm. A comparison of kinetic models applied to the adsorption of BY28 on the PMMA was evaluated for the pseudo first-order and the pseudo second-order kinetic models. It was found that used models were correlated the experimental data. Intra particle diffusion model was also used in these experiments. The thermodynamic parameters namely the enthalpy ΔH°, entropy ΔS° and free energy ΔG° of adsorption of BY28 on PMMA were determined. From the obtained results, the negative values of Gibbs free energy ΔG° indicated the spontaneity of the adsorption of BY28 by PMMA. The negative values of ΔH° revealed the exothermic nature of the process and the negative values of ΔS° suggest the stability of BY28 on the surface of SW PMMA.

Keywords—Removal; Waste PMMA; BY28 dye; Equilibrium; kinetic study; thermodynamic study.

Nadjib Dahdouh University of the Science and Technology H. Boumediene; Laboratory of the material technology (LTM); B.P. 32 - Alia 36111, Algiers, Algeria (phone: 213 (21) 24 71 69; fax: 213 (21) 24 71 69; e-mail: nadjibdahdouh@outlook.com).

Samira Amokrane, University of the Science and Technology H. Boumediene; Laboratory of the material technology (LTM); B.P. 32 - Alia 36111, Algiers, Algeria (phone: 213 (21) 24 71 69; fax: 213 (21) 24 71 69; e-mail: samiraramokrane@gmail.com).

Elhadj Mekatel University of the Science and Technology H. Boumediene; Laboratory of the material technology (LTM); B.P. 32 - Alia 36111, Algiers, Algeria (phone: 213 (21) 24 71 69; fax: 213 (21) 24 71 69; e-mail: hmekatel@yahoo.fr).

Djamel Nibou, University of the Science and Technology H. Boumediene; Laboratory of the material technology (LTM); B.P. 32 - Alia 36111, Algiers, Algeria (phone: 213 (21) 24 71 69; fax: 213 (21) 24 71 69; e-mail: dnibou@yahoo.fr).

Electrical Study of Schottky Diode with an Interfacial Porous SiC Layer for Gas Sensors

K. Bourenane, A. Keffous, G. Nezzal

***Abstract*—**The aim of this work is the comparison between pt (pd) / sic-psi and pt (pd) / psc / sic-psi schottky diode. the schottky diode was characterized in air ambient and in vacuum at pressure 8.10^{-2} mbar. these diodes could be used for exhaust gas monitoring as gas sensors for different gas (o_2, h_2, co, co_2 and hydrocarbure). the thin sic layer are realized on p-type silicon (si(100)) substrate by laser ablation method with krf laser (248 nm) using 6h-sic (purchased by goodfellow uk) as sputtered target and a thermal deposition of a thin metal layer (platinum (pt) and palladium (pd)). the electrical measurements were made at room temperature 295 k using an oxford cryostat. we investigate the effect of nature of surface sic and the nature of the metal on the electrical parameters such as ideality factor (n), barrier height (ϕ_{bp}) and series resistance (rs). analysis of current-voltage (i–v) characteristics showed that the forward current might be described by classic thermal emission theory. the ideality factor of the i–v characteristics was found to be dependent and vary only on a modified surface such as psc (interfacial layer) and also vary with the nature of the metal (pt or pd) for electrical measurements in air and in vacuum, it notes that schottky diode without an interfacial layer (psc), all electrical parameters does not change when the measurements were taking in vacuum or in air ambient.

***Keywords*—**Palladium, platinum, porous silicon carbide, schottky diode.

I. INTRODUCTION

THE present interest in the control of the pollutant emissions to the atmosphere has substantially stimulated the research and development in the field of gas sensors. It is very important to detect some harmful gases like O_2, H_2, CO, CO_2, hydrocarbure, such as CH_4 etc. for pollution control. Boilers, automobiles etc. are major source for these types of gases. Detection and controls of these gases in high temperature has great importance. A material, which can be used in high temperature and hazardous medium, is necessary for this type of application. Recently sensors using semiconductors with large energy band gap such as silicon carbide and diamond film as substrates are developed for high temperature operation [1, 2]. Widely used silicon carbides are 6H-SiC and recently thin SiC layers elaborated onto p-type silicon,grows more attention for its wider band gap. When the devices exposed to gas, the gas molecules adsorb dissociatively on the surface of the catalytic metal gate and diffuse through the metal gate to form a polarized layer at the metal-semiconductor or metal-insulator interface which shifts the *I-V* curve of a Schottky diode, which can be measured as their response to the gases. The first gas sensor was developed by Lundstrom et al. in 1975 [3], it was a MOS structure using silicon as a substrate and could only operate at temperatures below 150 °C. In order to develop gas sensors that can operate in the high temperature environment of aerospace and automobile applications, new technologies were created. One new technology is based on the development of high temperature semiconductors,especially silicon carbide (SiC) which allows to the sensor to operate up to 1000 °C [4-7]

In order to increase the sensitivity and selectivity to certain gases, these devices need to operate at high temperature, which cannot be fulfilled by the silicon devices. Thus, a material as silicon carbide (SiC) that has a large band gap that allows it to operate a temperature up to about 700 °C [8], is necessary for the fabrication of this type of gas sensor. Furthermore, SiC has a high chemical and physical resistance, and high thermal conductivity. However, the technology for the fabrication of these devices is still under development and the quality of the SiC wafers and of the insulating layer is far from the one of Si which hinders the correct modelling for the MOSiC devices.

In this work, we extended our investigations for improvement our sensor quality and using thin SiC and porous SiC layer (PSiC) fabricated onto p-type Silicon substrates and prepared catalytic metal gate Schottky diodes with palladium and platinum gate deposited by thermal evaporation and laser ablation respectively.

II. EXPERIMENTAL PROCEDURE

All Porous structure silicon carbide (PSiC) layers were fabricated by anodization in HF on SiC layer, deposited onto a p-type Si(100) substrate by pulsed laser deposition (PLD), using a hot pressed p-type 6H-SiC as a target. The p-type Si(100) substrate with a resistivity of 6 Ω cm was mounted on a plate. The plate was attached on top of a rotating cylinder and heated in-situ to 500 °C using halogen lamps mounted on a fixed water-cooled reflector. The target is a hot pressed (supplied by Goodfellow) polycrystalline 6H-SiC. The interaction of the laser beam with the target produced a highly oriented material stream, usually ejected normal to the target surface, which was deposited onto the substrate positioned in front of the target. The reaction chamber vacuum pressure was fixed at 10^{-6} Torr. The laser pulses were produced by a Lambda Physik Compex 205 KrF laser excimer. The most important parameters were: wavelength λ = 248 nm, maximum pulse energy Emax = 600 mJ and pulse duration τ = 25 ns. The SiC layer was deposited by laser ablation [9, 10]. After the growth of the SiC layer, an ohmic contact layer of Al with a thickness of 4900 Å was deposited by thermal evaporation on the back side of silicon substrate.

Development of porous structure in the SiC layers was performed by an electrochemical (anodization)method. Before this step, the samples were provided with an Al contact on the front side and were annealed at 650 °C for 1 hour in air ambience. The annealing step reduced the electrical resistivity of the SiC substrate. The electrochemical setup was a standard three electrode configuration with SiC/pSi(100) as a working electrode, a Platinum (Pt) sheet as a counter electrode and a saturated

K. Bourenane is with USTHB, Algeria (e-mail: bourima2003@yahoo.fr).

calomel electrode (SCE) as a reference. The electrochemical process was performed by using a potentiostat-galvanostat model EG&G PAR 362 [11]. After formation of the ohmic contact, the samples were placed into a deposition chamber in order to evaporate a thin palladium or platinum (99.9% purity) on the PSiC/pSi(100) sample to form Schottky. The layer served as a catalytic gate. The current-voltage measurements were performed at room temperature using a Keithley voltage/current source unit model 237 (SMU 237). Figures 1 illustrate cross section of Pt(Pd)-PSiC/pSi device Schottky diode.

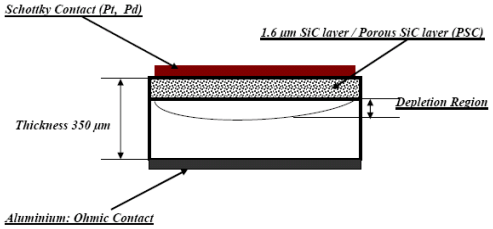

Fig. 1Schematic cross-section view of the designed Silicon Carbide Schottky diode.

III. RESULTS AND DISCUSSIONS

A. Current-voltage

The forward and reverse current–voltage (I-V) characteristics measured on Pt/SiC-pSi and Pt/PSC-pSi Schottky diode allow for quantitative determination of Schottky diode electrical parameters such as barrier height (ϕ_B), ideality factor (n) and series résistance (R_s) of the diodes. The I-V relationship based on the thermoionic emission-diffusion theory, can be expressed by [12-15]:

$$I = a.A^{**}.T^2.\exp(\frac{-q\phi_B}{kT})\left[\exp(\frac{qV}{nkT})-1\right] \qquad (1)$$

Where q is the electron charge, A^{**} is the effective Richardson constant and equal 72 A.cm^{-2}.K^{-2} for 6H-SiC [16], a is the diode area (cm^2), T the absolute temperature (295 K), k = 1.38 10^{-23} J/K is the Boltzmann constant and ϕ_B is the barrier height.

If the barrier height ϕ_B is assumed to vary linearly with bias, one writes:

$$\phi_B = \phi_{B0} + \beta V \qquad (2)$$

Where ϕ_{B0} is the barrier height at zero bias and $\beta = \frac{\partial V}{\partial \phi}$ is the change in the effective barrier height with bias voltage. Using substitution Eq.(2), Equation (1) becomes:

$$I = I_s.\exp(-\beta\frac{qV}{kT})\left[\exp(\frac{qV}{nkT})-1\right] \qquad (3)$$

Where I_s is the saturation current:

$$I_s = a.A^{**}.T^2.\exp(\frac{-q\phi_B}{kT}) \qquad (4)$$

By introduction a parameter n such that $\frac{1}{n} = 1-\beta$, Equation (3) can be written:

$$I = I_s.\exp(\frac{qV}{nkT})\left[1-\exp(\frac{-qV}{kT})\right] \qquad (5)$$

Where n is the ideality factor incorporating the tunnelling current in pratical diode. If the applied voltage V is much larger than kT/q, the second term in the Equation(5) become insignificant. The parameter n is included in the I-V relation to take into account the non-ideal behaviour. This factor is calculated from the slop of the linear region of the forward bias Ln(I)-V.

$$n = \frac{q}{kT}.\frac{dV}{dLn(I)} \qquad (6)$$

The barrier height ϕ_{B0} is determined from the extrapolated I_s and is given by the relation:

$$\phi_{B0} = \frac{kT}{q}Ln(\frac{a.A^{**}T^2}{I_s}) \qquad (7)$$

The I-V characteristics of Pt/SiC-pSi and Pd/SiC-pSi Schottky diode at room temperature (295 K) were measured by a Keithley Source Measure Unit model 237 in air and vacuum (8. 10^{-2} mbar) are shown in Figures 2 and 3 respectively.

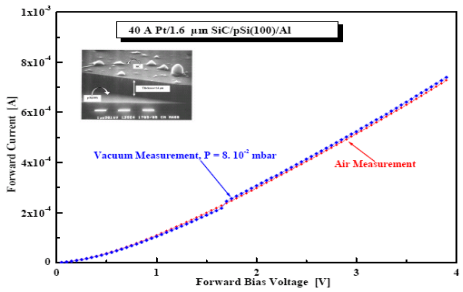

Fig. 2Experimental forward current-voltage characteristics of Pt / SiC-pSi measured in Air and Vacuum

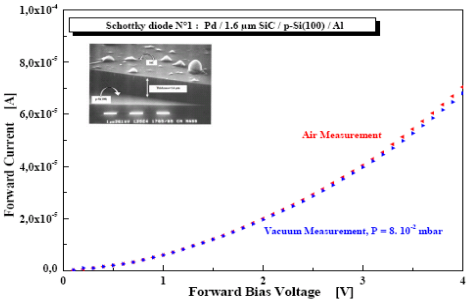

Fig. 3Experimental forward current-voltage characteristics of Pd / SiC-pSi measured in Air and Vacuum

B. Effect of an interfacial layer PSC

For Schottky diodes Pt/SiC-pSi and Pd/ SiC-pSi without an interfacial layer PSC, The electric parameters leave constants as shown in Table1.In contrary, for Schottky diode with an interfacial layer PSC, as Pt / PSC /SiC-pSi and Pd / PSC /SiC-pSi, the electrical parameters depend with the nature of the PSC surface and changes when the measured IV in air and vacuum.A summary is given below:

1. The ideality factor (n) increases in presence of an interfacial layer (PSC) or modified surface: n (PSC) > n (SiC)

2. The ideality factor (n) increases in air (gas) by report of the electrical measurements in vacuum (8. 10^{-2} mbar): n (air : gas) < n (vacuum)
3. The barrier height (ϕ_{Bp}) increases in air measurements by report in vacuum:
   ϕ_{Bp} (air : gas) > ϕ_{Bp} (vacuum)
4. Series resistance (Rs) increases in air measurements by report in vacuum:
   R_S (air : gaz) > R_S (vacuum)

TABLE 1
ELECTRICAL PARAMETERS BY IV MEASUREMENTS OF DIFFERENT SIC AND PSC SCHOTTKY DIODE.

	In Air				In Vacuum : 8.10^{-2} mbar			
Schottky diode	n	V_{bp} (V)	ϕ_{Bp} (eV)	R_s (kΩ)	n	V_{bp} (V)	ϕ_{Bp} (eV)	R_s (kΩ)
N°5:Pt / SiC-pSi (Unetched)	1.169	0.746	0.845	85.53	1.169	0.746	0.845	85.53
N°8 : Pt / PSC-pSi 50%HF/50%ETG, 2 min	1.087	2.807	0.935	42.01	1.657	0.849	0.797	12.40
N°1:Pd / SiC-pSi(Unetched)	1.286	0.600	0.804	12.60	1.434	0.807	0.805	10.74
N°7 :Pd / PSC-p-Si 50%HF/50%ETG, 1 min	1.390	0.690	0.771	2.94	1.569	0.761	0.770	2.78
N°9 : Pd / PSC-pSi 50%HF/50%ETG, 2 min	1.344	0.754	0.792	0.71	1.428	0.997	0.784	0.52

C. Effect of metal

A low value of ideality factor (n) and a high barrier height ($\boldsymbol{\phi_{Bp}}$) was obtained for Pt Schottky contact compared for the Pd one. This result shows that Schottky diode using Pt as catalytic gate allow to give a high electrical performances by report when using palladium contact.

IV. CONCLUSION

In this work, we have study the roles of the porous SiC layer (PSC) and the catalytic gate (platinum and palladium) on the electrical properties of Pt (Pd)-SiC/pSi(100)/Al Schottky diodes which can be used a gas sensor. The forward *I-V* plot, indicating that the diodes parameters are not voltage-dependent. It was possible to extract barrier height changes accurately from the value of the saturation current *Isat* obtained from *I-V* plots corrected for the voltage drop at series resistance. Good I-V characteristics were obtained on platinum and palladium Schottky diodes, which were fabricated as function of catalytic gate and porous structure SiC layers. A low value of *n* was found around 1.169 and 1.436 with a barrier height ϕ_{Bp} 0.746 eV and 0.804 eV for Pt and Pd Schottky contact respectively. In contrast, in the presence of an interfacial layer (PSC), the electrical properties of all the Schottky contact change, in fact, the ideality factor *n* increase 1.505 to 1.657 for the measurement carried out in vacumm (8. 10^{-2} mbar) by report of the one taking in the air (70 % N_2 gas), this result confirmed in the two metals (Pt and Pd), also we register a decrease in barrier height ϕ_{Bp} and in series resistance *Rs* for air measurements by report to vacuum measurements.

A. References

[1] Shabbir A. Khan, Elder A. de Vasconcelos, Hidekazu Uchida,Teruaki Katsube "Gas response and modeling of NO-sensitive thin-Pt SiC schottky diodes", *Sensors and Actuators B* Vol .92, pp. 181 – 5, 2003

[2] I. Lundström, " Why bother about gas-sensitive field effect devices?", *Sens. Actuators* A Vol.56 pp. 75 – 82, 1996

[3] I. Lundström, S. Shivaraman, C. Svensson and L. Lundkvist, "A hydrogen–sensitive MOS field–effect transistor", *Appl. Phys. Lett.* Vol. 26 pp.55 – 7, 1975

[4] W.M. Tang, P.T. Lai, J.P. Xu and C.L. Chan," Enhanced hydrogen-sensing characteristics of MISiC Schottky-diode hydrogen sensor by trichloroethylene oxidation", *Sens. Actuators A.* pp. 11963 – 67, 2005

[5] Wai-Kai Chen, *VLSI Handbook* CRC and IEEE Press, 2000

[6] Y.H. Tang, T.K. Sham, D. Yang and L. Xue, "Preparation and characterization of pulsed laser deposition (PLD) SiC films", *Appl. Surf. Science*. Vol. 252 pp.3386 – 89, 2006

[7] P. Tobias, B. Golding and R.N. Ghosh ," Sensing mechanisms of high temperature silicon carbide field-effect devices", *Transducers, 12th Int.,Conf on Solid State Sensors, Actuators and Microsystems* (Boston, June 8-12) pp 416 – 419, 2003

[8] A. Arbab, A. Spetz, I. Lundstrom ,"Gas sensors for high temperature based metal-Oxidesilicon carbide (MOSiC) devices" *Sens. and Actuators, Vol. B* 15-16 ,pp.19 – 23, 1993

[9] A.Keffous, K. Bourenane, M. Kechouane, N. Gabouze and T. Kerdja ,"Morphological,structural and optical properties of thin SiC layer growth onto silicon by pulsed laser deposition",*Vacuum*Vol.81, Issue 5pp. 632 – 5, 2007

[10] A. Keffous, K. Bourenane, O. Manseri, H. Maneri, F. Kezzoula, M. Kechouane,A.Bourenane, T. Kerdja, G. Nezzal and A. Boukezzata,"Structural and Optical Properties of Polycrystalline 6H-SiC and crystalline SiC film Grown onto Silicon substrate by PLD",*Modern Physics Letter B* Vol.22, N°1pp. 61 – 72, 2008

[11] A.Keffous, K. Bourenane, M. Kechouane, N. Gabouze, T. Kerdja, L. Guerbous and S. Lafane " Effect of anodization time on Photoluminescence of porous thin SiC layer grown onto Silicon",*Journal of Luminescence*Vol.126, pp.561 – 5, 2007

[12] S.M. Sze *Physics of Semiconductor Devices*,New York:second ed., Wiley, 1981

[13] Rhoderick EH, Williams RH,*Metal–Semiconductor Contacts*,Oxford: second. ed., Oxford University Press, 1988

[14] Rahab H, Keffous A, Siad M, Boussaa N and Menari H *Nucl Instr & methods Physics Research A* ***Vol.*** 453, p.413, 2001

[15] Cheung SK, Cheung NW. *Appl Phys Lett* Vol.49, p.85, 1986

[16] Waldrop JR, Grant RW, Wang YC, Davis RF *J Appl Phys* Vol.72, p. 4757, 1992

Biography: Karima Bourenane received her doctoral degree in chemical from Houari Boumediene University of Algiers in June 2010 and master degree in chemical from the National Polytechnic School of Algiers in Jannuary 2004.from 2004 to 2012 , she works in Silicon Technology Unit in Algiers. Since 2012 as teacher in Environment and chemical field at Houari Boumediene University of Algiers in Mechanical and Chemical Department. She is currently working in the field of sensors for automotive safety and exhaust gas monitoring for advanced environmental safety.

Elimination of Nickel from Aqueous Solution Using Paper of Newspaper

Redouane Laib, Samira Amokrane, Nadjib Dahdouh, Djamel Nibou

Abstract—Our work consists to the wastepaper valorizing of newspaper in the setting of the water treatment that constitutes of paper of newspaper to throw in the nature. The retraining and the means to follow for valorizing this garbage of way to save resources of wood. We achieved experiences of Nickel adsorption on the paper of newspaper used after washing with water distilled for the homogeneity of our adsorbent and the elimination of the anchor. These experiences showed that pH, temperature and initial concentration of Ni^{2+} are important parameters in the metallic ion fixing on the surface of the adsorbent. The Freundlich and the Langmuir models have been applied and the adsorption kinetics followed both adsorption isotherms.

For the survey of output of Nickel adsorption on the paper of newspaper we noted that it increases according to the report. The survey of the effect of the temperature as thermodynamic parameter was showed that for increasing variation of 10 until 60 °C a considerable increase of the capacity and output of the adsorption of Ni^{2+} (7 mg/g). Otherwise, we note that the time of balance is about 3 h for the survey of the adsorption kinetics.

Keywords—Removal; newspaper; Nickel; adsorption; kinetic study; thermodynamic study.

Redouane Laib University of the Science and Technology H. Boumediene; Laboratory of the material technology (LTM); B.P. 32 - Alia 36111, Algiers, Algeria (phone: 213 (21) 24 71 69; fax: 213 (21) 24 71 69; e-mail: oxredw@gmail.com).

Samira Amokrane, University of the Science and Technology H. Boumediene; Laboratory of the material technology (LTM); B.P. 32 - Alia 36111, Algiers, Algeria (phone: 213 (21) 24 71 69; fax: 213 (21) 24 71 69; e-mail: samiraramokrane@gmail.com).

Nadjib Dahdouh University of the Science and Technology H. Boumediene; Laboratory of the material technology (LTM); B.P. 32 - Alia 36111, Algiers, Algeria (phone: 213 (21) 24 71 69; fax: 213 (21) 24 71 69; e-mail: nadjibdahdouh@outlook.com).

Djamel Nibou, University of the Science and Technology H. Boumediene; Laboratory of the material technology (LTM); B.P. 32 - Alia 36111, Algiers, Algeria (phone: 213 (21) 24 71 69; fax: 213 (21) 24 71 69; e-mail: dnibou@yahoo.fr).

Photocatalytic Degradation of Bisphenol A Using ZnO Nanoparticles as Catalyst under UV/Solar Light: Effect of Different Parameters and Kinetic Studies

Farida Kaouah, Chahida Oussalah, Wassila Hachi, Salim Boumaza, Mohamed Trari

Abstract—A catalyst of ZnO nanoparticles was used in the photocatalytic process of treatment for potential use towards bisphenol A (BPA) degradation in an aqueous solution. To achieve this study, the effect of parameters such as the catalyst dose, initial concentration of BPA and pH on the photocatalytic degradation of BPA was studied. The results reveal that the maximum degradation (more than 93%) of BPA occurred with ZnO catalyst in 120 min of stirring at natural pH (7.1) under solar light irradiation. It was found that chemical oxygen demand (COD) reduction takes place at a faster rate under solar light as compared to that of UV light. The kinetic studies were achieved and revealed that the photocatalytic degradation process obeyed a Langmuir–Hinshelwood model and followed a pseudo-first order rate expression. This work envisages the great potential that sunlight mediated photocatalysis has in the removal of bisphenol A from wastewater.

Keywords—bisphenol A, photocatalytic degradation, sunlight, zinc oxide, Langmuir–Hinshelwood model, chemical oxygen demand

Corresponding Author
Farida Kaouah from University of Science and Technology Houari Boumediene, Algeria
e-mail: faridkaouah@yahoo.fr

Properties of Fuel from Agrifood By-Products

S. Elbey, R. Rihani, F. Z. Zoubiri, Y. Baghdadi, F. Bentahar

Abstract**—**Transport is one of the sectors that contribute most to energy consumption and the one that depends upon the use of fossil fuels. The continued burning of fossil fuels generates a significant greenhouse gas emission in the atmosphere. In the last years, the level of greenhouse gasses are increasing in atmosphere; causing global warming. These products still harmful to both the environment and human health.

This study consists of purifying hydrated bioethanol from agrifood by-products using two methods : fractional distillation and molecular sieves of A4 type. Moreover, the characterization of the fuels was carried out using the gasolines incorporated with 10% of biotehanol. The mixtures obtained were characterized in term of the ASTM distillation, density, the vapor Reid tension, Octane number, sulfur content, flash point. It has been found that the addition of bioethanol 10% to super gasoline allowed an improvement of the octane number of the gasoline from 98 to 100 with low sulfur amount 0.0023wt%.

Keywords**—**Agrifood by-products, biofuel, Octane number, sulfur content.

S. Elbey is with Laboratoire Phénomènes de transfert (LPDT), Université des Sciences et de la Technologie Houari Boumediene (USTHB),Bab-Ezzouar, 16111, Algiers, Algeria. (samira_st@hotmail.fr).

R. Rihani is with Laboratoire Phénomènes de transfert (LPDT), Université des Sciences et de la Technologie Houari Boumediene (USTHB),Bab-Ezzouar, 16111, Algiers, Algeria.(rachida_riha@yahoo.fr ; rrihani@usthb.dz).

F. Z. Zoubiri is with Laboratoire Phénomènes de transfert (LPDT), Université des Sciences et de la Technologie Houari Boumediene (USTHB),Bab-Ezzouar, 16111, Algiers, Algeria. (zoubirifatima@hotmail.fr).

Y. Baghdadi is with Laboratoire Phénomènes de transfert (LPDT), Université des Sciences et de la Technologie Houari Boumediene (USTHB),Bab-Ezzouar, 16111, Algiers, Algeria. (Yacine.167@hotmail.com).

F. Bentahar is with Laboratoire Phénomènes de transfert (LPDT), Université des Sciences et de la Technologie Houari Boumediene (USTHB),Bab-Ezzouar, 16111, Algiers, Algeria. (fatihabentahar@yahoo.fr).

The Relation between the Fluid Temperature of the Crude Oil Fouling and the Heat Exchangers of Algiers Refinery

Harche Rima, Mouheb Abdelkader

Abstract**—**Crude oil fouling in refinery preheat exchangers is a chronic operating problem that compromises energy recovery in these systems. Progress is hindered by the lack of quantitative knowledge of the dynamic effects of fouling on exchanger heat transfer [1]. Generally, crude oil flows through the tube side while various other hot streams and pump-around streams flow through the shell side in the heat exchangers [2].

Fouling in heat exchangers has been the subject of intensive research by several groups of investigators. For that, in this study, we will consider the fouling phenomenon of the heat exchangers tubes for the preheat circuit of the Algiers refinery E101 CBA and FED, which are used for the heating of the crude oil before its division, are exposed to the problem of fouling at the tube side of heat exchangers**.**

Keywords**—**Fouling, Crude oil, Tubular heat exchanger, fouling resistance, Transfer Phenomenon, Refinery, tube-calander.

Harche Rima, Laboratory of Heat Transfer Phenomenon, Department of Process Engineering, Faculty of Mechanical and Process Engineering, University of Sciences and Technology Houari Boumediene (USTHB), BP 32 EL-ALIA, 16111 Bab Ezzouar Algiers, Algeria (E-mail: s_r_harche@yahoo.fr).

Mouheb Abdelkader, Laboratory of Heat Transfer Phenomenon, Department of Process Engineering, Faculty of Mechanical and Process Engineering, University of Sciences and Technology Houari Boumediene (USTHB), BP 32 EL-ALIA, 16111 Bab Ezzouar Algiers, Algeria.

Chemical Pretreatment of Agro-Industrial Effluents for Eco-Fuel Production

F. Z. Zoubiri, R. Rihani, S. Elbey, Y. Baghdadi, F. Bentahar

Abstract**—**As the global oil reserves and raw materials are finite, a renewed interest in alternative fuels research has been conducted. Biofuels remain an alternative source of energy for the foreseeable future and may offer the basis of sustainable development towards by combining environmental, economic and social considerations. Concerns have arisen on the basis of the dwindling of oil and gas reserves as well as the growing worldwide consumption of fossil fuels and the increase in oil prices. Biofuels derived from agro-industrial effluents, promise to become attractive future sources of energy, in particularly in the transport sector.

This study was designed to assess chemical pretreatments to extract sugars from agro-industrial effluents, then transform them into ethanol. Different chemical compounds are tested: hydrogen peroxide, sulfuric acid and sodium hydroxide. Note that the chemical compounds concentration varied from 1 to 7% (v/v). The characteristics of agro-industrial effluents showed that effluents contained high total sugars, 89.54 g/L and low ash contents, 0.81% and protein 5.4 g/L. It can be seen that the total sugars extracted increased gradually till to reach a maximum sugar yield of about 93.05 g/L, this value was reached using 0.5% of H_2SO_4 and after 3 hours of hydrolysis.

Keywords**—**Agro-industrial effluents, biofuel, pretreatment, hydrolysis.

F. Z. Zoubiri is with Laboratoire Phénomènes de transfert (LPDT), Université des Sciences et de la Technologie Houari Boumediene (USTHB),Bab-Ezzouar, 16111, Algiers, Algeria. (zoubirifatima@hotmail.fr).

R. Rihani is with Laboratoire Phénomènes de transfert (LPDT), Université des Sciences et de la Technologie Houari Boumediene (USTHB),Bab-Ezzouar, 16111, Algiers, Algeria.(rachida_riha@yahoo.fr ; rrihani@usthb.dz).

S. Elbey is with Laboratoire Phénomènes de transfert (LPDT), Université des Sciences et de la Technologie Houari Boumediene (USTHB),Bab-Ezzouar, 16111, Algiers, Algeria. (samira_st@hotmail.fr).

Y. Baghdadi is with Laboratoire Phénomènes de transfert (LPDT), Université des Sciences et de la Technologie Houari Boumediene (USTHB),Bab-Ezzouar, 16111, Algiers, Algeria. (Yacine.167@hotmail.com).

F. Bentahar is with Laboratoire Phénomènes de transfert (LPDT), Université des Sciences et de la Technologie Houari Boumediene (USTHB),Bab-Ezzouar, 16111, Algiers, Algeria. (fatihabentahar@yahoo.fr).

Vitamin D Deficiency and Erectile Dysfunction among Men with Type 2 Diabetes among Men with Type 2 Diabetes

Shahjada Selim, Hafiza Lona

Abstract—Background and Aims: Several recent studies found a strong relationship of vitamin D deficiency (VDD) with erectile dysfunction (ED). Due to the growing epidemic of diabetes and VDD in Bangladesh, exploring the role of vitamin D in causing the complications of diabetes is crucial. The morbidity of men with diabetes is also becoming more increasingly recognized, which has been taken to have association again with VDD. The aim of this study was to determine the association between vitamin D status and ED Bangladeshi adult men with type 2 diabetes. Materials and Methods: The nested case-control study included 2860 patients with type 2 diabetes mellitus (T2DM) who had ED (aging between 30 to 69 years). The patients who found to have normal vitamin D level were categorized as control and those who had VDD were grouped as the case. The study was conducted in eight diabetes care centers, one from each of the eight administrative divisional cities of Bangladesh. Socio-demographic, personal, and family information were collected by face to face interview, and disease-specific data were recorded from the patient's record book. Body weight, height, waist circumference, hip circumference, and blood pressure were also recorded. Fasting blood samples were collected, and serum levels of vitamin D, glucose, and free testosterone were measured. Results: The diabetes patients with ED have more severe VDD [(25 OH)D < 10 ng/mL] than the controls (61.28% and 62.16%, respectively). The more severe form of ED found in the lowest level of serum vitamin D level. The multivariate logistic regression analysis found VDD has a linear relationship with ED [OR 2.83, CI 2.36, 3.97]. Conclusions: Vitamin D deficiency is an independent risk factor of ED in men with type 2 DM, and severity of ED is linearly associated with the degree of deficiency of vitamin D.

Keywords—vitamin D, deficiency, erectile dysfunction, diabetes

Corresponding Author
Shahjada Selim from Bangabandhu Sheikh Mujib Medical University, Bangladesh
e-mail: selimshahjada@gmail.com

Risk Factors for Osteoporosis in Hospitalized Type 2 Diabetes Mellitus Patients: A Cross Sectional Study in BIRDEM General Hospital, Bangladesh

Mohammad Saifuddin, Shahjada Selim

Abstract—Diabetes mellitus and osteoporosis are two frequent multifactorial medical conditions with an increasing prevalence in the aging population. Patients with type 2 diabetes mellitus have an increased fracture risk despite a higher bone mineral density (BMD). Objective of my study was to find out distribution of known risk factors of osteoporosis among type 2 diabetes mellitus and osteoporotic patients admitted in BIRDEM General Hospital. A descriptive cross sectional hospital based study was conducted in indoor of BIRDEM General Hospital from 1st January 2018 to 31th December 2018. All patients of type 2 diabetes mellitus with osteoporosis as and when available (nonprobability purposive sampling) were included. Total 100 patients took part in the study. Socio-demographic and personal information were recorded from patient through face to face interview with a semi-structured pre-tested questionnaire. Complete history and physical examination searching risk factors of osteoporosis was done. Secondary data about present state, diagnosis and related investigations were collected from treatment file. In this study the mean age of the respondents was 59.46 ± 12.36 years ranging from 42 to 97 years. Among study patients 74 (74%) were female and among females around 66 (89.1%) were postmenopausal women among whom 38 (57.5%) had history of premature menopause. Regarding BMI 9% were underweight, 37% were of normal weight and 28% were obese. In my study 54% were sedentary worker, 66% did not exercise regularly, 22% were smoker and 6% alcoholic. In my study 22% respondents had history of taking steroids, 8% homeopathic medicine and 12% were on thiazolidinediones. Regarding glycaemic status, in terms of fasting blood sugar level 71% had their diabetes uncontrolled. Based on post prandial blood sugar level 78% had their diabetes uncontrolled and in term of HbA1c 86% had their diabetes uncontrolled. In conclusion, Health care providers should carefully check the existence of risk factors of osteoporosis and fractures in their patients of type 2 diabetes mellitus. Strategies to prevent osteoporosis and/or falling may be especially warranted in elderly patients with type 2 diabetes.

Keywords—fracture, glycaemic status, osteoporosis, type 2 diabetes mellitus

Corresponding Author
Mohammad Saifuddin from Abdul Malek Ukil Medical College, Bangladesh
e-mail: saifk56dmc@yahoo.com

The Impact of Total Dust (LGS) and Mineral Dust (PM 10) in Cardio Vascular and Respiratory System, in Albania: A Longitudinal Study

Canga Mimoza, Irene Malagnino, Giulia Malagnino, Vito Malagnino

Abstract**—**Aim: This study aims at evaluating the impact of total dust (LGS) and mineral dust (PM10), in the cardio vascular and respiratory systems. Also proving that these air polluters are the cause of several diseases, such as: bronchopneumonia, pneumonia, bronchitis, angina pectoris and cardiac insufficiency. Material and Method: The study is concentrated in the cities of Fier and Vlora. This is a clinic-epidemiological study conducted during the time period 2014-2019. Some of the data of LGS and PM10 were obtained from the database of the Institute of Public Health. The formula to measure the mean value of LGS and PM10 is ΔX=X (mean) – Xi. Results: Based on the calculations made, we noticed that: The mean value of LGS in the city of Fieri was 227,33, while the mean value of LGS in the city of Vlora was 177,4. Whereas, the mean value of PM10 in the city of Fieri was 105.5 and the mean value of PM10 in the city of Vlore was 77.5. According to, our statistics the values of LGS were 1.2 times higher in Fier than in Vlora and the PM10 values were 1.36 times higher in Fier than in Vlora. Based on the data, in the city of Fier, the incidence of the bronchopneumonia was 56.53 sick patients /1000 inhabitants, but in Vlora it was 22 sick patients /1000 inhabitants, so the number of the sick patients was 2.5 times higher in the city of Fieri compared with Vlora city, (P=0.001). The number of the patients with bronchitis, in the city of Fier, was 18 patients /1000 inhabitants, whereas, in Vlora, it was 9 patients /1000 inhabitants, (P=0.005). Based on the data, 8 patients/1000 inhabitants in the city of Fier, suffered from the pneumonia disease, while in Vlora city, were 4 patients /1000 inhabitants, (P=0.005). Another disease taken in consideration was angina pectoris. This study can claim that in the city of Fier, 9.5 patients /1000 inhabitants suffered from this disease, while in Vlora city, were only 4 patients /1000 inhabitants, (P=0.001). Findings of the present study proved that 3.7 patients /1000 inhabitants in the city of Fieri, had cardiac insufficiency, whereas in the city of Vlora, were 1.8 patients /1000 inhabitants, (P=0.05). Conclusions: LGS and PM10 have an influential impact in the cardio vascular and respiratory system, that's why their levels should be kept under control. The pollution levels are 1.2 and 1.4 times higher in Fier than in Vlora, also the incidences of the diseases are 2 times higher in Fier than in Vlora. Recommendations: In order to prevent the cardio vascular and respiratory diseases, we should avoid places, where the pollution is higher than the norm. This can be achieved by frequenting places where the air pollution is lower, such as: parks, gardens, top floors, etc.

Keywords**—**Total dust LGS, mineral dust PM 10, cardio vascular pathologies, respiratory diseases.

Canga Mimoza is with Faculty of Public Health, University "Ismail Qemali" Vlore – Albania (e-mail: mimoza-canga@hotmail.com).

Irene Malagnino, Giulia Malagnino are with Private Practice, Rome, Italy.

Vito Malagnino is with the Chief of Endodonty Catheder, University "Gabriele D'Annunzio" Chiety – Italy.

Nigerian Medical Students and Medical Migration: A Cross-Sectional Survey of Their Views on Migration and Aspirations to Migrate after Graduation

Eddy Awire

Abstract—Background and objectives: Nigeria continue to lose medical doctors through international migration. One of the several 'push' factors implicated in the migration of doctors from Nigeria is a 'culture of migration' in the medical schools where the doctors are trained. This study set out to examine the attitude of Nigerian medical students to the international migration of Nigerian trained medical doctors. Method: a cross-sectional survey of final-year students in four medical schools. Ethical approval was granted by each institutional ethics review committee following the presentation of ethical approval from the National Health Research Ethics Committee of Nigeria. The survey data were entered into SPSS version 21 for analysis. Result: 211 (out of a total of 580) final year students participated and returned the survey questionnaire. Views on international migration of doctors were significantly associated religion, perception of the quality of academic training facilities, and perception of the quality of support from medical training institutions. Gender, family migration history, and views on migration were shown to be the predictors of aspirations to migrate after graduation. Conclusion: - Nigerian medical graduates continue to migrate from Nigeria because the culture in their training institutions encourages them to do so. Retention schemes aimed at keeping doctors in Nigeria must, therefore, include concerted efforts to change the institutional support for migration. This will require policies geared towards changing attitudes to the international migration of doctors, improvements in funding for medical education and healthcare system, and revamping of the national social infrastructure in Nigeria.

Keywords—Nigeria , medical students, views on migration , aspirations to migrate, international migration

Corresponding Author
Eddy Awire from Delta State University, Nigeria
e-mail: ighele@yahoo.com

The Effects of Sitagliptin on Free Androgen Index in Infertile Women with Polycystic Ovary Syndrome Undergoing ICSI

Delbar Daneshjou, Malek Soleimani Mehranjani, Seyyed Mohammad Ali Shariatzadeh, Shahrzad Zadehmodarres

Abstract**—**Background: Polycystic ovary syndrome (PCOS) is a *testosterone* heterogeneous disorder, the etiology of which is not well understood. Hyperandrogenism is the common biochemical abnormality in women with PCOS. Most of the PCOS Studies have focused on the evaluation and treatment of hirsutism, acne, alopecia, and infertility, health issues that are generally of greatest relevance to PCOS. PCOS patients often suffer from a glucose homeostasis disorder, insulin resistance, and obesity and are susceptible to type 2 diabetes. There is a hypothesis that insulin plays a role in the hyperandrogenism of women with PCOS. Sitagliptin, as an oral antihyperglycemic agent uses in treatment of type 2 diabetes, is considered recently in clinical investigations of PCOS.

Objective: The aim of the present study was to evaluate the effect of sitagliptin on the free androgen index(FAI) in patients with PCOS.

Materials and Methods: In this clinical trial, 40 infertile PCOS patients were selected based on the Rotterdam criteria. Then, they divided into two groups (n=20): sitagliptin group (treated with 50 mg of sitagliptin/ two times per day) and placebo group. All patients were undergoing treatment with antagonist GnRH protocol. Placebo and Sitagliptin were administrated from day 3 of menses of previous cycle until ovum pick-up. Total testosterone and SHBG concentrations in blood serum were assayed. To calculate the FAI, total testosterone value x 100 is divided by the sex hormone binding globulin value. The data were analyzed statistically using paired samples t-test and means difference was consider significantly different at $p<0.05$.

Result: FAI was significantly decreased after treatment with sitagliptin (3.80 ± 1.27vs. 8.74 ± 3.87)($p<0.05$).

Conclusion: Our obtained result from this clinical study showed that sitagliptin can decrease The FAI index in women with infertility due to PCOS. Therefore, it seems that sitagliptin has therapeutic efficiency for treatment of PCOS.

Keywords**—**Polycystic ovary syndrome, Sitagliptin, *Testosterone*, SHBG, FAI index.

Delbar Daneshjou is with Department of Biology, Arak University, Arak, Iran (e-mail: d.daneshjou@yahoo.com).

Malek Soleimani Mehranjani, Seyyed Mohammad Ali Shariatzadeh are with Department of Biology, Arak University, Arak, Iran.

Shahrzad Zadehmodarres is with Department of Gynecology and Obstetrics, Shahid Beheshti University of Medical Sciences, Tehran, Iran.

Impact of 6-Week Brain Endurance Training on Cognitive and Cycling Performance in Highly Trained Individuals

W. Staiano, S. Marcora

Abstract**—**Introduction: It has been proposed that acute negative effect of mental fatigue (MF) could potentially become a training stimulus for the brain (Brain endurance training [BET]) to adapt and improve its ability to attenuate MF states during sport competitions. Purpose: The aim of this study was to test the efficacy of 6 weeks of BET on cognitive and cycling tests in a group of well-trained subjects. We hypothesised that combination of BET and standard physical training (SPT) would increase cognitive capacity and cycling performance by reducing rating of perceived exertion (RPE) and increase resilience to fatigue more than SPT alone. Methods: In a randomized controlled trial design, 26 well trained participants, after a familiarization session, cycled to exhaustion (TTE) at 80% peak power output (PPO) and, after 90 min rest, at 65% PPO, before and after random allocation to a 6 week BET or active placebo control. Cognitive performance was measured using 30 min of STROOP coloured task performed before cycling performance. During the training BET group performed a series of cognitive tasks for a total of 30 sessions (5 sessions per week) with duration increasing from 30 to 60 min per session. Placebo engaged in a breathing relaxation training. Both groups were monitored for physical training and were naïve to the purpose of the study. Physiological and perceptual parameters of heart rate, lactate (LA) and RPE were recorded during cycling performances, while subjective workload (NASA TLX scale) was measured during the training. RESULTS: Group (BET vs. Placebo) x Test (Pre-test vs. Post-test) mixed model ANOVA's revealed significant interaction for performance at 80% PPO ($p = .038$) or 65% PPO ($p = .011$). In both tests, groups improved their TTE performance, however BET group improved significantly more compared to placebo. No significant differences were found for heart rate during the TTE cycling tests. LA did not change significantly at rest in both groups. However, at completion of 65% TTE it was significantly higher ($p = 0.043$) in the placebo condition compared to BET. RPE measured at ISO-time in BET was significantly lower (80% PPO, $p = 0.041$; 65% PPO $p= 0.021$) compared to placebo. Cognitive results in the STROOP task showed that reaction time in both groups decreased at post-test. However, BET decreased significantly ($p = 0.01$) more compared to placebo despite no differences accuracy. During training sessions, participants in the BET showed, through NASA TLX questionnaires, constantly significantly higher ($p < 0.01$) mental demand rates compared to placebo. No significant differences were found for physical demand. Conclusion: The results of this study provide evidences that combining BET and SPT seems to be more effective than SPT alone in increasing cognitive and cycling performance in well trained endurance participants. The cognitive overload produced during the 6-week training of BET can induce a reduction in perception of effort at a specific power, and thus improving cycling performance. Moreover, it provides evidence that including neurocognitive interventions will benefit athletes by increasing their mental resilience, without affecting their physical training load and routine.

Keywords**—**Cognitive Training, Perception of Effort, Endurance Performance, Neuro-performance.

Doctor W. Staiano is with Department of Physical Education and Sport, University of Valencia, Valencia, 46010, Spain (phone: +34663262239, e-mail: walterstaiano@gmail.com).

Professor S. Marcora is with Department of Sport and Exercise Sciences, University of Bologna, Bologna, 40123, Italy (e-mail: samuele.marcora@gmail.com).

A Quantitative Model for Identification of Key Factors That Cause Cardiac Hypertrophy and Variations in the Biomechanics of the Heart

V. A. Doss, K. Dharaniyambigai, K. Julia Rose Mary

***Abstract*—**Cardiac hypertrophy is the enlargement of the left ventricle of the heart myocardium which is the main muscle mass of the heart. Pathological conditions such as diabetes, hypertension etc., result in excessive deposition of collagenous and non-collagenous extracelluar matrix (ECM). This results in functional changes in the biomechanical and electrical properties of the heart such as contractility, passive stiffness and electrical conduction velocities of the heart. Myocardial stiffness can impair diastolic filling leading to heart failure. In order to predict the complex biochemical cascade reactions, deterministic modeling techniques such as Ordinary differential equation (ODE) and stochastic ordinary differential equation (S)ODE based model was used. Stochastic simulation and analysis was done using the tool COPASI. We used the model to explore the set of combination of molecules that will block the progression of cardiac hypertrophy so that the factors that compromise the biomechanics could be identified.

***Keywords*—**Cardiac hypertrophy, Cardiomyopathy, Fibrosis, Left Ventricular hypertrophy.

V. A. Doss, is the Associate Professor of Biochemistry, PSG College of Arts & Science, Coimbatore – India (phone: +919944641506; fax: 0422-2575622; e-mail: victordoss64@gmail.com).

K. Dharaniyambigai is the research scholar at PSG College of Arts & Science, Coimbatore – India (phone: +919790082487, e-mail: dharaniyambigai.kuberan@gmail.com).

K. Julia Rose Mary is the Associate Professor of Mathematics, at Nirmala College for Women, Coimbatore – India (phone: +919944641598, e-mail: juliakulandaisamy@gmail.com).

Mathematical Modeling and Elucidation of Potential Drug Targets in Altered Cardiac Biomechanics Due to Growth and Remodeling

K. Julia Rose Mary, V. A. Doss

***Abstract*—**Due to pathological conditions such as diabetes, hypertension, to compensate for the excessive neurochemical, chemical and mechanical cues, myocardium will switch over to adaptive process know as growth and remodeling which is an important cause for heart failure. As the heart failure progresses the heart size increases and its biomechanical functions deteriorate. Growth and remodeling is due to various interactions of many proteins and their interactions. Hence mathematical modeling becomes a powerful tool to understand the intricate molecular interactions. We used multi scale modeling, numerical methods, parameter testing and sensitivity analysis to validate the model and to analyse the complex protein networks using Ordinary differential equation (ODE) and stochastic ordinary differential equation (S)ODE. As these protein networks alter the biomechanics of the heart such as structural, kinematic and other dynamic constituents of the heart tissue, alterations of these reflect on the diastolic filling, pumping efficiency, ejections fraction etc., Thus this model suggests potential drug targets that could be tested in the actual biochemical experiments.

***Keywords*—**Cardiac hypertrophy, Cardiomyopathy, Fibrosis, Left Ventricular hypertrophy.

K. Julia Rose Mary is the Associate Professor of Mathematics, at Nirmala College for Women, Coimbatore – India (phone: +919944641598, e-mail: juliakulandaisamy@gmail.com).

V. A. Doss, is the Associate Professor of Biochemistry, PSG College of Arts & Science, Coimbatore – India (phone: +919944641506; fax: 0422-2575622; e-mail: victordoss64@gmail.com).

Detection of Bartonella Tamiae, Coxiella Burnetii and Rickettsiae in Arthropods and Tissues from Wild and Domestic Animals in North-Eastern Algeria

Hamza Leulmi, Atef Aouadi, Idir Bitam, Amina Bessas, Ahmed Benakhla, Didier Raoult,Philippe Parola

Abstract—Background: In recent years, the scope and importance of emergent vector-borne diseases has increased dramatically. In Algeria, only limited information is currently available concerning the presence and prevalence of these zoonotic diseases. For this reason, we conducted a survey of hematophagous ectoparasites of domestic mammals and/or spleens of wild animals in El Tarf and Souk Ahras, Algeria. Methods: Using real-time PCR, standard PCR and sequencing, the presence of Bartonella spp., Rickettsia spp., Borrelia spp. and Coxiella burnetii was evaluated in 268/1626 ticks, 136 fleas, 11 Nycteribiidae flies and 16 spleens of domestic and/or wild animals from the El Tarf and Souk Ahras areas. Results: For the first time in Algeria, Bartonella tamiae was detected in 12/19 (63.2 %) Ixodes vespertilionis ticks, 8/11 (72.7 %) Nycteribiidae spp. flies and in 6/10 (60 %) bat spleens (Chiroptera spp.). DNA from Coxiella burnetii, the agent of Q fever, was also identified in 3/19 (15.8 %) I. vespertilionis from bats. Rickettsia slovaca, the agent of tick-borne lymphadenopathy, was detected in 1/1 (100 %) Haemaphysalis punctata and 2/3 (66.7 %) Dermacentor marginatus ticks collected from two boars (Sus scrofa algira) respectively. Ri. massiliae, an agent of spotted fever, was detected in 38/94 (40.4 %) Rhipicephalus sanguineus sensu lato collected from cattle, sheep, dogs, boars and jackals. DNA of Ri. aeschlimannii was detected in 6/20 (30 %) Hyalomma anatolicum excavatum and 6/20 (30 %) Hy. scupense from cattle. Finally, Ri. felis, an emerging rickettsial pathogen, was detected in 80/110 (72.7 %) Archaeopsylla erinacei and 2/2 (100 %) Ctenocephalides felis of hedgehogs (Atelerix algirus). Conclusion: In this study, we expanded knowledge about the repertoire of ticks and flea-borne bacteria present in ectoparasites and/or tissues of domestic and wild animals in Algeria.

Keywords—Bartonella tamiae, Rickettsia, Coxiella burnetii, Ticks, Fleas, Algeria

Corresponding Author
Atef Aouadi from University of Souk Ahras, Algeria
e-mail: draouadiatef@gmail.com

Anatomical and Pathological Evaluation of Anomaly Cases Presented to the Department of Pathology at the Kafkas University Faculty of Veterinary Medicine, between 2017 and 2019

Gülseren Kırbaş Doğan, Emin Karakurt, Mushap Kuru, Hilmi Nuhoğlu

***Abstract*—**Developmental anomalies can be caused by defects in bone tissue, cartilage tissue, or primitive mesenchymal tissue. Genetic-, environmental-, teratogenic-, faulty breeding selection–, or feeding-related anomalies can be observed either locally or systemically. This study aimed to evaluate in detail the various anomalies in six calves according to pathological and anatomical investigations. Six calves were delivered to the Department of Pathology at the Kafkas University Faculty of Veterinary Medicine between 2017 and 2019. These calves comprised one with anencephaly, one with diencephalic syndrome, one with schistosoma reflexum, two with anasarca, and one with nasal and calvarium openings. After necropsy, samples were taken from the organs, foreseen and routine pathological examinations were performed. Following these procedures, the calves were brought to the anatomy laboratory and anatomically examined. As a result, various anomalies in 6 calves were evaluated according to pathological and anatomical investigations. These findings are believed to contribute to the literature.

***Keywords*—**Anatomy**,** Anomaly, Calf, Pathology.

G. K. D. The University of Kafkas, Faculty of Veterinary Medicine, Department of Anatomy, Kars/Turkey (e-mail: glsrn36@ gmail.com).

E. K. The University of Kafkas, Faculty of Veterinary Medicine, Department of Pathology, Kars/Turkey (mehmeteminkarakurt@hotmail.com).

M. K. The University of Kafkas, Faculty of Veterinary Medicine, Department of Obstetrics and Gynecology, Kars/Turkey (e-mail: mushapkuru @hotmail.com).

H. N. The University of Kafkas, Faculty of Veterinary Medicine, Department of Pathology, Kars/Turkey (hilminuhoglu@gmail.com).

Risk Assessment for Big Data in Cloud Computing: Trust as an Impact

Hazirah Bee Yusof Ali, Lili Marziana Abdullah, Mira Kartiwi, Azlin Nordin

***Abstract*—**Reduced IT cost, scalability, business continuity, collaboration efficiency and flexibility of work practice are some of the benefits that attract companies to move their business operation into the cloud. Cloud computing serves companies as IaaS, PaaS, and SaaS. Even though cloud has many benefits, it also has its own risks, the risk of being exposed unnecessarily as the cloud is owned and managed by a third party. Therefore, the risks need to be monitored and accessed by companies as they are the cloud customers who choose to use the cloud computing environment in handling their big data. Thus, the objective of this paper is to assess risk using trust measure as the impact.

***Keywords*—**Big data, cloud, risk, trust measures.

I. Introduction

TRADITIONALLY, we need many servers to be stored in our premise to keep and to process large amount of data that continuously accumulated by the day. The increased amount of data cause extra burden to the company as we need to purchase more servers and these servers are costly. In addition, more skilled workers are needed to manage the servers. The emergence of cloud computing with its attractive attributes of on-demand self-service, broad network access, elasticity and scalability, attracts companies to use cloud computing for data storage, data processing and data access.

The services of the cloud benefit the company when capital and operational cost can be reduced enormously. Expensive in-house servers are not required anymore and the same applies to manpower whereby the number of manpower needed to service the servers can be greatly reduced.

II. BACKGROUND

A. Big data

Big data are large amount of data generated exponentially through various channels such as email and social media. Data is then analyzed to enable us to see patterns and trends(Fujita, 2015). Patterns and trends help the company to predict customers' behaviors towards our products (Khosravi, Member, Nahavandi, Member, & Creighton, n.d.). Big-data technology can be used to "extract meaning and infer knowledge from very large datasets" (Fujita, 2015). Big-data technology is currently being used for human profiles creation, social behavior monitoring and decision making. It can show us the social trends and new business opportunities (Fujita, 2015).

B. Cloud Computing

Cloud computing on the other hand, enables us to rent only the services that we need. Cloud computing provides services of IaaS, PaaS and SaaS (Purcell, 2016). IaaS is Infrastructure as a Service, PaaS is Platform as a Service and finally SaaS is Software as a Service (Purcell, 2016). IaaS is a situation where Infrastructure is treated as a service. In IaaS, cloud provider serves companies with virtualized computing resources over the Internet. While IaaS looks into the infrastructure, PaaS looks into the platform to be utilized and SaaS looks into the software to be used in the cloud. PaaS enables companies to use the platform that they desire without buying the platform. This situation enables companies to utilize the platform with a very low cost compared to having the platform within the company. SaaS is a situation when Cloud provider leases application of software owned by them to cloud users. SaaS enables us to rent only the services that we need for the amount of time that we use and definitely, SaaS saves us a lot of money.

Cloud computing can be divided into three (3) areas: the public cloud, the private cloud, and the hybrid cloud. A public cloud is the "pay- as-you-go" services (Purcell, 2016). All companies are treated equally in the public cloud where companies share the cloud resources and storage among themselves. A private cloud on the other hand, is only used by a single business and the cloud is not shared with other companies, yet, it still uses the cloud structure (Purcell, 2016). The hybrid cloud is a mixture of public cloud and private cloud (Purcell, 2016).

Three major reasons why small to medium sized businesses use cloud computing for big data technology implementation are hardware cost reduction, processing cost reduction and the ability to test the value of big data. However, security and loss of control remain as the major concerns of cloud computing (Purcell, 2016).

C. Benefits of Big Data in Cloud

Having the capabilities of serving as IaaS, PaaS and SaaS (Purcell, 2016), cloud computing looks like a collection of data center to place and to manage our data. Cloud computing manages its resources while enables us to use and to manage our resources properly.

The ability to collect and mine data from the mass information in the cloud with less time and less space

Hazirah Bee Yusof Ali is with Kulliyah of Information and Communication Technology, International Islamic University Malaysia, Gombak, Malaysia (phone: +6019-222-9179; e-mail: hazirahbee@gmail.com).

Lili Marziana Abdullah is with Kulliyah of Information and Communication Technology, International Islamic University Malaysia, Gombak, Malaysia (phone: +603-6196-5657; e-mail: lmarziana@iium.edu.my).

Mira Kartiwi is with Kulliyah of Information and Communication Technology, International Islamic University Malaysia, Gombak, Malaysia (phone: +603-6196-5652; e-mail: mira@iium.edu.my).

Azlin Nordin is with Kulliyah of Information and Communication Technology, International Islamic University Malaysia, Gombak, Malaysia (phone: +603-6196-5659; e-mail: azlinnordin@iium.edu.my).

creates values to companies. Besides that, the companies can also utilize the "storage, management and calculation" capabilities of the cloud computing environment (Cui, 2016).

D.Risk

However, the benefits that cloud computing give to companies frequently come with a risk. "Information leakage, illegal access, interest first" can be easily found in cloud computing environment as data are not residing with the data owner (Arias-Cabarcos, Almenárez, Díaz-Sánchez, & Marín, 2018). The risk of losing the controlling power of the company's data exists because data are stored in external servers and are located anywhere in the cloud (Felici & Pearson, 2014). Because of that, some companies could not enjoy the cloud usage up to the maximum as some data need to stay in their premise.

E. Trust

When data are stored outside the premise of the company, it is very difficult to say that we can trust the situation easily (Felici & Pearson, 2014). Arias-Cabarcos, P (2018) claimed that "trust, dependencies and data security" create problems to big data security services. Data providers, users and cloud service provider are fully aware about this problem (Arias-Cabarcos et al., 2018). As a result, various techniques are being added to increase the trust level. One good example is SLA (Service level agreement) where trust is earned by putting all stages of control in writing. If the cloud provider fails to serve as promised, they should be ready to compensate with the breach of the SLA.

From the users' perspective, in order to reduce the feelings of distrust, they segregate the highly confidential data from the less confidential data. Highly confidential data are stored in premise while the less confidential data are stored in cloud. Unfortunately, this situation removes the benefits of cloud computing environment for the highly confidential data.

III. Methodology

We adopt a mixed method approach of data collection. Mixed method is a research approach, in which we collect, analyze, and integrate both qualitative and quantitative data to answer the research questions (Creswell, 2013).

Since there are several types of mixed method, we choose exploratory sequential mixed method design. An exploratory sequential mixed method is a design where the qualitative data is explored and analyzed (Creswell, 2013). The findings of the data analysis are used as an input to the quantitative phase. The purpose is to come up with a better measurement with samples of the population and to check if the data analysis from qualitative sample can be generalized to large sample in quantitative method (Creswell, 2013). Creswell, 2013 also mentioned that "if a concept or phenomenon needs to be explored and understood because little research has been done on it, then, it merits a qualitative approach". Qualitative research is the best when little is known about the variables to be examined (Creswell, 2013).

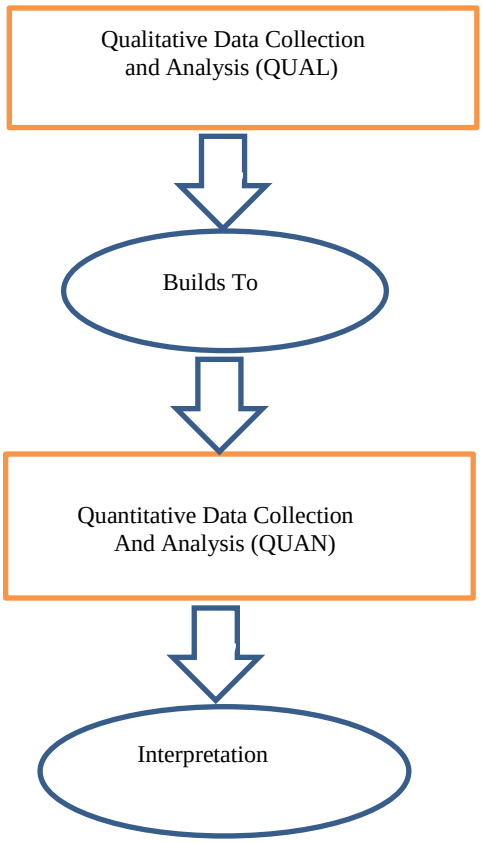

Fig. 1: Exploratory Sequential Mixed Method (Creswell, 2013)

Exploratory Sequential Mixed Method is chosen for the research because very few literatures discussed on risk assessment from the trust perspective. Therefore, we decided to use exploratory sequential mixed method instead.

In our exploratory sequential design, qualitative exploratory data is gained through interviews of few candidates. We will analyze the information and develop a psychometric instrument to be verified by a sample of population (Creswell, 2013). We will employ a three-phase procedure as the following:

- Exploratory
- Instrument development
- To verify the instrument by testing the instrument towards a population

(Creswell, 2013)

However, before any of the above can be done, we would like to have a good look at the interview questions. The interview should give us results that can lead us to the research questions. Since interviews are conducted at the early stages of exploratory, thorough check on the interview questions need to be done. Thorough check can be expedited by conducting a pilot interview prior to the real interview.

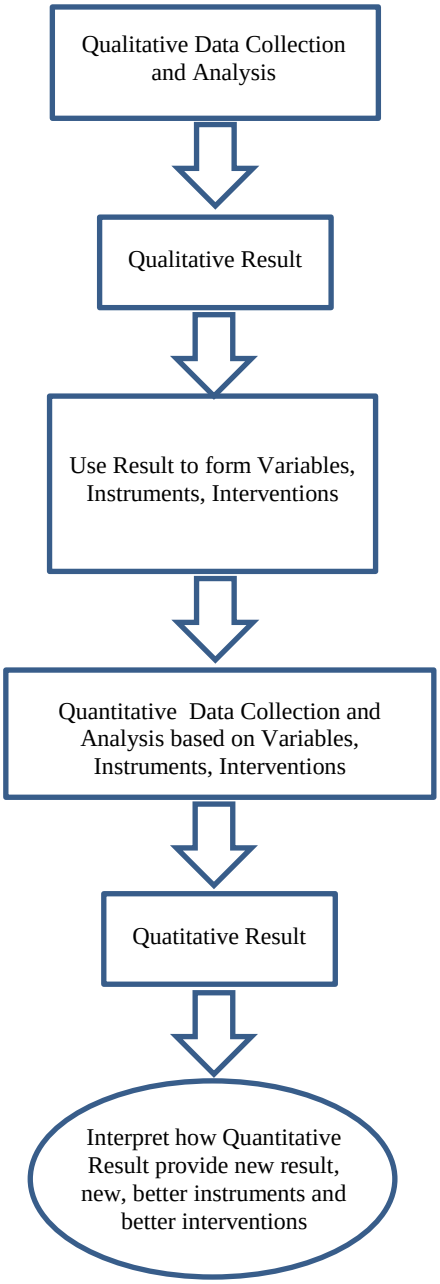

Fig. 2: Exploratory Sequential Design (Creswell, 2013)

Our research questions are the following:

1) RQ1: How do a client of cloud service processing big data **establish trust** with its service provider regarding the client's data?

2) RQ2: What are the risks affecting the trust between the client, and its cloud service provider regarding the client's data?

3) RQ3: What impact have the risks had on the trust between the client, and its cloud service provider regarding the client's data?

We design several questions that can lead us to the research questions. The questions are tested in our pilot test by conducting interviews to two candidates from the industry. The interviews are used to ensure that all questions asked to the interview candidates later, can be answered and can eventually lead us to the research questions. There are seven (7) questions for RQ1, four (4) questions for RQ2 and two (2) questions for RQ3.

The questions are asked in the order as listed below:

RQ1: How do a client of cloud service processing big data **establish trust** with its service provider regarding the client's data?

1) What cloud services processing big data have your organisation used or are using now?
2) Who are your organisation's service provider(s)?
3) What is the size of your data in the cloud?
4) On what basis, does your organisation trust the service provider with the organisation's data?
5) What security objectives of big data in the cloud set with the service provider?
6) Would your organisation be more trusting of the service provider if the service provider shows progress towards the security objectives?
7) How does your organisation monitor progress of the service provider towards the security objectives?

RQ2: What are the risks affecting the trust between the client, and its cloud service provider regarding the client's data?

1) Has your organisation changed big data and cloud service provider before?
2) What are the causes for the change?
3) What events that have occurred or could occur towards the organisation's data that affect the organisation's trust in the service provider?
4) What were the causes or would be the likely causes for the events?

RQ3: What impact have the risks had on the trust between the client, and its cloud service provider regarding the client's data?

1) How frequent did the events occur or how frequently likely for the events to occur?

2) What impact did the events have or would have towards the organisation's data that affect the organisation's trust in the service provider?

IV. ANALYSIS

We have interviewed two (2) candidates from two (2) GLC companies (government linked company) and we found out that some of the questions have to be reworded so that the interviewee can easily understand the questions and can provide a better answer that eventually lead to a better output.

A properly prepared interview questions can expedite us towards answering the research questions. We also found out that there are some conflicts when they tried to answer RQ1 (Question 4):

Question 4.

On what basis, does your organization trust the service provider with the organization's data?

Both said that they trust the service provider but they still need to segregate the highly confidential data from the less confidential data before they can put them in the cloud storage. Highly confidential data are stored in premise.

One of them even stated that they should be allowed to manage the operation of their data in the cloud.

Both of them claimed that they have never changed the cloud provider.

V. FINDINGS

The level of risk "vary significantly with the type of cloud architecture deployed" (Khosravani, Nicholson, & Wood-Harper, 2013). The same applies to our study where the companies store high risk data in house and low risk data in the cloud. Even though the cloud enables them to do a better data crunching and faster data analysis, they could not take the risk of putting high risk data in the cloud which are owned by the cloud provider and the cloud provider are external party.

VI. CONCLUSION

We conclude that checking and validating the interview question is important so that we get high quality interview questions that can lead us to our research questions. A pilot interview is very useful when we are not sure of the quality of our interview questions. This is because, the interview candidates coming from the industries may have different perception on certain terms used by us, the researcher. Therefore, by conducting a pilot interview may help us in correcting the interview questions so that the outcome of the real interview will lead us to the research question.

ACKNOWLEDGMENT

This research has been funded by Fundamental Research Grant Scheme (FRGS16-022-0521) supported by Ministry of Higher Education, Malaysia.

REFERENCES

[1] Arias-Cabarcos, P., Almenárez, F., Díaz-Sánchez, D., & Marín, A. (2018). FRiCS: A framework for risk-driven cloud selection. *Proceedings of the ACM Conference on Computer and Communications Security*, 18–26. https://doi.org/10.1145/3267357.3267362

[2] Creswell, J. W. (2013). Steps in Conducting a Scholarly Mixed Methods Study: What I am looking for core characteristics: Do you have a quantitative database? (closed- ended). *University of Nebraska - Lincoln*, 54.

[3] Cui, H. T. (2016). Research on the model of big data serve security in cloud environment. *2016 1st IEEE International Conference on Computer Communication and the Internet, ICCCI 2016*, 514–517. https://doi.org/10.1109/CCI.2016.7778976

[4] Felici, M., & Pearson, S. (2014). Accountability, Risk, and Trust in Cloud Services: Towards an Accountability-Based Approach to Risk and Trust Governance. *2014 IEEE World Congress on Services*, 105–112. https://doi.org/10.1109/SERVICES.2014.29

[5] Fujita, H. (2015). Big data based clouds healthcare web service forecasting: Research challenge. *2015 IEEE 10th Jubilee International Symposium on Applied Computational Intelligence and Informatics*, 529–534. https://doi.org/10.1109/SACI.2015.7208261

[6] Khosravani, A., Nicholson, B., & Wood-Harper, T. (2013). A case study analysis of risk, trust and control in cloud computing. *Science and Information Conference (SAI), 2013*, 879–887.

[7] Khosravi, A., Member, I., Nahavandi, S., Member, I. S., & Creighton, D. (n.d.). *Estimating Performance Indexes of a Baggage Handling System Using Metamodels*.

[8] Purcell, B. M. (2016). *Big data using cloud computing Big data using cloud computing*. (October).

Determination of Critical Success Factors (CSF) Necessary for Ensuring the Digital Transformation of Cities and the Creation of Digital City Maps (DCM) and Digital City Indexes (DCI) of Zonguldak Province Cities Depending on the CSFs

Mustafa Çoruh

Abstract**—**The integration of new mobile and digital technologies with digital meters (sensors) becomes important in the effective and productive implementation of municipal and urban services. For example, automatic reading of water, natural gas and electricity meters by mobile technologies, monitoring of air, road and traffic status with the relevant sensors and announcement to the relevant authorities and the public, such as providing fluidity, energy saving and efficiency in traffic, help to facilitate urban life and efficient use of urban resources. Smart City (SC) applications have started to provide important opportunities for ensuring urban security, finding addresses and activating municipal services. In line with all these developments, the dimensions, factors and indicators affecting the digitalization of cities are defined, and the digital indices of cities and the creation of Digital City Maps (DCM) are becoming new tools of city administrations. Particularly in cities, the DCM is important in terms of revealing or visualizing the codes of digital transformation. It is important to identify the dimensions of smart technology, smart people, smart governance and smart economics that affect cities, and Critical Success Factors (CSFs) that define each dimension. In order to measure each CSF with city data, the relevant indicative values were collected and analyzed from the city stakeholders, the municipality, Chamber of Commerce and Industry (TSO), Türk Telekom, Police Department, SSI, MoNE, district governor and national statistical institutions. The level of urban readiness for digital transformation or SC level can be measured. In this research, digital city maps and digital city indexes of Zonguldak districts were collected by collecting indicator data that will affect the digital transformation of eight districts in Zonguldak province and the digital transformation order of the districts was determined.

Keywords**—**Smart Cities, Digital Transformation, Digital City Index, Digital City Map, Information and Communication Technologies, Critical Success Factors, Analytical Hierarchy Procedure.

Mustafa Çoruh is with Sakarya University, Turkey (e-mail: mcoruh@mustafacoruh.com).